Understanding the role of C16orf72

in the DNA replication stress response



Joel Kosmin

Somerville College

A thesis submitted for the award of

DPhil in Interdisciplinary Bioscience

Michaelmas Term 2022

Abstract

The human genome continually undergoes DNA damage that is endogenous and exogenous in origin. To protect the genome from this DNA damage, cells have evolved a plethora of signalling pathways, known as the DNA damage response (DDR). The poly(ADP-ribose) polymerase (PARP) enzyme family can regulate a variety of DDR pathways by modifying substrates with ADP-ribose, a type of chemical post-translational modification. However, our understanding of these pathways, and the factors involved in them, remains in their infancy. Chemical inhibitors of PARPs (PARPi) have emerged as key therapeutic tools to combat human diseases, thereby underlining the importance of understanding the pathways controlled by this enzyme family.

To investigate whether additional PARP enzymes might function in the absence of PARP1 and PARP2 in response to DNA damage, a genetic approach using a small-scale siRNA screen was taken. From this, I found that loss of PARP6 or PARP14 may rescue the PARPi-induced further sensitisation of PARP1/PARP2 knockout cells to methyl methanesulfonate (MMS). This suggests that PARP6 or PARP14 may be trapped to DNA by olaparib and supports the notion that either of these PARPs may participate in the repair of MMS-induced DNA damage in the absence of PARP1 and PARP2.

To reveal novel DDR proteins that are synthetic lethal with the combined loss of PARP1 and PARP2, a genome-wide CRISPR dropout screen was performed. From this, I identified the poorly characterised protein C16orf72 as being synthetic lethal

with the combined loss of PARP1 and PARP2. Genetic deletion of C16orf72 sensitises cells to the DNA replication stress-inducing agents, hydroxyurea (HU) and aphidicolin (APH) indicating a function for C16orf72 in the DDR pathways that respond to DNA damage induced by these agents. Indeed, I find that C16orf72 is recruited to chromatin in response to exogenous replication stress, thereby localising it to damaged chromatin. In addition, I find that C16orf72 is required to limit replication catastrophe under conditions of prolonged replication stress. Together, these findings suggest that C16orf72 is a novel DDR factor that functions in response to DNA replication stress.

Collectively, my findings represent two major advances. Firstly, I identify PARP6 or PARP14 as novel PARP family members that may participate in the repair of MMS-induced DNA damage in the absence of PARP1 and PARP2. Secondly, I identify C16orf72 as a novel component of the DDR and show that it functions in response to DNA replication stress. Taken together, my findings expand our understanding of two important aspects of the DDR: ADP-ribosylation signalling and the DNA replication stress response.

Contents

Abstract ii

List of Figures ix

List of supplementary figures xii

List of tables xiii

Abbreviations xiv

Declaration xxii

Acknowledgments xxiii

Chapter 1. Introduction 1

1.1 PARPs 1

1.1.1 Post-translational modifications 1

1.1.2 ADP-ribosylation 1

1.1.3 Removal of ADP-ribosylation 11

1.1.4 An Overview of the PARP Family 2

1.1.5 PARP catalysis 8

1.1.6 Mechanism of PARP1, PARP2 and PARP3 activation 10

1.2 The involvement of PARPs in the DNA damage response 14

1.3 Mechanisms of repairing base lesions and single-strand breaks 15

1.3.1 Causes of DNA SSBs 15

1.3.2 BER and SSBR 16

1.3.3 The participation of PARPs in BER and SSBR 20

1.4 Mechanisms of DNA double-strand break repair 21

1.4.1 Causes of DNA DSBs 22
1.4.2 c-NHEJ 31
1.4.3 The involvement of PARPs in c-NHEJ 35
1.4.4 alt-NHEJ 36
1.4.5 The involvement of PARPs in alt-NHEJ 40
1.4.6 Homologous recombination 23
1.4.7 The involvement of PARPs in HR 30
1.4.8 Making the decision between DSB and c-NHEJ 41
1.5 DNA Replication stress 41
1.5.1 Causes of DNA replication stress 42
1.5.2 The DNA replication stress response 42
1.5.3 The involvement of PARPs in the DNA replication stress response 55
1.6 The cell cycle 60
1.6.1 Cell cycle phases 60
1.6.2 DNA damage checkpoints 62
1.7 Synthetic lethality 63
1.7.1 Discovery of synthetic lethality and the development of PARPi 63
1.7.2 PARPi: How do they work? 65
1.7.3 PARPi resistance 68
1.8 Aims 70
Chapter 2. Materials and Methods 71
2.1 Materials 71
2.1.1 Buffers 71
2.2 Methods 74

2.2.1 Cell Culture 74
2.2.2 Clonogenic Survival Assay 74
2.2.3 Immunofluorescence 75
2.3 Preparation of whole cell extracts 77
2.4 Chromatin fractionation 78
2.5 Western Blotting 79
2.6 Antibodies 80
2.7 siRNA transfections 82
2.8 siRNAs 83
2.9 Genome-wide CRISPR Dropout Screen 84
2.10 High-throughput Combination Assay 86
Chapter 3. Determining whether a PARP participates in the repair of MMS-induced DNA damage in cells lacking PARP1 and PARP2 88
3.1 Introduction 88
3.1.1 Alkylation base damage increases PARPi toxicity 88
3.1.2 A PARP may participate in the repair of MMS-induced DNA damage in cells lacking PARP1 and PARP2 88
3.1.3 Aims 90
3.2 Results 90
3.2.1 Chemical proteomic approach to investigate the olaparib selectivity profile in PARP1ΔPARP2Δ cells 90

3.2.2 PARP depletion screens to determine whether an additional PARP participates in the repair of MMS-induced DNA damage in cells lacking PARP1 and PARP2 96

3.3 Discussion 130

Chapter 4. Identifying novel synthetic lethal interactions with combined loss of PARP1 and PARP2 138

4.1 Introduction 138

4.1.1 CRISPR in genome editing 138

4.1.2 Discovery of novel DDR factors using CRISPR screens 139

4.1.3 Aims 140

4.2 Results 141

4.2.1 Identification of synthetic lethal interactions with combined deletion of PARP1 and PARP2 141

4.2.2 Validation of the synthetic lethal interaction between C16orf72 loss and combined PARP1 and PARP2 deletion 147

4.2.3 Investigating the key determinants of the synthetic lethal interaction between C16orf72 deficiency and combined PARP1 and PARP2 loss 149

4.2.4 Bioinformatic analysis of C16orf72 151

4.2.5 Loss of C16orf72 further sensitises U2OS cells to HU, APH, WEE1i and ATRi 159

4.2.6 Loss of C16orf72 further sensitises U2OS cells to ATRi-ATMi combinations 170

4.3 Discussion 178

Chapter 5. Investigating the function of C16orf72 in the DNA replication stress response 187

5.1 Introduction 187

5.1.1 C16orf72 may be a novel DNA replication stress response factor 187

5.2 Results 188

5.2.1 QIBC analysis of cell cycle distribution in C16orf72Δ cells 188

5.2.2 C16orf72 is recruited to chromatin in response to exogenous replication stress in an ATR-independent manner 192

5.2.3 QIBC analysis of G_1-phase 53BP1 nuclear body formation in C16orf72Δ cells in the absence and presence of exogenous replication stress 195

5.2.4 Western blot analysis of pRPA, pDNA-PK_{CS}, pCHK1 and γH2AX levels in C16orf72Δ cells in the absence and/or presence of exogenous replication stress 200

5.2.5 QIBC analysis of γH2AX and RPA70 levels in C16orf72Δ cells in the absence and presence of exogenous replication stress 206

5.2.6 QIBC analysis of RPA-γH2AX-positive cells in the absence and presence of exogenous replication stress 213

5.2.7 QIBC analysis of recovery of γH2AX levels in C16orf72Δ cells following removal of exogenous replication stress 216

5.3 Discussion 219

6. General Discussion 232

7. References 240

8. Appendices 288

List of Figures

1.1: Arrangement of domains within proteins of the PARP family……....7

1.2: Mechanism of addition and removal of serine ADP-ribosylation in response to DNA damage……13

1.3: Summary of BER……19

1.4: Summary of HR……..29

1.5: Summary of c-NHEJ……..34

1.6: Summary of alt-NHEJ……39

1.7: Summary of the DNA replication stress response……59

3.1: Another PARP may participate in the repair of MMS-induced DNA damage in cells lacking PARP1 and PARP2. ……89

3.2: Chemical proteomic assay workflow……..93

3.3: Chemical proteomic study suggests that PARP1 and PARP2 are present in PARP1ΔPARP2Δ cells. ……...95

3.4: Rationale for PARP depletion screen to assess whether PARP1ΔPARP2Δ cells are further sensitised to MMS following independent depletion of a PARP..……100

3.5: First PARP depletion screen to determine whether a PARP may participate in the repair of MMS-induced DNA damage……..105

3.6: Rationale for PARP depletion screen to assess whether independent depletion of a PARP rescues the olaparib-induced further sensitisation of PARP1ΔPARP2Δ cells to MMS……..……..……..……..……..……..……..……..……..……..……..……...114

3.7: PARP depletion screen to determine whether olaparib-mediated trapping of a PARP to DNA is responsible for the olaparib-induced further sensitisation of PARP1ΔPARP2Δ cells to MMS……...119

3.8: Repetition of PARP depletion screen to determine whether independent depletion of PARP6 or PARP14 rescues the olaparib-induced further sensitisation of PARP1ΔPARP2Δ cells to MMS..……..126

4.1: Genome-wide CRISPR dropout screen to identify novel synthetic lethal interactions with combined PARP1 and PARP2 deletion……143

4.2: Venn diagram summarising gene hits identified in the wild type U2OS and PARP1ΔPARP2Δ cell lines.……..146

4.3: C16orf72 depletion is synthetic lethal with combined PARP1 and PARP2 loss…..……..……..……..……..……..……..……..……..……..……..……...148

4.4: PARP1 and PARP2 are key determinants of the synthetic lethal interaction between C16orf72 deficiency and combined PARP1 and PARP2 loss.……..150

4.5: Predicted sites of phosphorylation and ubiquitination in human C16orf72……..152

4.6: Two motifs are highly conserved in C16orf72 orthologues from chordates and arthropods……154

4.7: The predicted structure of C16orf72 is highly conserved in vertebrates……..156

4.8: Validation of C16orf72 knockout and FLAG-HA-C16orf72-overexpressing cell lines……..……..……..……..……..……..……..……..……..……..……..…161

4.9: Loss of C16orf72 sensitises further sensitises U2OS cells to HU and APH.……164

4.10: Loss of C16orf72 sensitises further sensitises U2OS cells to WEE1i……168

4.11: C16orf72 depletion sensitises U2OS cells to ATRi……..169

4.12: Schematic of high-throughput ATRi-ATMi combination screen……..173

4.13: C16orf72 deletion further sensitises U2OS cells to ATRi-ATMi combinations……..……..……..……..……..……..……175

5.1: Cell cycle distribution is not altered in C16orf72Δ cells……..……..……..……...190

5.2: FLAG-HA-C16orf72 is recruited to chromatin in response to HU treatment but independently of ATR……194

5.3: G_1-phase 53BP1 nuclear body formation in C16orf72Δ cells in the absence and presence of APH……..……..199

5.4: Western blot analysis of pRPA, pDNA-PK_{CS}, pCHK1 and γH2AX levels in C16orf72Δ cells in the absence and presence of HU.……205

5.5: QIBC analysis of nuclear γH2AX intensity in C16orf72Δ cells in the absence and presence of HU.……..209

5.6: QIBC analysis of RPA70 levels in C16orf72Δ cells in the absence and presence of HU.……212

5.7: QIBC analysis of RPA70-γH2AX-positive cells in the absence and presence of HU.……215

5.8: QIBC analysis of recovery of γH2AX levels in C16orf72Δ cells following removal of HU.……218

List of supplementary figures

8.1: Validation of C16orf72 knockdown in U2OS, PARP1Δ and PARP1ΔPARP2Δ cells……...288

8.2: Extended alignment of C16orf72 orthologues from chordates, arthropods and ascomycetes……...289

8.3: Loss of C16orf72 sensitises further sensitises U2OS cells to ATRi……..291

8.4: C16orf72 loss further sensitises U2OS cells to ATRi-ATMi combinations……292

List of tables

2.1: Primary antibodies utilised in this study……..80

2.2: Secondary antibodies utilised in this study……82

2.3: siRNAs utilised in this study……..83

3.1: Summary of p-values for Figure 3.5 when evaluated by two-way ANOVA……..109

3.2: Summary of p-values for Figure 3.5 when evaluated by two-way ANOVA with Tukey's post hoc analysis……..110

3.3: Summary of p-values for Figure 3.7 when evaluated by two-way ANOVA……..123

3.4: Summary of p-values for Figure 3.7 when evaluated by two-way ANOVA with Tukey's post hoc analysis…..……124

3.5 Summary of p-values for Figure 3.8 a……128

3.6 Summary of p-values for Figure 3.11 c……..129

4.1: Human proteins aligned with motif 1 in human C16orf72……...157

4.2: Human proteins aligned with motif 2 in human C16orf72……...158

4.3. Summary of findings from the high-throughput combination screens……..177

Abbreviations

5’-dRP – 5’-deoxyribose phosphate

53BP1 – p53-binding protein 1

AAD – ATR activating domain

ABCB – ATP binding cassette subfamily B member

ABRO1 – Abraxas brother 1

ADPr – ADP-ribose

ALC1 – Amplified in liver cancer 1

Alt-NHEJ – Alternative non-homologous end joining

AP – Apurinic/apyrimidinic

APC/C – Anaphase-promoting complex/cyclosome

APE1 – Apurinic/apyrimidinic endoculease 1

APH – Aphidicolin

APLF – Aprataxin and PNKP Like Factor

APTX – Aprataxin,

ARH – (ADP-ribosyl)hydrolase

ART – ADP-ribosyltransferase

ARTD – Diptheria-toxin-like ADP-ribosyltrasferases

ATAD5 – ATPase Family AAA Domain Containing 5 (ATAD5)

ATM – Ataxia telangiectasia mutated

ATMi – ATM inhibitor

ATR – Ataxia and Rad3-related protein

ATRi – ATR inhibitor

ATRX – α-thalassemia mental retardation X-linked

BER – Base excision repair

BIR – Break-induced replication

BLM – Bloom syndrome

BOD1L – Biorientation of chromosomes in cell division 1-Like

BRCA – Breast Cancer gene

BRCT – Breast cancer susceptibility protein-1 C terminus

c-NHEJ – Classical non-homologous end joining

C16orf72 – Chromosome 16 Open Reading Frame 72

CARM1 – Coactivator associated arginine methyltransferase 1

Cas9 – CRISPR associated protein 9

CDC25 – Cell division cycle 25

CDK – Cyclin-dependent kinase

CHD2 – Chromodomain helicase DNA-binding protein 2

CK2 – Casein kinase

CRISPR – Clustered regularly interspaced short palindromic repeats

CtIP – CtBP-interacting protein

DDR – DNA damage response

DDRi – DDR inhibitor

DDT – DNA damage tolerance

dHJ – Double Holliday junction

DMEM – Dulbecco's Modified Eagle Media

DMSO – Dimethyl sulfoxide

DNA-PK – DNA-dependent protein kinase

DNA-PKcs – DNA-PK catalytic subunit

DNA2 – DNA replication helicase/nuclease 2

DNAJC9 – DNA J heat shock protein family (Hsp40) member C9

DSB - Double-strand break

DSBR – Double-strand break repair (DSBR)

DUF – Domain of unknown function

EdU – 5-ethynyl-2'-deoxyuridine

ER – Endoplasmic reticulum

ETAA1 – Ewing's tumor-associated antigen 1

EXD2 – Exonuclease 3'-5' domain containing 2 (EXD2)

EZH2 – Enhancer of zeste homolog 2

FANC – Fanconi anemia group

FBH1 – F-Box DNA Helicase 1

FBS – Foetal Bovine Serum

FDR – False Discovery Rate

FEN1 – Flap-endonuclease 1

gRNA – Guide RNA

H2AX – H2A histone family member X

HAPSTR – HUWE1-associated protein modifying stress responses

HD – Helical domain

HIRAN – HIP116/HLTF RAD6 N-terminus

HLTF – Helicase-like transcription factor

HPF1 – Histone PARylation factor 1

HR – Homologous recombination

HSA – Highest single agent

HU – Hydroxyurea

HUWE1 – HECT, UBA and WWE domain containing protein ligase 1

IRE1α – Inositol requiring enzyme 1α

LIG – DNA ligase

MAD2L2 – Mitotic arrest deficient 2-like 2

MAGeCK – Model-based Analysis of Genome-wide CRISRP/Cas9 Knockout

MAR – Mono(ADP-ribose)

MDC1 – Mediator of DNA damage checkpoint protein 1

MDM2 – Mouse double minute 2 homolog

MiDAS – Mitotic DNA synthesis

MLL Mixed-lineage leukemia

MMR – Mismatch repair

MMS – Methyl methanesulfonate

MMS22L – MMS-sensitivity protein 22-like (MMS22L)

MRN – MRE11-RAD50-NBS1

MRNIP – MRN complex interacting protein

MRPS34 – Mitochondrial ribosomal protein S34

MVP^{ID} – Major vault protein interaction domain

NAD^+ – Nicotinamide adenine dinucleotide

Nam – Nicotinamide

NER – Nucleotide excision repair

nLC-MS/MS – Nano liquid chromatography with tandem mass spectrometry

NVL – Nuclear VCP Like

PALB2 – Partner and localiser of BRCA2

PAM – Protospacer-adjacent motif

PAR – Poly(ADP-ribose)

PARG – Poly(ADP-ribose) glycohydrolase

PARI – PCNA-associated recombination inhibitor

PARP – Poly(ADP-ribose) polymerase

PARPi – PARP inhibitor

PAXX – Paralog of XRCC4 and XLF

PBS – Phosphate buffered saline

PCNA – Proliferating cell nuclear antigen

PERK – PKR-like ER kinase

PFGE – Pulse field gel electrophoresis

PFN1 – Profilin-1

PICH – Plk1-interacting checkpoint helicase

PIKK – Phosphoinositide 3-kinase-(PI3K)-related kinase (PIKK)

PMYT1 – Tyrosine-and threonine-specific cdc2-inhibitory kinase

PNKP – Polynucleotide kinase 3'-phosphatase

Pol – DNA polymerase

PolD – Polymerase domain

PRIMOL – Primase And DNA Directed Polymerase

PTBP1 – Polypyrimidine tract binding protein

PTIP – Pax transactivation domain-interacting protein

PTM – Post-translation modification

QIBC – Quantitative image-based cytometry

RADX – RPA related single stranded DNA binding protein, X-linked

RB – Retinoblastoma (RB)

RECQL – RecQ Like Helicase

RECQL5 – RecQ-like helicase 5

RER – Ribonucleotide excision repair

REV3L – Reversionless 3-like

REV7 – Revertibility protein 7 homologue

RFC – Replication factor C

RHINO – RAD9-RAD1-HUS1-interacting nuclear orphan

RIF1 – Replication timing regulatory factor 1

RLC – Replication-factor C-like complex

RMI – RecQ mediated genome instability

RNASEH2 – Ribonuclease H2

RNF8 – Ring finger Protein 8

RPL36 – Ribosomal protein L36

RRM – RNA recognition motif

RRM2 - Ribonucleotide reductase regulatory subunit M2

RT-qPCR – Reverse transcription quantitative real-time PCR

SAM – Sterile-alpha motif

SDSA – Synthesis-dependent strand annealing

seDSB – Single-ended DSBs

SETD1A – SET domain containing 1A

SHLD – Shieldin

SIRF – In situ detection of proteins at replication forks (SIRF)

siRNA – Small interfering RNA

SMARCAL1 – SWI/SNF subfamily A-like 1

SNF2H – Sucrose nonfermenting-2 homolog (SNF2H)

SPINDOC – Spindlin interactor and repressor of chromatin binding (SPINDOC)

SSA – Single strand annealing

SSB – Single-strand break

SSBR – SSB repair

Tankyrase/TNKS – TRF1-interacting ankyrin-related ADP-ribose polymerase

TAPR1 – Telomere attrition and p53 response 1

TBS-T – Tris-Buffered Saline

TDP1 – Tyrosyl-DNA phosphodiesterase 1

Tip60 – Tat interactive protein, 60 kDa

TKOv3 – Toronto KnockOut version 3

TLS – Translesion synthesis

TM – Transmembrane

TMEJ – Polθ-mediated end joining

TONSL – Tonsoku-like

TOP – DNA topoisomerase

Tpr – Translocated promoter region

TS – Template switching

UBM1 – Ubiquitin-binding motif 1

UIM – Ubiquitin-interacting motif

UPR – Unfolded protein response

UPS – Ubiquitin proteasome system

USP7 – Ubiquitin Specific Peptidase 7

UV – Ultraviolet

vWA – von Willebrand type A

WEE1i – WEE1 inhibitor

WGR – Tryptophan-glycine-arginine

WRN – Werner protein

WWE – Tryptophan-tryptophan-glutamate

XRCC – X-ray repair cross complementing

ZF – Zinc finger

ZFP161 – Zinc Finger Protein 161 homolog (ZFP161)

ZRANB3 – Zinc finger RANBP2-type containing 3

Declaration

I confirm that all of the data in my thesis is my own apart from the data presented in Figures 3.1 (Dr George Ronson); 3.3 a and b (Dr Fiona Pachl); 3.3 c (Dr Sabrina Liberatori); 4.1 (Dr George Ronson, Dr Daniel Ebner and Dr Mohammed Khairul Ramlee); 4.8 (Dr Mohammed Khairul Ramlee); 4.9 b (Dr Mohammed Khairul Ramlee), 8.1 (Dr Mohammed Khairul Ramlee); and 8.3 (Amy Wolstenholme).

Acknowledgments

Firstly, I am grateful to my supervisors Ian Gibbs-Seymour, Nicholas Lakin and Catherine Pears for providing their advice and expertise throughout this research. Secondly, I am thankful to all of the friends that I made during my time in the lab. In particular, I would like to thank Khairul Ramlee for collaborating with me on this project and for teaching me how to keep a lab in pristine condition. I am also grateful to George Ronson, Daniel Ebner and Amy Wolstenholme who made important contributions to this work. I would also like to thank the BBSRC and AstraZeneca for providing me with the opportunity to perform research at Oxford. Special thanks also go to Mark O'Connor, Josep Forment and Paul Wijnhoven at AstraZeneca for supervising me during my placement there; for providing me with access to state-of-the-art research equipment; and for allowing me to gain exciting insight into the pharmaceutical industry.

I cannot thank my friends enough for helping me across the finish line. David, Paddy, Robin, Connor, Jon, Joe, Charlie, Ben, Yuval, Toby, Gil, Yoni, Aaron, Victoria, Rebecca, Bea, Laura, Ally, Ella, Sam and Ruby – I am certain that I would not have finished this work without your continued support, sense of humour and supply of food. Equally, I would like to express my gratitude to my friends and flatmates Adam and Raphael who made my time in the flat hilariously bizarre. Thank you for putting up with me; for making me howl with laughter; and for offering your unwavering support throughout my studies. I am also grateful to the wider Somerville MCR community for making my time at college special and for always keeping me fed and watered at Welfare Tea.

Finally, I am incredibly grateful to my parents Alan and Jane; to my sister Ella; to my uncles David and Davi; to my aunties Sarah, Edi and Maryse; and to my cousins Danya, Gilad, Tal, Aviv, Nadav, Alon, Tani, and Jamie. Thank you for always believing in me; for making sure that I finish the DPhil; and for loving and supporting me unconditionally. I am blessed to have you all in my life.

Impact of COVID-19 on studies

My research was exclusively wet-lab based and required a number of critical molecular and cell biology facilities that were only available in the Department of Biochemistry. Furthermore, there was no aspect of my project that was computational and therefore transferable to a home working environment. Therefore, the lack of access to the Department of Biochemistry and my immediate research laboratory effectively put my lab work on complete hold from Friday 20th March 2020 until 26th May 2020. Upon return to the department on May 26th 2020, social distancing rules were put in place and I was only permitted to work half-days in the laboratory for the following 7 months. Subsequently, I completed an iCASE placement in AstraZeneca for 3 months where I was also only permitted to work half-days in the laboratory. Upon my return to the Department of Biochemistry, I was only permitted to work half-days in the laboratory for a further 4 months. Before the university was closed to non-COVID-19 research, I planned to perform the following experiments:

(1) To generate *C16orf72*Δ clones in additional cell lines in order to determine whether the phenotypes observed in this thesis are general to all human cell lines.

(2) To perform isolation of proteins on nascent DNA (iPOND) and In situ detection of proteins at replication forks (SIRF), in order to determine whether C16orf72 is recruited to replication forks under conditions of exogenous replication stress.

(3) To perform a DNA fibre assay in order to determine whether C16orf72 promotes the restart of stalled replication forks following exposure to replication stress.

Chapter 1. Introduction

1.1 PARPs

1.1.1 Post-translational modifications

Prevalent amongst organisms is their ability to permanently or reversibly alter members of their cellular proteome with a diverse repertoire of post-translational modifications (PTMs). Examples of such PTMs – of which in excess of 300 have been described – are glycosylation, phosphorylation, ubiquitination, methylation and ADP-ribosylation, which are often facilitated by enzymes (Conibear, 2020; Nørregaard Jensen, 2004; Palazzo et al., 2017, 2019; Wang et al., 2014). For example, members of the poly(ADP-ribose) polymerase (PARP) protein family catalyse ADP-ribosylation (Amé et al., 2004; Hottiger et al., 2010). PTMs are important, as they can be orchestrated by a myriad of cellular signalling pathways in cells to enable appropriate and timely responses to environmental fluctuations (Conibear, 2020).

1.1.2 ADP-ribosylation

The donation of one or more groups of nicotinamide adenine dinucleotide (NAD^+)-borne ADP-ribose to a specific biomolecule, such as to a protein, to RNA or to DNA, is referred to as ADP-ribosylation, which was originally identified in 1963 (Chambon et al., 1963; Jankevicius et al., 2016; Nakano et al., 2015; Palazzo et al., 2017, 2019; Talhaoui et al., 2016; Weixler et al., 2022). More specifically, the transfer of a single ADP-ribose (mono(ADP-ribose) (MAR)) group to a target protein is referred to as MARylation, whereas the production of an ADP-ribose chain (poly-ADP ribose (PAR)) on a target protein is referred to as PARylation. PAR chains can be synthesised up to 200 ADP-ribose moieties in length, and these chains can also include branched

structures (Kiehlbauch et al., 1993). ADP-ribosylation orchestrates a plethora of important events within cells, including transcription, senescence and the DNA damage response (DDR) (Palazzo et al., 2017). However, ADP-ribosylation is especially important in regulating the DDR as ADP-ribosylation acts as a principal intracellular sensor for DNA damage (Wei & Yu, 2016). Indeed, ADP-ribosylation is an important contributor to the DDR as the negative charge of this PTM and the negative charge of DNA repel one another, which help to remodel chromatin and therefore increase the localisation of DDR factors to sites of DNA damage (Liu et al., 2017; Poirier et al., 1982). Furthermore, PAR regulates the repair of DNA by facilitating the localisation of chromatin remodellers such as Amplified in liver cancer 1 (ALC1) to DNA damage (Ahel et al., 2009). In mammalian cells, ADP-ribosylation is catalysed by a group of enzymes, often referred to as PARPs (Amé et al., 2004; Hottiger et al., 2010). The most frequently ADP-ribosylated amino acids by PARPs are glutamate, aspartate and serine. With ADP-ribose, glutamate/aspartate and serine form ester bonds and *O*-glycosidic bonds, respectively (Bartlett et al., 2018; Crawford et al., 2018; Leidecker et al., 2016; Sharifi et al., 2013; Tao et al., 2009; Zhang et al., 2013). Importantly, ADP-ribosylation of histones and other proteins principally occurs on serine residues following accumulation of DNA damage (Hendriks et al., 2019; Larsen et al., 2018; Palazzo et al., 2018).

1.1.3 An Overview of the PARP Family

Six decades ago, the first constituent of the PARP family was discovered – PARP1 (Chambon et al., 1963). Since then, in humans, the PARP family (or the diptheria-toxin-like ADP-ribosyltransferases (ARTDs)) has been expanded to 17 members (Figure 1.1). All of these PARPs possess an ADP-ribosyltransferase (ART) fold within

their catalytic domain – a shared characteristic which led to their discovery (Hottiger et al., 2010). The PARPs can be further divided into subfamilies according to the mutual possession of additional domains (Barkauskaite et al., 2015).

PARP1, PARP2 and PARP3 form the DNA-dependent PARP subfamily. The catalytic activity of these PARPs are stimulated through the binding of these proteins with DNA – an interaction which is mediated by a tryptophan-glycine-arginine (WGR) domain which is present in each of these proteins (Langelier et al., 2012, 2014). PARP1 has a plethora of cellular functions and is capable of PAR synthesis (Vyas & Chang, 2014). For example, it regulates the repair of DNA damage, transcription, differentiation, and mitosis (Butler & Ordahl, 1999; Das et al., 2014; El-Khamisy et al., 2003; Gao et al., 2009; Kanai et al., 2003; Krishnakumar et al., 2008; Krishnakumar & Kraus, 2010; Quénet et al., 2008; Satoh & Lindahl, 1992). Other domains within PARP1, but not PARP2 or PARP3 include the zinc finger and breast cancer susceptibility protein-1 C terminus (BRCT) domains, which facilitate the binding of PARP1 to DNA (Ikejima et al., 1990; Ménissier-de Murcia et al., 1989; Rudolph et al., 2021). PARP2 is capable of PAR synthesis and regulates numerous cellular processes, including telomere integrity, metabolism, and mitosis (Bai et al., 2011; Dantzer et al., 2004; Saxena et al., 2002; Vyas et al., 2014). PARP3 is capable of MAR synthesis, and PARP2 and PARP3 perform functions in the DDR (Amé et al., 1999; Langelier et al., 2014; Ronson et al., 2018; Rulten et al., 2011; Vyas et al., 2014).

PARP9, PARP14 and PARP15 form the Macro PARP subfamily, which are so-called because they all possess macrodomains that have the ability to associate with PAR polymers (Aguiar et al., 2005; Karras et al., 2005). PARP9 regulates the repair of DSBs

and the inflammatory response (Iwata et al., 2016; Yan et al., 2013; Yang et al., 2017). Originally, PARP9 was shown to form a complex with the E3 ubiquitin ligase DT3XL, although it was suggested that this PARP was not capable of catalysing MAR or PAR synthesis (Aguiar et al., 2005; Takeyama et al., 2003; Vyas et al., 2014). However, a subsequent study revealed that PARP9-DT3XL complex facilitates c-NHEJ-dependent DSB repair, and PARP9-mediated MARylation activity represses the function of this complex within this DNA repair pathway (Yang et al., 2017). PARP14 is capable of MAR synthesis and regulates numerous cellular operations including the repair of DNA, transcription, inflammatory response and progression through the cell cycle (Dhoonmoon et al., 2022; Iwata et al., 2016; Mehrotra et al., 2011, 2013; Nicolae et al., 2015; O'Connor et al., 2021; Vyas et al., 2014). PARP 15 is capable of MAR synthesis (Vyas et al., 2014). The function of PARP15 is not yet clear, although it has been proposed that this protein may function to suppress gene transcription (Aguiar et al., 2005). Additionally, PARP15, along with PARP10 and PARP11 are capable of MARylating RNA, although it is not yet understood what function this serves (Munnur et al., 2019).

PARP7, PARP12 and PARP13, form the CCCH PARPs, as they all possess an RNA-interacting Zinc finger domain that falls within the CCCH class (Guo et al., 2004). PARP7 is capable of MAR synthesis and antagonises aryl hydrocarbon receptor activity and represses the IFN-I pathway in response to viral infection (MacPherson et al., 2013; Vyas et al., 2014; Yamada et al., 2016). PARP12 is capable of MAR synthesis (Vyas et al., 2014). This PARP accumulates at the Golgi apparatus and is recruited to stress granules within the cytoplasm in response to numerous stress stimuli in a PARP1-dependent manner. The localisation of PARP12 to stress granules

represses mRNA translation when the cell is under stress. Additionally, when cells are infiltrated by viruses, PARP12 modulates the inflammatory response to these pathogens (Anderson & Kedersha, 2008; Catara et al., 2017; Leung et al., 2011; Welsby et al., 2014). Furthermore, PARP12 controls trafficking of proteins from the *trans*-Golgi network to the cell membrane (Grimaldi et al., 2022). PARP13 is the only PARP family member that is not capable of catalysing MAR or PAR synthesis (Vyas et al., 2014). By interacting with the mRNA of genes that control apoptosis and the response to viral infection with its CCCH zinc finger domains, PARP13 facilitates the degradation of these mRNAs, thereby regulating these cellular responses (Guo et al., 2004; Seo et al., 2013; Todorova et al., 2014; Vyas et al., 2014). Additionally, PARP13 is localised to stress granules and is therefore believed to repress mRNA translation under conditions of stress (Leung et al., 2011). Furthermore, PARP13 acts as a molecular scaffold to promote the formation of the heat shock transcription factor 1 (HSF1)-PARP13-PARP1 complex, which modulates the DDR (Fujimoto et al., 2017).

PARP5a and PARP5b form the TRF1-interacting ankyrin-related ADP-ribose polymerase (Tankyrase) subfamily and are also known as Tankyrase 1 and Tankyrase 2, respectively (Smith et al., 1998). Both of these PARPs are capable of PAR synthesis (Vyas et al., 2014). PARP5a and PARP5b possess a sterile-alpha motif (SAM) domain and ankyrin repeats, which facilitate formation of tankyrase polymers and promotes association with protein targets, respectively (De Rycker et al., 2003; De Rycker & Price, 2004; Guettler et al., 2011; Sbodio et al., 2002; Seimiya & Smith, 2002). PARP5a and PARP5b regulate numerous processes within the cell such as telomere elongation, activation of the Wnt pathway, activation of the Hippo pathway, mitosis, the inflammatory response, glucose homeostasis and the repair of DNA damage

(Chang et al., 2005a; Chang et al., 2005b; Guo et al., 2012; Huang et al., 2009; Kim et al., 2012; Liu et al., 2022; Nagy et al., 2016; Smith & de Lange, 2000; Wang et al., 2015; Yang et al., 2017). Finally, PARP4, PARP6, PARP8, PARP10, PARP11 and PARP16 – all of which are capable of MAR synthesis – are not grouped into any PARP subfamilies (Vyas et al., 2014). Vault particles are ribonucleoproteins of unknown function (Kedersha & Rome, 1986). PARP4 co-localises with vault particles, although it is not clear what cellular functions this protein serves (Kickhoefer et al., 1999). PARP6 regulates the development of neurones, mitosis and activation of the Wnt signalling pathway (Huang et al., 2016; Tang et al., 2020; Wang et al., 2018; Vermehren-Schmaedick et al., 2021). The function of PARP8 is not yet clear. However, during interphase and mitosis its presence is confined to the nuclear envelope and the centrosomes, respectively (Vyas et al., 2013). PARP10 performs roles in the DNA replication stress response and associates with proliferating cell nuclear antigen (PCNA) (Schleicher et al., 2018). PARP11 regulates the generation of spermatids and the response to viral infection (Guo et al., 2019; Meyer-Ficca et al., 2015). PARP16 functions within the unfolded protein response (UPR) and possesses a tail-anchor domain that localises this PARP to the endoplasmic reticulum (ER). Under conditions of stress within the ER, PARP16 stimulates the kinase activity of inositol requiring enzyme 1α (IRE1α) and PKR-like ER kinase (PERK), thereby activating the UPR (Cox et al., 1993; Harding et al., 1999; Jwa & Chang, 2012, 2012; Wattenberg & Lithgow, 2001). Therefore, PARPs have varied roles in all aspects of cell biology.

At the organismal level, the potential redundant functions of PARP1 and PARP2 during embryogenesis are indicated by the inability of mouse embryos that lack both PARP1

and PARP2 to remain viable (Ménissier de Murcia et al., 2003). Similarly, PARP5a and PARP5b perform redundant roles during embryogenesis. Indeed, loss of either PARP5a or PARP5b does not affect the survival of mouse embryos, while mouse embryos lacking both PARPs fail to survive (Chiang et al., 2008). Thus, PARPs perform important roles in regulating the development of organisms.

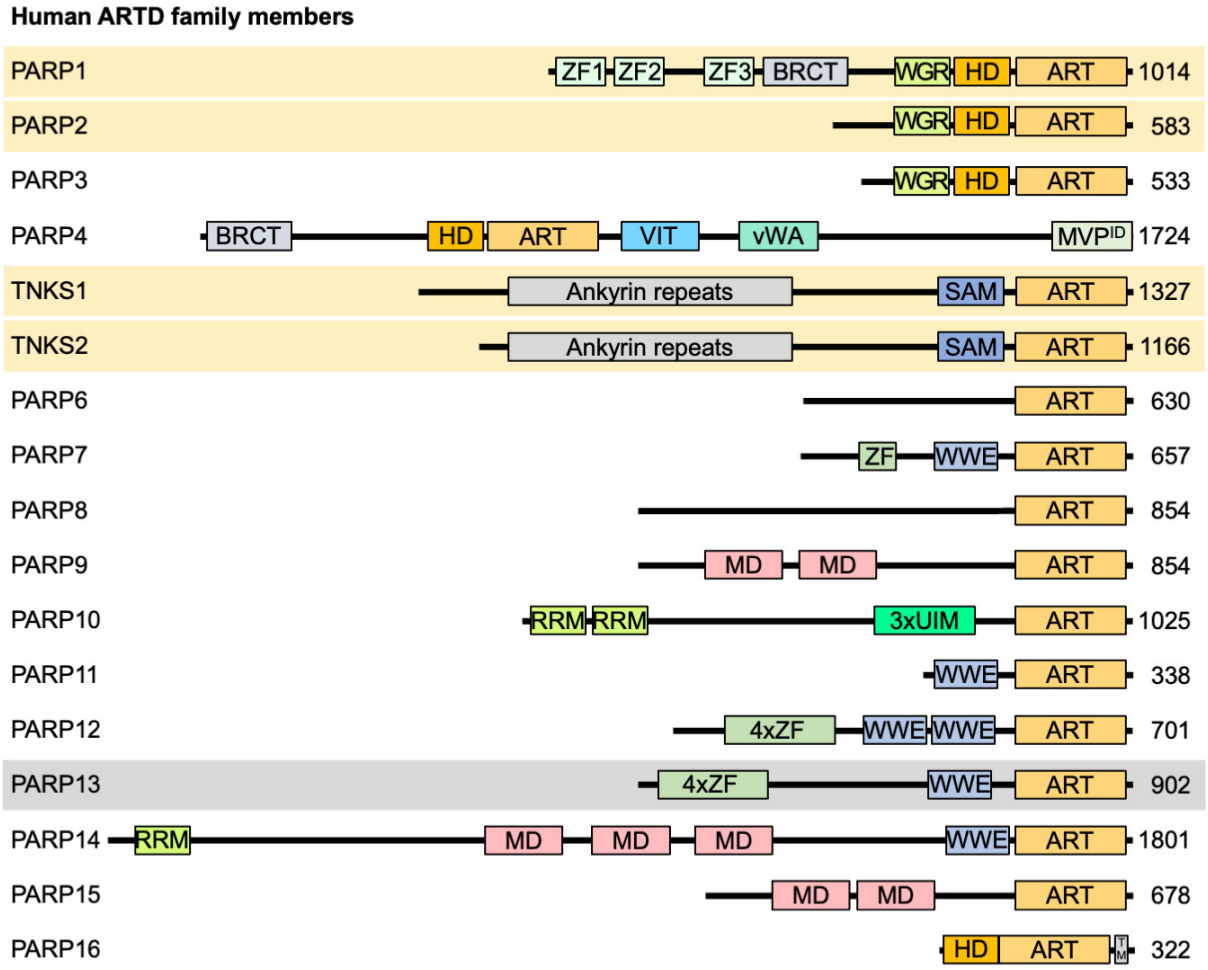


Figure 1.1: Arrangement of domains within proteins of the PARP family. The ART domain/subdomain binds to NAD^+ and catalyses ADP-ribosylation. The helical subdomain (HD) controls catalysis. The WGR domain, BRCT domain and ZF domains can bind to DNA. The functions of the major vault protein interaction domain (MVP^{ID}); the von Willebrand type A (vWA) domain; and the vault protein inter-α-trypsin (VIT)

domain are not clear. The SAM domain promotes the assembly of protein homomultimers. The ankyrin repeats promote the association between different proteins. The tryptophan-tryptophan-glutamate (WWE) domain can facilitate interactions with other proteins and regulate the stability of proteins. The macrodomain (MD) facilitates binding to other proteins and can catalyse the removal of ADPr from proteins. The ubiquitin-interacting motif (UIM) domain facilitates association with PCNA. The function of the RNA recognition motif (RRM) domain in PARPs is not clear. The transmembrane (TM) domain facilitates recruitment to the membrane of the ER. PARP1, PARP2, PARP5a (TNKS1) and PARP5b (TNKS2) can catalyse PAR synthesis (indicated in orange). PARP13 cannot catalyse MAR or PAR synthesis (indicated in grey). The remaining PARPs are capable of MAR synthesis (indicated in white). Adapted from Lüscher et al., 2022 and produced with BioRender.

1.1.4 PARP catalysis

The PARPs found in humans can be divided into three groups depending on the motif found within their catalytic domain (Lüscher et al., 2022): PARPs that possess the histidine-tyrosine-glutamate motif; PARPs in which the glutamate residue of the histidine-tyrosine-glutamate motif is exchanged with an isoleucine, leucine or tyrosine residue; and PARPs in which only the central tyrosine residue of the motif is present. The first group consists of PARP1, PARP2, PARP3, PARP4, PARP5a and PARP5b. The second group consists of PARPs that possess a histidine-tyrosine-isoleucine motif (PARP6, PARP7, PARP8, PARP10, PARP11 and PARP12) and PARPs that possess a histidine-tyrosine-leucine motif (PARP14 and PARP15). The third group consist of PARP9 which possesses a glutamine-tyrosine-threonine motif; PARP13 which possesses a tyrosine-tyrosine-valine motif; and PARP16 which possesses a

histidine-tyrosine-tyrosine motif (Kleine et al., 2008; Otto et al., 2005). PARP13 is catalytically inactive as its active site is impeded by its D-loop which averts NAD^+ binding (Karlberg et al., 2015).

A shared characteristic between the PARylating PARPs (PARP1, PARP2, PARP5a and PARP5b) is that they all possess a histidine-tyrosine-glutamate motif within their catalytic domain. It was initially proposed that the glutamate residue within this motif is vital for lengthening PAR polymers. This glutamate (Glu988 in PARP1) induces the polarisation of the NAD^+ donor and the PAR nucleophile acceptor by establishing hydrogen bonds with both substrates, which is believed to facilitate a S_N2 reaction in which the donor undergoes nucleophilic attack by the acceptor (Marsischky et al., 1995; Ruf et al., 1998). Interestingly, this residue is also believed to contribute to the formation of branched PAR structures (Rolli et al., 1997). A recent study revealed that following association of its N-terminus with PAR, PARP2 catalyses synthesis of branched PAR structures (Chen et al., 2018). Ruf et al. 1998 suggest that PAR branch formation is catalysed when the NAD^+ donor is turned 180 degrees with respect to the orientation of the donor that is required for PAR elongation.

Given that glutamate and aspartate residues have nucleophilic properties, it has been proposed that the catalytic glutamate residue in the histidine-tyrosine-glutamate motif is inessential for catalysing the addition of MAR on target proteins. In support of this notion is the observation that PARP6-PARP16 (which lack this glutamate residue) are not able to catalyse PAR synthesis, whereas PARP1, PARP2, PARP5a and PARP5b (which possess the glutamate residue) are capable of this activity. Yet, this notion has been challenged by the observation that the PARP3 and PARP4 – both of which are

MARylating PARPs – contain the histidine-tyrosine-glutamate motif, which suggests that there may be other key factors that determine whether a PARP is capable of MAR of PAR synthesis, such as the NAD^+ binding affinity and flexibility of the donor loop (Vyas et al., 2014).

1.1.5 Mechanism of PARP1, PARP2 and PARP3 activation

It has been proposed that in its inactive state, the numerous PARP1 domains are joined via flexible linkers, but do not interact with one another, in a manner akin to pearls on a necklace (Eustermann et al., 2015). Following interactions of the ZF1 and ZF2 zinc finger (ZF) domains of PARP1 to DNA damage, the various PARP1 domains fold together (Eustermann et al., 2011, 2015). This conformational change removes the helical subdomain (HD) from the active site of the ART subdomain, thus permitting PARP1-dependent PAR catalysis (Dawicki-McKenna et al., 2015). Similarly, activation of PARP2 and PARP3 also involves the removal of the HD domain from the ART catalytic site following binding of these PARPs to DNA. Yet, while the association with DNA and the DNA-mediated activation of PARP1 requires its N-terminal regulatory domains and C-terminal WGR domain, only the WGR domain is necessary for DNA-binding and activation of PARP2 and PARP3 (Langelier et al., 2014).

Additional factors associate with PARPs to fine-tune their catalytic activity. For example, histone PARylation factor 1 (HPF1) enables PARP1 and PARP2 to modify themselves and other proteins such as histones at serine residues, which is especially important for regulating the DDR (Bonfiglio et al., 2017; Gibbs-Seymour et al., 2016; Leidecker et al., 2016; Palazzo et al., 2018). Through interactions with PARP1/2, HPF1 facilitates PARP1/2-dependent serine ADP-ribosylation in a number of ways.

Firstly, it forms an essential part of the PARP1/2 active site and performs conformational changes to the active site that are required for this reaction (Sun et al., 2021; Suskiewicz et al., 2020). Secondly, it contains an amino acid motif that is believed to strengthen the interaction between PARP2 and histones (Suskiewicz et al., 2020). Thirdly, HPF1 forms transient associations with PARP1/2 and is exchanged between multiple PARP1/2 molecules. Given that HPF1 obstructs the acceptor site, this transient association with PARP1/2 is necessary to promote serine ADP-ribosylation without repressing PAR elongation (Langelier et al., 2021). Recently, coactivator associated arginine methyltransferase 1 (CARM1) and spindlin interactor and repressor of chromatin binding (SPINDOC) have also been revealed as PARP1-interacting proteins that stimulate PARP1 PARylation activity, although the functions of these accessory proteins are not well understood (Genois et al., 2021; Yang et al., 2021).

1.1.6 Removal of ADP-ribosylation

While DNA damage induces high levels of ADP-ribosylation, these modifications undergo reversal over time (Alvarez-Gonzalez & Althaus, 1989). In humans, bonds between ADP-ribose (ADPr) moieties and other molecules can be hydrolysed by five key proteins: TARG1, Poly(ADP-ribose) glycohydrolase (PARG), MACROD1, MACROD2 and ARH3. TARG1, PARG, MACROD1 and MACROD2 all possess macrodomains and are therefore members of the macrodomain protein family. In contrast, ARH3 is a member of the (ADP-ribosyl)hydrolase protein family. While numerous proteins contain macrodomains that are capable of mediating association with ADPr, the macrodomains within the above proteins also possess hydrolytic

activity (Barkauskaite et al., 2013; Jankevicius et al., 2013; Karras et al., 2005; Oka et al., 2006; Rosenthal et al., 2013; Sharifi et al., 2013; Slade et al., 2011).

PARG removes PAR chains by hydrolysing ADPr-ADPr bonds, although it is not capable of removing the final ADPr from PAR-modified proteins, thereby transforming PARylated proteins to MARylated proteins. Structural studies have demonstrated that PARG-mediated hydrolysis is facilitated by numerous amino acids within the macrodomain including Glu756 (Dunstan et al., 2012; Fontana et al., 2017; Slade et al., 2011; Tucker et al., 2012). In contrast, TARG1, MACROD1, MACROD2, and ARH3 are capable of removing ADPr from MARylated proteins by hydrolysing the bond between ADPr and an amino acid. Additionally, these proteins are capable of eliminating the final ADPr from PARG-processed proteins. MACROD1/2 -dependent hydrolysis is facilitated by a glycine and an asparagine residue within the macrodomain of these proteins (Jankevicius et al., 2013; Rosenthal et al., 2013; Sharifi et al., 2013). ARH3 has a specificity for removing ADPr from proteins that are MARylated at serine residues, and therefore performs an important role in regulating the DDR (Abplanalp et al., 2017; Palazzo et al., 2018). This protein also possesses slight ADPr-ADPr hydrolysis activity. Given that PARG is inefficient in hydrolysing shorter PAR chains, it is believed that this ARH3-dependent ADPr-ADPr hydrolysis assists PARG in reducing the length of these short chains (Hatakeyama et al., 1986; Mueller-Dieckmann et al., 2006). However, there are PAR branch structures that are only amenable to hydrolysis by PARG and not ARH3 (Rack et al., 2021). Structural studies have determined that the ARH3 active site possesses a pair of Mg^{2+} ions as well as a glutamate residue that facilitate catalysis. The Mg^{2+} ions assist in the binding

of MAR/PAR. Subsequently, the Mg^{2+} ions and the glutamate residue collaborate to catalyse the hydrolysis reaction (Mueller-Dieckmann et al., 2006; Rack et al., 2021).

PARG loss is lethal to mouse embryos during development and loss of this protein further sensitises cells to DNA damage. Additionally, ARH3 dysfunction prevents chromatin from returning to its non-damaged condition following the repair of DNA damage. Therefore, these findings underscore the importance of ADP-ribosylation removal in regulating embryogenesis and the DDR (Hanzlikova et al., 2020; Koh et al., 2004).

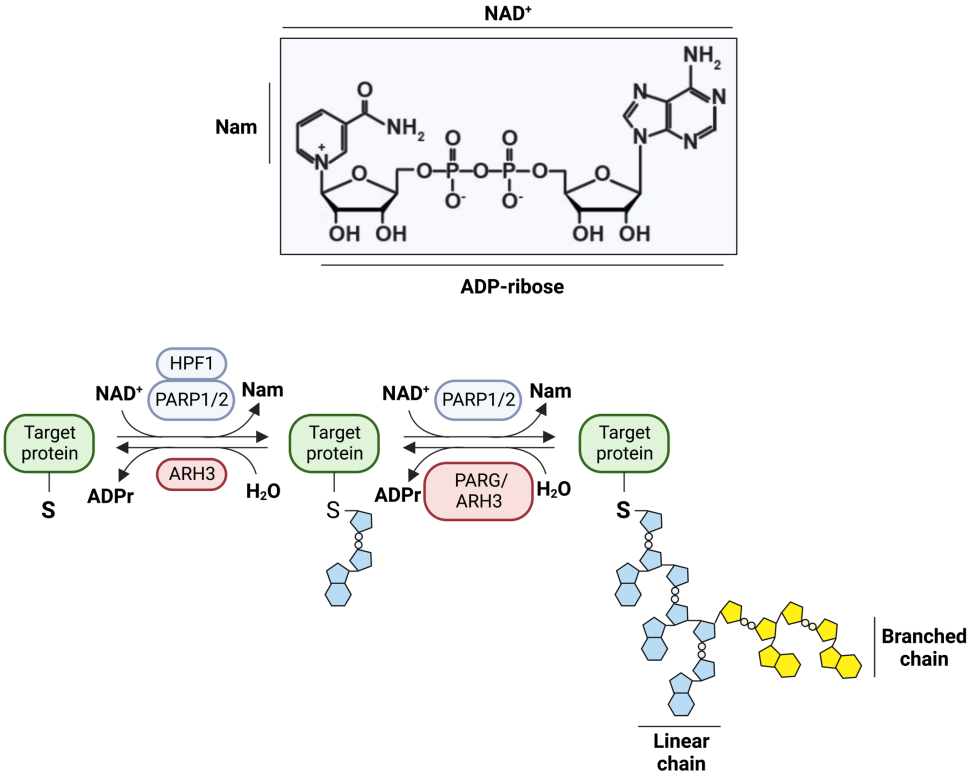


Figure 1.2: Mechanism of addition and removal of serine ADP-ribosylation. In response to DNA damage, serine residues (indicated with S) are ADP-ribosylated on target proteins such as histones. The PARP1/2-HPF1 complex utilises NAD^+ as a substrate to initiate the ADP-ribosylation reaction, producing a nicotinamide (Nam) by-

product. Subsequently, HPF1 dissociates from PARP1/2, which enables the PARP1/2-dependent synthesis of linear and branched chains of PAR. The ADP-ribosylation of proteins is a reversible process. The removal of individual ADPr from linear and branched PAR structures can be mediated by PARG or ARH3, which hydrolyse ADPr-ADPr bonds in these structures. The removal of the last ADPr from target proteins can only be mediated by ARH3, which hydrolyses ADPr-serine bonds. Adapted from Schützenhofer et al., 2021 and produced with BioRender.

1.2 The involvement of PARPs in the DNA damage response

DNA within the human cell is frequently subjected to damage that is exogenous and endogenous in origin. DNA damage can manifest in a plethora of forms such as DNA single-strand breaks (SSBs), double-strand breaks (DSBs), intrastrand crosslinks (ICLs), interstrand crosslinks, base mismatches, mis-incorporated ribonucleotides and bases that are oxidised, methylated or deaminated (Chatterjee & Walker, 2017; Sassa et al., 2019). Failure to repair such damage can result in genomic instability and consequently, senescence, programmed cell death, or carcinogenesis (Pilié et al., 2019). In order to mitigate the potentially deleterious consequences of DNA damage, cells have evolved a myriad of mechanisms, which are capable of managing such damage. Examples of these pathways include base excision repair (BER), nucleotide excision repair (NER), ribonucleotide excision repair (RER), mismatch repair (MMR), double-strand break repair (DSBR), intertrand crosslink repair and the DNA replication stress response (Chatterjee & Walker, 2017; Sassa et al., 2019). An important contributor to many of these repair mechanisms are members of the PARP protein

family. Therefore, DNA repair pathways that are pertinent to this thesis, as well as the involvement of PARPs within such pathways will be reviewed below.

1.3 Mechanisms of repairing base lesions and single-strand breaks

1.3.1 Causes of DNA SSBs

A disruption in the structure of an individual strand of DNA is known as a single-strand break (SSB), which often manifests as a single nucleotide gap flanked by 5' and 3' break ends that are aberrant in structure (Caldecott, 2008). SSBs are the most frequently observed type of DNA damage observed in mammalian cells, as this category of DNA damage represents three-quarters of all DNA damage within these cells (Tubbs & Nussenzweig, 2017). DNA topoisomerase I (TOP1) is an enzyme that facilitates replication and transcription of DNA by momentarily forming a TOP1-DNA cleavage complex and generating temporary DNA nicks in order to alleviate tension within the double helix. Yet, in instances where a TOP1-DNA cleavage complex is contiguous with certain types of DNA damage or the TOP1-DNA cleavage complex obstructs a DNA/RNA polymerase, a SSB can be generated that possesses a 3' break end that is bound covalently by TOP1 (Pommier et al., 2003; Wang, 2002). In addition, BER-mediated processing of DNA damage such as abasic sites or deaminated (e.g. xanthine), alkylated (e.g. 3-methylguanine) and oxidised DNA bases (e.g. formamidopyrimidine), can give rise to SSBs (Demple & DeMott, 2002; Hegde et al., 2008). An example of an exogenous source of alkylation base damage is methyl methanesulfonate (MMS) (O'Connor, 1981). Furthermore, SSBs can be generated by reactive oxygen species (ROS) that oxidise the DNA sugar-phosphate backbone.

Sources of ROS include cellular metabolism and ionising radiation (Pogozelski & Tullius, 1998). Given that there are multiple causes of SSBs, there is a need for DNA repair pathways to repair them.

1.3.2 BER and SSBR

Damage to DNA bases that do not cause substantial distortion of the DNA double helix, such as those described above, is repaired by the BER pathway (Figure 1.3) (Krokan & Bjørås, 2013). Firstly, the base damage is detected by a DNA glycosylase, of which 11 have been characterised to date (Jacobs & Schär, 2012; Krokan & Bjørås, 2013). While each DNA glycosylase is capable of detecting a different assortment of DNA base lesions, some DNA glycosylases share some selectivity for their targets (Krokan & Bjørås, 2013). DNA glycosylases broadly fit into two categories: monofunctional DNA glycosylases and bifunctional DNA glycosylases (Svilar et al., 2011). Examples of monofunctional and bifunctional DNA glycosylates are 3-methylpurine glycosylase (MPG) and 8-OxoG DNA glycosylase 1 (OGG1), respectively (Jacobs & Schär, 2012). MPG removes a variety of base alkylation damage such as 3-methylguanine and N7-methylguanine (O'Connor, 1993). OGG1 eliminates 7,8-dihydro-8-oxoguanine (8-oxoG), which forms as a consequence of oxidative damage to DNA (Radicella et al., 1997).

Following recognition of a base lesion, a monofunctional DNA glycosylase generates an abasic (also referred to as apurinic/apyrimidic (AP)) site by severing the *N*-glycosidic bond between the DNA sugar-phosphate backbone and the damaged base (Dianov & Hübscher, 2013). Subsequently, a SSB containing a 5' deoxyribose phosphate (5'-dRP) group and a 3'-hydroxyl group is generated through the action of

AP endonuclease 1 (APE1), which incises the DNA sugar phosphate backbone at a 5' position relative to where the AP site is situated (Demple et al., 1991; Levin & Demple, 1990). In contrast to monofunctional DNA glycosylases, following recognition of a base lesion, a bifunctional DNA glycosylase generates an AP site by cleaving the *N*-glycosidic-DNA sugar phosphate linkage via a mechanism that is similar, but not identical to monofunctional glycosylases. Subsequently, the same bifunctional DNA glycosylase makes an incision that is 3' to the AP site, generating a SSB that has a 3' break end containing a phosphate group or an αβ unsaturated aldehyde group (Caldecott, 2020; Jacobs & Schär, 2012). Consequently, SSBs containing a 3'-phosphate group are converted by polynucleotide kinase 3'-phosphatase (PNKP) to SSBs containing 3'-hydroxyl groups, whereas SSBs containing a 3'- αβ unsaturated aldehyde group are converted to the same end-product by APE1 (Caldecott, 2020; Wiederhold et al., 2004). Regardless of whether base lesions are excised by monofunctional or bifunctional DNA glycosylases, the BER pathway intersects with the single-strand break repair (SSBR) pathway at the end-processing stage (Hegde et al., 2012).

Following identification of a SSB, PARP1 binds to the lesion and ADP-ribosylates itself and other proteins surrounding the lesion (Ogata et al., 1981; Satoh & Lindahl 1992). Through its BRCT1 domain, X-ray repair cross complementing protein 1 (XRCC1) binds to the ADP-ribosylated proteins and to DNA, localising this protein to the SSB (Breslin et al., 2015; Li et al., 2013; Polo et al., 2019). XRCC1 acts as a platform for the recruitment of other repair factors that promote the resolution of SSBs, such as PNKP, Aprataxin, (APTX), DNA polymerase β (Polβ) and DNA ligase IIIα (LIGIIIα) (Caldecott et al., 1994, 1996; Clements et al., 2004; Loizou et al., 2004). Recently, it

was revealed that XRCC1 also functions to repress prolonged PARP1 binding to DNA which, if dysregulated, precludes access of repair factors to the SSB intermediates (Demin et al., 2021). Next, if necessary, the SSB break ends undergoes processing, as described previously.

Following appropriate processing of the SSB termini, the lesion can be channelled down one of two SSBR branches (Figure 1.3): short-patch and long-patch repair (Frosina et al., 1996). During short-patch repair, Polβ fills the one-nucleotide-wide SSB intermediate, and if present, Polβ removes a dRP group from the 5' terminus of an APE1-processed SSB intermediate. Finally, the SSB intermediate is ligated by the XRCC1-LIGIIIα complex. (Bennett et al., 1997; Caldecott et al., 1996; Matsumoto & Kim, 1995). If required, in order to avert abortive DNA ligation by LIGIIIα, APTX eliminates 5'AMP groups from SSB intermediates (Ahel et al., 2006; Reynolds et al., 2009). During long-patch repair, Polβ not only fills the gap of the SSB intermediate, but also synthesises up to 11 nucleotides past the lesion, which displaces the original 3' break terminus in the process and generates a DNA flap that is single-stranded. DNA polymerase δ has also been implicated in this process (Abbotts & Wilson, 2017; Klungland & Lindahl, 1997). Consequently, the DNA flap is incised by flap-endonuclease 1 (FEN1) and the break is ligated by DNA ligase I (LIGI) (Klungland & Lindahl, 1997; Levin et al., 2000). It is thought that LIGI recruitment is mediated through its interaction with proliferating cell nuclear antigen (PCNA) (Levin et al., 2000). It is important to note that functional redundancy exists between LIGI and LIGIIIα (Gao et al., 2011). Long-patch repair is utilised at SSB intermediates that possess oxidised abasic lesions with termini that are not compatible with Polβ-dependent lyase activity (DeMott et al., 2002).

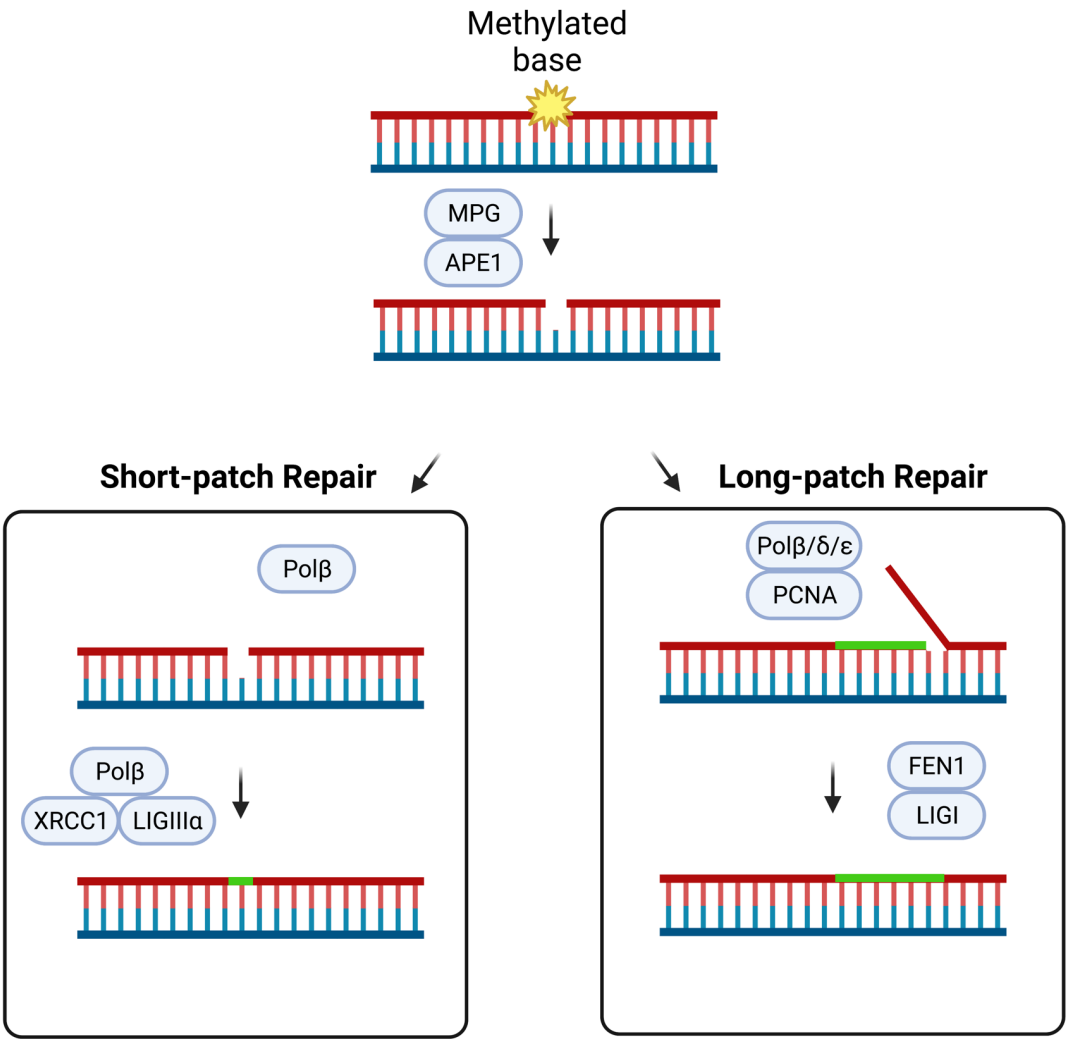


Figure 1.3: Summary of BER. Upon detection of a methylated base, MPG (a mono-functional DNA glycosylase) produces an AP site by excising the damaged base. The AP site is processed by APE1, producing an SSB which can be repaired via the short-patch or long-patch sub-pathway. In short-patch repair, the 5'-dRP terminus of the SSB is excised by the lyase function of Polβ. Subsequently, the single-nucleotide gap is filled by Polβ and ligation of the nick is mediated by XRCC1 and LIGIIIα. In long-patch repair, PCNA facilitates gap filling by DNA polymerases, which dislodge the 5' terminus of the break, thereby generating a ssDNA flap, which is cleaved by FEN1. Subsequently, ligation of the nick is mediated by LIGI. Adapted from Caldecott, 2022 and produced with BioRender.

1.3.3 The participation of PARPs in BER and SSBR

There is a variety of evidence that are supportive of the notion that PARPs participate in BER and SSBR. For example, through an interaction mediated by its BRCT domain, XRCC1 is localised to SSBs by binding to PAR-decorated PARP1 (Masson et al., 1998; El-Khamisy et al., 2003). Yet, whether PARP1 is an integral factor in BER and SSBR is a matter of controversy. For example, while one study suggested PARP1 may expedite the strand ligation step in BER, another study came to the opposite conclusion (Ström et al., 2010; Fisher et al., 2007). Additionally, on the one hand, the importance of PARP1 function in BER and SSBR is demonstrated in PARP1 deficient cells, which are sensitised to base damage and SSBs (Fisher et al., 2007; Ronson et al., 2018). In contrast, *in vitro* studies have suggested that BER and SSBR can be performed efficiently in the absence of PARP1 (Pascucci et al., 2002; Klungland et al., 1997).

The importance of PARP2 function in BER and SSBR is also not clear. While loss of PARP2 reduced the kinetics of strand ligation in mouse cells, loss of PARP2 in human cells did not reduce strand ligation kinetics (Fisher et al., 2007; Schreiber 2002). However, in a recent study, PARP1 and PARP2 were shown to perform redundant functions in BER in response to alkylation base damage. Indeed, as demonstrated by alkaline comet assay, in cells exposed to alkylation base damage, individual loss of PARP1 or PARP2 did not result in a substantial increase in the accumulation of SSBs, whereas a marked increase in the accumulation this type of lesion was observed in cells lacking both PARP1 and PARP2 (Ronson et al., 2018). Consistent with a redundant role for PARP1 and PARP2 in SSBR, another recent study demonstrated that PARP1 and PARP2 are each independently able to recruit XRCC1 and PNKP to

SSBs induced by oxidative damage (Hanzlikova et al., 2017). Yet, given that PARP2 localises to laser-induced DNA lesions consequent to the localisation of PARP1 to these lesions, it has been proposed that PARP2 may perform PARP1-independent roles in the DDR and perhaps in BER/SSBR (Mortusewicz et al., 2007). It remains to be determined if PARP2 has separate functions to PARP1 in BER and SSBR.

PARP3 has also been implicated in SSBR. Indeed, loss of PARP3 in chicken cells reduces repair kinetics of ionizing radiation-induced DNA damage, which can consist of SSBs. Furthermore, PARP3 is activated by DNA nicks that possess a terminus containing a 5' phosphate, and consequently MARylates histones within nucleosomes at these sites of damage (Grundy et al., 2016; Langelier 2014). Additionally, an *in vitro* study demonstrated that human PARP3 can directly MARylate DNA at DNA nicks that possess a 5' phosphate, which is proposed to act as an initiator for PARP1/2-dependent PARylation at these sites. Therefore, while it is conceivable that PARP3 functions in the SSBR, its role within this pathway remains to be confirmed in human cell lines (Belousova et al., 2018).

1.4 Mechanisms of DNA double-strand break repair

Mammalian cells have evolved numerous mechanisms for the repair of DNA DSBs, such as classical non-homologous end joining (c-NHEJ), alternative non-homologous end joining (alt-NHEJ) and homologous recombination (HR). These repair mechanisms will be described below.

1.4.1 Causes of DNA DSBs

Lesions in which both DNA strands are disrupted are known as double-strand breaks (DSBs), which are thought to be highly cytotoxic (Chapman et al., 2012; Jackson, 2002). There are numerous causes for the intentional generation of DSBs. For example, DSBs are produced during meiosis I, in order to facilitate meiotic recombination; during V(D)J recombination, which facilitates the construction of a diverse range of B- and T- cell receptors genes; and during isotypic commutation (de Massy, 2013; Soulas-Sprauel et al., 2007). DSBs can also be formed unintentionally by numerous sources. For example, ionising radiation can induce a pair of SSBs that occur near one another on opposite DNA strands, which can result in the conversion of these lesions into a DSB (Cannan & Pederson, 2016). The radiomimetic bleomycin can also induce DSBs (Povirk, 1996). Protracted exposure of cells to hydroxyurea (HU) – which blocks ribonuclease reductase activity – stalls replication forks by draining the cellular stores of dNTPs, which can subsequently collapse into DSBs (Bianchi et al., 1986; Petermann et al., 2010; Toledo et al., 2017; Toledo et al., 2013). In the event that a replication fork meets a SSB within the leading or lagging strand, the SSB can be converted into a DSB (Kuzminov, 2001; Ensminger et al., 2014; Vrtis et al., 2021). During DNA replication, manipulations to the DNA structure, such as DNA relaxation or segregation of linked DNA is facilitated by topoisomerase II (TOP2) by inducing transient DSBs that are subsequently repaired once the required spatial manipulation to the DNA is complete (Nitiss, 2009). The TOP2 poison etoposide prevents the repair of TOP2-induced DSBs by causing permanent association of TOP2 to the unrepaired DSBs (Nitiss, 2009).

1.4.2 Homologous recombination

The repair of DSBs by homologous recombination (HR) is constrained to the S/G_2 and mitotic cell cycle phases, as opposed to c-NHEJ which functions throughout all cell cycle phases apart from during mitosis (Takata et al., 1998; Orthwein et al., 2014) (Figure 1.4). This is due to the requirement for the presence of a sister chromatid which acts as a template. An important responder to DSBs is Ataxia telangiectasia mutated (ATM) – a member of the PIKK protein family – which also oversees numerous other cellular responses such as activation of the cell cycle checkpoints (Savitsky et al., 1995; Shiloh & Ziv, 2013). It has been proposed that in unperturbed cells, ATM exists as an inactive dimer, whereas following accumulation of DSBs, ATM dimers detach to form active ATM monomers – a process which may be facilitated by the MRN complex (Bakkenist & Kastan, 2003; Lee & Paull, 2004, 2005; Uziel et al., 2003). However, a subsequent study challenged this model and suggested that in response to damage, monomeric, inactive ATM can be activated following changes to its conformation (Baretić et al., 2017). Activated ATM influences the response to DNA damage by phosphorylating a plethora of protein targets at their serine/threonine-glutamine S/T-Q motifs (Bensimon et al., 2010; Matsuoka et al., 2007; Kim et al., 1999). One such example is the ATM-dependent phosphorylation of H2A histone family member X (H2AX) at its serine 139 residue (γH2AX) at DSB loci (Burma et al., 2001; Rogakou et al., 1998). Mediator of DNA damage checkpoint protein 1 (MDC1) associates with these modified histones at these lesions. The MDC1-γH2AX interaction at DSBs is strengthened by ATM-dependent phosphorylation of MDC1, which induces the formation of MDC1 dimers (Jungmichel et al., 2012; Liu et al., 2012; Stucki et al., 2005). Subsequently, MDC1 is phosphorylated by casein kinase (CK2), which enables interactions between NBS1 and MDC1, augmenting the localisation of

the MRN complex to γH2AX-decorated loci (Chapman & Jackson, 2008; Melander et al., 2008; Spycher et al., 2008). It has been proposed that the MDC1-dependent localisation of the MRN complex to DSBs forms a positive feedback loop in which more ATM is localised to these lesions, which further increases γH2AX levels and consequently increases the spread of additional MDC1, MRN and ATM proteins on chromatin flanking the DSBs. In turn, this feedback loop may magnify the signalling of these lesions (Blackford & Jackson, 2017).

Homologous recombination is initiated by resection of the DSB termini to form 3' overhangs. Through its endonuclease activity, the MRN complex makes an incision within each 5' strand. Subsequently, through its exonuclease activity, the MRN complex engages in the short-range resection of the 5' strands in the direction approaching the break until 3' overhangs are formed (Shibata, 2017). It is generally believed that the initial incision and subsequent short-range resection of the break is mediated by MRE11, although RAD50 and CtIP stimulate these MRN-dependent functions (Anand et al., 2016). An additional nuclease, EXD2, as well as the BRCA1-BARD1 complex have also been implicated in this stage. (Broderick et al., 2016; Chen et al., 2008; Zhong et al., 1999). In order to facilitate this MRN-dependent resection, CtIP is phosphorylated at its Thr847 residue via cyclin-dependent kinase (CDK)-mediated catalysis (Huertas & Jackson, 2009). This CDK-regulated initiation of resection is integral to restrict HR to S/G_2 cell cycle phases, in which a homologous template is present (Scully et al., 2019). While it has been suggested that CtIP is a nuclease, it is yet to be determined whether CtIP-dependent catalysis contributes to the resection stage (Makharashvili et al., 2014; Wang et al., 2014). Rather, it has been proposed that when necessary, CtIP eliminates DNA-protein adducts at break termini

(Anand et al., 2016; Deshpande et al., 2016). Subsequently, in a DNA2- and EXO1-dependent manner, the 5' strands undergo long-range resection to produce extended 3' overhangs (Nimonkar et al., 2008, 2011; Zhu et al., 2008). The localisation of these long-range resection factors is facilitated by the MRN complex (Nimonkar et al., 2011). Subsequently, the ssDNA at the extended 3' overhangs is shielded by RPA, which prevents the 3' overhangs from undergoing DNA2-dependent attack; promotes DNA2-dependent attack of the 5' DNA at the overhangs; and represses ssDNA annealing within the overhang, thereby averting DNA secondary structure formation (Cejka et al., 2010; Niu et al., 2010; Wold, 1997). Next, the RPA that is associated with the 3' overhangs is exchanged with RAD51 to generate a nucleoprotein filament. The replacement of RPA with RAD51 and its subsequent assembly into a nucleoprotein filament is facilitated by BRCA2 via interactions of the BRCA2 BRC domains with RAD51 (Carreira et al., 2009; Jensen et al., 2010; Yuan et al., 1999). Additionally, RAD54 and the BRCA1-BARD1 complex are also believed to contribute to this process (Sy et al., 2009; Wolner & Peterson, 2005). The localisation of BRCA1 and BRCA2 to the DSB is facilitated by Partner and Localiser of BRCA2 (PALB2) (Sy et al., 2009). BRCA2-PALB2 binding is facilitated through interactions of the coiled-coil domains within each of these proteins (Sy et al., 2009). However, the precise mechanism by which BRCA1, PALB2 and RAD54 contribute to the assembly of RAD51 nucleoprotein filaments is yet to be determined. Furthermore, RAD51 paralogues are believed to promote the formation of RAD51 nucleoproteins. RAD51 paralogues can interact to produce the BCDX2 complex (consisting of RAD51B, RAD51C, RAD51D, XRCC2 and XRCC3) and the CX3 complex (consisting of RAD51C and XRCC3). A study revealed that the RAD51B and RAD51C subunits of the BCDX2 complex facilitate the replacement of RPA with RAD51 and the

subsequent formation of RAD51 nucleoprotein filaments (Masson et al., 2001; Sigurdsson et al., 2001). Once formed, the stability of the RAD51 nucleoprotein filaments is promoted by the SWI5-SFR1 complex which, in collaboration with BRCA1-BARD1, assist in subsequent strand invasion (Akamatsu & Jasin, 2010; Tsai et al., 2012; Zhao et al., 2017). In somatic cells, the broken strand usually invades a template strand by forming Watson-Crick interactions with a homologous sequence within a sister chromatid. As the base-pairing is established between the 3' overhang and the template strand, the strand originally bound to the template strand is shifted out of place, forming a D-loop. Within the displaced ssDNA strand of the D-loop, RAD51 is ousted by RAD54, and this strand is protected by RPA (Eggler et al., 2002; Mason et al., 2015; Solinger et al., 2002). Next, typically Polδ and ε conduct DNA synthesis of the annealed 3' strand (Hicks et al., 2010; Li et al., 2009; Maloisel et al., 2008).

At this juncture, HR can proceed via two main routes: synthesis-dependent strand annealing (SDSA) and canonical DSB repair (DSBR) (Ranjha et al., 2018). The SDSA sub-pathway involves the dissociation of the synthesised strand from the DNA template, which is subsequently captured by the other 3' terminus of the resected DSB. Consequently, DNA is synthesised to fill the arising gaps and the DNA phosphodiester backbones undergo ligation, which leads solely to non-crossover events. Therefore, this sub-pathway repairs DSBs in a manner that has an exceedingly low rate of mutation. In contrast, an important feature of the DSBR pathway is the formation of a double Holliday junction (dHJ) (see below). The invaded strand remains annealed to the template strand, while the extruded strand of the D-loop anneals to the other 3' terminus of the DSB. The annealed strand subsequently undergoes DNA synthesis, and the DNA phosphodiester backbone is ligated, thereby forming a dHJ.

Subsequently, dHJs can be processed by two distinct methods: dissolution and resolution. Dissolution dismantles dHJs with the BTR complex, which is comprised of RecQ Mediated Genome Instability 1/2 (RMI1/2), Bloom syndrome (BLM) and topoisomerase IIIα (Singh et al., 2008; Wu & Hickson, 2003). Furthermore, there is evidence to suggest that RPA facilitates dHJ dissolution by associating with RMI1 (Xue et al., 2013). As with SDSA, dHJ dissolution results solely in non-crossover events. In instances in which, dHJ dissolution cannot be performed, dHJ resolution is employed instead. Furthermore, there are scenarios in which single HJs may arise, which must also undergo resolution (Shah Punatar et al., 2017). The SLX1-SLX4 and MUS81-EME1 complexes can resolve dHJs by performing incisions that can be either symmetrical or asymmetrical (Chen et al., 2001; Ciccia et al., 2003; Fekairi et al., 2009; Muñoz et al., 2009; Svendsen et al., 2009; Wyatt et al., 2013). In contrast, GEN1 resolves dHJs by performing dual incisions that are always symmetrical in nature (Ip et al., 2008; Rass et al., 2010). Due to the stochasticity of the nucleases that are employed in dHJ resolution, either non-crossover or crossover events can arise from this process (Shah Punatar et al., 2017).

An alternative HR sub-pathway that cells employ is single strand annealing (SSA). Like the other HR sub-pathways, SSA is also initiated by extended resection of DSB termini followed by RPA protection of the ssDNA overhangs, and this resection is mediated by the same resection machinery as the other RAD51-mediated HR pathways outlined above. However, next, RAD52, as opposed to RAD51, facilitates the formation of Watson-Crick base pairing between homologous sequences that are found within the RPA-protected ssDNA overhangs (Rothenberg et al., 2008). Due to the presence of nonhomologous sequences that neighbour the homologous

sequences in the ssDNA overhangs, ssDNA flaps are generated at the annealed overhangs. Subsequently, the removal of these ssDNA flaps is performed in a XPF-ERCC1-dependent manner (Motycka et al., 2004). Finally, gap filling of any residual gaps is carried out, followed by ligation of the DNA phosphodiester backbone.

BIR is an HR sub-pathway that cells can employ to repair seDSBs, such as those that are generated as a consequence of prolonged replication fork stalling. BIR is initiated by the invasion of the resected 3' terminus of the seDSB to a homologous template, forming a D-loop. Subsequently, conservative DNA replication is performed, with the D-loop progressing along the template until the entire template has been replicated (Donnianni & Symington, 2013; Epum & Haber, 2022; Saini et al., 2013). In comparison to other HR DSBR sub-pathways, BIR is considerably more error-prone (Kramara et al., 2018).

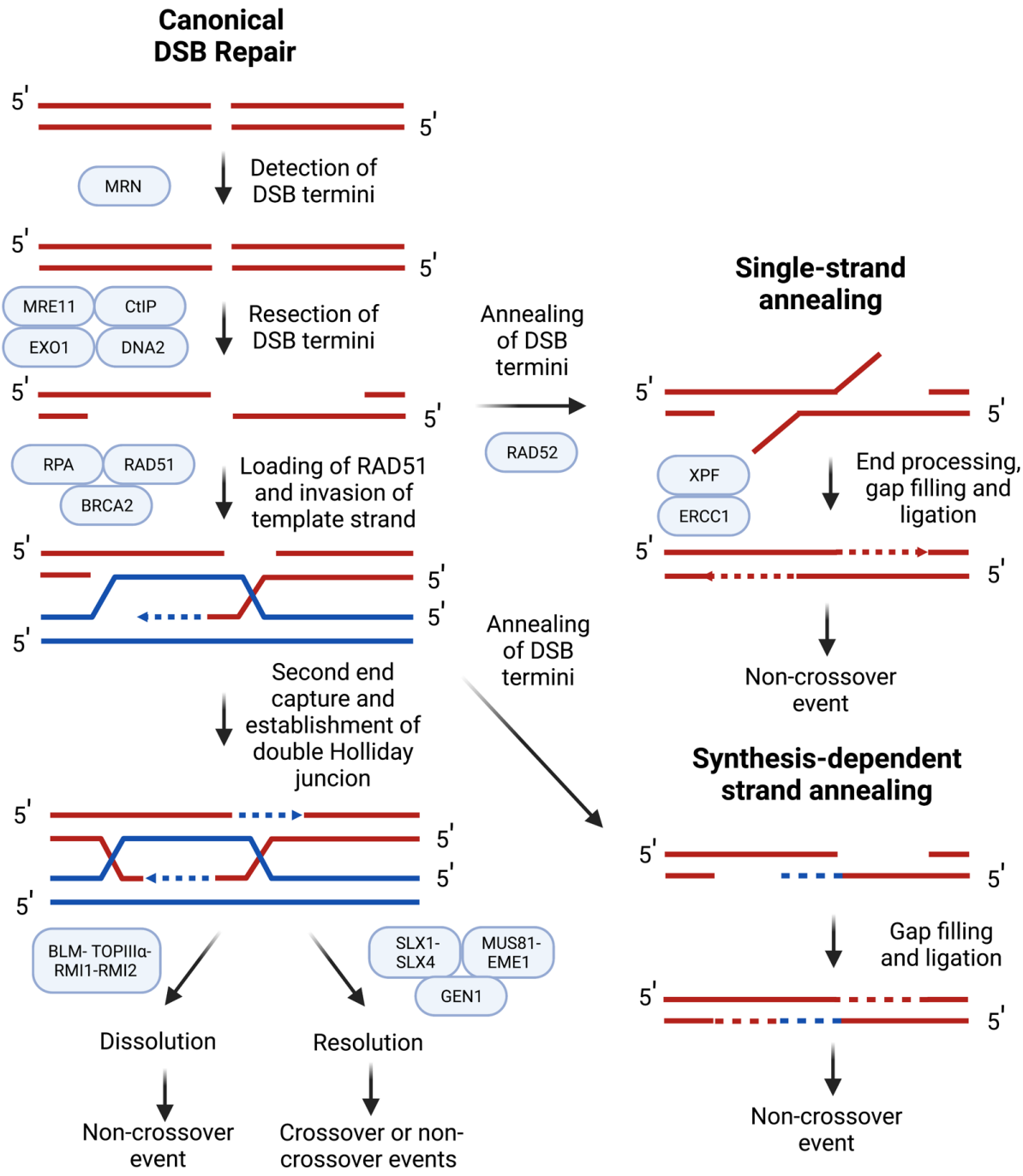


Figure 1.4: Summary of HR. The MRN complex initiates HR by detecting the DSB termini. Subsequently, 3' ssDNA overhangs are generated at the DSB in a MRE11/CtIP/EXO1/DNA2-dependent manner. Following resection, RPA associates with the 3' ssDNA overhangs. At this stage, the lesion can be repaired by 3 HR sub-pathways: canonical DSBR, SSA and SDSA. In SSA, the 3' ssDNA overhangs at each break terminus anneal at homologous sequences in a RAD52-dependent manner,

forming ssDNA flaps at non-homologous sequences. Subsequently, the ssDNA flaps are cleaved by the XPF-ERCC1 complex and the break undergoes gap filling and ligation. In canonical DSBR or SDSA, BRCA2 and PALB2 associate to facilitate the replacement of RPA with RAD51 nucleoprotein filaments on the ssDNA overhangs. Consequently, the RAD51-associated ssDNA on the first break terminus invades the homologous DNA template and DNA synthesis is performed. In SDSA, following DNA synthesis using the homologous template, the invaded strand is extruded and captured by the ssDNA overhang on the second break terminus, and the break subsequently undergoes gap filling and ligation. In canonical DSBR, following DNA synthesis using the homologous template, the extruded strand of the D-loop can anneal with the 3' ssDNA overhang on the second DSB terminus, generating a double Holliday Junction (dHJ). The dHJ can be processed by dissolution or resolution. Dissolution is mediated by the BTR complex (consisting of BLM, TOPIIIα, RMI1 and RMI2) whereas resolution is mediated by the nucleases GEN1, MUS81-EME1 or SLX1-SLX4. Adapted from Ranjha et al., 2018 and produced with BioRender.

1.4.3 The involvement of PARPs in HR

An early study claimed that rather than playing a direct role in HR, PARP1 may form a regulatory role to repress this repair pathway. Indeed, while PARP1 does not co-localise with RAD51 foci at DSBs and HR kinetics are unperturbed in PARP1-deficient cells, the same cells, or wild type cells treated with PARP inhibitor (PARPi) exhibit increased levels of HR at DSBs (Schultz et al., 2003). In contrast, a subsequent study provided compelling evidence in support of the notion that PARP1 has a direct role in HR. The study demonstrated via immunoprecipitation that PARP1 binds to MRE11 *in vivo* and via a nitrocellulose-PAR binding assay, *in vitro*, that MRE11 also binds to

PAR via its PAR-binding domain. Furthermore, the same study showed that PARP1 promotes the localisation of MRE11 and NBS1 to laser microirradiation-induced DSBs (Haince et al., 2008). Therefore, this study suggested that PARP1 may promote the resection stage of HR. Consistent with this, the localisation of BRCA2 to I-SceI-dependent DSBs is dependent on PARP1 catalytic activity. Indeed, following the generation of IR-induced DSBs, BRCA2 binds to PAR via its OB-folds, which promotes the EXO1-dependent resection step of HR (Soutoglou et al., 2007; Yang et al., 2002; Zhang, Shi, Bian, et al., 2015). Interestingly, EXO1 binds to PAR via its PIN domain, which contributes to its localisation to DSBs (Zhang, Shi, Chen, et al., 2015). Furthermore, the localisation of BRCA1-BARD1 to DSBs is facilitated by the PAR-associating BRCT domains of BARD1 (Li & Yu, 2013).

While the precise role of PARP14 in HR is not clear, a study showed that PARP14 is not required for the assembly of RAD51 nucleoprotein filaments, but instead, may function to facilitate the invasion of RAD51-coated ssDNA strands or the dismantlement of RAD51 nucleoprotein filaments. Indeed, PARP14-depletion reduces the viability of cells following bleomycin exposure; results in a reduction in HR efficiency; and causes delayed resolution of RAD51 foci following exposure to camptothecin (Nicolae et al., 2015).

1.4.4 c-NHEJ

By ligating the ends of DSBs, the classical non-homologous end-joining (c-NHEJ) pathway can repair DSBs in the absence of a homologous template at most points within the cell cycle, although it is generally believed that it is inactive during mitosis (Figure 1.5) (Chaudhuri & Nussenzweig, 2017; Mao et al., 2008; Meek et al., 2008;

Orthwein et al., 2014). This repair pathway is prone to error (Chang et al., 2017). Repair of a DSB via c-NHEJ can be instigated by detection of a DSB by the dimeric protein Ku, which consists of Ku70 and Ku80 (Mimori et al., 1986). At each break terminus, an individual Ku complex envelops DNA by forming a ring structure, which acts as a molecular scaffold for the localisation of downstream NHEJ factors (Britton et al., 2013; Ma et al., 2004; Walker et al., 2001). Subsequently, the DNA-dependent protein kinase catalytic subunit (DNA-PKcs) – a member of the phosphoinositide 3-kinase-(PI3K)-related kinase (PIKK) family – binds to the Ku80 C-terminal domain within the Ku heterodimer to form the DNA-dependent protein kinase (DNA-PK) complex (Gottlieb & Jackson, 1993; Hartley et al., 1995; Yaneva et al., 1997). Recently, a cryo-EM study demonstrated that a single DNA-PK complex forms at each break terminus, which dimerise via interactions between the Ku80 C-terminal domains at each terminus. This forms a molecular scaffold that increases the proximity of the DSB ends and facilitates the recruitment of other c-NHEJ proteins to the break (Chaplin et al., 2021). Following the assembly of the DNA-PK complex at the DSB, DNA-PK phosphorylates itself at numerous residues, and consequently phosphorylates Artemis, which promotes the end-processing activity of this nuclease (Ding et al., 2003; Goodarzi et al., 2006; Niewolik et al., 2006). Artemis contributes to end-processing by removing structures such as 3'-phosphoglycolates from DSB termini although tyrosyl-DNA phosphodiesterase 1 (TDP1) can also facilitate this process (Povirk et al., 2007; Zhou et al., 2005). Furthermore, additional proteins also contribute to DSB end-processing including Aprataxin and PNKP Like Factor (APLF) and APTX (Li et al., 2011). Following appropriate nuclease-dependent processing of the DSB termini, gap filling is performed by DNA polymerase μ (Polμ) and DNA polymerase λ (Polλ) at the DSB termini (Pryor et al., 2015). Finally, the DSB termini

are ligated by the DNA ligase IV (LIGIV)-X-ray repair cross complementing 4 (XRCC4)-XLF complex and subsequent to the repair of a DSB, the Ku complex is ubiquitinated, which facilitates its eviction from the DNA damage site (Ahnesorg et al., 2006; Brown et al., 2015; Ma et al., 2004; Postow et al., 2008). XRCC4 and XLF assemble into complexes with a conformation that is sleeve-like, which tether the DSB termini in order to facilitate repair (Brouwer et al., 2016; Ropars et al., 2011). Recently, an additional c-NHEJ factor – Paralog of XRCC4 and XLF (PAXX) – has been revealed, which promotes c-NHEJ by increasing the stability of c-NHEJ factors at DSBs via its interactions with the Ku complex (Ochi et al., 2015).

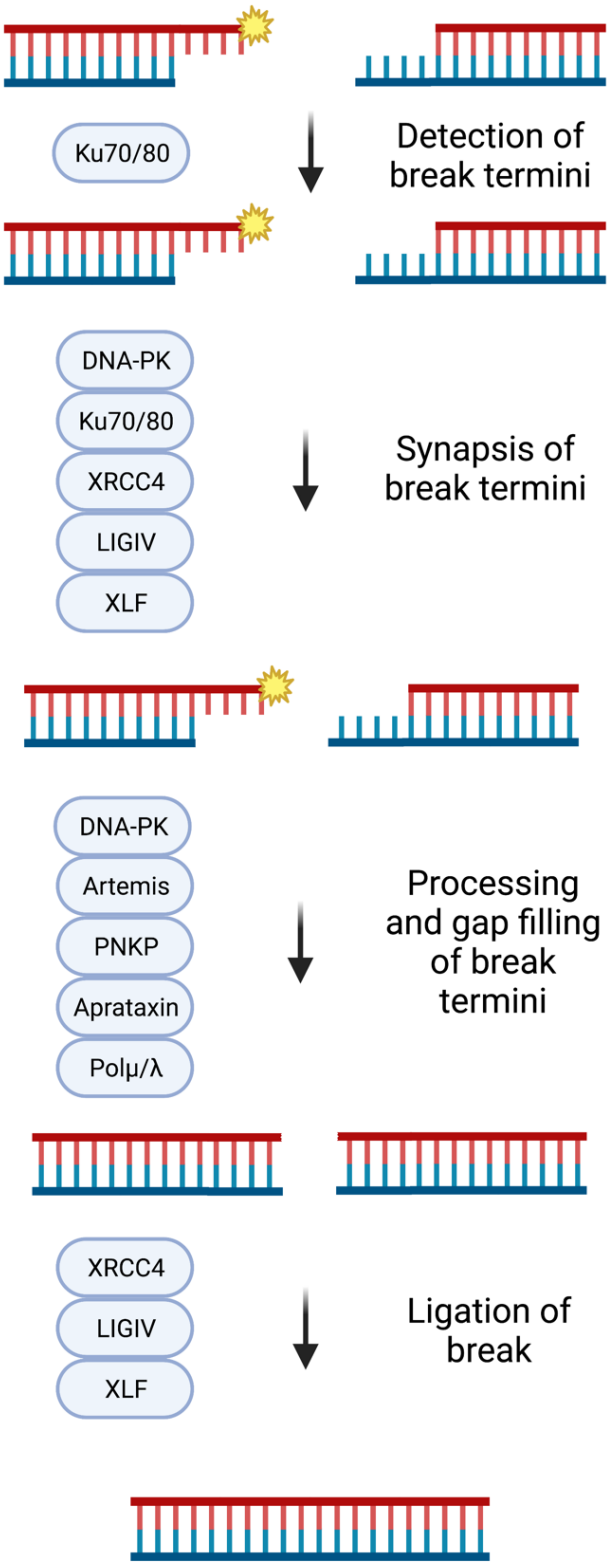


Figure 1.5: Summary of c-NHEJ. c-NHEJ is initiated following the detection of a DSB by the Ku complex, which consists of Ku70 and Ku80. Subsequently, DNA-PKcs associates with the Ku complex to form an active DNA-PK complex. DNA-PK

promotes the localisation of other c-NHEJ repair factors and draws the DSB termini closer together. DNA-PK also stimulates Artemis, which is one of many other proteins such as PNKP and aprataxin that process the break termini. Gap filling of the break termini is facilitated by Polμ and Polλ. Finally, ligation of the break is performed by the LIGIV-XRCC4-XLF complex. Adapted from Zhao et al., 2020 and produced with BioRender.

1.4.5 The involvement of PARPs in c-NHEJ

PARP1 was first proposed to have an involvement in c-NHEJ in an *in vitro* study, which demonstrated that PARP1 interacts with and ADP-ribosylates DNA-PKcs, in a Ku-independent manner, which consequently increases the DNA-PK-dependent phosphorylation of its downstream targets (Ruscetti et al., 1998). Consistent with this, DNA-PK was found to interact with PAR (Gagné et al., 2008). Later, the DNA-PK-PARP1 interaction was confirmed by electron microscopy using purified DNA-bound DNA-PK-PARP1 (Spagnolo et al., 2012). In addition, a number of c-NHEJ factors have been shown to be recruited to DSBs in an ADP-ribosylation-dependent manner. For example, chromodomain helicase DNA-binding protein 2 (CHD2) – a chromatin remodeller – was shown to be recruited to DSBs via its PAR-binding domain at its C-terminus in a manner that is dependent on PARP1-mediated PARylation. The PARP1-dependent recruitment of CHD2 to DSBs helps remodel chromatin in a manner that is proposed to assist in the congregation of c-NHEJ factors at DSBs, thereby expediting c-NHEJ repair kinetics (Gagné et al., 2008; Luijsterburg et al., 2016). Recently, it was demonstrated that ZNF384 – a zinc finger protein – interacts with DSBs and promotes the recruitment of the Ku complex to DSBs via a mechanism that is dependent on the remodelling of chromatin into a relaxed state by PARP1-mediated PARylation.

Recruitment of ZNF384 to DSBs promotes the assembly of c-NHEJ factors at these lesions in a DNA-PKcs-independent manner (Singh et al., 2021).

There are also several lines of evidence demonstrating that PARP3 participates in c-NHEJ. Firstly, PARP3 binds to numerous components of the c-NHEJ pathway, such as the Ku complex, DNA-PKcs and APLF (Rouleau et al., 2007; Rulten et al., 2011). Indeed, the ligation of break termini by the LIG IV-XRCC4-XLF complex is thought to be expedited by the PARP3-APLF interaction (Rulten et al., 2011). Furthermore, PARP3 stimulates the c-NHEJ-mediated repair of DSBs by promoting the localisation and/or stability of the Ku complex at these lesions, which represses the substantial resection of break termini required for HR or alt-NHEJ (Beck et al., 2014).

1.4.6 alt-NHEJ

Until recently, little was known about the mechanism of the alternative-NHEJ (alt-NHEJ) DSB repair pathway. The alt-NHEJ pathway was first identified following the observation that the end-joining-mediated repair of DSBs could occur in eukaryotic cells in the absence of numerous c-NHEJ repair factors (Boulton & Jackson, 1996; Kabotyanski et al., 1998; Liang & Jasin, 1996). Due to the often observed, yet non-compulsory involvement of the A-family polymerase DNA polymerase θ (Polθ) in the alt-NHEJ pathways of the majority of eukaryotic organisms, alt-NHEJ is often referred to as Polθ-mediated end joining (TMEJ) (Ramsden et al., 2022; Seki et al., 2003). Like c-NHEJ, alt-NHEJ repair is prone to error (Ramsden et al., 2021). A recent study demonstrated that the utilisation of the alt-NHEJ pathway to repair DSBs – particularly single-end DSBs (seDSBs) generated via replication fork collapse – is restricted until mitosis, as this gives the cell sufficient time to replicate the other side of the DSB so that alt-NHEJ can be performed (Llorens-Agost et al., 2021).

A full mechanistic understanding of alt-NHEJ and the proteins involved in this pathway are still being revealed, but the following model has been proposed for this pathway (Figure 1.6). A pre-requisite to the alt-NHEJ-mediated repair of a DSB is that the DSB termini must undergo processing by CtBP-interacting protein (CtIP) and MRE11-RAD50-NBS1 (MRN) to form a 3'overhang at one or both break termini that are 30 to 70 nucleotides in length (Deriano & Roth, 2013; Lee-Theilen et al., 2011; Ma et al., 2003; Ramsden et al., 2022; Truong et al., 2013; Wyatt et al., 2016; Xie et al., 2014). Following resection of the DSB termini, the localisation of Polθ to the DSB is dependent upon PARP1 and Fanconi anemia group D2 (FANCD2) (Kais et al., 2016; Mateos-Gomez et al., 2015). Subsequently, the 3' overhangs anneal at sequences that share microhomology that are typically at least 3 nucleotides in length (Carvajal-Garcia et al., 2020; He & Yang, 2018; Wyatt et al., 2016). The annealing of the break termini is thought to be facilitated by Polθ (Newman et al., 2015). DNA hairpins can be formed at DSB termini that contain complementary nucleotide sequences, which prevents the annealing step of alt-NHEJ. To avoid this scenario, it has been proposed that these DNA hairpins can be removed by the C-terminal polymerase domain (PolD) of Polθ, which allows alt-NHEJ-mediated repair of the DSB to ensue (Seki et al., 2003; Zahn et al., 2021). Following annealing of the 3' ssDNA DSB overhangs, 3' flaps form which must be cleaved by a nuclease. The identity of this nuclease is yet to be confirmed, but the Polθ PolD and the XPF-ERCC1 heterodimer have been proposed as candidates that may perform this 3' nuclease function (Ahmad et al., 2008; Ramsden et al., 2022; Tsodikov et al., 2005; Zahn et al., 2021). Subsequently, Polθ synthesises DNA in an error-prone manner on both sides of the annealed termini, which fills the gaps at this repair intermediate, although Polδ may also contribute to

this stage of alt-NHEJ (Arana et al., 2008; Layer et al., 2020; Ramsden et al., 2022). Finally, the break is ligated predominantly via LIGIII, although in certain instances LIGI may also have functional overlap with LIGIII in the ligation step (Boboila et al., 2012; Masani et al., 2016; Simsek et al., 2011).

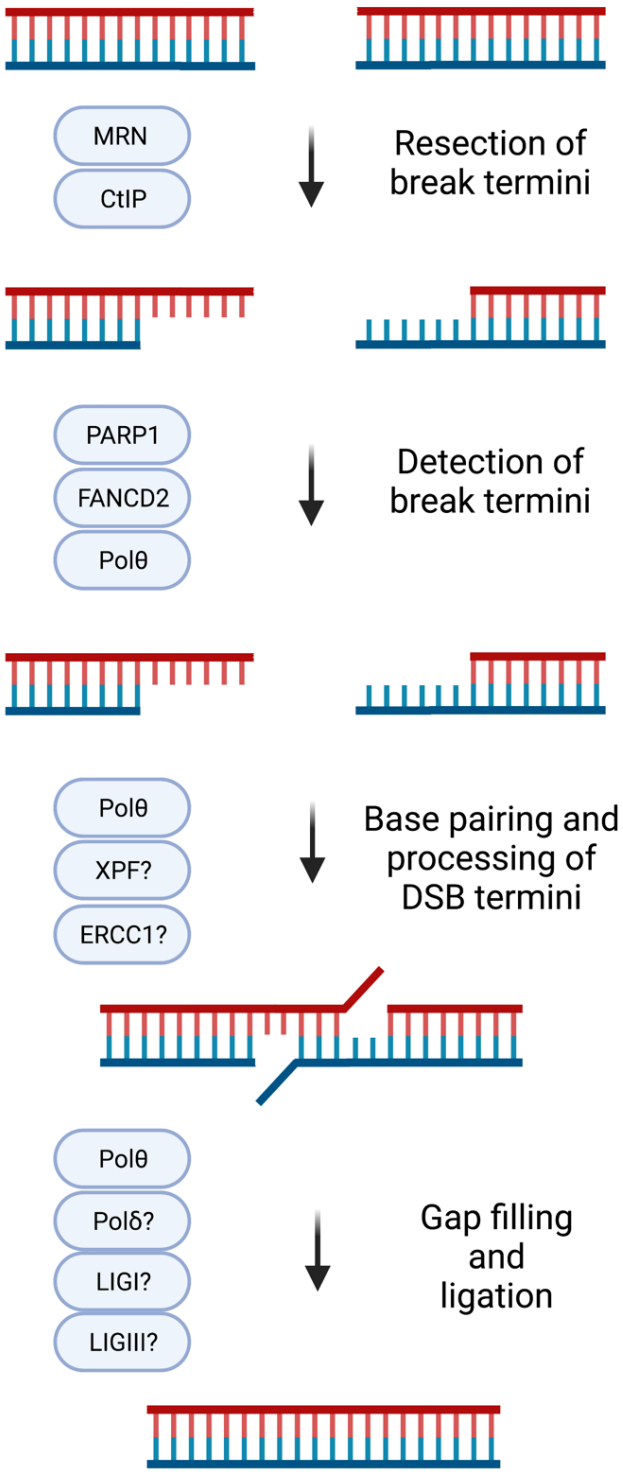


Figure 1.6: Summary of alt-NHEJ. alt-NHEJ is initiated after the MRN/CtIP-dependent resection of the DSB termini, which generates ssDNA overhangs. Next, PARP1 and FANDC2 detect the DSB termini and assist in the localisation of Polθ to the DSB termini. Consequently, Polθ facilitates the processing of the ssDNA

overhangs and facilitates the annealing of the strands at regions that have microhomologous sequences, forming ssDNA flaps. The removal of the ssDNA flaps is believed to be mediated by the XPF-ERCC1 complex. Next, gap filling is performed by Polθ and possibly Polδ. Finally, ligation of the break may be performed by either LIGI or LIGIII. Adapted from Ramsden et al., 2022 and produced with BioRender.

1.4.7 The involvement of PARPs in alt-NHEJ

The first lines of evidence that suggested a role for PARP1 in alt-NHEJ were the observations that PARP1 inhibition or depletion sensitised cells to DSBs and diminished the efficiency of an end joining pathway that functions independently to c-NHEJ (Audebert et al., 2004; Mansour et al., 2010; Wang et al., 2006). Subsequently, a study showed that depletion of PARP1 ablated the recruitment of Polθ to DSBs induced by laser-micro-irradiation, which demonstrated that Polθ is recruited to DSBs in a PARP1-dependent manner (Mateos-Gomez et al., 2015). Recently, a study showed that PARP1 and PARP2-mediated PARylation stimulates the resection of DSB termini, which encourages alt-NHEJ-mediated repair of these lesions. Indeed, loss of PARP1 and PARP2 mediated PARylation prevented the resection of DSBs, leading to their repair via c-NHEJ. It has been proposed that the PARP1 and PARP2-mediated PARylation enables the localisation of the resection factors required for alt-NHEJ-mediated repair (Luedeman et al., 2022).

1.4.8 Making the decision between HR and c-NHEJ

Numerous mechanisms can control whether a two-ended DSB is repaired by c-NHEJ or HR. Resection of the DSB termini results in the ejection of the Ku complex from the lesion, and consequently enables the cell to channel this lesion down the HR pathway. Key mediators of DSBR pathway choice are Breast Cancer gene 1 (BRCA1) and p53-binding protein 1 (53BP1), which stimulate and limit DSB resection, respectively (Bunting et al., 2010; Chen et al., 2008; Zhong et al., 1999). In addition to 53BP1, its interacting partners Revertibility Protein 7 Homologue (REV7), Replication Timing Regulatory Factor 1 (RIF1) and the shieldin (SHLD) complex (consisting of SHLD1, SHLD2, SHLD3) also contribute to the antagonisastion of DNA resection (Dev et al., 2018; Di Virgilio et al., 2013; Escribano-Díaz et al., 2013; Gao et al., 2018; Ghezraoui et al., 2018; Gupta et al., 2018; Noordermeer et al., 2018; Tomida et al., 2018; Zimmermann et al., 2013). In order to ensure that HR is only initiated when appropriate (during S-phase and G_2-phase), DSB resection must be tightly controlled by CDKs, which stimulate the activation of DSB resection factors and other proteins that function within downstream steps of HR at these cell cycle phases (Aylon et al., 2004; Ira et al., 2004; Scully et al., 2019; Tomimatsu et al., 2014).

1.5 DNA Replication stress

While the replisome has been optimised to execute DNA replication with minimal error, there are numerous endogenous and exogenous impediments to DNA replication that elicit deceleration or stalling of replication forks (Gaillard et al., 2015). Collectively, these impediments are referred to as DNA replication stress. However, it is important to note that within the literature, numerous definitions of DNA replication stress are

utilised, which can often lead to confusion. An important product of DNA replication stress is the accumulation of ssDNA, which arise at perturbed replication forks due to the disengagement of the MCM helicase and the DNA polymerase (Byun et al., 2005).

1.5.1 Causes of DNA replication stress

There is a plethora of endogenous and exogenous inducers of replication stress. Examples of endogenous inducers of DNA replication stress include alkylated bases, SSBs, DNA hairpins, G-quadruplexes, R-loops that can arise due to oncogene activation-induced aberrant origin firing, transcription-replication conflicts (TRCs) and common fragile sites (CFSs). CFSs are typically large genes that frequently undergo transcription but are challenging to replicate as they contain low frequencies of dormant replication origins, which are required to complete replication following fork stalling. Examples of exogenous inducers of DNA replication stress include MMS, the DNA cross-linking agent mitomycin C, Top1 poisons, the ribonuclease reductase inhibitor HU which diminishes dNTP pools required during DNA replication, and the DNA polymerase α/ε inhibitor aphidicolin (APH) (Cheng & Kuchta, 1993; Ikegami et al., 1978; O'Connor, 1981; Bianchi et al., 1986).

1.5.2 The DNA replication stress response

Replication stress can incite two key effects on the replication fork: fork stalling and fork breakage. Replication fork breakage can occur in a number of ways. If a replication fork encounters an unrepaired SSB, the fork can continue to progress, converting this lesion to a single-ended DSB (seDSB) (Kuzminov, 2001; Ensminger et al., 2014; Vrtis et al., 2021). Additionally, when a replication fork stalls after

encountering DNA replication stress, the nascent strands of the replication fork can anneal, forming a four-armed configuration called a reversed fork (Sogo et al., 2002). In the event that a reversed fork remains stalled for extensive periods, it can be susceptible to nucleolytic processing and MUS81-dependent incision to generate seDSBs (Hanada et al., 2007). Nuclear-wide seDSB induction can also occur in response to prolonged dNTP deprivation – an event known as replication catastrophe (Toledo et al., 2013). A response to prolonged fork stalling is to complete DNA replication with additional replication forks which are initiated by firing of dormant replication origins (Ge et al., 2007; Woodward et al., 2006). Therefore, it has been proposed that following protracted fork stalling, additional replication origins are fired, generating an abundance of replication forks that stall to generate high levels of ssDNA. The ssDNA at the forks is consequently protected by RPA, until the cellular reserves of RPA is consumed. In this eventuality, the unprotected stalled replication forks accumulate, which are cleaved, resulting in replication catastrophe (Toledo et al., 2013).

Given the potentially deleterious nature of DNA replication stress, cells have evolved a DNA replication stress response to mitigate the effects of this stress (Figure 1.7). Since our understanding of the responses of cells to DNA replication stress is continuously improving, there is no clear definition of the DNA replication stress response in the literature. As such, in this thesis, the DNA replication stress response is defined as a network of DDR pathways that function together to promote the completion of DNA replication during or after replication forks encounter DNA replication stress.

A crucial impresario of the DNA replication stress response is ataxia and Rad3-related protein (ATR) – a member of the PIKK family (Cimprich et al., 1996). Following fork stalling, or resection of stalled forks, RPA assembles on the replication stress-induced ssDNA, which leads to the localisation of ATR and ATR-interacting protein (ATRIP) to these lesions – an interaction that is a prerequisite for ATR activation (Cortez et al., 2001; Zou & Elledge, 2003). A pair of ATR-ATRIP heterodimers dimerise to form an ATR-ATRIP complex with a cordate conformation (Rao et al., 2018). ATR activation can subsequently be facilitated by DNA topoisomerase II binding protein 1 (TOPBP1) or Ewing's tumor-associated antigen 1 (ETAA1), which homodimerise at their ATR activating domains (AADs) to expedite ATR activation kinetics (Bass et al., 2016; Lee et al., 2007; Thada & Cortez, 2019, 2021). TOPBP1 localisation to perturbed replication forks is facilitated by the 9-1-1 complex (consisting of RAD9, RAD1 and HUS1) which is primed at replication stress-induced ssDNA-dsDNA intersections by the RAD17-Replication factor C (RFC) complex (Bermudez et al., 2003; Delacroix et al., 2007; Ellison & Stillman, 2003; Lee et al., 2007; Zou et al., 2003). On the other hand, ETAA1-dependent ATR activation is mediated by binding of ETAA1 to RPA-bound ssDNA at stressed replication forks, via its dual RPA-binding domains (Bass et al., 2016; Haahr et al., 2016). It has also been suggested that RAD9-RAD1-HUS1-interacting nuclear orphan (RHINO) and the MRN complex also contribute to the localisation of TOPBP1 to stressed forks, although precisely how these factors perform this function is yet to be determined (Cotta-Ramusino et al., 2011; Duursma et al., 2013; Lindsey-Boltz et al., 2015). Interestingly, a recent study demonstrated that ATR phosphorylates TOPBP1 to induce the formation of TOPBP1 aggregates via interactions between the TOPBP1 b6-8 domain, which in turn amplifies the activation of ATR (Frattini et al., 2021). Subsequent to its activation, ATR modifies a plethora of

protein targets through its kinase activity, with the CHK1 kinase being one of the best characterised targets (Liu et al., 2000; Matsuoka et al., 2007). It is through this ATR-CHK1 signalling cascade that the cell orchestrates numerous aspects of the DNA replication stress response such as halting cell cycle progression, repressing aberrant firing of replication origins, promoting the stabilisation of stalled forks, stimulating restart of stalled forks and facilitating repair of broken forks, in order to reduce the likelihood that mitotic entry is initiated when DNA replication is incomplete (Saldivar et al., 2017). However, it is important to note that the cell also has mechanisms of dealing with replication intermediates that enter mitosis (see below).

An important response to DNA replication stress is fork reversal. Initially, fork reversal was considered to be a deleterious outcome of fork instability (Sogo et al., 2002). However, subsequent studies have challenged this notion by revealing via electron microscopy that fork reversal is a highly regulated and common process in cells, which is initiated following exposure to a wide variety of DNA replication stresses (Ray Chaudhuri et al., 2012; Zellweger et al., 2015). It is generally believed that fork reversal is advantageous to cells for three key reasons. Firstly, it may be utilised when DNA damage in the leading strand is encountered by a replication fork, and therefore enables the repair of these DNA lesions (e.g. by using aforementioned DDR pathways), and then fork restart (Berti, Cortez, et al., 2020; Wassing & Esashi, 2021). Secondly, it may convert the stalled fork into a configuration that reduces the likelihood of nuclease-induced seDSB formation (Zellweger et al., 2015). Thirdly, nuclease-dependent incision of reversed forks can generate seDSBs which can promote fork restart (Hanada et al., 2007).

An important facilitator of fork reversal is the HR protein RAD51, although the precise mechanism by which this protein mediates this function is yet to be determined (Zellweger et al., 2015). Given that RAD51 performs fork reversal in a BRCA2-independent manner, this recombinase assists in fork reversal via a process that is distinct to its modus operandi in HR (Kolinjivadi et al., 2017; Lemaçon et al., 2017; Mason et al., 2019; Mijic et al., 2017). RAD51-dependent fork reversal is also supported via the action of the Methyl methanesulfonate-sensitivity protein 22-like (MMS22L)-Tonsoku-like (TONSL) complex, which binds to RAD51 via the MMS22L C-terminal domain and promotes the assembly of RAD51-coated ssDNA while repressing the formation of RAD51-coated dsDNA (Duro et al., 2010; O'Donnell et al., 2010; Piwko et al., 2016). MMS2L-TONSL localises to stalled forks by interacting with nucleosomes containing H4 non-methylated at K20 (H4K20me0)-decorated histones – a marker of newly synthesised DNA (Saredi et al., 2016). Fork reversal is also promoted by three DNA translocases – Helicase-like transcription factor (HLTF), zinc finger RANBP2-type containing 3 (ZRANB3) and SWI/SNF subfamily A-like 1 (SMARCAL1). Recent studies have revealed the involvement of the RAD51 paralogue-containing BCDX2 complex in this process, which collaborates with RAD51 in facilitating SMARCAL1-dependent and ZRAN3B-dependent fork reversal (Berti, Teloni, et al., 2020; Halder et al., 2022). In response to DNA replication stress, PCNA can be polyubiquitinated, thereby promoting fork reversal (Hoege et al., 2002). Indeed, ZRANB3 localises to stalled forks by via interactions with polyubiquitinated PCNA, which subsequently enables this DNA translocase to mediate fork reversal (Ciccia et al., 2012; Vujanovic et al., 2017; Weston et al., 2012). In contrast, SMARCAL1 initiates fork reversal by binding to RPA-coated ssDNA at stalled replication forks that contain replication barriers within the leading strand (Bétous et al., 2012, 2013; Couch et al.,

2013). SMARCAL1-dependent fork reversal is also stimulated by ATM, which promotes the localisation of SMARCAL1 to stalled forks. This ATM-mediated function is thought to be promoted by Tat interactive protein, 60 kDa (TIP60)-dependent acetylation of ATM (Kamine et al., 1996; Schleicher et al., 2022). SMARCAL1-dependent fork reversal is negatively regulated by ATR via SMARCAL1 phosphorylation at its Ser652 residue (Couch et al., 2013). Recently, RAD52 was also shown to antagonise SMARCAL1-dependent fork reversal by preventing SMARCAL1 from binding to stalled forks (Malacaria et al., 2019). The HIP116/HLTF RAD6 N-terminus (HIRAN) domain of HLTF facilitates its localisation to stalled forks by binding to 3' termini at these structures (Blastyák et al., 2007, 2010; Iyer et al., 2006; Kile et al., 2015). Interestingly, HLTF also participates in the modification of PCNA with polyubiquitin and functions to reduce fork velocity when a fork encounters replication stress (Bai et al., 2020). A recent study revealed that fork reversal occurs in two discrete phases: initiation and extension. The initiation phase is instigated by SMARCAL1, HLTF and ZRANB3, generating topological stress in the annealed nascent strands. Subsequently, the elongation phase is performed by TOP2α and the DNA helicase Plk1-interacting checkpoint helicase (PICH), which alleviate the topological stress that is accrued during the initiation phase (Kolinjivadi et al., 2017; Tian et al., 2021). While their mechanism of action in promoting fork reversal is not fully understood, other proteins such as the DNA helicases RecQ-like helicase 5 (RECQL5), WRN and BLM; the translocases Fanconi anemia group M (FANCM) and RAD54; and the Exonuclease 3'-5' domain containing 2 (EXD2) nuclease have been implicated in this process (Bugreev et al., 2011; Flaus et al., 2006; Gari et al., 2008; Kanagaraj et al., 2006; Machwe et al., 2006; Nieminuszczy et al., 2019; Z. Yan et al., 2010). ATR also facilitates the localisation of RAD51 to stalled forks by promoting the

ATPase Family AAA Domain Containing 5 (ATAD5)-Replication Factor C-like complex (RLC)-dependent exclusion of PCNA from forks that have undergone stalling. It has been proposed that this ATAD5-dependent function promotes fork reversal because PCNA may act as a barrier to the reversal of replication forks (Park et al., 2019). Recently, DNA-PKcs and Ku were also revealed as a novel facilitators of replication stress-induced reduction in fork velocity and fork reversal (Dibitetto et al., 2022). Therefore, numerous factors are required to facilitate fork reversal.

Reversed replication forks can be processed by the DNA replication helicase/nuclease 2 (DNA2) nuclease in tandem with Werner protein (WRN) helicase, in order to facilitate fork restart (Thangavel et al., 2015). Regulated resection at reversed forks by the nuclease MRE11 may also promote fork restart (Dhoonmoon et al., 2022; Kolinjivadi et al., 2017; Lemaçon et al., 2017; Mijic et al., 2017). MRE11 can be localised to stalled forks by interacting with histones that are methylated by Pax transactivation domain-interacting protein (PTIP) in conjunction with the mixed-lineage leukemia 3/4 (MLL3/4) complex (Cho et al., 2007; Ray Chaudhuri et al., 2016). However, unsolicited processing of reversed forks by a variety of nucleases is repressed by fork protection. While important for mediating fork reversal, RAD51 also contributes to fork protection from MRE11-dependent processing by forming stable nucleofilaments on the nascent strands of reversed forks (Hashimoto et al., 2010; Schlacher et al., 2011; Zadorozhny et al., 2017). This RAD51-dependent fork protection is facilitated by BRCA1, BRCA2 and FANCD2 (Schlacher et al., 2012). The BRCA2-RAD51 interaction is mediated by a motif within the BRCA2 C-terminus (Schlacher et al., 2011). In a CDK1/2-dependent manner, the BRCA1 subunit of the BRCA1-BARD1 heterodimer is phosphorylated, resulting in a BRCA1 species that is recognised and bound by PIN1, a peptidyl-prolyl

isomerase. This binding event facilitates the localisation of RAD51 to the nascent strands of reversed forks by strengthening the association between BARD1 and RAD51, and thus, promotes fork protection (Daza-Martin et al., 2019; Steger et al., 2013). Recent studies demonstrated that MRE11-dependent revered fork degradation is also supressed by MRN Complex Interacting Protein (MRNIP) and α-thalassemia mental retardation X-linked (ATRX) via an interaction with MRN, as well as by Mitotic arrest deficient 2 like 2 (MAD2L2) in collaboration with the translesion synthesis (TLS) DNA polymerases REV1 and Reversionless 3-like (REV3L) (Bennett et al., 2020; Gibbs et al., 1998; Lin et al., 1999; Paniagua et al., 2022). Furthermore, the RAD51 paralogues XRCC2, XRCC3 and RAD51C also perform the same function (Somyajit et al., 2015). Reversed forks are guarded from aberrant DNA2-dependent processing by a number of proteins including Regulatory factor 1 (RIF1), Biorientation of chromosomes in cell division 1-like protein (BOD1L) and Abraxas brother 1 (ABRO1) and CtIP (Higgs et al., 2015; Mukherjee et al., 2019; Przetocka et al., 2018; Xu et al., 2017). Recently, a study demonstrated that BOD1L interacts with SETD1A – a methyltranstransferase – which function together to protect reversed replication forks from DNA2-dependent degradation by promoting RAD51 nucleofilament stability at these structures. Additionally, the SET domain containing 1A (SETD1A)-mediated methylation of histone H3 at lysine K4 (H3K4) stimulates the histone chaperone functionality of FANCD2 which in turn, is believed to promote RAD51 nucleofilament stability at reversed forks (Bledau et al., 2014; Sato et al., 2012; Higgs et al., 2018). Recently, a study revealed that Profilin-1 (PFN1) and sucrose nonfermenting-2 homolog (SNF2H) associate to stimulate fork reversal and resection of nascent DNA by promoting chromatin remodelling at stalled forks whilst also repressing the protection of the reversed forks by BOD1L (Collins et al., 2002; C. Zhu et al., 2022).

Additionally, the catalytic activity of the WEE1 kinase has recently been shown to prevent DNA2-dependent stalled fork degradation (Elbæk et al., 2022).

The disassembly of RAD51 nucleoprotein filaments needs to be tightly coordinated in order to resume DNA replication following the resolution of replication barriers (Wassing & Esashi, 2021). Furthermore, if left unregulated, RAD51 nucleoprotein filament formation at the nascent strands of reversed forks may lead to aberrant HR, which can have deleterious consequences such as the generation of genomic rearrangements (Lambert et al., 2010). Numerous negative regulators of RAD51 nucleoprotein filament stability have been reported. For example, F-Box DNA helicase 1 (FBH1) destabilises the association of RAD51 with ssDNA through both its DNA translocase function and by ubiquitinating RAD51 through both its F-box domain (Chu et al., 2015; Fugger et al., 2009; Kim et al., 2002; Kim et al., 2004; Simandlova et al., 2013). Another example is RPA related single stranded DNA binding protein, X-linked (RADX) which represses RAD51-ssDNA interactions. RADX mediates this process by associating with ssDNA via its OB-folds, thereby outcompeting RAD51 at interacting with these structures (Bhat et al., 2018; Dungrawala et al., 2017; Schubert et al., 2017). Additionally, the DNA helicases RECQL5, BLM and PCNA-associated recombination inhibitor (PARI) also repress RAD51 nucleoprotein filament formation at reversed replication forks (Hu et al., 2007; Mochizuki et al., 2017; Moldovan et al., 2012; Tripathi et al., 2007).

Following the resolution of replication barriers, reversed forks can also be restarted by remodelling these structures into normal, 3-way junctions (Petermann & Helleday, 2010). To date, two pathways are known to contribute to this process. The first

pathway is promoted by DNA helicase RecQ-Like helicase 1 (RECQL1), and repressed by PARP1 (Berti et al., 2013; Ray Chaudhuri et al., 2012). The PARP1-dependent repression of RECQL1 activity is counteracted by the mouse double minute 2 homolog (MDM2)-dependent ubiquitination of PARP1, which causes PARP1 to be degraded by the proteasome (Giansanti et al., 2022; Haupt et al., 1997; Kubbutat et al., 1997). The second pathway is promoted by the ubiquitination of histone H2A at the annealed nascent DNA which is believed to stimulate the localisation of proteins that facilitate this process (Schmid et al., 2018). Recent work also demonstrated that the BTR complex associates with RPA-bound ssDNA in order to facilitate fork restart, although the precise function of this complex in this process is yet to be determined (Shorrocks et al., 2021). Furthermore, DNA-PKcs and PARP1 interact with nascent DNA at reversed replication forks which have not undergone resection. It is believed that these interactions stimulate the localisation of XRCC1 to these forks which may perform excision of replication barriers and subsequently facilitate fork restart (Ying et al., 2016). Finally, p53 has been shown to facilitate fork restart by stimulating an ill-defined repair mechanism (Roy, Tomaszowski, et al., 2018).

An alternative mechanism for tolerating leading strand replication barriers is repriming, which is stimulated by ATR in instances where fork reversal is not possible (Quinet et al., 2020). This mechanism entails the resumption of disrupted DNA synthesis by circumventing DNA lesions in a Primase and DNA directed polymerase (PRIMPOL)-dependent manner, which leads to the accumulation of ssDNA gaps at the fork (Bianchi et al., 2013; García-Gómez et al., 2013; Lopes et al., 2006; Mourón et al., 2013). It has been proposed that PRIMPOL is recruited to forks encountering replication stress by interacting with RPA-bound ssDNA (Guilliam et al., 2015; Wan et

al., 2013). Typically, PRIMPOL-dependent ssDNA gaps are filled by TLS (Quinet et al., 2021). However, PRIMPOL-dependent ssDNA gaps that arise due to bulky DNA lesions are repaired by RAD51-mediated post-replicative HR repair (Adar et al., 2009; Piberger et al., 2020). Another DDT pathway is template switching (TS), which is controlled by SUMOylation and ubiquitination of PCNA (Hoege et al., 2002; Mohiuddin et al., 2018). TS can circumvent DNA lesions at perturbed replication forks by utilising the opposing nascent strand as a homologous DNA template (Ashour & Mosammaparast, 2021). In yeast, the dissolution of TS intermediates is similar to the process involved in dHJ dissolution (Giannattasio et al., 2014). TLS facilitates the circumvention of DNA damage such as UV-induced thymine-thymine dimers at stalled forks by temporarily exchanging canonical DNA polymerases with specially adapted translesion DNA polymerases, although TLS is prone to inaccurate DNA synthesis (Johnson et al., 1999; Lange et al., 2011). The exchange of canonical DNA polymerases with TLS polymerases is mediated by the monoubiquitination of PCNA (Kannouche et al., 2004). Collectively, TLS and TS are pathways within the DNA replication stress response that are often referred to as DNA damage tolerance (DDT) pathways, since the rate of fork progression is minimally affected when they are utilised to mitigate DNA replication stress. (Quinet et al., 2021).

Following the accrual of stalled or reversed forks for extensive durations, these structures can be processed by a number of nucleases such as MUS81 into seDSBs (Hanada et al., 2006, 2007). MUS81 is localised to reversed forks by the Enhancer of zeste homolog 2 (EZH2)-mediated methylation of histone H3 (Rondinelli et al., 2017). seDSBs can also be generated due to aberrant nuclease-dependent processing of insufficiently protected replication forks (Lemaçon et al., 2017). In either case,

subsequent to the generation of seDSBs, replication can ensue by using the BIR sub-pathway of HR (see section 1.4.6). Alternatively, alt-NHEJ may be utilised by the cell to repair collapsed replication forks (Wang et al., 2019).

In instances where a replication fork stalls, a dormant replication origin can initiate a new replication fork that progresses in the opposing direction in order to complete DNA replication (Ge et al., 2007; Woodward et al., 2006). It has been proposed that under these conditions, dormant replication origins are activated in clusters and when the opposing forks meet, they fuse (Ashour & Mosammaparast, 2021; McIntosh & Blow, 2012). However, under conditions of severe replication stress, ATR represses dormant origin firing in order to avert cellular depletion of RPA pools and replication catastrophe (Toledo et al., 2013).

A more recently discovered aspect of the DNA replication stress response is mitotic DNA synthesis (MiDAS) (Minocherhomji et al., 2015). MiDAS is utilised by cells to promote DNA replication during mitosis at incompletely replicated (or under-replicated) DNA that can arise as consequence of fork stalling at CFSs and TRCs (Groelly et al., 2022). It has been proposed that these lesions can pass through the G_2/M checkpoint undetected and into mitosis because they are induced by mild DNA replication stress, which does not cause the accumulation of high enough levels of DNA lesions to halt cell cycle progression (Koundrioukoff et al., 2013; Mocanu & Chan, 2021). MiDAS is considered to operate in a similar manner to BIR, with early studies showing that RAD52, POLD3 and MUS81 are involved in this pathway. While the exact mechanistic details of MiDAS are still being uncovered, it is believed that MiDAS can be initiated by MUS81-dependent cleavage of a stalled replication fork, generating a

seDSB which can subsequently resume DNA synthesis through the strand annealing and DNA synthesis activities of RAD52 and DNA polymerase delta 3 (POLD3), respectively (Bhowmick et al., 2016; Di Marco et al., 2017; Minocherhomji et al., 2015). A recent investigation demonstrated that there is also a RAD51-dependent MiDAS mechanism that facilitates semi-conservative replication, unlike RAD52-dependent MiDAS. It has been proposed that the RAD51-dependent mechanism can be utilised at stalled replication forks in mitosis that are still capable of fork restart and therefore do not require MUS81-dependent processing into seDSBs. It is believed that RAD51 associates with ssDNA at this subset of stalled replication forks in order to reduce the susceptibility of this ssDNA to MUS81-dependent cleavage (Wassing et al., 2021).

In the event that under-replicated DNA – particularly at CFSs – cannot be resolved during mitosis, these loci can be transferred from parent cells to daughter cells following cell division. In the daughter cells, these lesions can be protected by 53BP1 nuclear bodies, which also function to repress the 'second chance' RAD52-dependent HR repair of this damage from G_1-phase until late S-phase, at which point the 53BP1 nuclear bodies disassemble (Harrigan et al., 2011; Lukas et al., 2011; Spies et al., 2019). Interestingly, a recent study revealed that not all under-replicated DNA is protected by 53BP1 in daughter cells. Indeed, under-replicated telomeric loci can be transmitted into daughter cells and the ssDNA is protected by RPA in G_1-phase, at which point these lesions can be resolved by a novel and ill-defined pathway termed post-mitotic DNA synthesis (post-MiDAS) (Lezaja et al., 2021).

1.5.3 The involvement of PARPs in the DNA replication stress response

PARPs have been implicated in the DNA replication stress response in a variety of studies. By associating with stalled forks, PARP1 is thought to promote the localisation of MRE11 to these structures, which stimulates MRE11-dependent fork processing and restart. This is supported by the observations that cells lacking PARP1 accumulate less RPA foci; PAR and MRE11 foci co-localise at stalled forks; and PARP inhibition or depletion increases the frequency of stalled forks in cells (Bryant et al., 2009). Conversely, another study challenged this view and suggested that PARP1 acts to repress MRE11-dependent resection of stalled forks. Indeed, combined exposure of cells to HU and PARPi promoted stalled fork resection, which could be rescued when also combined MRE11 inhibitor treatment (Ying et al., 2012).

PARP1 antagonises RECQL1-dependent fork restart in order to prevent inappropriate resumption of fork progression. Indeed, following inhibition of PARP1 and treatment with the TOP1 inhibitor camptothecin, cells accumulated increased levels of DSBs, as demonstrated via Pulse Field Gel Electrophoresis (PFGE). RECQL1 associates with PARP1 following treatment with camptothecin as demonstrated by co-immunoprecipitation. Under these conditions, the PARP1 DNA binding domain, the PARP1 BRCT domain, as well as PAR chains on PARP1 associate with the RecQ-C-terminal domain of RECQL1. This interaction is strengthened by PARP1-dependent auto-PARylation. Indeed, RECQL1-PARP1 interactions were diminished following PARP1 inhibition (Berti et al., 2013; Hsiang et al., 1989).

Recently, in human cells, the localisation of HLTF, ZRANB3 and SMARCAL1 were shown to be facilitated by PARP1 in response to replication stress. Following MMS

exposure, PARP1-deficient cells exhibited fewer HLTF, ZRANB3 and SMARCAL1 foci, as demonstrated by the in situ detection of proteins at replication forks (SIRF) technique (Roy et al. 2018; Ho et al., 2022). Therefore, PARP1 has a role in promoting fork reversal under condition of replication stress.

A recent study revealed that PARP1 functions in collaboration with p53 and p21 in a pathway that is responsible for recognising DNA damage that is in close proximity to approaching active replication forks. Following detection of these lesions this pathway induces fork slowing or stalling (Maya-Mendoza et al., 2018). Indeed, inhibition of PARP1 increases replication fork velocity as demonstrated by DNA fibre analysis (Maya-Mendoza et al., 2018; Nieminuszczy et al., 2016). Similarly, Coactivator Associated Arginine Methyltransferase 1 (CARM1) promotes PARP1-dependent fork slowing and stalling in response to replication stress. CARM1 facilitates this PARP1-dependent function by binding to PARP1 at HU-induced stalled forks and stimulating PARP1 catalysis (Genois et al., 2021).

The concerted action of PARP1 and PARP2 maintain the stability of forks that meet incompletely repaired BER products such as SSBs by repressing the FBH1-mediated disassembly of RAD51 nucleoprotein filaments at compromised replication forks. Indeed, following treatment with MMS, the formation of RAD51 foci is defective in *PARP1ΔPARP2Δ* cells, but these cells gain the ability to form unrestricted quantities of RAD51 foci following depletion of FBH1 (Ronson et al., 2018).

It has also been proposed that PARP1/ Polθ-mediated alt-NHEJ can be utilised by cells to repair seDSBs at collapsed replication forks, especially in cancers that possess

HR-dysfunction (Ceccaldi et al., 2015; Feng et al., 2019; Wang et al., 2019). Indeed, Polθ-depleted cells are hypersensitised to a variety of replication stress-inducing agents. Additionally these cells accumulate elevated levels of γH2AX following prolonged HU exposure, which is indicative of increased accumulation of collapsed forks under these conditions (Petermann et al., 2010; Wang et al., 2019).

Interestingly, in unperturbed cells undergoing DNA replication, PARP1, LIGIII and XRCC1 contribute to the maturation of Okazaki fragments in a pathway that acts in parallel to the FEN1-LIG1I-dependent pathway (Goulian et al., 1990; Hanzlikova et al., 2018; Harrington & Lieber, 1994; Ishimi et al., 1988; Waga et al., 1994). In the PARP1-dependent pathway, PARP1 recognises the ssDNA gaps that accumulate at Okazaki fragments that have not undergone ligation (Hanzlikova et al., 2018).

By associating with PCNA via a PCNA-interacting protein-motif within its N-terminus, PARP10 promotes TLS at stalled forks by facilitating the localisation of TLS polymerases. Indeed, cells lacking PARP10 are hypersensitive to HU; exhibit a reduction in PCNA ubiquitination following HU treatment; and exhibit a reduction in the TLS polymerase foci in response to ultraviolet (UV) radiation (Nicolae et al., 2014; Shahrour et al., 2016).

A recent investigation showed that the MRE11-dependent restrained processing of unresected nascent DNA at reversed forks is regulated by PARP14 and the Ku complex (Dhoonmoon et al., 2022). The SIRF technique revealed that PARP14 binds to newly synthesised DNA at HU-induced stalled replication forks, and the quantity of SIRF PARP14 foci increased upon combined HU and RAD51 inhibitor treatment.

These are conditions that induce MRE11-dependent processing of reversed forks, thus indicating that PARP14 associates with reversed forks under these conditions (Roy, Luzwick, et al., 2018; Taglialatela et al., 2017). Additionally, using the same assay, PARP14 knockdown combined with RAD51 inhibition reduced the localisation of MRE11 to reversed forks, indicating that the localisation of MRE11 to reversed forks is PARP14-dependent. Overall, the findings from this study suggested that Ku associates with the nascent strand terminus at reversed forks which guards this structure from EXO1-dependent resection. Subsequently, PARP14-bound MRE11 is localised to the nascent DNA terminus by Ku, initiating MRE11-dependent processing, which expels Ku from the terminus and generates a ssDNA terminus that can be protected by RAD51 nucleoprotein filaments (Chanut et al., 2016; Dhoonmoon et al., 2022).

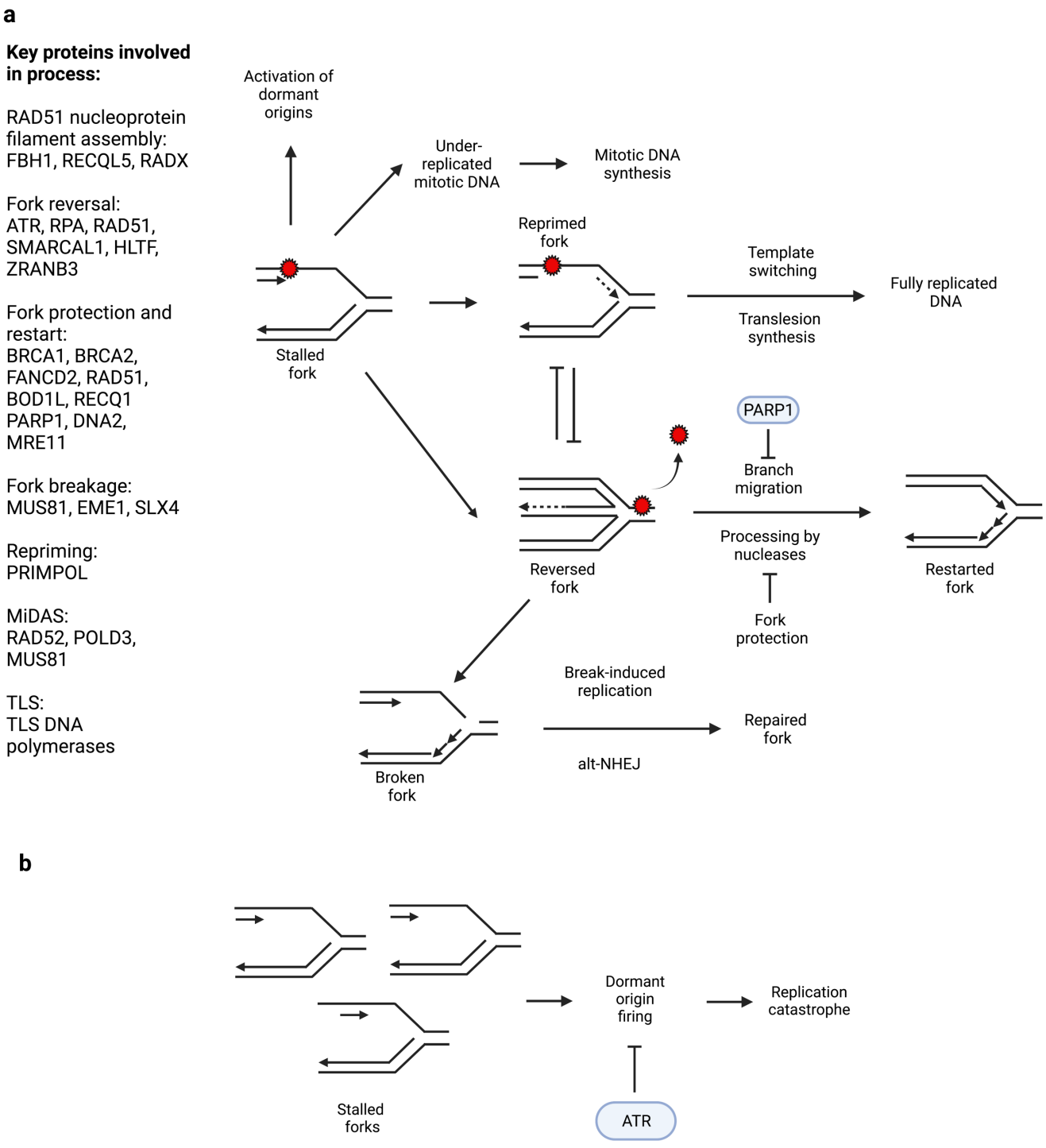


Figure 1.7: Summary of the DNA replication stress response. (a) In the event that a replication fork meets DNA damage in the leading strand, replication fork stalling can occur. Several mechanisms are utilised to restart the replication fork, such as fork repriming and fork reversal (which antagonise one another); activation of dormant origins; and MiDAS. Fork repriming generates ssDNA gaps which remain in the

template strand. Subsequently, TLS or TS (DDT pathways) perform post-replication repair of the ssDNA gaps, which enables the complete replication of the DNA. Following fork reversal, the DNA damage that induced fork stalling is repaired. Subsequently, the reversed fork can be restarted by branch migration which is repressed by PARP1, or by nuclease-dependent processing which is regulated by fork-protection factors. Alternatively, activation of dormant origins enables a fork that is progressing in the opposing direction to complete DNA replication and merge with the stalled fork. Fork stalling can also result in the accumulation of under-replicated DNA in mitosis. In order to repair under-replicated DNA during mitosis, MiDAS is utilised. When the fork remains stalled for protracted durations, it is susceptible to nuclease-dependent fork breakage, which generates a seDSB. In this event, forks are repaired by BIR or alt-NHEJ. **(b)** In response to prolonged nucleotide shortage, pan-nuclear fork stalling occurs. In this event, ATR prevents aberrant firing of dormant origins in order to limit replication catastrophe. The key proteins that are involved in each of these responses to DNA replication stress are indicated. Adapted from Berti, Cortez, et al., 2020 and Toledo et al., 2013 and produced with BioRender.

1.6 The cell cycle

1.6.1 Cell cycle phases

Progression throughout the cell cycle must occur in a controlled manner to make certain that the genome is properly replicated, and that appropriate division of the cell is performed. The cell cycle is commonly divided into the following phases: G_0/G_1, S, G_2 and M (mitosis). The advancement of cells throughout this cycle is orchestrated by

an abundance of cyclin-dependent kinases (CDKs) which associate with their required cyclins (Otto & Sicinski, 2017). The majority of cells are halted in a condition of cell cycle arrest known as G_0 phase, such as quiescent or senescent cells. Due to the transience of quiescence, cells in this state can resume cell cycle progression by utilising pathways that stimulate interaction between CDK4/6 and cyclin D proteins and promote transition from G_0 or G_1 to S-phase (Otto & Sicinski, 2017). This CDK4/6-dependent function is antagonised by the INK4 CDK inhibitors (Jeffrey et al., 2000; Russo et al., 1998; Serrano et al., 1993). CDK4/6 bound to cyclin D can promote transition from G_0 or G_1 to S-phase by phosphorylating retinoblastoma (RB), p107 and p130, which allows the E2F transcription factors to instigate transcription of genes that promote progression through these cell cycle phases, such as cyclin E (Chellappan et al., 1991; Kato et al., 1993; Weinberg, 1995). When the cell approaches late G_1-phase, cyclin E associates with CDK2 to promote cell cycle progression, which also performs RB phosphorylation, thus amplifying the E2F-dependent promotion of cell cycle progression (Otto & Sicinski, 2017). Inhibitors of cyclin E include $p21^{CIP1}$ and $p27^{KIP1}$(Harper et al., 1993; Polyak et al., 1994). Furthermore, CDK2 activity is repressed by WEE1 by phosphorylating CDK2 at Tyr15, although the cell division cycle 25 (CDC25) protein family members can reverse this modification through their phosphatase activity (Gu et al., 1992). When the cell progresses through G_2 phase, CDK1 activity is initiated through its association with cyclin A and cyclin B which promotes mitotic entry. Following initiation of mitosis, CDK1 retains its association with cyclin B, which phosphorylates target proteins to coordinate mitosis. In contrast, towards the end of mitosis, cyclin A is broken down in an anaphase-promoting complex/cyclosome (APC/C)-dependent manner, which ablates CDK1 function and enables the final stages of cell division to ensue (Gavet & Pines, 2010; Geley et al.,

2001; Gong & Ferrell, 2010; Otto & Sicinski, 2017). CDK1 is negatively regulated by membrane-associated tyrosine-and threonine-specific cdc2-inhibitory kinase (PMYT1) and WEE1. PMYT1 mediates the inhibitory phosphorylation of CDK1 at both Thr14 and Tyr15, whereas WEE1 only catalyses the latter modification. The CDC25 protein family members can remove this WEE1-dependent CDK1 modification (Mueller et al., 1995; Parker & Piwnica-Worms, 1992).

1.6.2 DNA damage checkpoints

In order to mitigate the accumulation of mutations when cell division takes place, cells have evolved numerous cell cycle checkpoints (Matthews et al., 2022). These DNA damage checkpoints are activated in response to DNA damage in order to cease cell cycle progression, thus enabling the appropriate repair of these lesions before the cell divides (Otto & Sicinski, 2017). The G_2/M checkpoint, G_1/S checkpoint and the S-phase checkpoint are the most commonly studied cell cycle checkpoints. Following the accrual of DSBs during G_1-phase, these lesions result in the activation of ATM, which modifies numerous protein targets with phosphate groups (Bensimon et al., 2010; Matsuoka et al., 2007). Indeed, ATM catalyses the phosphorylation of CHK2, resulting in its activation. In its active state, CHK2 phosphorylates and consequently activates p53, which stimulates the up-regulation of $p21^{CIP1}$. The elevated expression of $p21^{CIP1}$ initiates the G_1/S checkpoint by repressing cyclin E. In response to certain types of DNA damage that contain ssDNA, CHK1 can be phosphorylated and activated by ATR (Liu et al., 2000; Zhao & Piwnica-Worms, 2001). In its active state, CHK1 can trigger the S or G_2/M cell cycle checkpoints by inactivating CDC25 family proteins, which consequently represses the removal of Tyr15 phosphate groups from CDK1 and CDK2 (Liu et al., 2006; Mailand et al., 2000; Peng et al., 1997; Sanchez et

al., 1997; Sørensen et al., 2003; Zhao et al., 2002). Via its kinase activity, CHK1 also modifies and stimulates WEE1 activity. Active WEE1 catalyses the phosphorylation of CDK1 at Tyr15, which also contributes to the enforcement of the G_2/M checkpoint (O'Connell et al., 1997). Interestingly, WEE1 performs other important cellular functions. For example, during unperturbed DNA replication in S-phase cells, WEE1 activity ensures that aberrant MUS81-dependent processing of progressing replication forks does not occur by repressing CDK1. Under these conditions, WEE1 also ensures that there are sufficient stores of dNTPs within the cell by repressing two additional CDK-dependent events – the degradation of Ribonucleotide Reductase Regulatory Subunit M2 (RRM2) and the initiation of DNA replication origins (Beck et al., 2012; Domínguez-Kelly et al., 2011; Thelander & Reichard, 1979).

1.7 Synthetic lethality

1.7.1 Discovery of synthetic lethality and the development of PARPi

More than a century has passed since the notion of synthetic lethality was proposed by Calvin Bridges, with the term being coined by Theodosius Dobzhansky in 1946 (Bridges, 1922; Dobzhansky, 1946). Traditionally, synthetic lethality is defined as a scenario whereby separate faults in each gene within a gene pair does not result in any consequences, but simultaneous faults within both genes within a gene pair results in cellular death (Ashworth et al., 2011). However, for the purposes of this thesis, the definition of synthetic lethality will be extended to include scenarios in which a single genetic change does not cause any negative effects, but simultaneous genetic changes cause cellular death, with each genetic change consisting of modifications in one or more genes. Synthetic lethal interactions often occur between two DDR genes,

most likely due to the fact that the genes contribute to separate mechanisms that reduce the incidence of cell death-inducing damage to DNA (Nijman, 2011; Ashworth & Lord 2018).

The phenomenon of synthetic lethality was verified experimentally almost 20 years ago in a pair of breakthrough publications by the Ashworth and Helleday labs, which demonstrated synthetic lethal interactions between PARP1 inhibition/knockdown and BRCA1/2 (Bryant et al., 2005; Farmer et al., 2005). It is widely believed that the selective cytotoxic effect of PARPi in BRCA1/2-deficient cells is predominantly caused by PARPi-induced trapping of PARPs such as PARP1 to DNA, rather than by a genetic alteration in PARP1 (see section 1.7.2), although this is commonly referred to as a synthetic lethal interaction (Murai et al., 2012).

Following the successful proof-of-concept experiments described above, olaparib (Lynparza) was granted clinical approval in 2014 for the treatment of ovarian cancers that harboured germline mutations in *BRCA* genes (Kaufman et al., 2015). Almost a decade later, additional PARPi have been granted clinical approval such as rucaparib, niraparib and talazopraib. At present, clinical trials have significantly widened the scope of the genetic background and type of cancers that can be treated by these PARPi, such as certain tumours that possess homologous recombination dysfunction but do not possess germline *BRCA* mutations – a condition known as ‘BRCAness’ (Bitler et al., 2017; Turner et al., 2004).

1.7.2 PARPi: How do they work?

Numerous hypotheses have been put forward to explain how PARPi elicits its cell-killing effects in *BRCA*-deficient cells. Initially, it was proposed that this synthetic lethal interaction arises because PARPi induces the accumulation of unresolved SSBs, which are transformed into DSBs subsequent to the impact of replication forks with SSBs. It was believed that in *BRCA*-proficient cells, the DSBs can undergo high-fidelity HR repair whereas in BRCA-deficient cells, the DSBs are repaired by alternative DSBR pathways that are more likely to induce error and result in cell death (Farmer et al., 2005). Yet, the validity of this model was contested by the following observations. Firstly, XRCC1 knockdown does not affect the viability of *BRCA2*-deficient cells (Patel et al., 2011). Secondly, there is no notable difference in the frequency of SSBs that arise in PARPi-exposed *BRCA*-deficient and *BRCA*-proficient cells, respectively (Gottipati et al., 2010). Thirdly, seminal work by the Pommier lab demonstrated that *PARP1*-null cells are less sensitive to PARPi relative to wild-type cells (Murai et al., 2012). Together, these findings indicate that the cell-killing effects of PARPi in *BRCA*-deficient cells may not solely be due to SSBR dysfunction.

Instead, the influential work by Murai et al. 2012 suggested that PARPi-dependent trapping of PARP1 to DNA is responsible for this synthetic lethal interaction, which challenged the previous model of PARPi action (Murai et al., 2012). Indeed, PARP1-DNA complexes are believed to induce fork stalling and in some cases, fork breakage (Dias et al., 2021). In BRCA-deficient cells, fork protection is impaired, further increasing the likelihood that stalled forks undergo aberrant nucleolytic processing, resulting in the accumulation of more cytotoxic seDSBs (Cong & Cantor, 2022). There are several additional experimental findings that support the model proposed by Murai

et al. 2012. Firstly, treatment of cells with a variety of PARPi's with approximately the same PARP1 catalytic inhibition ability revealed that the more potent a trapper of PARP1, the greater the cell-killing effects of a PARPi (Murai, Huang, et al., 2014b). The PARPi ranked in order of strongest to weakest PARP1 trapping ability are: 1. talazoparib, 2. Niraparib 3. olaparib and rucaparib 4. Veliparib (Lord & Ashworth, 2017; Murai et al., 2012; Murai, Huang, et al., 2014b). Secondly, loss of SPRTN – a gene that is thought to remove trapped PARP1 from DNA – considerably sensitises cells to talazoparib and olaparib, but not to veliparib (Saha et al., 2021). Thirdly, chemical inhibition of p97 – another factor believed to removed trapped PARP1 from DNA – further sensitises BRCA-deficient cells to talazoparib (Krastev et al., 2022). Fourthly, loss of Family with sequence similarity 111 member A (FAM111A) – a protease that promotes the progression of forks that meet PARP1-DNA complexes – further sensitises cells to the niraparib (Kojima et al., 2020).

Findings from *in vitro* studies suggested there are two key mechanisms by which PARPi traps PARP1 to DNA. Firstly, PARPi represses PARP1 catalytic inhibition by displacing NAD^+ within the catalytic pocket of PARP1, which prevents the PARP1-dependent autoPARylation required for release from DNA lesions (Lord & Ashworth, 2017). Secondly, by displacing NAD^+ within the catalytic pocket of PARP1, PARPi such as olaparib and talazoparib provoke pro-trapping allosteric changes in PARP1 conformation. However, PARPi-induced PARP1 catalytic inhibition, rather than allosteric changes is thought to be the principal factor in driving PARP1 trapping (Langelier et al., 2018; Xue et al., 2022; Zandarashvili et al., 2020). While the PARP1-trapping theory is widely accepted, a study presented findings which challenge this model. Indeed, the authors of the study claimed that numerous PARP1 molecules are

frequently substituted at DNA lesions and PARPi reduces the flux of the PARP1 exchange, forming longer-lasting PARP1 foci at these lesions, which can be mistaken for trapped PARP1 (Shao et al., 2020).

Recently, several lines of evidence support the notion that replication stress-induced ssDNA that accumulates as a consequence of PARP1 trapping and a reduction in Okazaki fragment maturation is a principal driver for PARPi cytotoxicity in *BRCA*-deficient backgrounds (Cong et al., 2021; Hanzlikova et al., 2018; Panzarino et al., 2021; Vaitsiankova et al., 2022). Following PARPi exposure, cells that are resistant to PARPi due to their ability to express functional BRCA, exhibit lower levels of ssDNA relative to cells that are sensitive to PARPi due to *BRCA* defects. This suggests that BRCA1 and BRCA2 contribute to the suppression of PARPi-induced ssDNA (Cong et al., 2021). While it is not clear precisely how ssDNA contributes to the cytotoxicity of PARPi in BRCA-deficient cells, it has been proposed that they are converted to cytotoxic DSBs in the subsequent cell cycle during DNA replication (Simoneau et al., 2021). On the other hand, it has also been suggested that PARPi-induced ssDNA alone induces cell death in BRCA-deficient cells and that apoptotic cell death is the cause of DSB formation (Panzarino et al., 2021).

It is important to note that it is unlikely that a single model can explain this synthetic lethal interaction in *BRCA*-deficient cells. Rather, it is conceivable that that PARPi elicits simultaneously all of the proposed effects described above, which together contribute to the synthetic lethal effect observed in BRCA-deficient cells.

1.7.3 PARPi resistance

In many instances, PARPi treatment acts as an effective short-term treatment for BRCA-deficient patients. However, inevitably, the majority of cancer sufferers receiving this treatment over longer durations develop PARPi-resistant disease (Dias et al., 2021). There are six main processes by which PARPi resistance can arise in cells. The first mechanism involves the reduction in the accrual of PARPi within the cell by increasing the cellular abundance of drug efflux transporters. Indeed, *BRCA1*-deficient and *BRCA2*-deficient breast cancer mouse models exposed to olaparib for protracted durations acquire PARPi resistance by upregulating the ATP binding cassette subfamily B member 1 (ABCB1) transporter. Furthermore, following acquisition of PARPi-resistance, exposure of both of these mouse models to tariquidar – an ABCB1 inhibitor – re-sensitised their tumours to olaparib (Jaspers et al., 2015; Rottenberg et al., 2008). The second mechanism involves the acquisition of mutations that thwart PARP1 trapping. In support of this notion, a PARPi-resistant ovarian cancer sufferer was shown to possess a *PARP1* mutation within the WGR domain that was predicted to prevent PARP1 trapping to DNA in *BRCA1*-mutated cells (Pettitt et al., 2018). The third mechanism, which was first observed in a *BRCA2*-deficient pancreatic cancer cell models is mediated by the acquisition of 'reversion mutations' within *BRCA*-deficient cells that permit hypomorphic or wild type BRCA1/2 expression. Following exposure to olaparib, *BRCA1*-deficient patient-derived xenograft (PDX) mouse models acquired secondary *BRCA1* mutations which re-established the *BRCA1* open reading frame, enabling the expression of functional *BRCA1*. Additionally, hypermethylation of the *BRCA1* promoter represses BRCA1 expression. Exposure of the same PDX model to olaparib resulted in the acquisition of secondary mutations that prevented *BRCA1* promoter methylation which consequently restored

BRCA1 expression (Edwards et al., 2008; Esteller et al., 2000; ter Brugge et al., 2016). The fourth mechanism involves the re-establishment of HR in *BRCA1*-deficient cells. Indeed, deletion of 53BP1 in *BRCA1*-deficient mouse and human models induces PARPi resistance by re-instating resection (Bouwman et al., 2010; Bunting et al., 2010). In this genetic background, HR-dependent resection is re-established by the ubiquitylation of histone H2A, which promotes the localisation of PALB2 to resected DNA at DSBs, allowing RAD51 loading to ensue (Luijsterburg et al., 2017; Zong et al., 2019). Similarly, mutations within members of the shieldin complex re-establishes HR-dependent resection in *BRCA1*-deficient human cell lines (Dev et al., 2018; Gupta et al., 2018; Noordermeer et al., 2018). The fifth mechanism involves the re-establishment of fork stability in cells deficient in *BRCA1*/2 which prevents the accumulation of cytotoxic seDSBs. MUS81-dependent degradation of stalled forks is averted by loss of EZH2 in *BRCA2*-deficient cells, which thwarts the localisation of MUS81 to these structures (Rondinelli et al., 2017). Similarly, deletion of *PTIP* in *BRCA2*-deficient mouse models results in PARPi resistance as in this genetic background, the PTIP-dependent localisation of MRE11 to these structures is diminished, which reduces MRE11-dependent fork degradation (Ray Chaudhuri et al., 2016). The sixth mechanism involves the acquired resistance of BRCA-deficient cells to PARPi-induced ssDNA, although the precise mechanisms through which this can occur are currently under investigation (Cong et al., 2021; Panzarino et al., 2021).

1.8 Aims

It is well established that PARP1 and PARP2 participate in the repair of MMS-induced DNA damage. However, whether other PARPs facilitate the repair of this damage in the absence of PARP1 and PARP2 is yet to be defined. Additionally, although our understanding of the DNA replication stress response continues to improve, factors that function within this response continue to be discovered. Therefore, it is likely that there are numerous DNA replication stress response proteins that are yet to be revealed.

In this thesis, I aimed to explore the following. Firstly, to determine whether in cells lacking both PARP1 and PARP2, other PARPs participate in the repair of MMS-induced DNA damage. Secondly, to identify novel DDR factors by determining whether any uncharacterised genes are synthetic lethal with combined loss of PARP1 and PARP2. Thirdly, to characterise these DDR protein-coding genes and to determine whether the novel DDR factors participate in the DNA replication stress response.

Chapter 2. Materials and Methods

2.1 Materials

2.1.1 Buffers

Phosphate Buffered Saline pH 7.4 (PBS):

2.7 mM KCl

10 mM phosphate buffer

137 mM NaCl

PBS including 0.2% Triton X-100:

2.7 mM KCl

10 mM phosphate buffer

137 mM NaCl

0.2% Triton X-100

PBS including 0.01% Tween-20

2.7 mM KCl

10 mM phosphate buffer

137 mM NaCl

0.01% Tween-20

Tris-Buffered Saline (TBS-T) pH 7.4

137 mM NaCl

2.48 mM Tris-Cl

10X Tris-Glycine SDS Running Buffer:

192 mM glycine

0.1% SDS

25 mM Tris-Cl

Triton X-100 buffer:

50 mM Tris-HCl pH 8

100 mM NaCl

1% Triton X-100

Immediately before use for whole cell extracts, the Triton X-100 buffer was supplemented with the following additives:

5mM NEM

1mM DDT

Protease Inhibitor Cocktail (Sigma-Aldrich)

1 mM NaF

10 mM β-glycerophosphate

0.1 mM Sodium orthovanadate

Buffer A

Protease Inhibitor Cocktail (Sigma-Aldrich)

10% glycerol

1.5 mM $MgCl_2$

0.34 M sucrose

10 mM KCl

Buffer B

Protease Inhibitor Cocktail (Sigma-Aldrich)

0.2 mM EGTA

3 mM EDTA

4X SDS-PAGE loading buffer:

40% glycerol

200 mM Tris-Cl pH 6.8

0.4% bromophenol blue

400 mM DTT

8% SDS

Click-iT® Reaction Cocktail

1X Click-iT® reaction buffer

Click-iT® reaction buffer additive

$CuSO_4$

Alexa Fluor® Azide

2.2 Methods

2.2.1 Cell Culture

U2OS cell lines were cultured in Dulbecco's Modified Eagle Media (DMEM) (Thermo Fisher Scientific) including 1% GlutaMAX (Thermo Fisher Scientific) and 10% Foetal Bovine Serum (FBS) (Thermo Fisher Scientific). U2OS cell lines were grown in T-75 flasks (Corning) in 20 ml of cell culture media. T-75 flasks were kept in an incubator (Thermo Fisher Scientific) set to conditions of 5% CO_2 and 37°C.

2.2.2 Clonogenic Survival Assay

Cells were detached from T-75 flasks with TrypLE Express (1X) (Thermo Fisher Scientific) and counted with an automated cell counter (DeNovix). Individual wells of 6-well plates were each seeded with 400 cells. The following day, cells were treated with genotoxins or DNA damage repair inhibitors (DDRi). In the instances where cells were treated with both MMS (Sigma-Aldrich) and olaparib (AZD2281) (Cambridge Bioscience), cells were pre-incubated with olaparib for 1 h and subsequently treated with MMS for an additional hour. In instances where cells were treated with MMS alone, cells were pre-incubated with vehicle (DMSO) (Sigma-Aldrich) for 1 h. Cells were treated with hydroxyurea (HU) (Sigma-Aldrich), aphidicolin (APH) (Sigma Aldrich) or WEE1 inhibitor (WEE1i) (AZD1775) (AstraZeneca) for 24 h, or with ATRi (AZD6738) (Selleck Chemicals) for 48 h or for 9 days (constant exposure). In the instances where cells were treated with any of the above compounds for 24 h or 48 h, following treatment, cells were washed twice with PBS and replenished in fresh growth media. At 9-14 days post-treatment, cells were washed twice with PBS and fixed in ice-cold methanol at -20°C for 20 min. Subsequently, cells were stained with 0.5%

crystal violet (Sigma-Aldrich) at room temperature for 20 min. Following treatment of cells with ATRi for 9 days, cells were fixed and stained as described previously. Finally, 6-well plates were rinsed with water and dried. The ability of cells to form colonies in response to a particular treatment was analysed. A colony was considered to be a group of 50 cells or more.

2.2.3 Immunofluorescence

2.2.3.1 EdU labelling

Cells were detached from T-75 flasks following incubation of cells with TrypLE Express (1X) (Gibco). Cells were counted using an automated cell counter (DeNovix) and $2x10^5$ cells suspended in growth media were seeded onto four 13 mm glass cover slips placed in each well of 6-well plates. The following morning, cells were labelled with of 5-ethynyl-2'-deoxyuridine (EdU) by treating cells with 10 μM EdU (Invitrogen) for 1 h. Cover slips were washed twice with PBS and fixed in PBS including 3.7% formaldehyde for 15 min at 22°C. Subsequently, the fixing agent was removed, and cover slips were washed twice with PBS including 3% BSA. Cells were permeabilised by treating cover slips with PBS including 0.5% Triton X-100 for 20 min at 22°C. Consequently, the permeabilising agent was removed from the cells, and cover slips were washed twice with PBS including 3% BSA. The cells were then treated with Click-iT® reaction cocktail for 30 min at 22°C and kept in dark conditions. After, the reaction cocktail was removed from the cells and cover slips were washed with PBS including 3% BSA. Nuclei were stained by incubating cover slips with growth media including

0.01% DAPI for 1 h at 22°C. Finally, cover slips were washed with Milli-Q water; left to dry for 1 h at 22°C; and mounted onto microscope slides with Mowiol (Sigma-Aldrich).

2.2.3.2 Labelling of γH2AX, RPA70, 53BP1 and cyclin A

Cells were detached from T-75 flasks with TrypLE Express (1X) (Gibco); counted with an automated cell counter; and seeded onto cover slips as described above. The next day, cells were treated with DNA damaging agents as follows. In instances where the frequency of G_1-phase 53BP1 nuclear bodies per nucleus and mean cyclin A intensity per nucleus were analysed, cells were treated with the vehicle dimethyl sulfoxide (DMSO) for 1 min or 0.2 μM APH for 24 h. In instances where only mean γH2AX intensity was quantified, cells were treated with vehicle (Milli-Q water) for 1 min, with 200 μM HU for 24 h, or with 200 μM HU for 24 h followed by a 6 h recovery in fresh growth media. In instances where both mean γH2AX intensity and mean RPA70 intensity were analysed, cells were treated with vehicle (Milli-Q water) for 1 min, or with 2 mM HU for 2 h, 8 h and 24 h. When required, cells were washed 3 times with cold (4°C) PBS and were subsequently pre-extracted by treating the cover slips with cold PBS including 0.2% Triton X-100 for 5 min. Next, in all instances, the cover slips were washed 3 times with cold PBS; fixed in 4% formaldehyde for 15 min at 22°C; and subsequently washed 3 times in cold PBS. Following fixation, cells were permeabilised with cold PBS including 0.2% Triton X-100 for 5 min and then washed three times with cold PBS. Next, cover slips were incubated with growth media including the required primary antibodies for 2 h at 22°C. Cover slips were then washed four times with cold PBS including 0.01% Tween-20. Next, cover slips were incubated with growth media including the required secondary antibodies and DAPI (1:10,000) for 1 h and were

then washed four times with cold PBS including 0.01% Tween-20. Finally, cover slips were dried and mounted with Mowiol onto microscope slides as described above.

2.2.3.3 QIBC

Images of cells were captured for QIBC analysis on the ScanR IX-83 inverted microscope (Olympus) using the ScanR Acquisition Software (Olympus). The microscope was fitted with a fast emission filter wheel for DAPI, TRITC, Cy5 and FITC excitation/emission wavelengths and an ORCA-Fusion BT Digital CMOS camera (Hamamatsu). All images were acquired using the UPLSAPO 20X objective (Olympus). Using the ScanR Acquisition Software, individual nuclei were detected via the DAPI signal. Next, with the same software, frequency of G_1-phase 53BP1 nuclear bodies per nucleus (FITC), mean nuclear intensity of γH2AX (FITC), RPA70 (TRITC), cyclin A (TRITC) and EdU (Cy3) were detected where appropriate. Finally, data were visualised on scattered plots with Prism (GraphPad) or with jittered scatter plots with Spotfire (TIBCO).

2.3 Preparation of whole cell extracts

Cells were detached from T-75 flasks (Sigma Aldrich) using TrypLE Express (1X) (Gibco) and counted with an automated cell counter (DeNovix) as described above. 10 cm tissue culture-treated dishes (Greiner Bio-One) were seeded with $2x10^6$ cells. In instances where levels of pCHK1 (Ser317), pDNA-PK_{cs} (Ser2056), γH2AX (Ser139) and pRPA (Ser4/Ser8) were analysed, cells were treated with vehicle (Milli-Q water) for 1 min or with 2 mM HU for 1 h, 2 h, 8 h or 24 h. In instances where cellular levels

of C16orf72-FLAG-HA protein were analysed, cells were treated with vehicle (Milli-Q water) for 1 min or with 2 mM HU for 24 h. When preparing whole cell extracts, harvested cells were washed 3 times in cold PBS and were treated with Triton X-100 lysis buffer. Lysate was rotated for 20 min at 4°C and was centrifuged (13,000 x *g*) for 10 min at 4°C. The concentration of the clarified protein lysate was analysed by Bio-Rad Protein Assay Dye (Bio-Rad) by following the manufacturer's protocol. 4X NuPAGE LDS sample buffer (Thermo Fischer Scientific) was added to an appropriate volume of each clarified protein lysate to ensure that all protein samples within an experiment contained the same concentration of protein and samples were boiled for 5 min at 95°C.

2.4 Chromatin fractionation

As described previously, cells were detached from T-75 flasks following treatment with TrypLE Express (1X) (Gibco) and counted with an automated cell counter (DeNovix). 20 cm tissue culture-treated dishes (Greiner Bio-One) were each seeded with $3x10^6$ cells. The following day, cells were exposed to vehicle (DMSO), 2 mM HU, 1 μM ATRi, or ATRi in combination with HU for 24 h. Harvested cells were washed 3 times in cold PBS and counted with an automated cell counter (DeNovix). $4x10^6$ cells from each sample were resuspended in Buffer A including Triton X-100 (0.01%) and kept for 1 min at 4°C. Samples were centrifuged (1,300 x *g*) for 5 min at 4°C and the supernatant (cytosolic fraction) was removed, leaving the pellet (nuclei) behind. The pellets (nuclei) were washed with Buffer A and centrifuged (1,300 x *g*) for 5 min at 4°C. Nuclei were resuspended in Buffer A and kept at 4°C for 30 min. Throughout the incubation time, samples were vortexed every 5 min. Next, samples were centrifuged (1,300 x *g*) for 5

min at 4°C. The supernatants (nuclear protein fractions) were removed, and the pellets (chromatin protein fractions) were washed with buffer B. Samples were centrifuged (1,300 x *g*) for 5 min at 4°C and supernatants were discarded. Pellets were resuspended in 1X SDS-PAGE loading buffer (diluted to 1X) and samples were boiled for 5 min at 95°C.

2.5 Western Blotting

Proteins were separated in cell extracts with SDS-PAGE by loading samples into Invitrogen NuPAGE Bis-Tris 4-12% (Thermo Fisher Scientific) protein gels or in Invitrogen NuPAGE Bis-Tris 8% protein gels (Thermo Fisher Scientific). The gels were run at 140 V for 1.5 h in 1 X NuPAGE MOPS SDS Running Buffer (Thermo Fisher Scientific), 1 X NuPAGE MES SDS Running Buffer (Thermo Fisher Scientific) or 1 X Tris-Glycine SDS Running Buffer. The mass of 10-250 kDa proteins was analysed with the PageRuler Plus Prestained Protein Ladder (Thermo Fisher Scientific) or SeeBlue Plus2 Pre-strained Protein Standard (Thermo Fisher Scientific), whereas proteins with a mass of 250-460 kDa were analysed with the HiMark Prestained Protein Standard (Thermo Fisher Scientific). The proteins were transferred from the gel to a PVDF membrane with a Trans-Blot Turbo Midi PVDF transfer pack (BioRad) and the semi-dry Trans-Blot Turbo Transfer System (BioRad), as described by the manufacturer's protocol. Next, the PVDF membrane was blocked for 1 h in TBS-T including 5% milk and the blocked PVDF membrane was incubated overnight in TBS-T including 5% milk and the required primary antibodies. The following day, the PVDF membrane was washed 3 times in TBS-T and incubated in TBS-T including 5% milk and the required secondary antibodies. Subsequently, the PVDF membrane was

washed 3 times in TBS-T and exposed to Pierce ECL Western Blotting Substrate (Thermo Fisher Scientific). Finally, proteins levels were detected on autoradiography film (GE Healthcare).

2.6 Antibodies

The primary antibodies that were utilised in this study were:

Antibody	Host and Type	Dilution (IF)	Dilution (WB)	Source
PARP6	Rabbit polyclonal	-	1:1000	GeneTex (GTX122488)
pDNA-PKcs (Ser2056)	Rabbit monoclonal	-	1:2000	Abcam (ab124918)
DNA-PKcs	Rabbit monoclonal	-	1:1000	Abcam (ab32566)
pCHK1 (Ser317)	Rabbit monoclonal	-	1:1000	Cell Signalling (D12H3)
CHK1	Mouse monoclonal	-	1:1000	Cell Signalling (2G1D5)
pRPA32 (Ser4/Ser8)	Rabbit polyclonal	-	1:1000	Bethyl (A300-245A)
RPA32	Rabbit polyclonal	-	1:5000	Bethyl (A300-244A)
RPA70	Rabbit monoclonal	1:1000	-	Abcam (ab79398)

γH2AX (Ser319)	Mouse monoclonal	1:500	-	Biolegend (613402)
γH2AX (Ser319)	Rabbit polyclonal	-	1:2000	Abcam (ab11174)
p53-HRP conjugate	Mouse monoclonal	-	1:500	Santa Cruz (sc-126-HRP)
Vinculin-HRP conjugate	Mouse monoclonal	-	1:1000	Santa Cruz (sc-73614-HRP)
β-Actin	Mouse monoclonal	-	1:5000	Santa Cruz (sc-47778)
HA	Rabbit monoclonal	-	1:1000	Cell signalling (#3724)
53BP1	Rabbit polyclonal	1:500	-	Novus Biologicals (NB100-305)
Cyclin A	Rabbit polyclonal	1:250	-	Santa Cruz (sc-751)
H3	Goat polyclonal	-	1:10000	Abcam (ab12079)
C16orf72	Rabbit polyclonal	-	1:1000	Eurogentech (Custom antibody)

Table 2.1: Primary antibodies utilised in this study.

The secondary antibodies that were utilised in this study were:

Antibody	Host and Type	Dilution (IF)	Dilution (WB)	Source
Anti-mouse Alexa Fluor 488-conjugate	Goat polyclonal	1:500	-	Thermo Fisher Scientific (A-11001)
Anti-rabbit Alexa Fluor 555-conjugate	Donkey polyclonal	1:500	-	Thermo Fisher Scientific (A-21206)
Anti-rabbit HRP-conjugate	Donkey polyclonal	1:500	-	Jackson ImmunoResearch 715-035-150
Anti-mouse HRP-conjugate	Donkey polyclonal	-	1:2000	Jackson ImmunoResearch 715-035-151
Anti-goat HRP-conjugate	Rabbit polyclonal	1:10,000	-	DAKO (P0449)

Table 2.2: Secondary antibodies utilised in this study.

2.7 siRNA transfections

The day before transfection, $3x10^5$ cells were seeded into wells of 6-well plates (Greiner Bio-One). Using Dharmafect-1 (Horizon) cells were twice transfected (24 h for each transfection) with ON-TARGET plus Non-targeting pool siRNA (Horizon); with ON-TARGET plus siRNA SMARTpool targeting PARP3-16 or C16orf72; or with four

individual ON-TARGET plus siRNAs targeting C16orf72 by following the manufacturer's protocol. Subsequently, the transfected cells were left to recover in fresh growth media for 24 h, after which, they were suitable for use in experiments. The ON-TARGET plus siRNA SMARTpools each consisted of four distinct siRNAs that targeted the same gene for depletion.

2.8 siRNAs

The siRNAs that were utilised in this study were:

ON-TARGET plus siRNA	Dharmacon Catalogue Number
PARP3 SMARTpool	L-009297-00-0005
PARP4 SMARTpool	L-007244-00-0005
PARP5a SMARTpool	L-004740-00-0005
PARP5b SMARTpool	L-004741-00-0005
PARP6 SMARTpool	L-013797-00-0005
PARP7 SMARTpool	L-013948-00-0005
PARP8 SMARTpool	L-015784-03-0005
PARP9 SMARTpool	L-014734-00-0005
PARP10 SMARTpool	L-014997-00-0005

PARP11 SMARTpool	L-016115-00-0005
PARP12 SMARTpool	L-013740-00-0005
PARP13 SMARTpool	L-017449-01-0005
PARP14 SMARTpool	L-023583-00-0005
PARP15 SMARTpool	L-017186-00-0005
PARP16 SMARTpool	L-020837-00-0005
C16orf72 SMARTpool	L-031072-00-0005
C16orf72 siRNA #1	J-031072-05
C16orf72 siRNA #2	J-031072-06
C16orf72 siRNA #3	J-031072-07
C16orf72 siRNA #4	J-031072-08
Non-targeting pool (control)	D-001810-10-05

Table 2.3: siRNAs utilised in this study.

2.9 Genome-wide CRISPR Dropout Screen

$1.5x10^8$ wild type U2OS and *PARP1ΔPARP2Δ* cells were grown in growth media in two separate T-175 flasks (Sigma Aldrich). As outlined previously, cells were detached from T-175 flasks with TrypLE Express (1X) (Gibco) and counted with an automated

cell counter (DeNovix). To the detached cells suspended in growth media, polybrene (8 µg/ml) (Sigma Aldrich) was added to lentivirus including the Toronto KnockOut version 3 (TKOv3) sgRNA library (Addgene) (MOI = 0.3). Subsequently, the virus-cell-growth media combination was plated onto 15 cm tissue culture-treated plates (Greiner Bio-One) and incubated for 24 h. Next, the virus-cell-growth media combination was removed from the 15 cm plates, replaced with fresh growth media and the cells were incubated for 24 h. Subsequently, cells were replenished with growth media including puromycin (20 µg/ml) and were incubated for 24 h. The following day, cells were replenished with growth media including the same concentration of puromycin and incubated for 24 h. The next day (T = 0 days), cells were detached from 15 cm plates with TrypLE Express (1X) and counted using an automated cell counter as described previously. $4x10^7$ cells of each cell line in growth media were evenly distributed across four 50 ml conical tubes. The cells were centrifuged at 500 x *g* for 5 min and each pellet was washed with warm PBS. Subsequently, the cells were transferred to 15 ml centrifuge tubes (Thermo Fisher Scientific) and were centrifuged again as before. Consequently, the PBS was removed from the pellets with an aspirator; the dry pellets were snap frozen in liquid nitrogen; and the pellets were stored at -80°C. The remainder of the cells from each cell line were plated onto 15 cm plates in growth media and incubated for 24 h. The following day, cells were detached from the plates and counted using an automated cell counter as described before. $1.5x10^8$ cells of each cell line were seeded onto 15 cm plates in growth media and incubated for 24 h. The previous step was repeated every 3 days until T=18 days and T=24 days in the wild type U2OS and *PARP1ΔPARP2Δ* cell lines, respectively. At these time points, cell pellets were snap frozen and stored at -80°C as described previously. QIAGEN Ribonuclease A and the QIAamp DNA Blood Maxi

Kit were used to extract and precipitate genomic DNA from the cell pellets by following the manufacturer's protocol. Next, sgRNAs that integrated into the genome were amplified by two-step PCR amplification and the amplified gRNAs were sequenced by Illumina Next-Generation Sequencing. Finally, the MaGeCK pipeline was used to reveal gene hits (False Discovery Rate (FDR) < 0.01).

2.10 High-throughput Combination Assay

Each of the wells of black clear-bottom 384 well microplates (Greiner Bio-One) were seeded with 500 cells in growth media using a multi-channel pipette (Thermo Fisher Scientific). The following day, with an Echo 555 Liquid Handler (LabCyte) cells were exposed for 5 days to a 6x6 compound concentration matrix of AZD6738 (ATRi) (0, 0.032, 0.1, 0.357, 1.071, 3.214 μM) and AZD1390 (ATMi) (0, 0.003214, 0.01, 0.036, 0.017, 0.321 μM). On the same day, for each cell line, CellTitre Glo 2.0 reagent (Promega) was added to wells of a microplate including untreated cells (control microplate) and the live cell count of the cells was analysed by quantifying the mean luminescence of the cells with a SpectraMax i3x microplate reader (Molecular Devices). Following exposure of the cells to the ATRi-ATMi concentration matrix, the live cell count of the cells were analysed as described previously. By comparing the live cell count from the treated microplates with the live cell count from their respective control microplates, the GeneData Screener software was used to calculate the experimental activity (% growth inhibition) and synergy score for each ATRi-ATMi concentration combination. Synergy scores were calculated by comparing experimental activity scores to the Highest Single Agent (HSA) additivity model.

2.11 Statistical Analysis

Statistical significance was evaluated by One-Way ANOVA with Bonferroni's post hoc analysis; Two-Way ANOVA; Two-Way ANOVA with Tukey's post hoc analysis;; or Student's t-test. Prism 9 (GraphPad) software was used to perform these statistical analyses. In all statistical analyses, p-values are signified by, ns, not significant; * $p < 0.05$, ** $p < 0.01$; *** $p < 0.001$; **** $p < 0.0001$.

Chapter 3. Determining whether a PARP participates in the repair of MMS-induced DNA damage in cells lacking PARP1 and PARP2

3.1 Introduction

3.1.1 Alkylation base damage increases PARPi toxicity

In wild-type chicken DT40 bursal lymphoma cells, the alkylating agent MMS increases the toxicity of olaparib (Baba et al., 1985; Murai et al., 2012; Winding & Berchtold, 2001). As an intermediary step in the BER pathway, it is generally thought that alkylation base damage induced by MMS is processed by APE1 into SSBs that possess a 5'dRP end. These 5'dRP groups act as PARP1 substrate, which causes PARP1 to be localised to the SSBs and stimulates the repair of this damage (Cistulli et al., 2004). Therefore, a commonly held view that I am also in agreement with, is that following generation of alkylating agent induced-SSBs, olaparib traps PARP1 to DNA, forming high levels of cytotoxic PARP1-DNA lesions (Murai et al., 2012, 2014a, 2014b).

3.1.2 A PARP may participate in the repair of MMS-induced DNA damage in cells lacking PARP1 and PARP2

Previously, the Lakin lab demonstrated that PARP1 and PARP2 have functional redundancy in the repair of MMS-induced DNA damage. Indeed, PARP1 and PARP2 are thought to partake in intersecting roles in two DDR pathways to repair this form of DNA damage. The first DDR pathway is BER, although the precise role(s) shared by

these PARPs in this pathway are not yet clear. The second DDR pathway is the DNA replication stress response, in which PARP1 and PARP2 stimulate the HR-mediated stabilisation/repair of replication forks that are stalled/damaged after meeting incompletely resolved products of BER. Together, these PARPs perform this role by counteracting the FBH1-dependent dissolution of RAD51 filaments at these stalled/damaged replication forks (Chu et al., 2015; Fugger et al., 2009; Ronson et al., 2018; Simandlova et al., 2013). The Lakin lab also showed that olaparib treatment results in additional sensitisation of *PARP1ΔPARP2Δ* cells to MMS (Figure 3.1) (Ronson, 2017). This observation suggested that olaparib may elicit an effect on another PARP that may participate in the repair of MMS-induced DNA damage in cells lacking PARP1 and PARP2 (see sections 3.2.1 and 3.2.2). However, to date, a PARP that performs this function has not yet been identified.

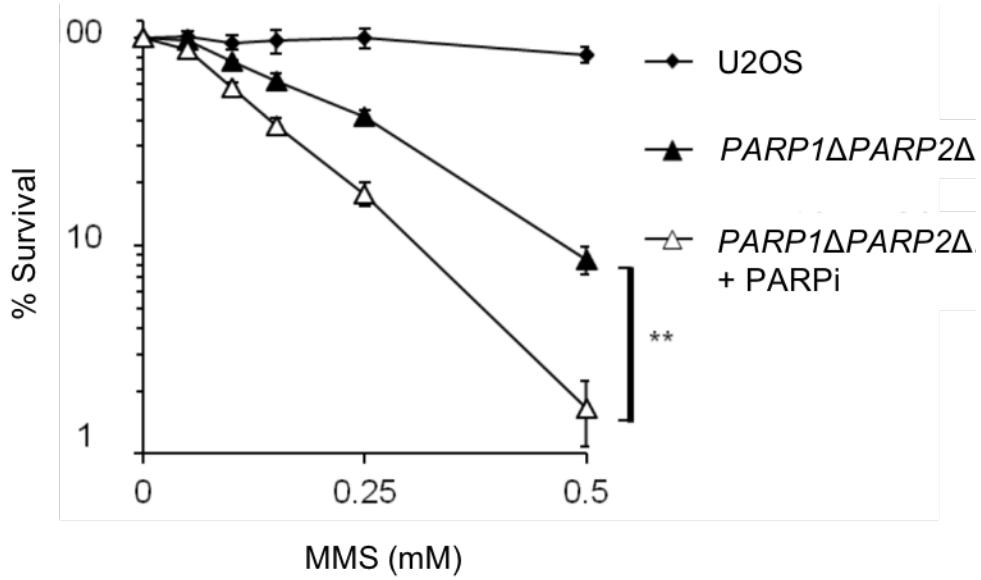


Figure 3.1: Another PARP may participate in the repair of MMS-induced DNA damage in cells lacking PARP1 and PARP2. Wild type U2OS and *PARP1ΔPARP2Δ* cells were treated with MMS in the presence or absence of olaparib (10 μM) and their ability to form colonies was analysed via clonogenic survival assay. Error bars at each

data point represent the standard error of the mean from three separate biological replicates. The statistical significance between relevant conditions was evaluated by two-way ANOVA. The experiment and data presented in this figure was produced by Dr George Ronson. Figure adapted from Ronson, 2017.

3.1.3 Aims

While the roles of PARP1 and PARP2 in the repair of MMS-induced DNA damage have been subject to investigation, whether or not another PARP is involved in the repair of this form of DNA damage in *PARP1ΔPARP2Δ* cells is not yet clear. Therefore, the aim of this chapter is to determine whether a PARP participates in the repair of MMS-induced DNA damage in cells lacking PARP1 and PARP2.

3.2 Results

3.2.1 Chemical proteomic approach to investigate the olaparib selectivity profile in *PARP1ΔPARP2Δ* cells

I hypothesised that the olaparib-mediated further sensitisation of *PARP1ΔPARP2Δ* cells to MMS may be due to the effect of a strong interaction between olaparib and a PARP that may participate in the repair of MMS-induced DNA damage in cells lacking PARP1 and PARP2. This hypothesis is based on the assumption that a single PARP, rather than multiple PARPs, may participate in the repair of MMS-induced DNA damage in cells lacking PARP1 and PARP2. To explore this hypothesis, a mass spectrometry-based chemical proteomic assay was performed in collaboration with AstraZeneca, in which the competition profile of olaparib was assessed in the lysate

of *PARP1ΔPARP2Δ* cells (Figure 3.2 and 3.3 a-b). The *PARP1ΔPARP2Δ* cells were generated by Dr George Ronson by using a pair of Cas9 nickases (SSB-inducing) with gRNAs (guide RNAs) that targeted distinct *PARP1* loci that were in close proximity, to generate a DSB and subsequently, frameshift indel mutations in *PARP1*. Consequently, the same approach was taken in *PARP1Δ* cells to disrupt *PARP2* expression, thereby generating *PARP1ΔPARP2Δ* cells. This cell line was validated by western blot (using antibodies specific to PARP1 and PARP2) and PCR (Ronson et al., 2017). As a positive control, the competition profile of olaparib was also assessed in the lysate of wild type U2OS cells. In decreasing order of selectivity, in wild type U2OS cells lysates, olaparib was selective for PARP1, 2, 3, 4 and 10. This selectivity profile was similar to previous reports, which indicates that the assay worked as expected in the lysates of wild type U2OS cells (Thorsell et al., 2017; Wahlberg et al., 2012). The olaparib selectivity profile in lysates of *PARP1ΔPARP2Δ* cells in decreasing order of selectivity was PARP1, 2, 3, 4, and 10. It was surprising that peptides of PARP1 and PARP2 were detected in the *PARP1ΔPARP2Δ* cells, as this observation raised the possibility that either the *PARP1ΔPARP2Δ* cell line may not be a full CRISPR double-knockout or there may have been cross-contamination between the wild type U2OS and *PARP1ΔPARP2Δ* lysates when performing the LC-MS/MS analysis. To investigate these possibilities further, lysates from the wild type U2OS and *PARP1ΔPARP2Δ* cell lines were analysed for the presence of PARP1 and PARP2 via mass spectrometry in collaboration with Dr Sabrina Liberatori and Dr Shabaz Mohammed at the Advanced Proteomics Facility, University of Oxford (Figure 3.3 c). No unique peptides for PARP1 or PARP2 were identified in the *PARP1ΔPARP2Δ* cell line, which is consistent with previous validation of this cell line (Ronson et al., 2018). Therefore, these data suggest that the *PARP1ΔPARP2Δ* cell line is a full double-

knockout, which supports the notion that the *PARP1ΔPARP2Δ* lysates from the chemical proteomics assay may have been cross-contaminated with wild type U2OS lysate. Overall, it was not possible to determine the identities of novel PARPs that may participate in the repair of MMS-induced DNA damage. From here, additional independent repeats of this experimental approach will be required to further characterise the binding profile of olaparib in *PARP1ΔPARP2Δ* cells, in order to identify candidates for the PARP that may participate in the repair of MMS-induced DNA damage in cells lacking PARP1 and PARP2.

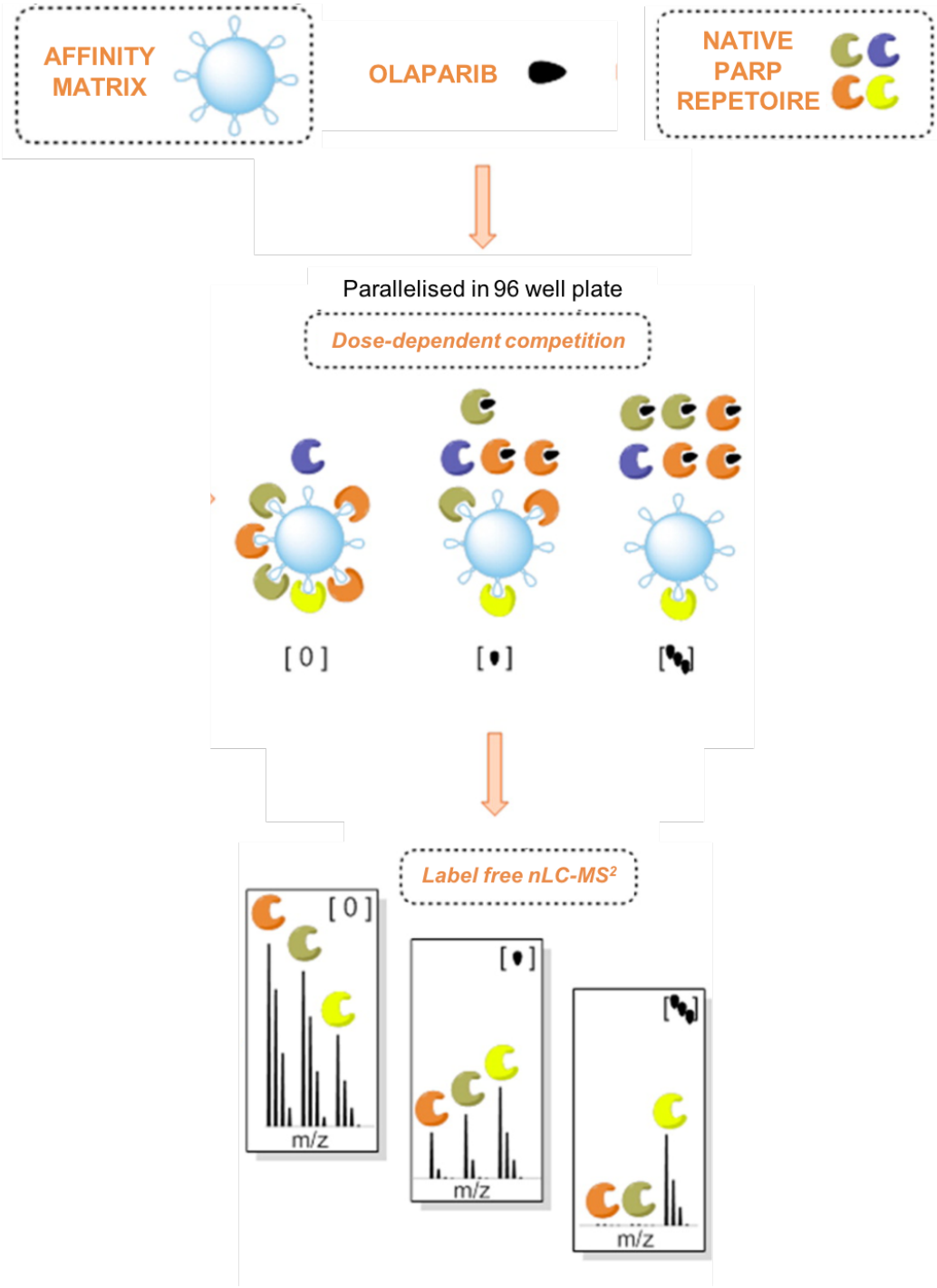
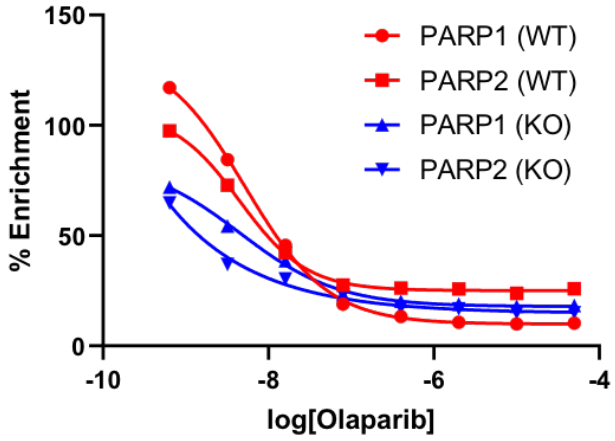

AFFINITY MATRIX
OLAPARIB
NATIVE PARP REPETOIRE
Parallelised in 96 well plate
Dose-dependent competition
[0]
[•]
[••]
Label free nLC-MS²
[0]
[•]
[••]
m/z
m/z
m/z

Figure 3.2: Chemical proteomic assay workflow.

A competition affinity pulldown was performed to investigate the olaparib selectivity profile in cells lacking PARP1 and PARP2. Wild type U2OS and *PARP1ΔPARP2Δ* cell pellets were lysed and the lysate was incubated with increasing concentrations of olaparib. The lysates were subsequently incubated with an affinity matrix consisting of pan-PARP inhibitor (undisclosed) bound to Sepharose beads. Finally, analysis of the PARPs that were enriched on the affinity matrix was performed by Nano Liquid Chromatography with tandem mass spectrometry (nLC-MS/MS). PARPs that bind strongly to olaparib are not enriched on the affinity matrix. These data were analysed to provide dose-dependent binding inhibition curves for olaparib in wild type U2OS and *PARP1ΔPARP2Δ* cells (Médard et al., 2015). Figure adapted from Médard et al., 2015.

a



b

PARP	WT Kd (nM)	Knockout Kd (nM)	Peptide spectral match (WT)	Peptide spectral match (KO)
1	0.3	0.7	***692***	***18***
2	0.9	0.025	***68***	***4***
3	43.1	15.4	12	10
4	588.7	990.2	124	110
10	16240	9754	81	75

c

Gene name	PARP1	PARP2
Mol. weight [kDa]	113.08	64.804
Sequence length	1014	570
Peptides in *parp1Δparp2Δ*	0	0
Peptides in U2OS wild-type	30	3
Unique peptides in *parp1Δparp2Δ*	0	0
Unique peptides in U2OS wild-type	30	3
Sequence coverage *parp1Δparp2Δ* [%]	0	0
Sequence coverage U2OS wild-type [%]	38.5	7
Intensity	5.57E+09	5.23E+07
Intensity *parp1Δparp2Δ*	0.00E+00	0.00E+00
Intensity U2OS wild-type	5.57E+09	5.23E+07

Figure 3.3: Chemical proteomic study suggests that PARP1 and PARP2 are present in *PARP1ΔPARP2Δ* cells. (a) A competition affinity pulldown was performed on wild type U2OS and *PARP1ΔPARP2Δ* lysates. The percentage enrichment of PARP1 and PARP2 on the affinity matrix is indicated for wild type U2OS (red line) and *PARP1ΔPARP2Δ* (blue line) cell lysates. **(b)** Table summarising the olaparib selectivity profile in wild type U2OS and *PARP1ΔPARP2Δ* cell lysates. A lower apparent K_d indicates a greater affinity of olaparib for a given PARP. **(c)** Table summarising internal mass-spectrometry analysis to validate the *PARP1ΔPARP2Δ* cell line. Experiments in **(a)** and **(b)** were performed in collaboration with AstraZeneca. Experiment **(c)** was performed in collaboration with the Advanced Proteomics Facility, University of Oxford. WT – Wild type U2OS cell line, KO – *PARP1ΔPARP2Δ* cell line.

3.2.2 PARP depletion screens to determine whether an additional PARP participates in the repair of MMS-induced DNA damage in cells lacking PARP1 and PARP2

When the clonogenic survival assays in this chapter were performed, the statistical significance between multiple pairs of observations within the same experiment was evaluated by two-way ANOVA – a method of statistical analysis that was accepted in peer-reviewed publications at the time (Ronson et al., 2018). The findings from these statistical analyses were used as the rationale for subsequent experiments in this chapter. However, four years later, it has since become standard practice to evaluate the statistical significance between multiple pairs of observations within the same experiment by two-way ANOVA with Tukey's post hoc analysis (Demin et al., 2021). Therefore, I have evaluated the statistical significance of multiple observations within

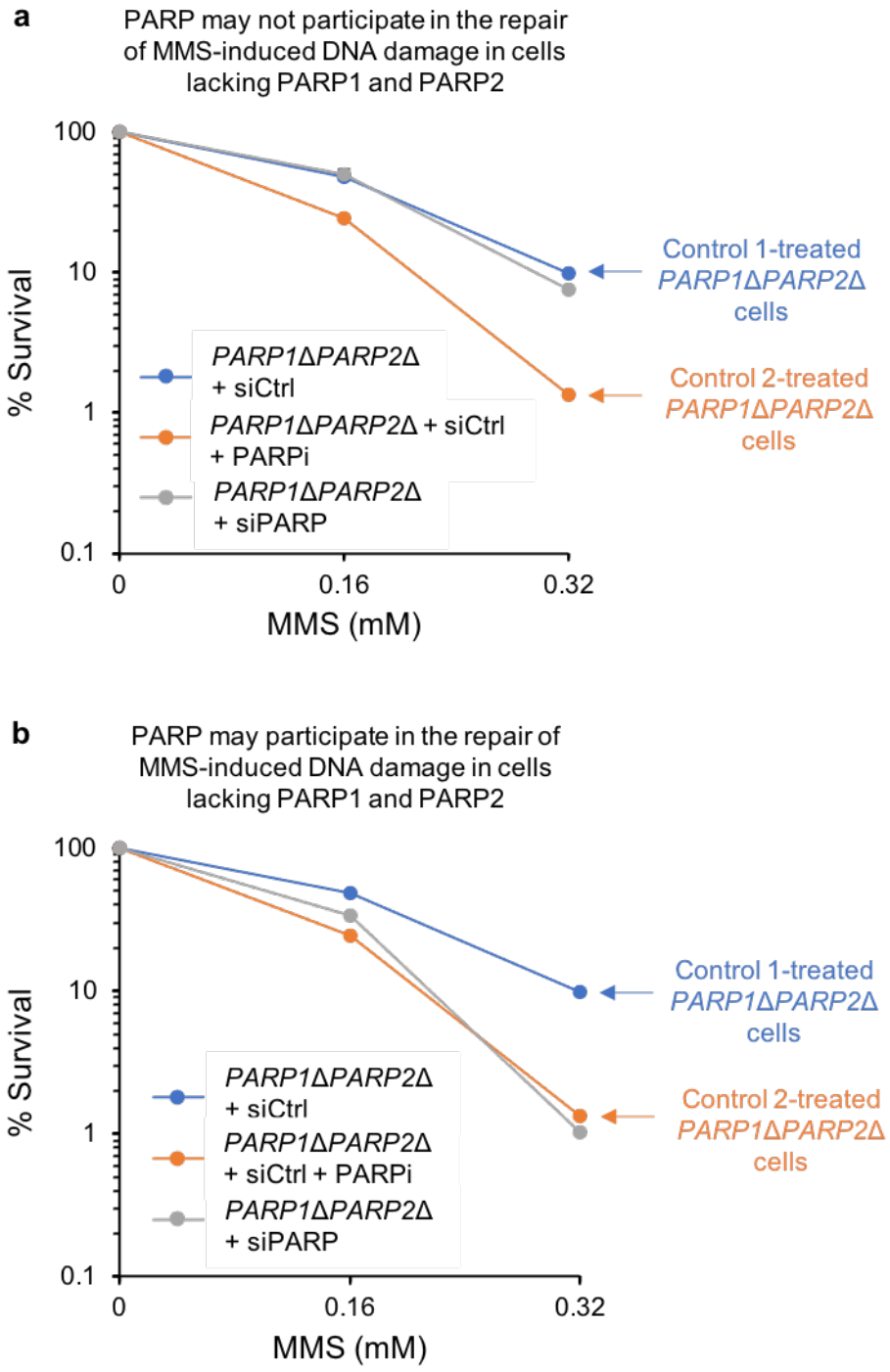
the same experiment by two-way ANOVA and by two-way ANOVA with Tukey's post hoc analysis.

Loss of PARP1 (which participates in the repair of MMS-induced DNA damage) and therefore loss of PARP1 catalytic activity, can further sensitise U2OS cells to MMS (Ronson et al., 2018). Therefore, I hypothesised that the olaparib-induced further sensitisation of *PARP1ΔPARP2Δ* cells to MMS may be due to the olaparib-dependent catalytic inhibition of a PARP that may participate in the repair of MMS-induced DNA damage in cells lacking PARP1 and PARP2. I reasoned that if *PARP1ΔPARP2Δ* cells are further sensitised to MMS following independent depletion of a given PARP to a similar extent to olaparib and MMS-treated *PARP1ΔPARP2Δ* cells, then this PARP may participate in the repair of MMS-induced DNA damage in cells lacking PARP1 and PARP2 (Figure 3.4 a). Alternatively, I reasoned that if depletion of a PARP does not further sensitise *PARP1ΔPARP2Δ* cells to MMS then this PARP may not participate in the repair of MMS-induced DNA damage in cells lacking PARP1 and PARP2 (Figure 3.4 b). To investigate this hypothesis further, I performed a PARP depletion screen (the first PARP depletion screen) in which each of the remaining PARP superfamily members (PARP3-16) were independently depleted in the *PARP1ΔPARP2Δ* cells via PARP3-16-targeting SMARTpool siRNA transfection and the cells were treated with increasing concentrations of MMS for 1 h (Figure 3.5 a-o). A control for this screen was included in which *PARP1ΔPARP2Δ* cells were transfected with non-targeting control siRNA (control siRNA) and treated with increasing concentrations of MMS for 1 h (control 1-treated cells) (Figure 3.4 a and b). This control provided insight into whether the MMS treatment sensitised this cells line as expected and also provided insight into whether depletion of a given PARP further

sensitised *PARP1ΔPARP2Δ* cells to MMS compared to this control (Ronson, 2017). Another control was also included in which *PARP1ΔPARP2Δ* cells were transfected with control siRNA; pre-incubated with olaparib for 1 h; treated with increasing concentrations of MMS for 1 h; and subsequently treated with olaparib for 24 h (control 2-treated *PARP1ΔPARP2Δ* cells) (Figure 3.4 a and b). This control provided insight into whether olaparib further sensitised control siRNA-transfected *PARP1ΔPARP2Δ* cells to MMS as expected, and also provided insight into whether depletion of a given PARP resulted in additional sensitisation of *PARP1ΔPARP2Δ* cells to MMS to a similar extent to this control. The ability of these cells to form colonies in response to the treatments described above was assessed via clonogenic survival assay. Depletion of a given PARP was considered to further sensitise *PARP1ΔPARP2Δ* cells to MMS if all of the following criteria were met when analysing the clonogenic survival assays within this PARP depletion screen: (1) A statistically significant and convincing decrease in cell viability was observed in *PARP1ΔPARP2Δ* cells depleted of a given PARP and also treated with MMS, relative to control 1-treated *PARP1ΔPARP2Δ* cells; (2) No statistically significant difference in cell viability/a statistically significant yet unconvincing difference in cell viability was observed in *PARP1ΔPARP2Δ* cells depleted of a given PARP and treated with MMS, relative to control 2-treated *PARP1ΔPARP2Δ* cells; (3) Within each experiment, a statistically significant and convincing decrease in cell viability was observed in control 2-treated *PARP1ΔPARP2Δ* cells relative to control 1-treated *PARP1ΔPARP2Δ* cells.

Interpretation of the first PARP depletion screen is based on three key assumptions: (1) In *PARP1ΔPARP2Δ* cells, olaparib catalytically inhibits a single PARP that may participate in the repair of MMS-induced DNA damage without trapping it to DNA; (2)

In *PARP1ΔPARP2Δ* cells, the olaparib-targeted PARP is the only remaining PARP that may participate in the repair of MMS-induced DNA damage; (3) The olaparib-induced further sensitisation of *PARP1ΔPARP2Δ* cells to MMS is a genuine phenotype. Therefore, any instances where there is no significant difference between the survival of control 2-treated *PARP1ΔPARP2Δ* cells and control 1-treated *PARP1ΔPARP2Δ* cells are due to a lack of statistical power.


a
PARP may not participate in the repair of MMS-induced DNA damage in cells lacking PARP1 and PARP2
100
10
1
0.1
% Survival
0
0.16
0.32
MMS (mM)
PARP1ΔPARP2Δ + siCtrl
PARP1ΔPARP2Δ + siCtrl + PARPi
PARP1ΔPARP2Δ + siPARP
Control 1-treated PARP1ΔPARP2Δ cells
Control 2-treated PARP1ΔPARP2Δ cells
b
PARP may participate in the repair of MMS-induced DNA damage in cells lacking PARP1 and PARP2
100
10
1
0.1
% Survival
0
0.16
0.32
MMS (mM)
PARP1ΔPARP2Δ + siCtrl
PARP1ΔPARP2Δ + siCtrl + PARPi
PARP1ΔPARP2Δ + siPARP
Control 1-treated PARP1ΔPARP2Δ cells
Control 2-treated PARP1ΔPARP2Δ cells

c

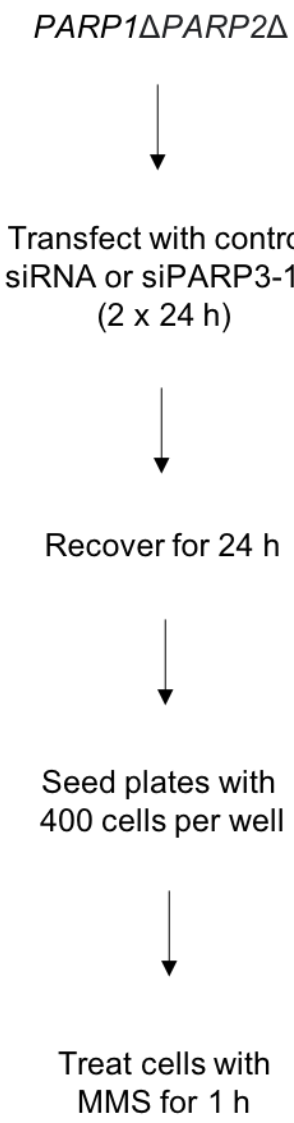


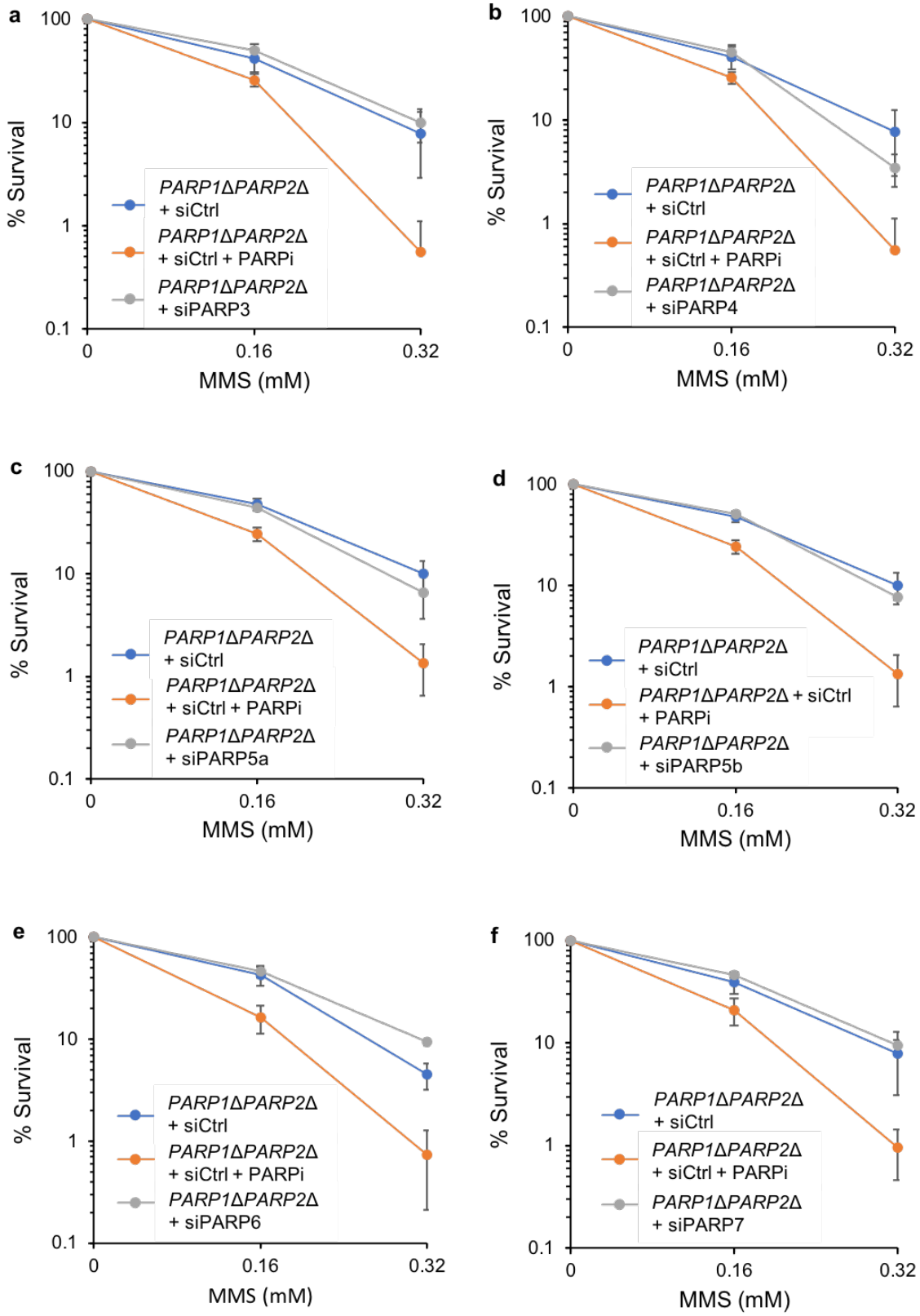
Figure 3.4: Rationale for PARP depletion screen to assess whether *PARP1ΔPARP2Δ* cells are further sensitised to MMS following independent depletion of a PARP. (a) If independent depletion of a PARP does not sensitise *PARP1ΔPARP2Δ* cells to MMS then the PARP may not participate in the repair of MMS-induced DNA damage in cells lacking PARP1 and PARP2. **(b)** If independent depletion of a PARP further sensitises *PARP1ΔPARP2Δ* cells to MMS, then the PARP may participate in the repair of MMS-induced DNA damage in cells lacking PARP1 and PARP2. **(c)** Summary of experimental procedure for this screen.

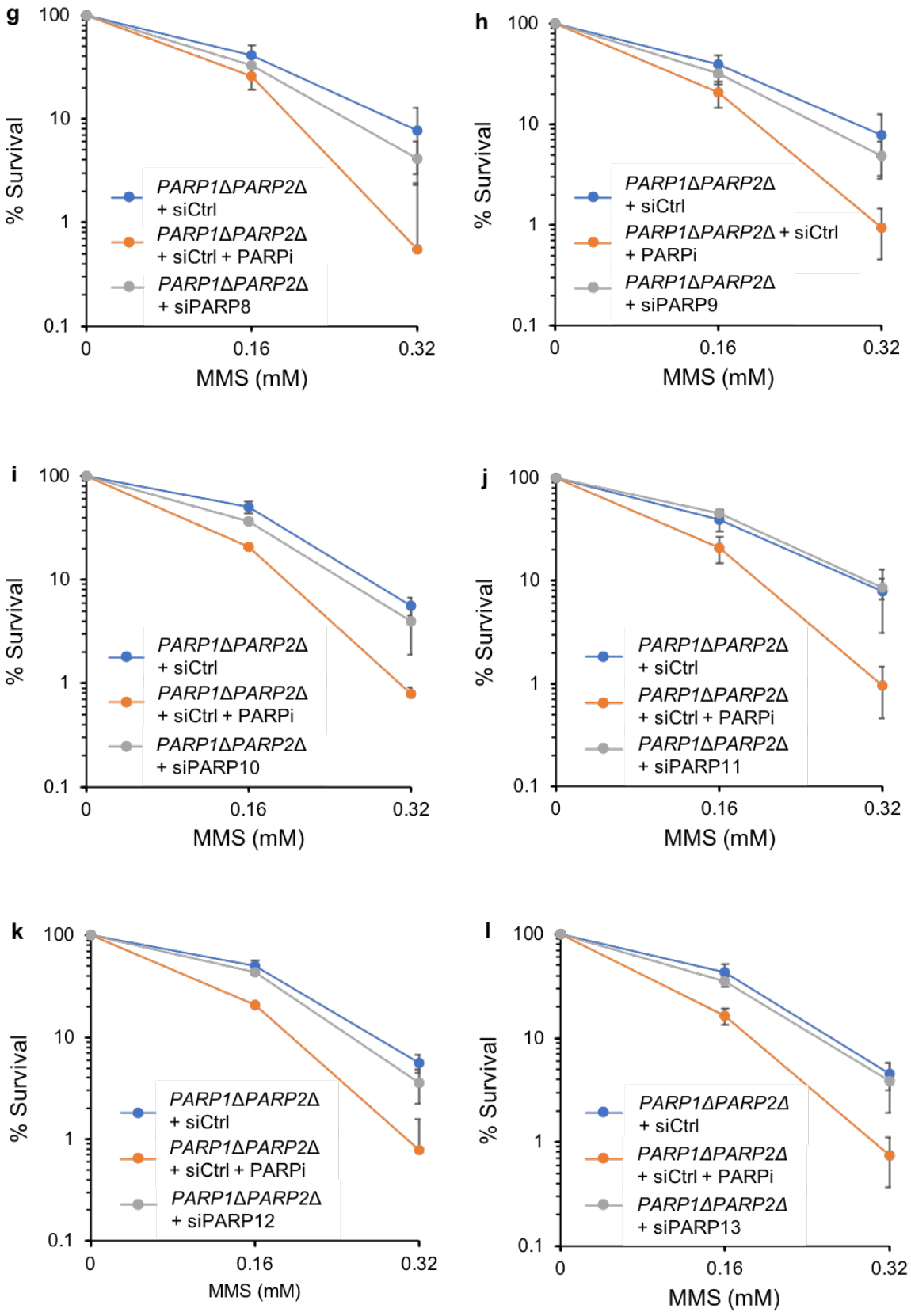
When evaluated by two-way ANOVA, the following observations were made from the first PARP depletion screen (Table 3.1). It was not possible to assess whether *PARP1ΔPARP2Δ* cells were further sensitised to MMS following independent depletion of PARP3, PARP4, PARP7, PARP8, PARP9 and PARP11, given that there was not a statistically significant difference between control 2-treated *PARP1ΔPARP2Δ* cells and control 1-treated *PARP1ΔPARP2Δ* cells in each of these experiments. It was not possible to assess whether *PARP1ΔPARP2Δ* cells were further sensitised to MMS following PARP16 depletion, since the viability of PARP16-depleted *PARP1ΔPARP2Δ* cells treated with MMS was not significantly different to the viability of control 1-treated *PARP1ΔPARP2Δ* cells or to the viability control 2-treated *PARP1ΔPARP2Δ* cells. *PARP1ΔPARP2Δ* cells were not further sensitised to MMS following depletion of PARP5a, PARP5b, PARP6, PARP10, PARP12, PARP13 and PARP14. Initially, *PARP1ΔPARP2Δ* cells were further sensitised to MMS following depletion of PARP15. However, when repeating the assay described above with the same MMS concentration range, but with additional MMS concentration intervals in order to increase the resolution of the clonogenic surivival assay, *PARP1ΔPARP2Δ* cells were not further sensitised to MMS following PARP15 depletion (data not shown). Together, when evaluated by two-way ANOVA, these data suggest the following. Firstly, it was not possible to assess whether PARP3, PARP4, PARP7, PARP8, PARP9 or PARP16 may participate in the repair of MMS-induced DNA damage in cells lacking PARP1 and PARP2. Secondly, PARP5a, PARP5b, PARP6, PARP10, PARP12, PARP13 and PARP14 may not participate in the repair of MMS-induced DNA damage in cells lacking PARP1 and PARP2. Thirdly, it is not clear

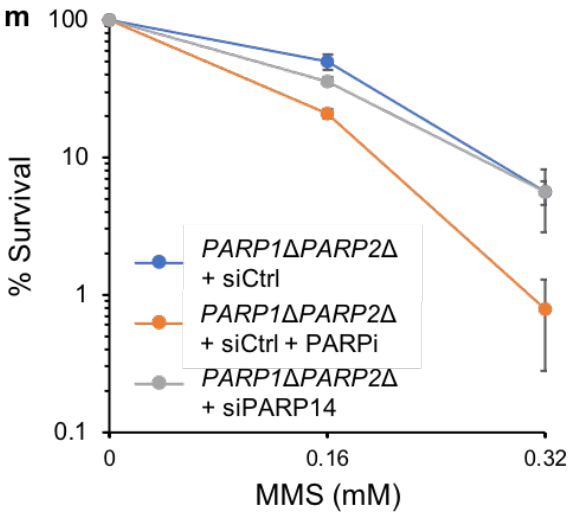
whether PARP15 may participate in the repair of MMS-induced DNA damage in cells lacking PARP1 and PARP2.

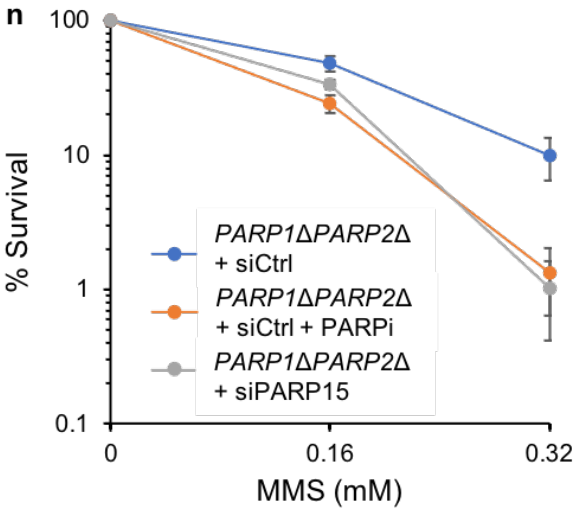
When evaluated by two-way ANOVA with Tukey's post hoc analysis, the first PARP depletion screen revealed the following observations (Table 3.2). Given that within each of the experiments in which PARP3, PARP4, PARP7, PARP8, PARP9, PARP11 and PARP16 were independently depleted there was not a statistically significant and notable difference between control 2-treated *PARP1ΔPARP2Δ* cells and control 1-treated *PARP1ΔPARP2Δ* cells, it was not possible to assess whether *PARP1ΔPARP2Δ* cells were further sensitised to MMS following depletion of these PARPs. *PARP1ΔPARP2Δ* cells were not further sensitised to MMS following depletion of PARP5a, PARP5b, PARP6, PARP10, PARP12, PARP13 and PARP14. Initially, it was not possible to determine whether *PARP1ΔPARP2Δ* cells were further sensitised to MMS following PARP15 depletion because the survival of PARP15-depleted *PARP1ΔPARP2Δ* cells was not significantly different to the survival of control 1-treated *PARP1ΔPARP2Δ* cells or to the survival of control 2-treated *PARP1ΔPARP2Δ* cells. However, following repetition of this experiment with the same MMS concentration range, but including more MMS concentration intervals in order to increase the resolution of the clonogenic survival assay, *PARP1ΔPARP2Δ* cells were not further sensitised to MMS following depletion of this PARP (data not shown). Together, when evaluated by two-way ANOVA with Tukey's post hoc analysis, these data suggest the following. Firstly, it was not possible to assess whether PARP3, PARP4, PARP7, PARP8, PARP9, PARP11 or PARP16 may participate in the repair of MMS-induced DNA damage in cells lacking PARP1 and PARP2. Secondly, PARP5a, PARP5b, PARP6, PARP10, PARP12, PARP13, PARP14 and PARP15 may

not participate in the repair of MMS-induced DNA damage in cells lacking PARP1 and PARP2.


a
100
10
1
0.1
% Survival
0
0.16
0.32
MMS (mM)
PARP1ΔPARP2Δ
+ siCtrl
PARP1ΔPARP2Δ
+ siCtrl + PARPi
PARP1ΔPARP2Δ
+ siPARP3
b
PARP1ΔPARP2Δ
+ siCtrl
PARP1ΔPARP2Δ
+ siCtrl + PARPi
PARP1ΔPARP2Δ
+ siPARP4
c
PARP1ΔPARP2Δ
+ siCtrl
PARP1ΔPARP2Δ
+ siCtrl + PARPi
PARP1ΔPARP2Δ
+ siPARP5a
d
PARP1ΔPARP2Δ
+ siCtrl
PARP1ΔPARP2Δ + siCtrl
+ PARPi
PARP1ΔPARP2Δ
+ siPARP5b
e
PARP1ΔPARP2Δ
+ siCtrl
PARP1ΔPARP2Δ
+ siCtrl + PARPi
PARP1ΔPARP2Δ
+ siPARP6
f
PARP1ΔPARP2Δ
+ siCtrl
PARP1ΔPARP2Δ
+ siCtrl + PARPi
PARP1ΔPARP2Δ
+ siPARP7


g
% Survival
100
10
1
0.1
0
0.16
0.32
MMS (mM)
PARP1ΔPARP2Δ
+ siCtrl
PARP1ΔPARP2Δ
+ siCtrl + PARPi
PARP1ΔPARP2Δ
+ siPARP8
h
% Survival
100
10
1
0.1
0
0.16
0.32
MMS (mM)
PARP1ΔPARP2Δ
+ siCtrl
PARP1ΔPARP2Δ + siCtrl
+ PARPi
PARP1ΔPARP2Δ
+ siPARP9
i
% Survival
100
10
1
0.1
0
0.16
0.32
MMS (mM)
PARP1ΔPARP2Δ
+ siCtrl
PARP1ΔPARP2Δ
+ siCtrl + PARPi
PARP1ΔPARP2Δ
+ siPARP10
j
% Survival
100
10
1
0.1
0
0.16
0.32
MMS (mM)
PARP1ΔPARP2Δ
+ siCtrl
PARP1ΔPARP2Δ
+ siCtrl + PARPi
PARP1ΔPARP2Δ
+ siPARP11
k
% Survival
100
10
1
0.1
0
0.16
0.32
MMS (mM)
PARP1ΔPARP2Δ
+ siCtrl
PARP1ΔPARP2Δ
+ siCtrl + PARPi
PARP1ΔPARP2Δ
+ siPARP12
l
% Survival
100
10
1
0.1
0
0.16
0.32
MMS (mM)
PARP1ΔPARP2Δ
+ siCtrl
PARP1ΔPARP2Δ
+ siCtrl + PARPi
PARP1ΔPARP2Δ
+ siPARP13


m
100
10
1
0.1
% Survival
PARP1ΔPARP2Δ
+ siCtrl
PARP1ΔPARP2Δ
+ siCtrl + PARPi
PARP1ΔPARP2Δ
+ siPARP14
0
0.16
0.32
MMS (mM)


n
100
10
1
0.1
% Survival
PARP1ΔPARP2Δ
+ siCtrl
PARP1ΔPARP2Δ
+ siCtrl + PARPi
PARP1ΔPARP2Δ
+ siPARP15
0
0.16
0.32
MMS (mM)

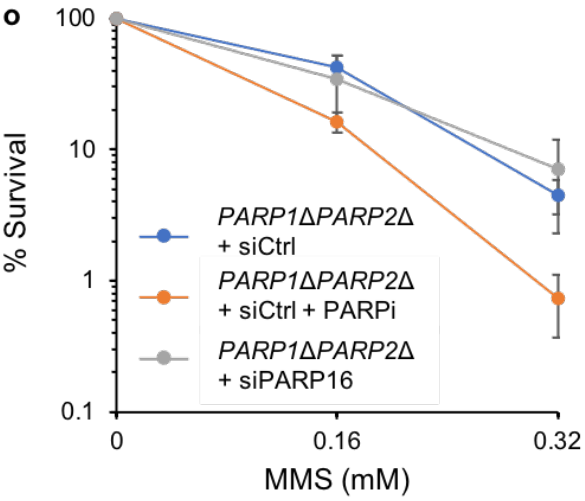

o
100
10
1
0.1
% Survival
PARP1ΔPARP2Δ
+ siCtrl
PARP1ΔPARP2Δ
+ siCtrl + PARPi
PARP1ΔPARP2Δ
+ siPARP16
0
0.16
0.32
MMS (mM)

Figure 3.5: First PARP depletion screen to determine whether a PARP may participate in the repair of MMS-induced DNA damage. *PARP1ΔPARP2Δ* cells were transfected with non-targeting control siRNA, siPARP3 SMARTpool **(a)**, siPARP4 SMARTpool **(b)**, siPARP5a SMARTpool **(c)**, siPARP5b SMARTpool **(d)**, siPARP6 SMARTpool **(e)**, siPARP7 SMARTpool **(f)**, siPARP8 SMARTpool **(g)**, siPARP9 SMARTpool **(h)**, siPARP10 SMARTpool **(i)**, siPARP11 SMARTpool **(j)**, siPARP12 SMARTpool **(k)**, siPARP13 SMARTpool **(l)**, siPARP14 SMARTpool **(m)**, siPARP15 SMARTpool **(n)** or siPARP16 SMARTpool **(o)** and treated with MMS. For each experiment, a control was included in which *PARP1ΔPARP2Δ* cells were transfected with non-targeting control siRNA and treated with MMS and vehicle (control 1-treated *PARP1ΔPARP2Δ* cells). Additionally, for each experiment, a control was included in which *PARP1ΔPARP2Δ* cells were transfected with non-targeting control siRNA and treated with MMS and olaparib (10 μM) (control 2-treated *PARP1ΔPARP2Δ* cells). The viability of these cells was analysed via clonogenic survival assay. Error bars at each data point represent the standard error of the mean from three independent biological replicates.

	Two-way ANOVA		
PARP	*PARP1ΔPARP2Δ* + siCtrl vs *PARP1ΔPARP2Δ* + siCtrl + PARPi	*PARP1ΔPARP2Δ* + siCtrl vs *PARP1ΔPARP2Δ* + siPARP	*PARP1ΔPARP2Δ* + siCtrl + PARPi vs *PARP1ΔPARP2Δ* + siPARP
3	0.0821 ns	0.4832 ns	0.0040 **
4	0.0821 ns	0.9953 ns	0.0228 *
5a	0.0018 **	0.4001 ns	0.0005 ***
5b	0.0018 **	0.9926 ns	< 0.0001 ****
6	0.0091 **	0.4726 ns	0.0002 ***
7	0.0558 ns	0.4896 ns	0.0003 ***
8	0.8210 ns	0.3800 ns	0.2072 ns
9	0.0558 ns	0.4353 ns	0.1387 ns
10	0.0003 ***	0.0629 ns	< 0.0001 ****
11	0.0558 ns	0.5718 ns	0.0008 ***
12	0.0003 ***	0.2319 ns	< 0.0001 ****
13	0.0091 **	0.4242 ns	0.0014 **

14	0.0003 ***	0.0843 ns	0.0002 ***
15	0.0018 **	0.0113 *	0.0759 ns
16	0.0091 **	0.7825 ns	0.2130 ns

Table 3.1: Summary of p-values for Figure 3.5 when evaluated by two-way ANOVA. Statistical significance was evaluated by two-way ANOVA. For all statistical tests performed, * $p < 0.05$; ** $p < 0.01$; *** $p < 0.001$; ****; ns not significant.

	Two-way ANOVA with Tukey's post-hoc analysis		
PARP	*PARP1ΔPARP2Δ* + siCtrl vs *PARP1ΔPARP2Δ* + siCtrl + PARPi	*PARP1ΔPARP2Δ* + siCtrl vs *PARP1ΔPARP2Δ* + siPARP	*PARP1ΔPARP2Δ* + siCtrl + PARPi vs *PARP1ΔPARP2Δ* + siPARP
3	0.2175 ns	0.7976 ns	0.0361 *
4	0.1624 ns	> 0.9999 ns	0.1600 ns
5a	0.0003 ***	0.7037 ns	0.0039 **
5b	0.0010 **	>0.9999 ns	0.0011 **
6	0.0129 *	0.7895 ns	0.0013 **
7	0.0655 ns	0.8185 ns	0.0046 **

8	0.1354 ns	0.6199 ns	0.7273 ns
9	0.0840 ns	0.7432 ns	0.4561 ns
10	<0.0001 ****	0.0520 ns	0.0084 **
11	0.0890 ns	0.9226 ns	0.0232 *
12	<0.0001 ****	0.3276 ns	0.0003 ***
13	0.0037 **	0.7013 ns	0.0459 *
14	<0.0001 ****	0.0719 ns	0.0080 **
15	0.0040 **	0.0502 ns	0.6981 ns
16	0.2070 ns	0.9796 ns	0.3781 ns

Table 3.2: Summary of p-values for Figure 3.5 when evaluated by two-way ANOVA with Tukey's post hoc analysis. Statistical significance was evaluated by two-way ANOVA with Tukey's post hoc test. For all statistical tests performed, * $p < 0.05$; ** $p < 0.01$; *** $p < 0.001$; **** $p < 0.0001$; ns not significant.

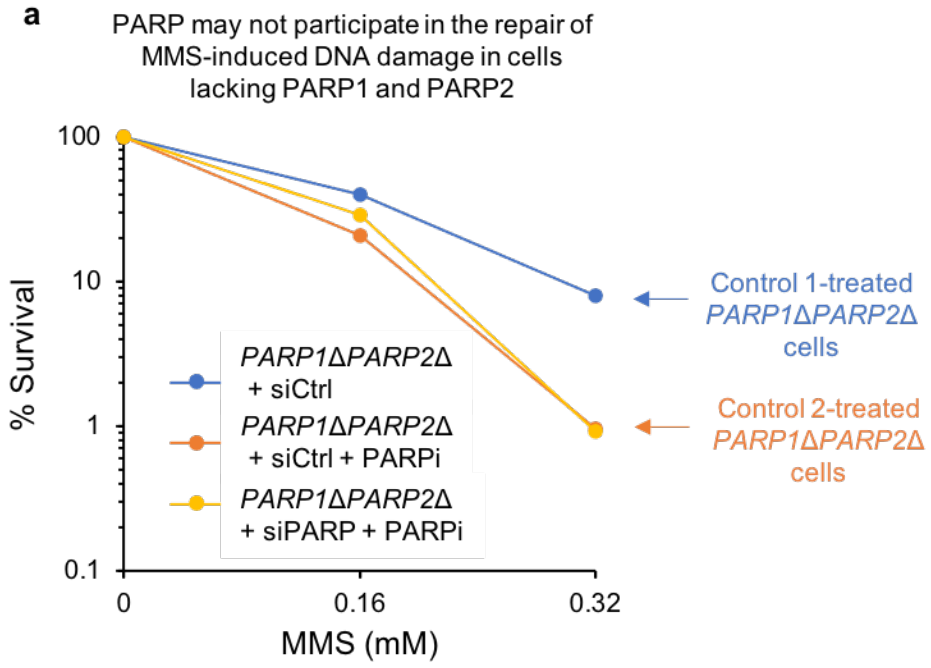
Olaparib-induced trapping of PARP1 (a PARP that participates in the repair of MMS-induced DNA damage) to DNA can hypersensitise wild type DT40 cells to MMS (Baba et al., 1985; Murai et al., 2012; Winding & Berchtold, 2001). Indeed, olaparib-treated *PARP*1Δ DT40 cells are sensitised to MMS to a lesser extent relative to DT40 cells exposed to the same treatment, indicating that PARP1-DNA complexes that are induced by olaparib are cytotoxic lesions in cells treated with MMS (Murai et al., 2012).

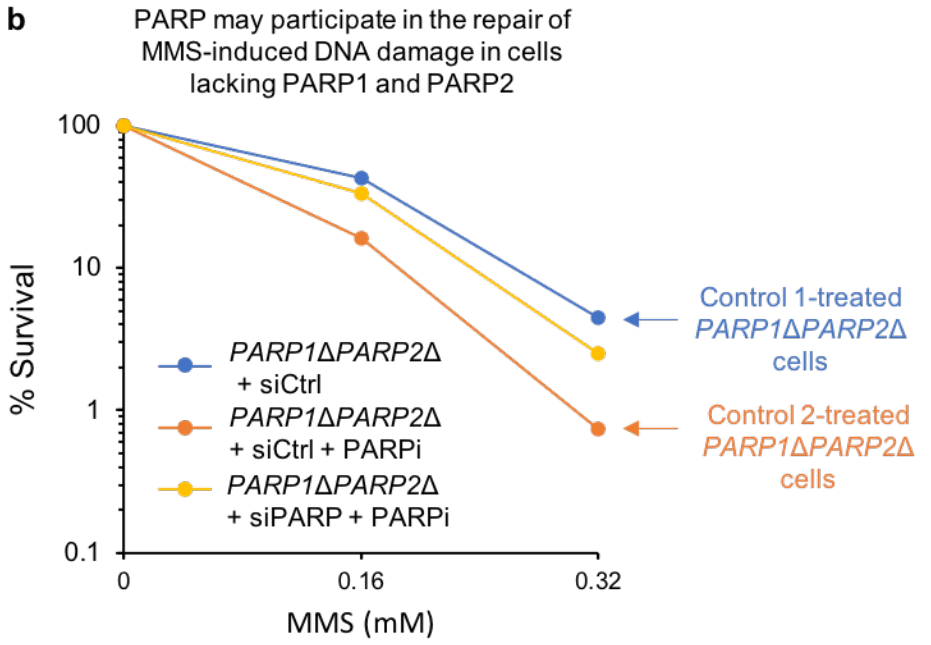
Therefore, I hypothesised that the olaparib-induced further sensitisation of *PARP1ΔPARP2Δ* cells to MMS may be due to the olaparib-dependent trapping of a PARP to DNA that may participate in the repair of MMS-induced DNA damage in cells lacking PARP1 and PARP2. I reasoned that if depletion of a given PARP rescues the olaparib-induced further sensitisation of *PARP1ΔPARP2Δ* cells to MMS then this PARP may participate in the repair of MMS-induced DNA damage (Figure 3.6 a). Alternatively, I reasoned that if depletion of a given PARP does not rescue the further sensitisation of *PARP1ΔPARP2Δ* cells to MMS, then this PARP may not participate in the repair of MMS-induced DNA damage (Figure 3.6 b).

To explore this hypothesis, I carried out a PARP depletion screen (the second PARP depletion screen) in *PARP1ΔPARP2Δ* cells which was performed in parallel with the first PARP depletion screen described previously, and therefore contained the same controls (control 1-treated cell and control 2-treated cells) (Figure 3.7 a-o and 3.8 a and c). PARP3-16 were independently depleted in the *PARP1ΔPARP2Δ* cells via PARP3-16-targeting SMARTpool siRNA transfection. These cells were pre-incubated with olaparib for 1 h and subsequently exposed to increasing concentrations of MMS for 1 h, followed by a further 24 h of olaparib treatment. When examining the clonogenic survival assays within this PARP depletion screen, independent depletion of a given PARP was considered to rescue the further sensitisation of *PARP1ΔPARP2Δ* cells to MMS if all of the following criteria were met: 1) A statistically significant and convincing increase in cell viability was observed in *PARP1ΔPARP2Δ* cells depleted of a given PARP and also treated with MMS, relative to control 2-treated *PARP1ΔPARP2Δ* cells. 2) No statistically significant difference in cell viability/a statistically significant yet unconvincing difference in cell viability was observed in

PARP1ΔPARP2Δ cells depleted of a given PARP and treated with MMS, relative to control 1-treated *PARP1ΔPARP2Δ* cells. 3) Within each experiment, a statistically significant and convincing decrease in cell viability was observed in control 2-treated *PARP1ΔPARP2Δ* cells relative to control 1-treated *PARP1ΔPARP2Δ* cells.

Interpretation of the second PARP depletion screen rested on three key assumptions: (1) In the absence of PARP1 and PARP2, olaparib traps a single PARP to DNA without catalytically inhibiting it; (2) In cells lacking PARP1 and PARP2, the PARP that is trapped to DNA by olaparib is the only remaining PARP that may participate in the repair of MMS-induced DNA damage; (3) The decrease in the survival of control 2-treated *PARP1ΔPARP2Δ* cells relative to the survival of control 1-treated *PARP1ΔPARP2Δ* cells is a genuine phenotype. Therefore, any cases where there is no significant difference between the survival of control 2-treated *PARP1ΔPARP2Δ* cells and control 1-treated *PARP1ΔPARP2Δ* cells occur as a consequence of a lack of statistical power.


a
PARP may not participate in the repair of
MMS-induced DNA damage in cells
lacking PARP1 and PARP2
100
10
1
0.1
% Survival
0
0.16
0.32
MMS (mM)
PARP1ΔPARP2Δ
+ siCtrl
PARP1ΔPARP2Δ
+ siCtrl + PARPi
PARP1ΔPARP2Δ
+ siPARP + PARPi
Control 1-treated
PARP1ΔPARP2Δ
cells
Control 2-treated
PARP1ΔPARP2Δ
cells


b
PARP may participate in the repair of
MMS-induced DNA damage in cells
lacking PARP1 and PARP2
100
10
1
0.1
% Survival
0
0.16
0.32
MMS (mM)
PARP1ΔPARP2Δ
+ siCtrl
PARP1ΔPARP2Δ
+ siCtrl + PARPi
PARP1ΔPARP2Δ
+ siPARP + PARPi
Control 1-treated
PARP1ΔPARP2Δ
cells
Control 2-treated
PARP1ΔPARP2Δ
cells

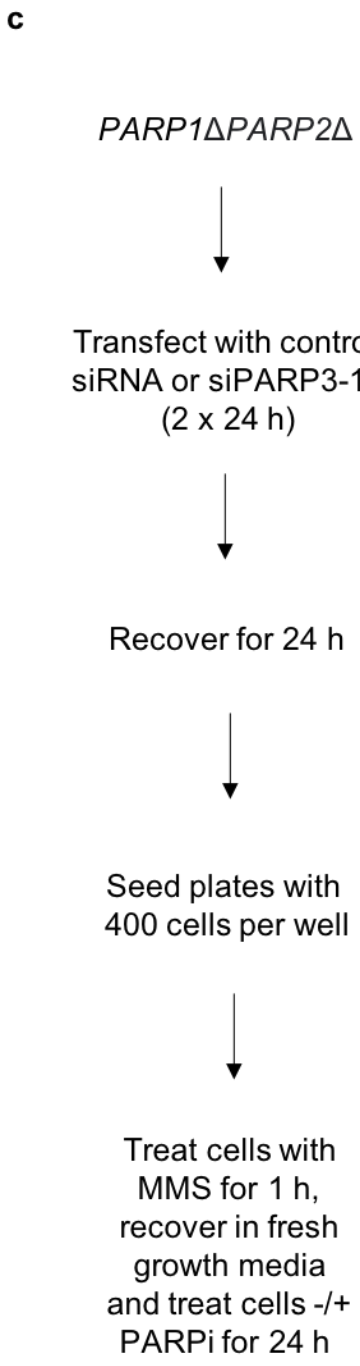


Figure 3.6: Rationale for PARP depletion screen to assess whether independent depletion of a PARP rescues the olaparib-induced further sensitisation of *PARP1ΔPARP2Δ* cells to MMS. (a) If independent depletion of a PARP does not rescue the olaparib-induced further sensitisation of *PARP1ΔPARP2Δ* cells to MMS then the PARP may not participate in the repair of MMS-induced DNA damage in cells lacking PARP1 and PARP2. **(b)** If independent depletion of PARP rescues the

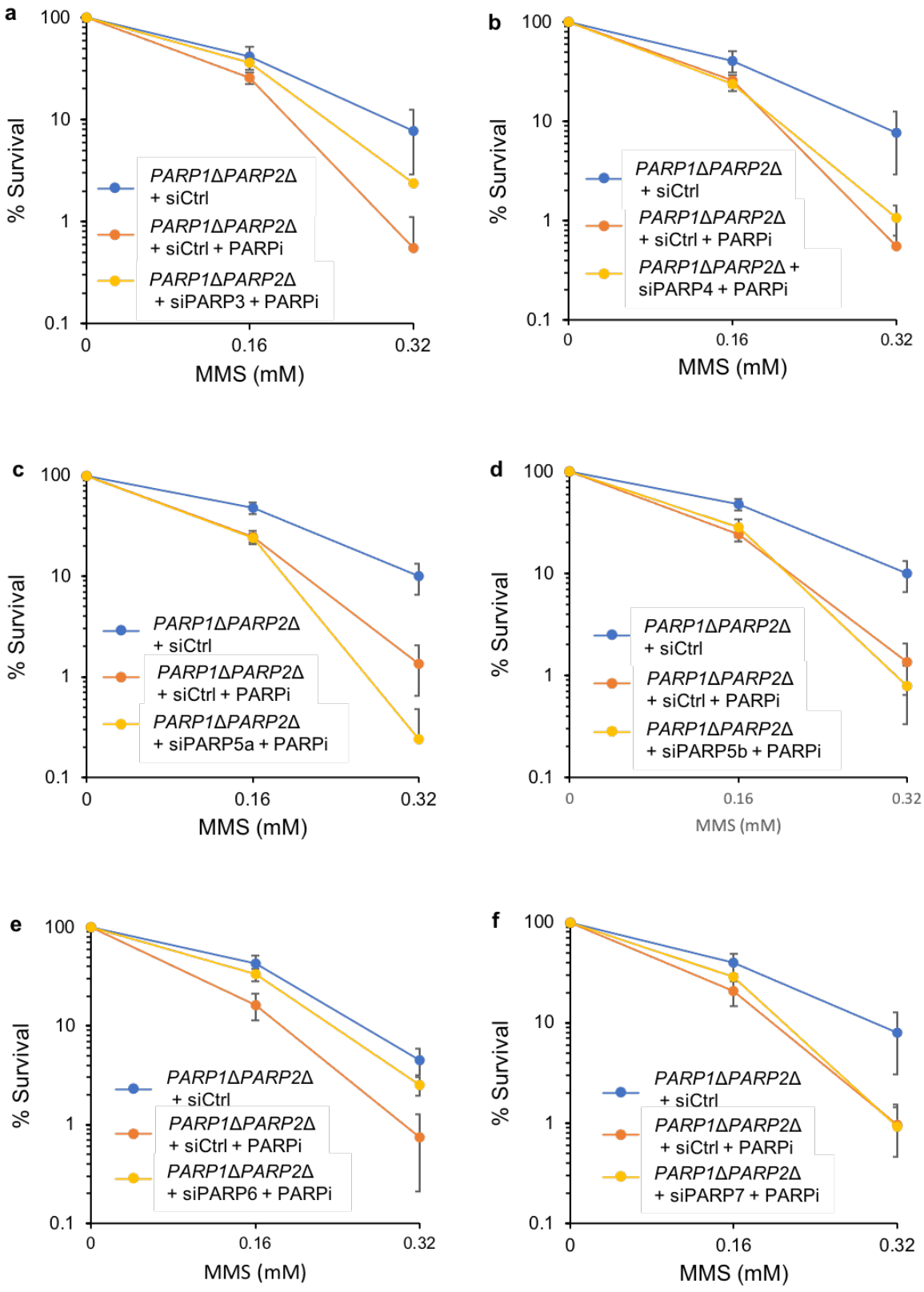
olaparib-induced further sensitisation of *PARP1ΔPARP2Δ* cells to MMS then the PARP may participate in the repair of MMS-induced DNA damage in cells lacking PARP1 and PARP2. (c) Summary of experimental procedure for this screen.

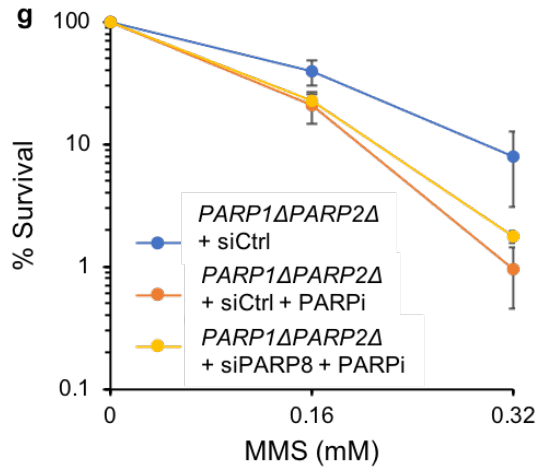
When the second PARP depletion screen was evaluated by two-way ANOVA, the following observations were made (Table 3.3, 3.5 and 3.6). It was not possible to assess whether independent depletion of PARP3, PARP4, PARP7, PARP8, PARP9 or PARP11 rescued the olaparib-induced further sensitisation of *PARP1ΔPARP2Δ* cells to MMS, as the survival of control-2 treated *PARP1ΔPARP2Δ* cells was not statistically different to the survival of control 1-treated *PARP1ΔPARP2Δ* cells in these experiments. Independent depletion of PARP5a, PARP5b, PARP10, PARP12, PARP13, PARP15 and PARP16 did not rescue the olaparib-induced further sensitisation of *PARP1ΔPARP2Δ* cells to MMS. Initially, independent depletion of PARP6 or PARP14 rescued the olaparib-induced further sensitisation of *PARP1ΔPARP2Δ* cells to MMS. In order to determine whether these initial findings were reproduceable, I repeated the experiment described above in PARP6-depleted and PARP14-depleted *PARP1ΔPARP2Δ* cells including all of the relevant controls, but cells were treated with more MMS concentration intervals to increase the resolution of the clonogenic survival assay. As before, PARP6 depletion rescued the olaparib-induced further sensitisation of *PARP1ΔPARP2Δ* cells to MMS and depletion of PARP6 protein levels in wild type U2OS cells was confirmed via western blot (Figure 3.8 b). However, it was not possible to assess whether PARP14 depletion rescued the olaparib-induced further sensitisation of *PARP1ΔPARP2Δ* cells to MMS, since the viability of PARP14-depleted *PARP1ΔPARP2Δ* cells treated with MMS and olaparib was not significantly different to the viability of control 1-treated *PARP1ΔPARP2Δ* cells

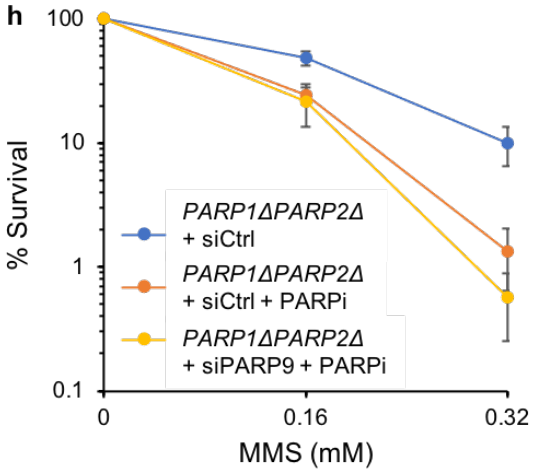
or significantly different to the viability of control 2-treated *PARP1ΔPARP2Δ* cells. Together, when evaluated by two-way ANOVA, these data suggest the following. Firstly, it was not possible to assess whether PARP3, PARP4, PARP7, PARP8, PARP9 or PARP11 may participate in the repair of MMS-induced DNA damage in cells lacking PARP1 and PARP2. Secondly, PARP5a, PARP5b, PARP10, PARP12, PARP13, PARP15 and PARP16 may not participate in the repair of MMS-induced DNA damage in cells lacking PARP1 and PARP2. Finally, PARP6 or PARP14 may participate in the repair of MMS-induced DNA damage in cells lacking PARP1 and PARP2, but there is more evidence supporting the notion that PARP6 may participate in the repair of MMS-induced DNA damage in cells lacking PARP1 and PARP2.

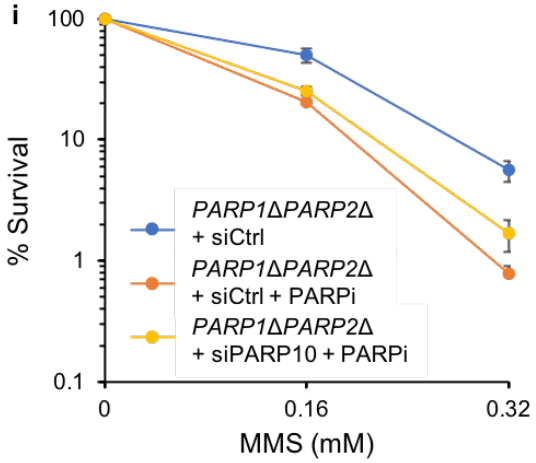
When evaluated by two-way ANOVA with Tukey's post hoc analysis, the second PARP depletion screen revealed the following observations (Table 3.4, 3.5 and 3.6). It was not possible to assess whether depletion of PARP3, PARP4, PARP7, PARP8, PARP9 or PARP11 rescued the olaparib-induced further sensitisation of *PARP1ΔPARP2Δ* cells to MMS because in each of these experiments, there was no statistically significant difference between the survival of control 2-treated *PARP1ΔPARP2Δ* cells and the viability of control 1-treated *PARP1ΔPARP2Δ* cells. Additionally, it was not possible to assess whether depletion of PARP16 rescued the olaparib-induced further sensitisation of *PARP1ΔPARP2Δ* cells to MMS, as the survival of PARP16-depleted *PARP1ΔPARP2Δ* treated with olaparib and MMS was not significantly different to the survival of control 1-treated *PARP1ΔPARP2Δ* cells or significantly different to the survival of control 2-treated *PARP1ΔPARP2Δ* cells. Depletion of PARP5a, PARP5b, PARP10, PARP12, PARP13 and PARP15 did not rescue the olaparib-induced further sensitisation of *PARP1ΔPARP2Δ* cells to MMS.

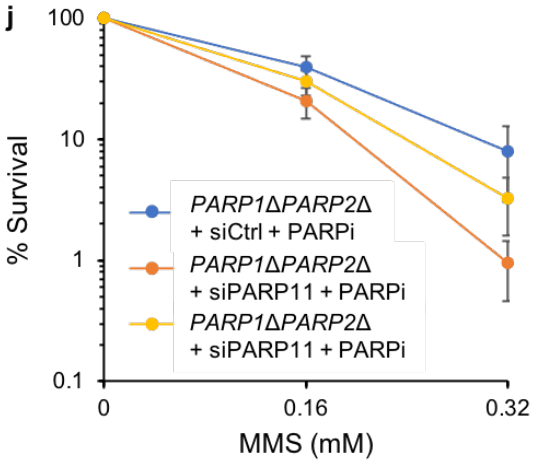
Initially, it was not possible to assess whether PARP6 depletion rescued the olaparib-induced further sensitisation of *PARP1ΔPARP2Δ* cells to MMS because the viability of PARP6-depleted *PARP1ΔPARP2Δ* cells treated with MMS and olaparib was not significantly different to the viability of control 1-treated *PARP1ΔPARP2Δ* cells or significantly different to the viability of control 2-treated *PARP1ΔPARP2Δ* cells. Furthermore, initially, it was not possible to assess whether PARP14 depletion rescued the olaparib-induced further sensitisation of *PARP1ΔPARP2Δ* cells to MMS, as there was a statistically significant decrease in the survival of PARP14-depleted *PARP1ΔPARP2Δ* cells treated with olaparib and MMS relative to control 1-treated *PARP1ΔPARP2Δ* cells, but the survival of PARP14-depleted *PARP1ΔPARP2Δ* cells treated with olaparib was not significantly different to the survival of control 2-treated *PARP1ΔPARP2Δ* cells. Following repetition of the clonogenic survival assays in which PARP6 and PARP14 were depleted as described previously, it was not possible to assess whether depletion of either of these PARPs rescued the olaparib-induced further sensitisation of *PARP1ΔPARP2Δ* cells to MMS, because in each of these experiments, the survival of control 2-treated *PARP1ΔPARP2Δ* cells was not significantly different to the survival of control 1-treated cells. As mentioned previously, depletion of PARP6 protein levels was validated by western blot in wild type U2OS cells. Together, when evaluated by two-way ANOVA with Tukey's post hoc analysis, the second PARP depletion screen suggests the following. Firstly, it was not possible to assess whether PARP3, PARP4, PARP6, PARP7, PARP8, PARP9, PARP11, PARP14 or PARP16 may participate in the repair MMS-induced DNA damage in cells lacking PARP1 and PARP2. Secondly, PARP5a, PARP5b, PARP10, PARP12, PARP13 and PARP15 may not participate in the repair of MMS-induced DNA damage in cells lacking PARP1 and PARP2.

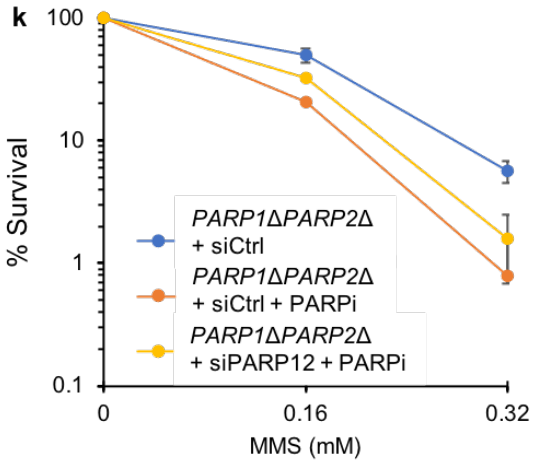

a
100
10
1
0.1
% Survival
0
0.16
0.32
MMS (mM)
PARP1ΔPARP2Δ
+ siCtrl
PARP1ΔPARP2Δ
+ siCtrl + PARPi
PARP1ΔPARP2Δ
+ siPARP3 + PARPi
b
PARP1ΔPARP2Δ
+ siCtrl
PARP1ΔPARP2Δ
+ siCtrl + PARPi
PARP1ΔPARP2Δ +
siPARP4 + PARPi
c
PARP1ΔPARP2Δ
+ siCtrl
PARP1ΔPARP2Δ
+ siCtrl + PARPi
PARP1ΔPARP2Δ
+ siPARP5a + PARPi
d
PARP1ΔPARP2Δ
+ siCtrl
PARP1ΔPARP2Δ
+ siCtrl + PARPi
PARP1ΔPARP2Δ
+ siPARP5b + PARPi
e
PARP1ΔPARP2Δ
+ siCtrl
PARP1ΔPARP2Δ
+ siCtrl + PARPi
PARP1ΔPARP2Δ
+ siPARP6 + PARPi
f
PARP1ΔPARP2Δ
+ siCtrl
PARP1ΔPARP2Δ
+ siCtrl + PARPi
PARP1ΔPARP2Δ
+ siPARP7 + PARPi

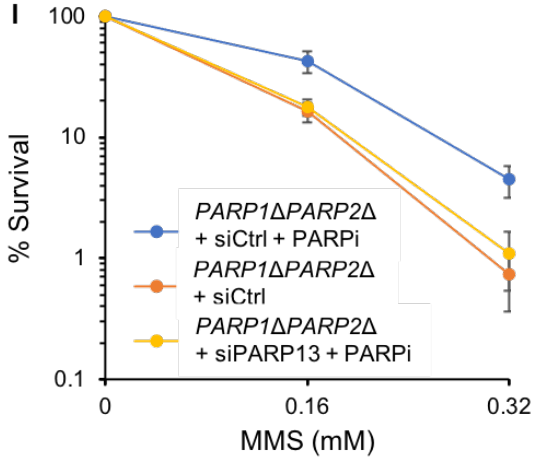

g
100
10
1
0.1
% Survival
PARP1ΔPARP2Δ
+ siCtrl
PARP1ΔPARP2Δ
+ siCtrl + PARPi
PARP1ΔPARP2Δ
+ siPARP8 + PARPi
0
0.16
0.32
MMS (mM)


h
100
10
1
0.1
% Survival
PARP1ΔPARP2Δ
+ siCtrl
PARP1ΔPARP2Δ
+ siCtrl + PARPi
PARP1ΔPARP2Δ
+ siPARP9 + PARPi
0
0.16
0.32
MMS (mM)


i
100
10
1
0.1
% Survival
PARP1ΔPARP2Δ
+ siCtrl
PARP1ΔPARP2Δ
+ siCtrl + PARPi
PARP1ΔPARP2Δ
+ siPARP10 + PARPi
0
0.16
0.32
MMS (mM)


j
100
10
1
0.1
% Survival
PARP1ΔPARP2Δ
+ siCtrl + PARPi
PARP1ΔPARP2Δ
+ siPARP11 + PARPi
PARP1ΔPARP2Δ
+ siPARP11 + PARPi
0
0.16
0.32
MMS (mM)


k
100
10
1
0.1
% Survival
PARP1ΔPARP2Δ
+ siCtrl
PARP1ΔPARP2Δ
+ siCtrl + PARPi
PARP1ΔPARP2Δ
+ siPARP12 + PARPi
0
0.16
0.32
MMS (mM)


l
100
10
1
0.1
% Survival
PARP1ΔPARP2Δ
+ siCtrl + PARPi
PARP1ΔPARP2Δ
+ siCtrl
PARP1ΔPARP2Δ
+ siPARP13 + PARPi
0
0.16
0.32
MMS (mM)

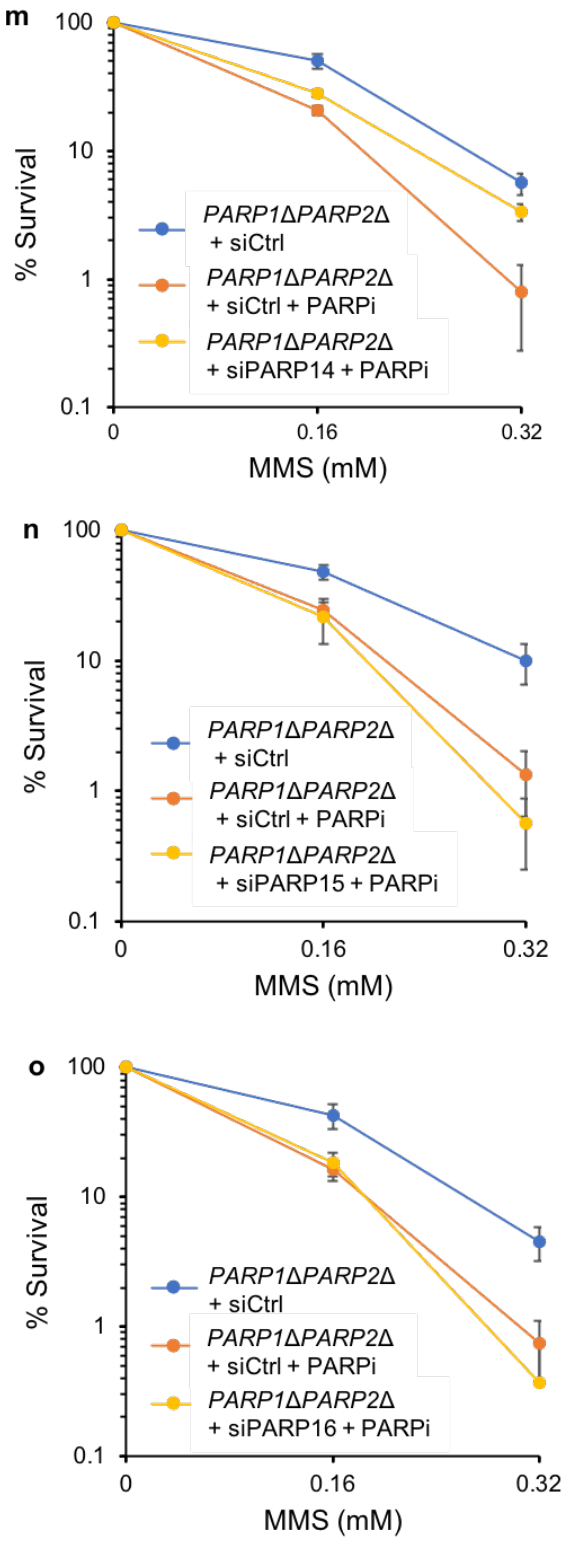

m
100
10
1
0.1
% Survival
PARP1ΔPARP2Δ
+ siCtrl
PARP1ΔPARP2Δ
+ siCtrl + PARPi
PARP1ΔPARP2Δ
+ siPARP14 + PARPi
0
0.16
0.32
MMS (mM)
n
100
10
1
0.1
% Survival
PARP1ΔPARP2Δ
+ siCtrl
PARP1ΔPARP2Δ
+ siCtrl + PARPi
PARP1ΔPARP2Δ
+ siPARP15 + PARPi
0
0.16
0.32
MMS (mM)
o
100
10
1
0.1
% Survival
PARP1ΔPARP2Δ
+ siCtrl
PARP1ΔPARP2Δ
+ siCtrl + PARPi
PARP1ΔPARP2Δ
+ siPARP16 + PARPi
0
0.16
0.32
MMS (mM)

Figure 3.7: PARP depletion screen to determine whether olaparib-mediated trapping of a PARP to DNA is responsible for the olaparib-induced further sensitisation of *PARP1ΔPARP2Δ* cells to MMS. *PARP1ΔPARP2Δ* cells were transfected with non-targeting control siRNA, siPARP3 SMARTpool **(a)**, siPARP4 SMARTpool **(b)**, siPARP5a SMARTpool **(c)**, siPARP5b SMARTpool **(d)**, siPARP6 SMARTpool **(e)**, siPARP7 SMARTpool **(f)**, siPARP8 SMARTpool **(g)**, siPARP9 SMARTpool **(h)** siPARP10 SMARTpool **(i)**, siPARP11 SMARTpool **(j)**, siPARP12 SMARTpool **(k)**, siPARP13 SMARTpool **(l)**, siPARP14 SMARTpool **(m)**, siPARP15 SMARTpool **(n)** and siPARP16 SMARTpool **(o)** and treated with MMS and olaparib (10 μM). For each experiment, controls were included in which *PARP1ΔPARP2Δ* cells were transfected with non-targeting control siRNA and treated with MMS (control 1-treated *PARP1ΔPARP2Δ* cells) or with MMS and olaparib (control 2-treated *PARP1ΔPARP2Δ* cells). Additionally, within each experiment, a control was included in which *PARP1ΔPARP2Δ* cells were transfected with non-targeting control siRNA and treated with MMS and olaparib (10 μM) (control 2-treated *PARP1ΔPARP2Δ* cells). The survival of these cells was analysed via clonogenic survival assay. Error bars at each data point represent the standard error of the mean from three independent biological replicates.

	Two-way ANOVA		
PARP	*PARP1ΔPARP2Δ* + siCtrl vs *PARP1ΔPARP2Δ* + siCtrl + PARPi	*PARP1ΔPARP2Δ* + siCtrl vs *PARP1ΔPARP2Δ* + siPARP + PARPi	*PARP1ΔPARP2Δ* + siCtrl + PARPi vs *PARP1ΔPARP2Δ* + siPARP + PARPi
3	0.0821 ns	0.4377 ns	0.1180 ns
4	0.0821 ns	0.0653 ns	0.7466 ns
5a	0.0018 **	0.0008 ***	0.7500 ns
5b	0.0018 **	0.0074 **	0.6080 ns
6	0.0091 **	0.2987 ns	0.0078 **
7	0.0558 ns	0.1117 ns	0.2451 ns
8	0.8210 ns	0.0243 *	0.1134 ns
9	0.0558 ns	0.0556 ns	0.6826 ns
10	0.0003 ***	0.0016 **	0.0482 *
11	0.0558 ns	0.2978 ns	0.2365 ns
12	0.0003 ***	0.0074 **	< 0.0001 ****
13	0.0091 **	0.0123 *	0.6667 ns

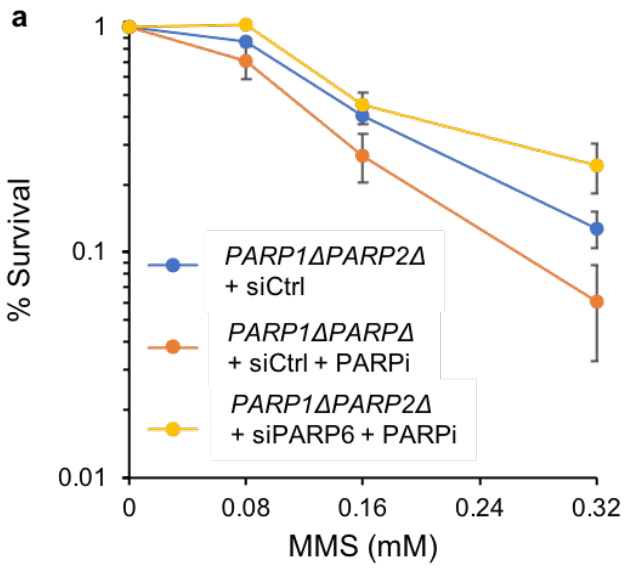
14	0.0003 ***	0.0043 **	0.0002 ***
15	0.0018 **	0.0065 **	0.7015 ns
16	0.00091 **	0.0147 *	0.7413 ns

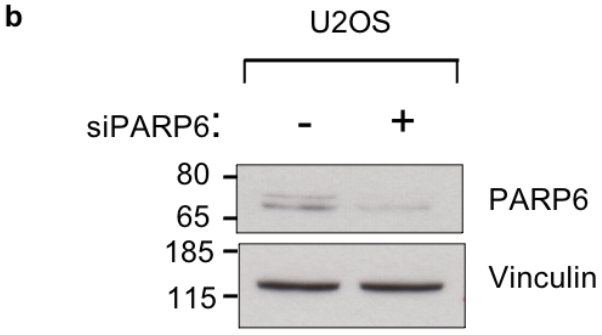
Table 3.3: Summary of p-values for Figure 3.7 when evaluated by two-way ANOVA. Statistical significance was evaluated by two-way ANOVA. For all statistical tests performed, * $p < 0.05$; ** $p < 0.01$; *** $p < 0.001$; **** $p < 0.0001$; ns not significant.

	Two-way ANOVA with Tukey's post-hoc analysis		
PARP	*PARP1ΔPARP2Δ* + siCtrl vs *PARP1ΔPARP2Δ* + siCtrl + PARPi	*PARP1ΔPARP2Δ* + siCtrl vs *PARP1ΔPARP2Δ* + siPARP + PARPi	*PARP1ΔPARP2Δ* + siCtrl + PARPi vs *PARP1ΔPARP2Δ* + siPARP + PARPi
3	0.2175 ns	0.7920 ns	0.7101 ns
4	0.1624 ns	0.1214 ns	0.9986 ns
5a	0.0003 ***	0.0002 ***	0.9960 ns
5b	0.0010 **	0.0034 **	0.9652 ns
6	0.0129 *	0.5876 ns	0.1858 ns
7	0.0655 ns	0.1974 ns	0.8234 ns

8	0.1354 ns	0.0273 *	0.8657 ns
9	0.0840 ns	0.1423 ns	0.9927 ns
10	<0.0001 ****	0.0001 ***	0.7430 ns
11	0.0890 ns	0.5485 ns	0.6682 ns
12	<0.0001 ****	0.0013 **	0.1070 ns
13	0.0037 **	0.0065 **	0.9954 ns
14	<0.0001 ****	0.0011 **	0.3032 ns
15	0.0040 **	0.0014 **	0.9774 ns
16	0.2070 ns	0.2489 ns	0.9995 ns

Table 3.4: Summary of p-values for Figure 3.7 when evaluated by two-way ANOVA with Tukey's post hoc analysis. Statistical significance between was evaluated by two-way ANOVA with Tukey's post hoc analysis. For all statistical tests performed, * $p < 0.05$; ** $p < 0.01$; *** $p < 0.001$; **** $p < 0.0001$; ns not significant.


a
1
0.1
0.01
% Survival
PARP1ΔPARP2Δ
+ siCtrl
PARP1ΔPARPΔ
+ siCtrl + PARPi
PARP1ΔPARP2Δ
+ siPARP6 + PARPi
0
0.08
0.16
0.24
0.32
MMS (mM)


b
U2OS
siPARP6:
-
+
80
65
185
115
PARP6
Vinculin

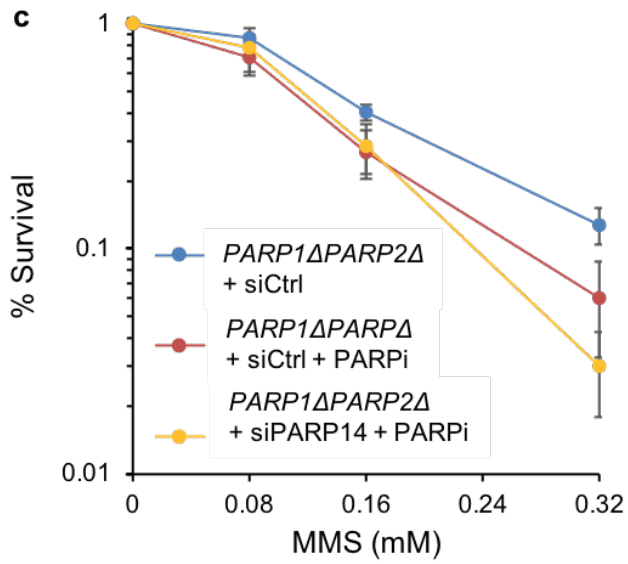

c
1
0.1
0.01
% Survival
PARP1ΔPARP2Δ
+ siCtrl
PARP1ΔPARPΔ
+ siCtrl + PARPi
PARP1ΔPARP2Δ
+ siPARP14 + PARPi
0
0.08
0.16
0.24
0.32
MMS (mM)

Figure 3.8: Repetition of PARP depletion screen to determine whether independent depletion of PARP6 or PARP14 rescues the olaparib-induced further sensitisation of *PARP1ΔPARP2Δ* cells to MMS. (a) *PARP1ΔPARP2Δ* cells were transfected with non-targeting control siRNA or siPARP6 and treated with MMS and olaparib (10 μM). A negative control was included in which *PARP1ΔPARP2Δ* cells were transfected with non-targeting control siRNA and treated with MMS. The viability of these cells was analysed via clonogenic survival assay. **(b)** Wild type U2OS cells were transfected with non-targeting control siRNA or siPARP6 and whole cell extracts were visualised via western blot analysis using the indicated antibodies. Vinculin acted as a loading control. **(c)** *PARP1ΔPARP2Δ* cells were transfected with non-targeting control siRNA or siPARP14 and treated with MMS and olaparib (10 μM). A negative control was included in which *PARP1ΔPARP2Δ* cells were transfected with non-targeting control siRNA and treated with MMS. The viability of these cells was analysed via clonogenic survival assay. Error bars at each data point represent the standard error of the mean from three independent biological replicates. A two-way ANOVA was used to determine the statistical significance between conditions.

	PARP1ΔPARP2Δ + siCtrl vs *PARP1ΔPARP2Δ* + siCtrl + PARPi	*PARP1ΔPARP2Δ* + siCtrl vs *PARP1ΔPARP2Δ* + siPARP6 + PARPi	*PARP1ΔPARP2Δ* + siCtrl + PARPi vs *PARP1ΔPARP2Δ* + siPARP6 + PARPi
Two-way ANOVA	0.0241 *	0.0049 **	0.0002 ***
Two-way ANOVA with Tukey's post-hoc test	0.1607 ns	0.2070 ns	0.0012 **

Table 3.5 Summary of p-values for Figure 3.8 a. Statistical significance was evaluated by two-way ANOVA or by two-way ANOVA with Tukey's post hoc test. For all statistical tests performed, * $p < 0.05$; ** $p < 0.01$; *** $p < 0.001$; ns not significant.

	PARP1ΔPARP2Δ + siCtrl vs *PARP1ΔPARP2Δ* + siCtrl + PARPi	*PARP1ΔPARP2Δ* + siCtrl vs *PARP1ΔPARP2Δ* + siPARP14 + PARPi	*PARP1ΔPARP2Δ* + siCtrl + PARPi vs *PARP1ΔPARP2Δ* + siPARP14 + PARPi
Two-way ANOVA	0.0241 *	0.1373 ns	0.7967 ns
Two-way ANOVA with Tukey's post-hoc test	0.4535 ns	0.6048 ns	0.9944 ns

Table 3.6 Summary of p-values for Figure 3.11 c. Statistical significance was evaluated by two-way ANOVA or by two-way ANOVA with Tukey's post hoc test. For all statistical tests performed, * $p < 0.05$; ns not significant.

3.3 Discussion

The work in this chapter was based on the previous finding that olaparib treatment results in the additional sensitisation of *PARP1ΔPARP2Δ* cells to MMS, indicating that olaparib elicits an effect on a PARP that may participate in the repair of MMS-induced DNA damage in cells lacking PARP1 and PARP2 (Figure 3.1) (Ronson, 2017). Therefore, the overall aim of this chapter was to determine whether a PARP may participate in the repair of MMS-induced DNA damage in the cells lacking PARP1 and PARP2.

I performed two PARP depletion screens in parallel to determine whether a PARP may participate in the repair of MMS-induced DNA damage in the absence of PARP1 and PARP2. The first PARP depletion screen assessed whether olaparib catalytically inhibits a PARP that may participate in the repair of MMS-induced DNA damage in cells lacking PARP1 and PARP2 (Figures 3.4 and 3.5) (Ronson et al., 2018). The second PARP screen investigated whether olaparib traps a PARP to DNA, which may participate in the repair of MMS-induced DNA damage in cells lacking PARP1 and PARP2 (Figures 3.6-3.8) (Murai et al., 2012). It is important to note that when the clonogenic survival assays in these PARP depletion screens were initially analysed, it was acceptable to evaluate the statistical significance between multiple pairs of observations within the same experiment by performing numerous, independent two-way ANOVAs (Ronson et al., 2018). However, more recently, it has become standard practice to evaluate the statistical significance between multiple observations within the same experiment by two-way ANOVA with Tukey's post hoc analysis (Demin et al., 2021). In light of this, I will discuss the interpretation of the results from the

experiments in this chapter when evaluated by two-way ANOVA and by two-way ANOVA with Tukey's post hoc test.

Evaluation of the first PARP depletion screen by two-way ANOVA revealed the following observations. It was not possible to assess whether *PARP1ΔPARP2Δ* cells were further sensitised to MMS following independent depletion of PARP3, PARP4, PARP7, PARP8, PARP9 and PARP11 and PARP16. *PARP1ΔPARP2Δ* cells were not further sensitised to MMS following depletion of PARP5a, PARP5b, PARP6, PARP10, PARP12, PARP13 and PARP14. Initially, *PARP1ΔPARP2Δ* cells were not further sensitised to MMS following PARP15 depletion. However, in a subsequent clonogenic survival assay, *PARP1ΔPARP2Δ* cells were not further sensitised to MMS following depletion of PARP15 (data not shown). Overall, when evaluated by two-way ANOVA, these data suggest the following. Firstly, PARP5a, PARP5b, PARP6, PARP10, PARP12, PARP13, and PARP14 may not participate in the repair of MMS-induced DNA damage cells lacking PARP1 and PARP2. Secondly, it is not clear whether PARP15 may participate in the repair of MMS-induced DNA damage in cells lacking PARP1 and PARP2. Thirdly, it was not possible to assess whether the remaining PARPs may participate in the repair of MMS-induced DNA damage in the absence of PARP1 and PARP2.

Evaluation of the first PARP depletion screen by two-way ANOVA with Tukey's post hoc analysis revealed the following observations. It was not possible to assess whether *PARP1ΔPARP2Δ* cells were further sensitised to MMS following independent depletion of PARP3, PARP4, PARP7, PARP8, PARP9, PARP11 and PARP16. Initially, it was not possible to assess whether *PARP1ΔPARP2Δ* cells were further

sensitised to MMS following depletion of PARP15. Furthermore, in a subsequent clonogenic survival assay, it was still not possible to assess whether *PARP1ΔPARP2Δ* cells were further sensitised to MMS following PARP15 depletion. *PARP1ΔPARP2Δ* cells were not further sensitised following depletion of PARP5a, PARP5b, PARP6, PARP10, PARP12, PARP13 and PARP14. Together, the findings from this PARP depletion screen suggest the following. Firstly, PARP5a, PARP5b, PARP6, PARP10, PARP12, PARP13 and PARP14 may not participate in the repair of MMS-induced DNA damage in cells lacking PARP1 and PARP2. Secondly, it was not possible to assess whether the remaining PARPs may participate in the repair of MMS-induced DNA damage.

Evaluation of the second PARP depletion screen by two-way ANOVA revealed the following observations. It was not possible to assess whether the olaparib-induced further sensitisation of *PARP1ΔPARP2Δ* cells to MMS was rescued following independent depletion of PARP3, PARP7, PARP8, PARP9 or PARP11. Initially, the olaparib-induced further sensitisation of *PARP1ΔPARP2Δ* cells to MMS was rescued by independent depletion of PARP6 and PARP14. However, subsequent clonogenic survival assays demonstrated that PARP6 depletion, but not PARP14 depletion rescued the olaparib-induced further sensitisation of *PARP1ΔPARP2Δ* cells to MMS. Additionally, siRNA-mediated PARP6 protein depletion in wild type U2OS cells was confirmed via western blot (Figure 3.8 b). The olaparib-induced further sensitisation of *PARP1ΔPARP2Δ* cells to MMS was not rescued following independent depletion of the remaining PARPs. Therefore, when evaluated by two-way ANOVA, these data suggest the following. Firstly, it was not possible to assess whether PARP3, PARP7, PARP9 or PARP11 may participate in the repair of MMS-induced DNA damage in cells

lacking PARP1 and PARP2. Secondly, PARP6 or PARP 14 may participate in the repair of MMS-induced DNA damage, but there is more evidence to support the notion that PARP6 may participate in the repair of this type of DNA damage in cells lacking PARP1 and PARP2. Thirdly, the remaining PARPs may not participate in the repair of MMS-induced DNA damage in cells lacking PARP1 and PARP2.

When analysing both PARP depletion screens by two-way ANOVA or by two-way ANOVA with Tukey's post hoc analysis, in some cases, it was not possible to assess whether a given PARP participates in the repair of MMS-induced DNA damage in cells lacking PARP1 and PARP2 when the following issues were encountered within an experiment: (1) There was no significant difference between the survival of control 2-treated *PARP1ΔPARP2Δ* cells and the survival of control 1-treated *PARP1ΔPARP2Δ* cells. (2) The survival of PARP-depleted *PARP1ΔPARP2Δ* treated with MMS (with or without olaparib) was not significantly different to both the survival of control 1-treated *PARP1ΔPARP2Δ* cells and the survival of control 2-treated *PARP1ΔPARP2Δ* cells. A potential cause of these issues is that the experiments in these PARP depletion screens lacked sufficient statistical power. Therefore, in the future, additional independent biological repeats of these screens should be performed to increase the statistical power of these experiments and to determine whether the findings from these screens, when evaluated by two-way ANOVA, still hold true following evaluation by two-way ANOVA with Tukey's post hoc analysis.

Overall, the conclusions drawn from these data are dependent on which method of statistical analysis is considered acceptable. Given that when the experiments in this chapter were performed, it was considered acceptable to evaluate the statistical

significance between multiple observations by two-way ANOVA, I conclude that taken together, the data from the PARP depletion screens suggest that the olaparib-induced further sensitisation of *PARP1ΔPARP2Δ* cells to MMS may be due to olaparib-induced trapping of PARP6 or PARP14 to DNA and not due to olaparib-dependent catalytic inhibition of either of these PARPs. This supports the notion that PARP6 or PARP14 may participate in the repair of MMS-induced DNA damage in cells lacking PARP1 and PARP2. However, given that there is more evidence supporting the notion that PARP6 may participate in this DNA repair pathway in cells lacking PARP1 and PARP2, it is more likely that PARP6 performs this function. Due to the issues described previously, it was not possible to assess whether these conclusions hold true when the data from the PARP depletion screens were evaluated by two-way ANOVA with Tukey's post hoc analysis. This could be due to the more conservative nature of two-way ANOVA with Tukey's post hoc analysis compared to two-way ANOVA. In order to assess, by two-way ANOVA with Tukey's post hoc analysis, whether PARP6 or PARP14 may participate in the repair of MMS-induced DNA damage in cells lacking PARP1 and PARP2, it may be beneficial to perform additional biological repeats of these experiments, as this will increase the statistical power of these experiments. Alternatively, it may be beneficial to conduct additional experiments using different experimental approaches (see below).

PARP6 regulates activation of the Wnt signalling pathway, mitosis and cell division (Huang et al., 2016; Tang et al., 2020; Wang et al., 2018; Vermehren-Schmaedick et al., 2021; Tuncel et al., 2016). PARP14 regulates HR, reversed fork resection, the inflammatory response and advancement through the cell cycle (Dhoonmoon et al., 2022; Iwata et al., 2016; Mehrotra et al., 2011, 2013; Nicolae et al., 2015; O'Connor

et al., 2021). However, precisely how PARP6 or PARP14 might participate in the repair of MMS-induced DNA damage in cells lacking PARP1 and PARP2, is not clear. Furthermore, it is also not clear how PARP6 or PARP14 may be trapped to DNA by olaparib without being catalytically inhibited by this PARPi. Interestingly, a recent publication demonstrated that in *PARP1Δ* cells, PARP2 can be trapped to DNA by olaparib via an ill-defined mechanism that occurs independently of olaparib-mediated PARP2 catalytic inhibition (Lin et al., 2022). Given that PARPs can be trapped to DNA by olaparib via multiple mechanisms, it is conceivable that PARP6 or PARP14 may be trapped to DNA by olaparib in a manner that is independent of catalytic inhibition.

While the PARP depletion screens were successful in generating a shortlist of PARP candidates that may participate in the repair of MMS-induced DNA damage in cells lacking PARP1 and PARP2, it was not possible from these data, to identify the individual PARP that may perform this function. Therefore, to determine with greater confidence if the identity of the PARP that may be trapped to DNA by olaparib in MMS-treated *PARP1ΔPARP2Δ* cells is PARP6 or PARP14, a chromatin fractionation experiment should be performed and visualised by western blot (Murai et al., 2012). Given that MMS-induced alkylation base damage is primarily repaired by BER, it is conceivable that either PARP6 or PARP14 participate in this repair pathway in response to this type of DNA damage in cells lacking PARP1 and PARP2 (Lindahl & Wood, 1999). Should olaparib-induced trapping of one of these PARPs be confirmed in MMS-treated *PARP1ΔPARP2Δ* cells via chromatin fractionation, the potential involvement of this PARP in BER should be investigated by performing the newly developed alk-BER assay in *PARP1ΔPARP2Δ*PARP6Δ cells (Li et al., 2021).

Through a chemical proteomics approach, it was not possible to identify the PARPs that have the strongest interactions with olaparib in *PARP1ΔPARP2Δ* cells and therefore it was not possible to identify potential candidates for the PARP that may participate in the repair of MMS-induced DNA damage in cells lacking PARP1 and PARP2 (Figure 3.2, 3.3 a-b) (Médard et al., 2015). Indeed, analysis of the *PARP1ΔPARP2Δ* cell lysates in this experiment revealed the presence of PARP1 and PARP2 peptides. However, independent mass-spectrometry and western blot analysis of the *PARP1ΔPARP2Δ* cell lysates confirmed that this cell line was a CRISPR double-knockout (Figure 3.3 c) (Ronson, 2017). A possible explanation for these observations is that PARP1 and PARP2 from the wild type U2OS cell lysate may have remained in the mass spectrometer between sample runs, resulting in contamination of the *PARP1ΔPARP2Δ* cell lysates with PARP1 and PARP2. Given that there were technical issues with the chemical proteomic approach and that the experiment was only performed once, additional biological replicates are required before confidently proposing potential candidates for the PARP that may participate in the repair of MMS-induced DNA damage in cells lacking PARP1 and PARP2. Interestingly, *in vitro*, it is not known whether olaparib catalytically inhibits PARP6, but it is thought that PARP14 is not catalytically inhibited by olaparib (Thorsell et al., 2017; Wahlberg et al., 2012).

In summary, in this chapter, I have demonstrated that following evaluation of two PARP depletion screens by two-way ANOVA, PARP6 or PARP14 may be trapped to DNA by olaparib independently of olaparib-induced catalytic inhibition. This indicates that one of these PARPs may participate in the repair of MMS-induced DNA damage in cells lacking PARP1 and PARP2. However, the design and execution of these

PARP depletion screens may need to be altered in order to determine whether these findings can be confirmed following evaluation of these screens by two-way ANOVA with Tukey's post hoc analysis. Given that the observations in this chapter yielded subtle phenotypes which often lacked statistical significance, the remainder of the research in this thesis focused on identifying novel proteins that function within the DDR, which are synthetic lethal with combined loss of PARP1 and PARP2 (see chapters 4 and 5).

Chapter 4. Identifying novel synthetic lethal interactions with combined loss of PARP1 and PARP2

4.1 Introduction

4.1.1 CRISPR in genome editing

The CRISPR-Cas system functions as an immune system that is utilised by prokaryotes as a barrier against repeated invasion of exogenous nucleotides such as viruses (Barrangou et al., 2007; Makarova et al., 2006). The subsequent modification of this system to act as programmable genetic scissors has undoubtedly expedited the identification of important discoveries across a multitude of fields, including DNA damage repair. As such, for their pioneering work in the development of the CRISPR-Cas system, Jennifer Doudna and Emmanuelle Charpentier shared the Nobel Prize in Chemistry 2020 (The Nobel Prize in Chemistry 2020, 2020). The most prevalent CRISPR-Cas tool that is used for targeted genome editing is the Cas9 nuclease that is derived from *Streptococcus pyogenes* (SpCas9) (Jinek et al., 2012; Pickar-Oliver & Gersbach, 2019). Furthermore, the first examples of programmable editing of mammalian genomes used SpCas9 (Cong et al., 2013; Mali et al., 2013). Cas9 can be programmed with a single guide RNA (sgRNA) to induce a locus-specific DSB via its RuvC and HNH domains, provided that the incision site is next to a protospacer-adjacent motif (PAM) sequence. The sgRNA contains a sequence that is complementary to the target locus and can therefore recruit Cas9 to the locus of interest (Cong et al., 2013; Garneau et al., 2010; Jinek et al., 2012; Mali et al., 2013). Error-prone NHEJ-dependent repair of Cas9-induced DSBs can result in insertions

and deletions that produce frameshift mutations at target loci, thus negating expression of specific genes (Pickar-Oliver & Gersbach, 2019).

Following its discovery, the CRISPR-Cas technology has been further developed to enable pooled screens, through which, researchers can systematically assess the effect of individually altering each gene within a given genome. For example, CRISPR dropout or positive selection screens can be performed to assess whether disruption of a given gene decreases or increases cell viability, respectively. The effect of these gene disruptions can be investigated in unperturbed cells, or in response to treatment with specific compounds such as DDR inhibitors (DDRi) or DNA damaging agents (Doench, 2018). Studies of this nature were first performed in human cells in 2014 (Shalem et al., 2014; Wang et al., 2014). For a more detailed description of pooled screens, refer to section 4.2.1.

4.1.2 Discovery of novel DDR factors using CRISPR screens

Pooled CRISPR screens have been instrumental in discovering novel DDR factors. For example, through the use genome-wide CRISPR dropout screens, two independent research groups concurrently identified that C17orf53 confers resistance to ICLs. This protein was identified as a potential DDR factor since it was a high ranking hit in genome-wide CRISPR dropout screens investigating genes that confer resistance to ATRi and PARPi (Hustedt, Saito, et al., 2019; Hustedt, Álvarez-Quilón, et al., 2019; Wang, Chen, et al., 2019; Wang et al., 2020; Zimmermann et al., 2018). Notably, in a recent publication, several CRISPR screens were performed in order to identify genes which, when disrupted, sensitise human cells to treatment with 27 different genotoxic agents, providing a genetic map for human cells in response to a

plethora of types of DNA damage. Through this screen, numerous novel DDR factors were identified, including the ATPase ERCC6L2, which was revealed as a novel c-NHEJ factor (Olivieri et al., 2020; Zhang et al., 2016). In another study, C20orf196/SHLD1, which forms the Shieldin complex with REV7, SHLD2, and SHLD3, was discovered in a CRISPR-based screen that sought to identify genes which, when disrupted, conferred PARPi resistance by re-establishing HR in *BRCA1*-hypomorphic or *BRCA1* knockout cell lines (Noordermeer et al., 2018). Therefore, pooled CRISPR screens are a valuable experimental tool that can be used to identify genetic determinants of sensitivity or resistance to genotoxic agents and DDRi in an unbiased manner. Furthermore, pooled CRISPR screens can be harnessed to uncover novel synthetic lethal interactions between genes, which can also identify novel DDR genes (Nijman, 2011; Ashworth & Lord, 2018).

4.1.3 Aims

It has been proposed that synthetic lethal interactions can occur between genes that are redundant in cellular function (Nijman 2011; Ashworth & Lord, 2018). Given that PARP1 and PARP2 have well characterized roles in the DDR, the Lakin lab performed a genome-wide CRISPR dropout screen in wild type U2OS and *PARP1ΔPARP2Δ* cells in order to identify synthetic lethal interactions with combined loss of PARP1 and PARP2. This screen may in turn, reveal novel DDR factors and therefore reveal hitherto unknown mechanisms in the DDR. Previously, genome-wide CRISPR dropout screens have exposed synthetic lethal interactions with olaparib, which are generally thought to be dependent predominantly on olaparib-induced trapping to DNA and catalytic inhibition of PARP1 (Knezevic et al., 2016; Murai et al., 2012; Thorsell et al., 2017; Zimmermann et al., 2018). Furthermore, olaparib is known to trap PARP2 to

DNA and inhibit its catalytic activity (Murai et al., 2012). However, the Lakin lab's screen is unique in that it has the potential to identify novel synthetic lethal interactions that do not occur due to PARP1 and/or PARP2 trapping to DNA. Identifying and increasing our mechanistic understanding of novel synthetic lethal interactions is important as these findings may have the potential to be exploited to develop novel therapeutics to treat cancers in the clinic. As such, by analysing the hits from the Lakin lab's screen, the aims of this chapter are:

1. To determine whether synthetic lethal interactions with combined loss of PARP1 and PARP2 may reveal potential novel DDR factors.

2. To validate any synthetic lethal interaction(s) of interest from the genome-wide CRISPR dropout screen and to determine whether PARP1 and/or PARP2 is the key determinant of the synthetic lethal interaction(s).

3. To learn more about the cellular function and other characteristics of the novel potential DDR factor(s) of interest.

4.2 Results

4.2.1 Identification of synthetic lethal interactions with combined deletion of PARP1 and PARP2

To determine whether synthetic lethal interactions with combined deletion of PARP1 and PARP2 may reveal potential novel DDR factors, a genome-wide CRISPR dropout screen was performed in wild type U2OS and *PARP1ΔPARP2Δ* cells by Dr George

Ronson in collaboration with Daniel Ebner's group at the Target Discovery Institute, University of Oxford (Figure 4.1). 150 million wild type U2OS or *PARP1ΔPARP2Δ* cells were infected with the Toronto Knockout CRISPR Library (TKOv3) via lentiviral transduction. This library contains 70,948 guide RNAs (gRNAs) that collectively target 18,053 protein-producing genes. The library also encodes the gene for SpCas9. Therefore, each gene was targeted by four independent gRNAs in an SpCas9-dependent manner (Hart et al., 2017; Olivieri & Durocher, 2021). The transduced U2OS and *PARP1ΔPARP2Δ* cells were treated with a 3-day puromycin selection pressure. Subsequently, at t = 0 days, the DNA was extracted from 40 million cells of each cell line and the integrated gRNAs were amplified and sequenced by 2-step PCR and Illumina Next Generation Sequencing, respectively. This sequencing data was used to estimate the representation of gRNAs in the wild type U2OS and *PARP1ΔPARP2Δ* pools at this time point. Subsequently, the transduced cells were subcultured until the cells doubled 12 times and the DNA was extracted, amplified and sequenced as described above. This sequencing data was used to identify the gRNAs that were still represented in each of the cell lines (Olivieri & Durocher, 2021). The wild type U2OS cells took 18 days to double 12 times (t = 18), whereas the *PARP1ΔPAPR2Δ* cells took 24 days to double 12 times (t = 24). Finally, the effect of knocking out a given gene on the viability of wild type U2OS or *PARP1ΔPARP2Δ* cells was calculated using the Model-based Analysis of Genome-wide CRISRP/Cas9 Knockout (MAGeCK) platform (analysis performed by Dr Khairul Ramlee) (Li et al., 2014). A strict false discovery rate (FDR) cut-off value of 0.01 was applied to increase the stringency of the hits. Using this approach, 193 genes were identified that reduced the viability of wild type U2OS cells, but not *PARP1ΔPARP2Δ* cells when disrupted. Additionally, 49 genes reduced the viability of both of these cell lines when disrupted.

Furthermore, 10 genes reduced the viability of *PARP1ΔPAPR2Δ*, but not wild type U2OS cells when disrupted, which suggests that the genome-wide CRISPR dropout screen yielded 10 potential synthetic lethal interactions with combined deletion of PARP1 and PARP2.

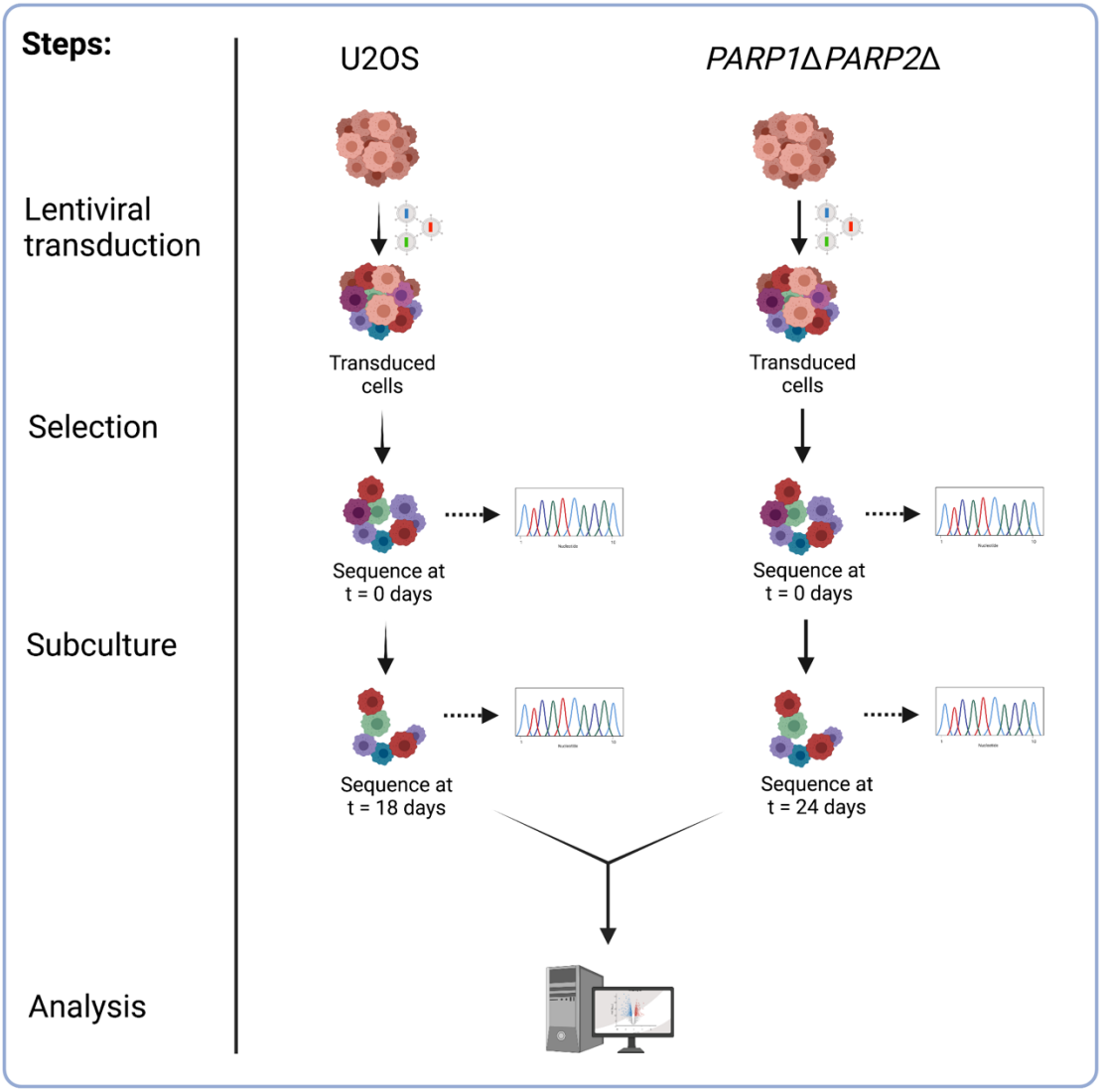


Figure 4.1: Genome-wide CRISPR dropout screen to identify novel synthetic lethal interactions with combined *PARP1* and *PARP2* deletion. Schematic diagram summarising the genome-wide CRISPR dropout screen performed in wild type U2OS and *PARP1ΔPARP2Δ* cell lines. U2OS and *PARP1ΔPAPR2Δ* cells were

transduced with the TKOv3 library and subjected to a puromycin selection pressure for 3 days. At t = 0 days, DNA was extracted from each of the cellular pools and integrated gNRAs were amplified by 2-step PCR and sequenced by Illumina. Transduced U2OS and *PARP1ΔPAPR2Δ* cells were subcultured for a further 18 and 24 days, respectively, in order to allow the cells to undergo 12 cell divisions. At t = 18 days (wild type U2OS cells) or t = 24 days (PARP1ΔPAPR2Δ), DNA was extracted, amplified and sequenced as described above. gRNA representation at the beginning and end of the screen was evaluated using MAGeCK. The screen was performed by Dr George Ronson and Dr Daniel Ebner's group at the Target Discovery Institute, University of Oxford. Subsequent anaylsis of the screen was performed by Dr Khairul Ramlee. Produced with BioRender.

The 10 gene candidates, in rank order, from the screen were: *DNA J Heat Shock Protein Family (Hsp40) Member C9* (*DNAJC9*), *Ribonuclease H2 Subunit A (RNAS2H2A)*, *Nuclear VCP Like* (*NVL*), *SARS*, *Ribosomal Protein L36* (*RPL36*), *Fanconi anemia group F* (*FANCF*), *Mitochondrial Ribosomal Protein S34* (*MRPS34*), *ATP-binding Cassette Subfamily C Member 6* (*ABCC6*), *Polypyrimidine tract binding protein* (*PTBP1*), and *Chromosome 16 Open Reading Frame 72* (*C16orf72*) (Figure 4.2). Recently, DNAJC9 has been identified as a contributor to the maintenance of the integrity of histones (Hammond et al., 2021). RNASEH2 is a protein trimer that consists of RNASEH2A, RNASEH2B and RNASEH2C. As DNA replication proceeds, RNASEH2 is involved in the resolution of R-loops and also excises incorrectly incorporated ribonucleotides from DNA. RNASEH2 catalysis is mediated by the RNAS2H2A subunit (Chon et al., 2013; Crow et al., 2006; Hiller et al., 2012; Jeong et al., 2004; Pizzi et al., 2015; Williams et al., 2017). NVL performs a number of functions,

but most notably, it is involved in the cellular production of ribosomes (Nagahama et al., 2006). *SARS* encodes seryl-tRNA synthetase although its cellular function is ill-defined (The UniProt Consortium, 2021). *RPL36* encodes a canonical ribosomal protein, as well as a newly discovered alt-RPL36 protein. Both of these proteins contribute to the regulation of translation in distinct ways (Cao et al., 2021). FANCF is a component of the FA core complex, that also consists of FAAP20, FAAP100, FANCA, FANCB, FANCC, FANG and FANCL. The core complex contributes to the resolution of ICLs via the Fanconi anaemia pathway (Walden & Deans, 2014). MRPS34 is a component of the small subunit of the mitochondrial ribosome and is vital for the translation of mitochondria-specific proteins. It also functions to stabilise a component of the small ribosomal subunit 12S rRNA, and also stabilises the small ribosomal subunit as a whole (Koc et al., 2001; Richman et al., 2015; Suzuki et al., 2001). *ABCC6* is a gene that encodes a protein that actively transports negatively-charged organic compounds (Iliás et al., 2002). PTBP1 is involved in the metabolism of RNA in numerous biomolecular contexts. For example, it inhibits alternative splicing of mRNA and also promotes mRNA stability (Tillmar et al., 2002; Tillmar & Welsh, 2002; Wagner & Garcia-Blanco, 2001). Given that FANCF and RNASEH2A were identified as synthetic lethal hits in this screen, this validates the use this approach to identify DDR factors. Taken together, analysis of this screen identified 10 potential novel synthetic lethal interactions with combined loss of PARP1 and PARP2 and therefore also identified numerous potential DDR factors: DNAJC9, NVL, SARS, RPL36, MRPS34, ABCC6, PTBP1 and C16orf72. At the time that this analysis was performed, the cellular function of C16orf72 was entirely unknown. Therefore, C16orf72 was an ideal candidate to pursue further, as a potential novel DDR factor.

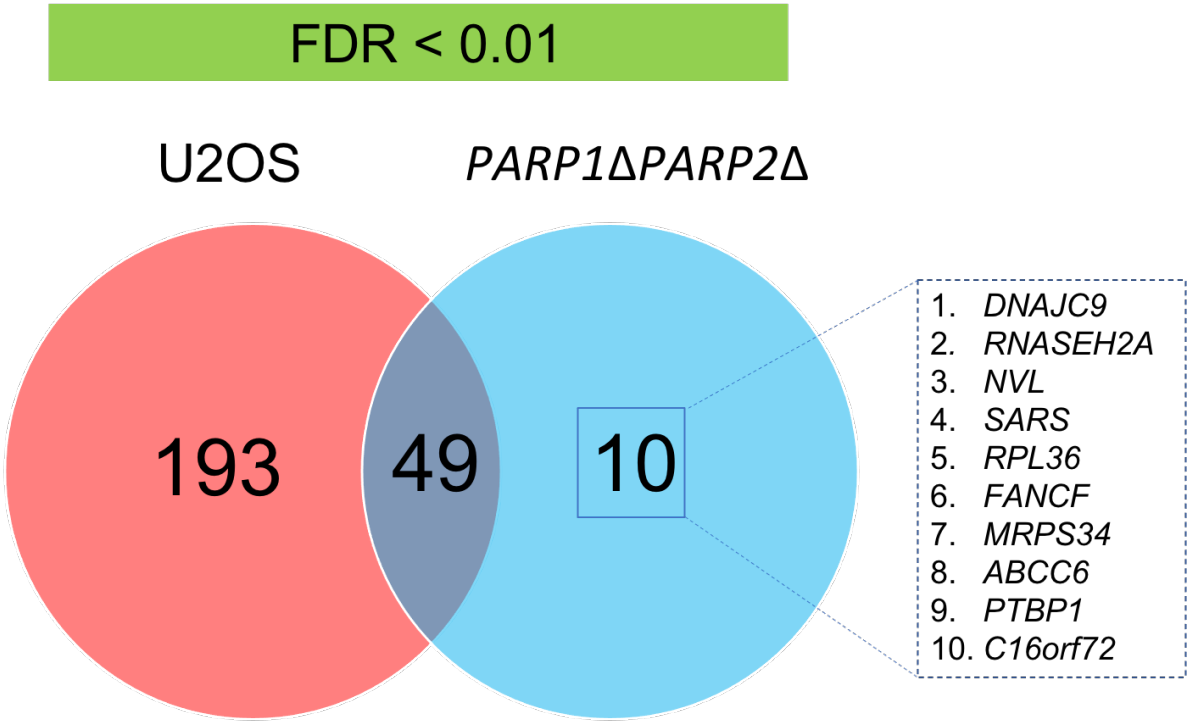


Figure 4.2: Venn diagram summarising gene hits identified in the wild type U2OS and *PARP1ΔPARP2Δ* cell lines. Depletion of 193 genes reduced the viability of U2OS cells. Depletion of 49 genes reduced the viability of both U2OS and *PARP1ΔPARP2Δ* cells. Depletion of 10 genes reduced the viability of *PARP1ΔPARP2Δ* cells. In rank order, these gene hits were *DNAJC9*, *RNASEH2A*, *NVL*, *SARS*, *RPL36*, *FANC*F, *MRPS34*, *ABCC6*, *PTBP*1 and *C16orf72*. Analysis of the screen hits was performed by Dr Khairul Ramlee.

4.2.2 Validation of the synthetic lethal interaction between C16orf72 loss and combined PARP1 and PARP2 deletion

To validate the synthetic lethal interaction between C16orf72 loss and combined deletion of PARP1 and PARP2, I transfected U2OS and *PARP1ΔPARP2Δ* cells with non-targeting control siRNA, C16orf72-targeting SMARTpool siRNA, or four independent C16orf72-targeting siRNAs (siRNA #1, siRNA #2, siRNA #3 and siRNA #4) and assessed the ability of these cells to form colonies via clonogenic survival assay (Figure 4.3 a and b). Excitingly, the synthetic lethal interaction could be recapitulated with 3 independent C16orf72-targeting siRNAs (siRNA #2 ($p < 0.0001$), siRNA #3 ($p = 0.0258$) and siRNA #4 ($p = 0.0036$)), although not with siRNA #1 ($p = 0.3941$)). Moreover, the severity of the synthetic lethal interaction directly correlated with C16orf72 knockdown efficiency (Appendices Figure 1). Additionally, as expected, the synthetic lethal interaction could be recapitulated with the C16orf72-targeting SMARTpool siRNA (Figure 4.3 a ($p = 0.0013$) and b ($p = 0.0003$)). Together, these data validate the synthetic lethal interaction between C16orf72 loss and combined PARP1 and PARP2 deletion.

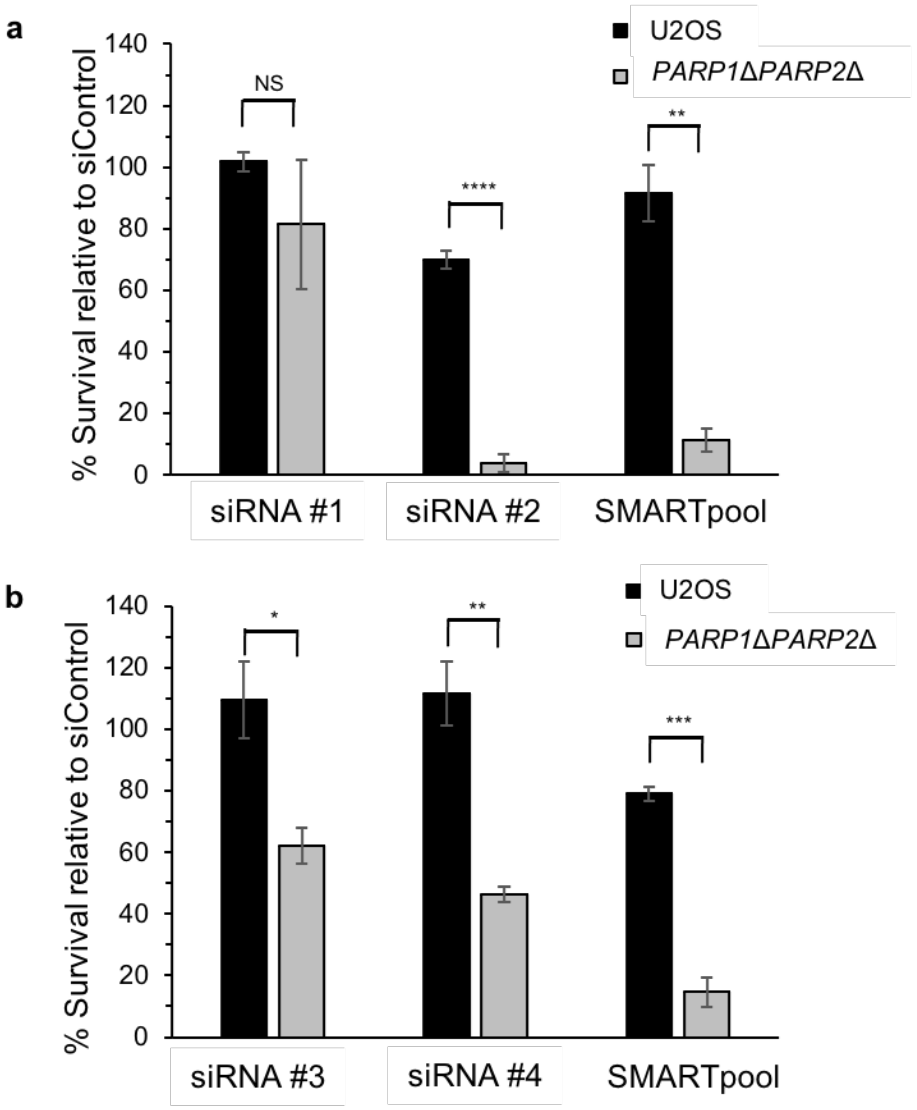


Figure 4.3: C16orf72 depletion is synthetic lethal with combined PARP1 and PARP2 loss. (a) Wild type U2OS and *PARP1ΔPARP2Δ* cells were transfected with non-targeting control siRNA, C16orf72-targeting siRNA#1, C16orf72-targeting siRNA#2, or a C16orf72-targeting siRNA SMARTpool. The viability of each cell line transfected with non- targeting control siRNA was set to 100%. The viability of each cell line transfected with the C16orf72-targeting siRNAs was analysed relative to the viability of each respective cell line transfected with non-targeting control siRNA, via clonogenic survival assay. **(b)** Wild type U2OS and *PARP1ΔPARP2Δ* cells were transfected with non-targeting control siRNA, C16orf72-targeting siRNA#3, C16orf72-

targeting siRNA#4, or a C16orf72-targeting siRNA SMARTpool. The viability of each cell line transfected with non-targeting control siRNA was set to 100%. The viability of each cell line transfected with the C16orf72-targeting siRNAs was analysed via clonogenic survival assay as described previously. Unpaired t-tests were used to determine the statistical significance between conditions and. The data represents three independent biological repeats and error bars represent the SEM. For all statistical tests performed, ns, not significant; * $p < 0.05$; ** $p < 0.01$; *** $p < 0.001$; **** $p < 0.0001$.

4.2.3 Investigating the key determinants of the synthetic lethal interaction between C16orf72 deficiency and combined PARP1 and PARP2 loss

Next, I investigated whether PARP1 and/or PARP2 are the key determinant(s) of the synthetic lethal interaction by transfecting wild type U2OS, *PARP1Δ*, *PARP2Δ* and *PARP1ΔPARP2Δ* cell lines with a C16orf72-targeting siRNA SMARTpool and assessed their ability to form colonies via clonogenic survival assay (Figure 4.4). A statistically significant reduction in cell survival was not observed in C16orf72-depleted *PARP1Δ* cells compared to C16orf72-depleted wild type U2OS cells ($p = 0.0793$). Similarly, a statistically significant reduction in viability was not observed in C16orf72-depleted *PARP2Δ* cells compared to C16orf72-depleted wild type U2OS cells ($p > 0.9999$). However, a 62.73% reduction in viability was observed in C16orf72-depleted *PARP1ΔPARP2Δ* cells compared to C16orf72-depleted wild type U2OS cells ($p = 0.0132$). Taken together, these data represent a novel synthetic lethal interaction in human cells and suggest that both PARP1 and PARP2 may be key determinants of the synthetic lethal interaction.

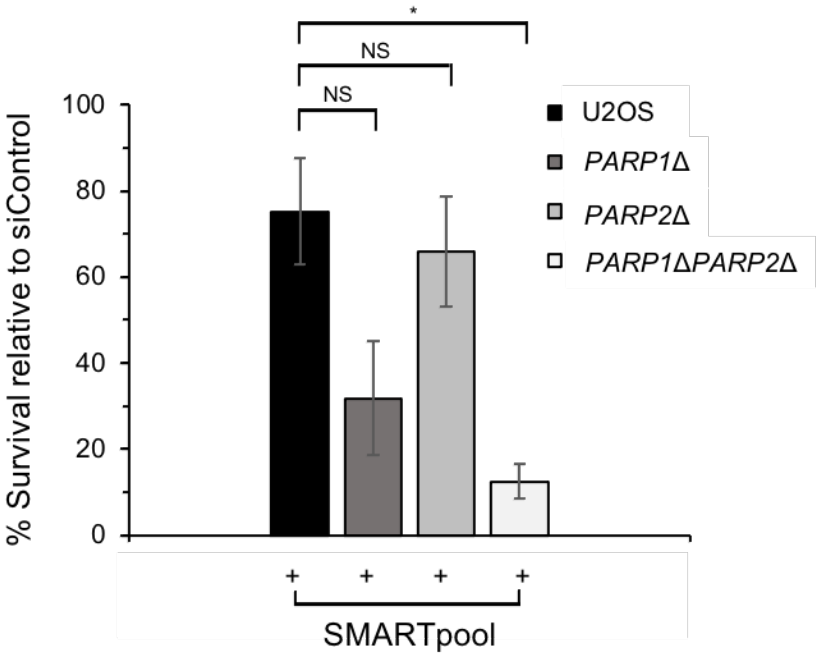


Figure 4.4: PARP1 and PARP2 may be key determinants of the synthetic lethal interaction between C16orf72 deficiency and combined PARP1 and PARP2 loss. Wild type U2OS, *PARP1Δ*, *PARP2Δ* and *PARP1ΔPARP2Δ* cells were transfected with non-targeting control siRNA, or with C16orf72-targeting siRNA SMARTpool. The viability of each cell line transfected with non- targeting control siRNA was set to 100%. The viability of each cell line transfected with the C16orf72-targeting siRNA SMARTpool was analysed relative to the viability of each respective cell line transfected with non-targeting control siRNA via clonogenic survival assay. The data represents three independent biological repeats and error bars represent the SEM. A one-way ANOVA, followed by a Bonferroni post hoc test was used to determine the statistical significance between conditions. ns, not significant; * $p < 0.05$.

4.2.4 Bioinformatic analysis of C16orf72

At the time that the synthetic lethal interaction between C16orf72 loss and combined *PARP1* and *PARP2* deletion was validated, the function of C16orf72 was ill-defined. Therefore, to determine potential functions of C16orf72 within and outside the DDR, and to characterise this protein, I performed bioinformatic analyses on C16orf72. Through analysis with Ensembl, I found that human *C16orf72* encodes 4 exons which are predicted to form two isoforms. The long isoform (275 amino acids) contains exons 1-4 whereas the short isoform (150 amino acids) contains exons 1-3. The estimated molecular weights of the long and short isoforms are 30.9 kDa and 17.1 kDa, respectively (Cunningham et al., 2022). Additionally, an InterProScan search suggested that a domain of unknown function – the DUF4588 domain – spans across the majority of C16orf72 (Jones et al., 2014) (Figure 4.5). Using the PhosphoSitePlus database, I determined that there are 6 sites of phosphorylation that all occur within the DUF4588 domain – Ser167, Ser197, Ser202, Ser204, Ser208, Ser212 and Ser266. The database also revealed that there are 2 sites of ubiquitination at Lys5, Lys23 that are outside of the DUF4588 domain and another two ubiquitination sites at Lys55 and Lys150 that fall within the DUF4588 domain. It is important to note that the Ser167 phosphosite has been identified in 15 separate studies which demonstrates that it is a consistent finding, whereas the other PTMs have been reported considerably less frequently and therefore may not represent true sites of phosphorylation or ubiquitination (Hornbeck et al., 2015). Taken together, these analyses identify numerous PTM sites in C16orf72, but it is not clear how these PTMs regulate C16orf72 function.

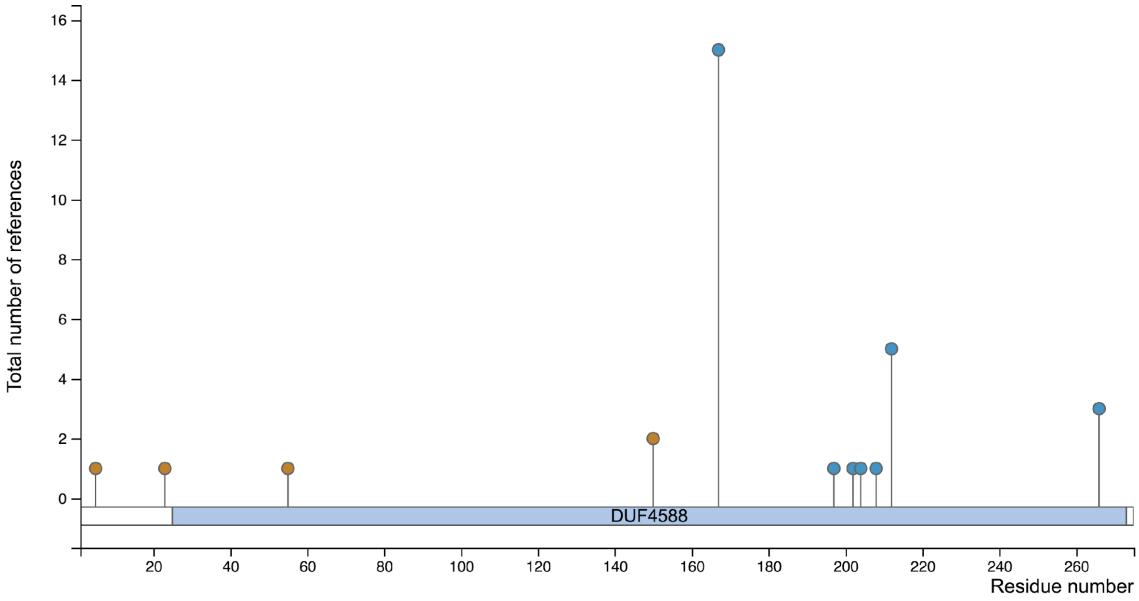


Figure 4.5: Predicted sites of phosphorylation and ubiquitination in human C16orf72. Prediction of sites of phosphorylation (blue marker) and ubiquitination (brown marker) in human C16orf72 from the PhosphoSitePlus database (Hornbeck et al., 2015).

Consequently, to identify highly conserved motifs that might suggest a potential cellular function for C16orf72, I performed an alignment of human C16orf72 with C16orf72 orthologues from the arthropods, chordates and ascomycetes, using the Clustal Omega tool (Sievers et al., 2011, Siever et al., 2020; Sievers & Higgins, 2018) (Figure 4.6 and Appendices Figure 2). The alignment showed that there are two highly conserved motifs in chordates and arthropods, but not in ascomycetes. These highly conserved motifs are 'WXXFQXXAXXXTXXYKXS' (motif 1) and 'WXXKXRXRXIRREXLXXXLXGXXXP' (motif 2), where 'X' represents any amino acid. While the structure of the known isoform of human C16orf72 is yet to be solved, it has been predicted with high confidence using the AI-based in silico model AlphaFold 2.0 (Figure 4.7). The model predicts that vertebrate C16orf72 has two central alpha helixes which span the entire diameter of the protein, as well as 3 shorter, peripheral

alpha helixes. In contrast, C16orf72 from the ascomycete *Saccharomyces cerevisiae* contains a long alpha helix which spans the entire diameter of the protein, and two peripheral alpha helixes (Jumper et al., 2021). In vertebrates, motif 1 is found within the longest central alpha helix, whereas motif 2 is found in a peripheral alpha helix. These findings suggest that there are highly conserved sequences of amino acids withinin C16orf72 in chordates and arthropods, and the predicted structure of this protein is highly conserved in the vertebrates. A search of the BLASTP database using motif 1 revealed immunoglobulin heavy chain junction region, DNAH10, FPRL2, T cell receptor alpha chain and CSMD1 as the top 5 hits. A summary of the cellular functions of these proteins can be found in Table 4.1. A search of the BLASTP database using motif 2 uncovered CCG1, TFIID subunit 1, CDP/cut, HECT, UBA and WWE Domain Containing Protein Ligase 1 (HUWE1) and SHF isoform o as the top 5 hits. The cellular functions of these proteins are summarised in Table 4.2. Of all of these identified hits, HUWE1 was particularly intriguing given that HUWE1 is a ubiquitin ligase that has a multitude of functions within the cell, but importantly, it is known to partake in multiple DDR pathways, including the DNA replication stress response (Choe et al., 2016; Hall et al., 2007; Kao et al., 2018; Mandemaker et al., 2017; Parsons et al., 2009; Sander et al., 2017; Zhong et al., 2005). Interestingly, parts of motif 2 show similarity with human HUWE1 at amino acids 2980-2994, which forms part of the ubiquitin-binding motif 1 (UBM1) domain that spans amino acids 2951-3100 of human HUWE1 (Hunkeler et al., 2021) (Figure 4.6). Therefore, collectively, these analyses indicate that C16orf72 may have numerous cellular functions, and importantly, may participate in the DNA replication stress response and other DDR pathways.

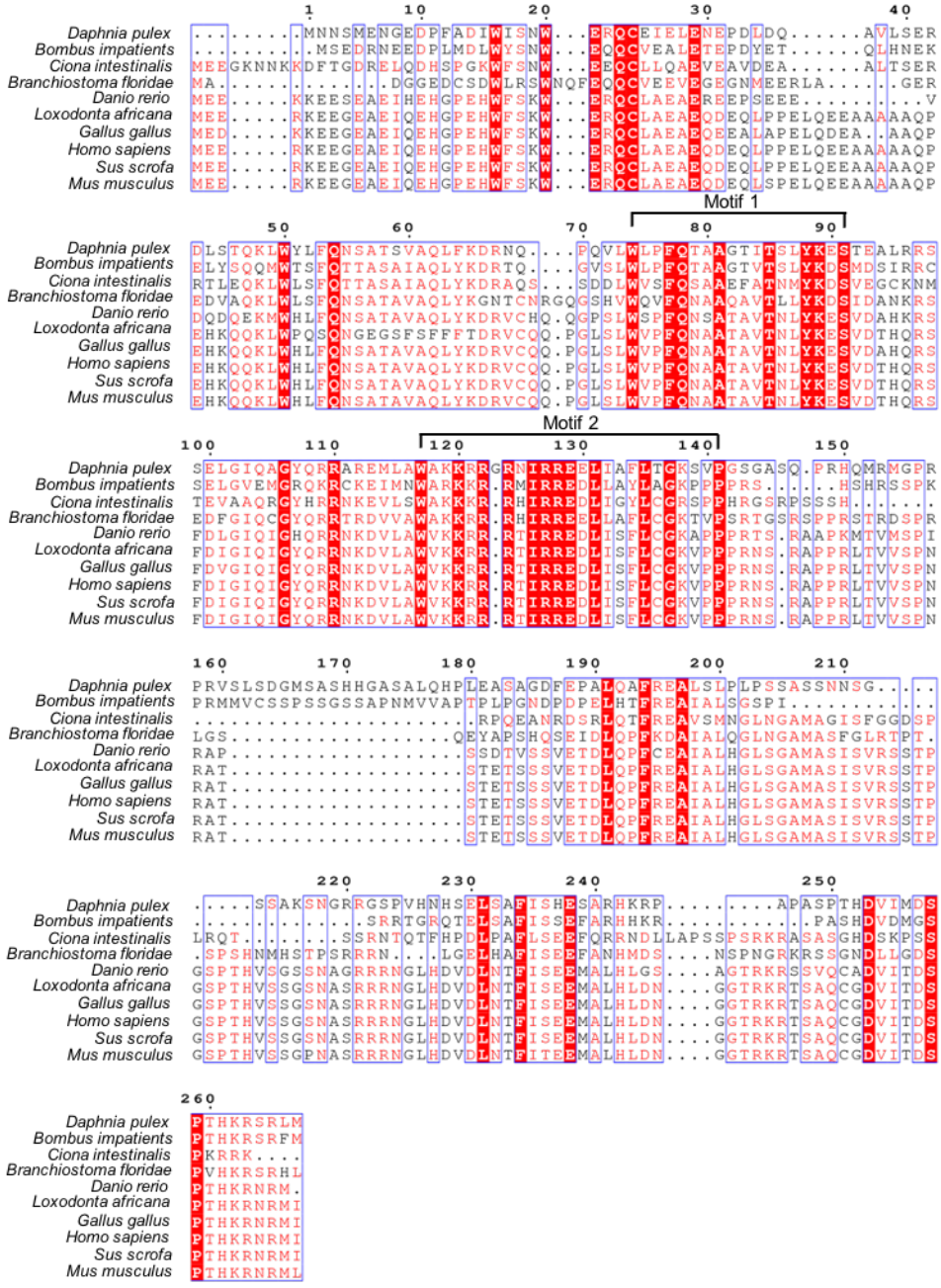

Motif 1
Motif 2
Daphnia pulex
Bombus impatients
Ciona intestinalis
Branchiostoma floridae
Danio rerio
Loxodonta africana
Gallus gallus
Homo sapiens
Sus scrofa
Mus musculus

Figure 4.6: Two motifs are highly conserved in C16orf72 orthologues from chordates and arthropods. Alignment of C16orf72 orthologues from *Daphnia pulex*, *Bombus impatients*, *Ciona intestinalis*, *Danio rerio*, *Loxodonta africana*, *Gallus gallus*, *Homo sapiens*, *Sus scrofa* and *Mus musculis*. The alignments were prepared with Clustal Omega and visualised with EndScript 3.0 (Robert & Gouet, 2014; Sievers et al., 2011, 2020; Sievers & Higgins, 2018). Completely conserved amino acids are indicated with white letters on a red background. Similar amino acids are indicated with red letters on a white background and are surrounded by a blue box. Amino acids with low similarity are indicated with black letters on a white background.

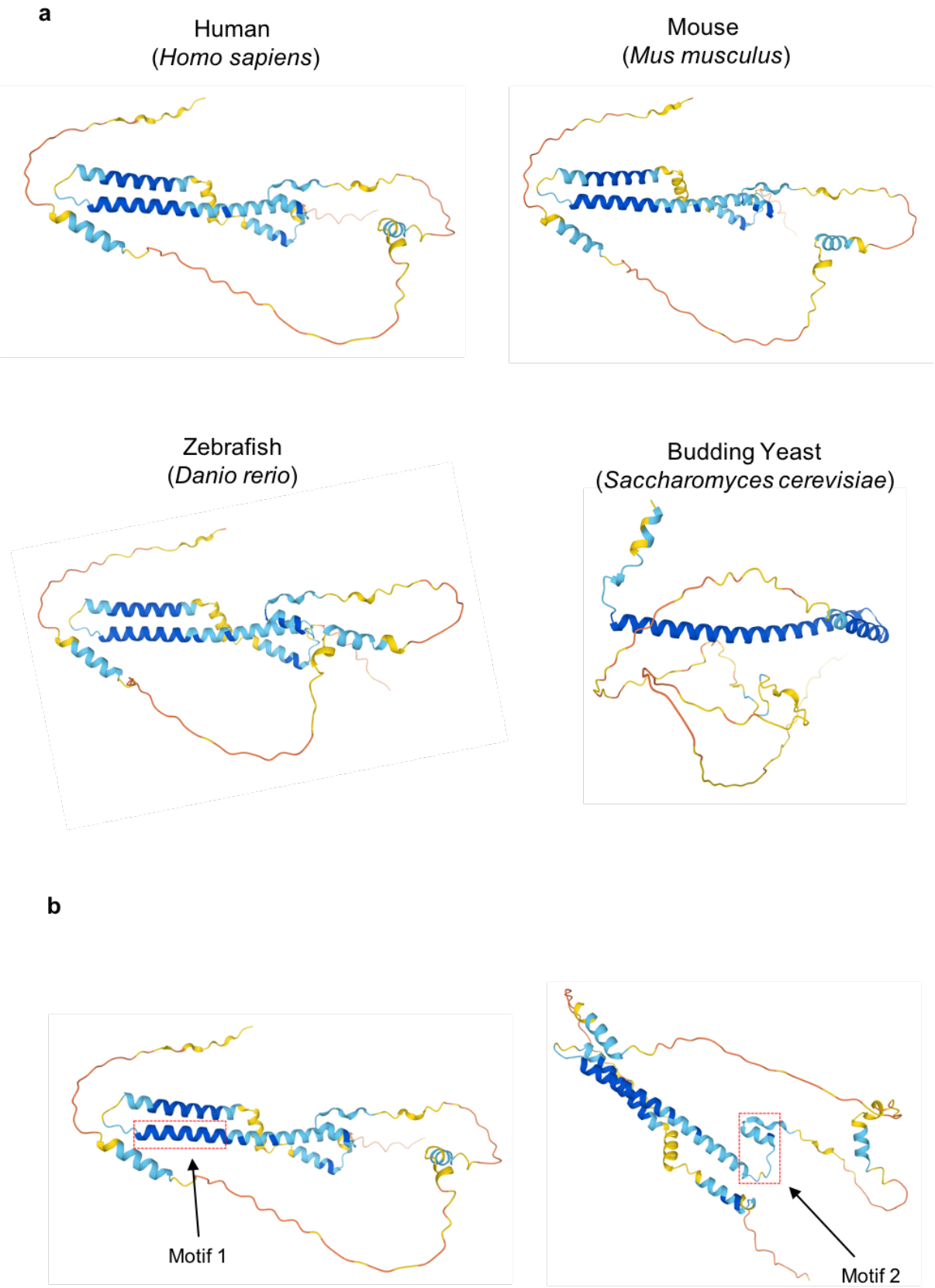


Figure 4.7: The predicted structure of C16orf72 is highly conserved in vertebrates. (a) AlphaFold prediction of the structure of C16orf72 orthologues from

Homo sapiens, *Mus musculus*, *Danio rerio* and Saccharomyces cerevisiae (Jumper et al., 2021). **(b)** The predicted position of motif 1 and motif 2 in C16orf72 from *Homo sapiens*. Conserved motifs are indicated in red boxes.

Protein	Aligned sequence	E-value	Example(s) of Function(s)
Immunoglobulin heavy chain junction region	**FQ**VA**A**ARQ**T**TD**YK**	618	Humoral immunity (Greenspan & Cavacini, 2019)
DNAH10	**FQ**TL**A**KKM**T**VL**YK**	805	Unknown
FPRL2	**W**FP**FQ**LV**A**LLG**T**	3162	Regulates immune system (Gronert et al., 1998; Ye et al., 1992)
T cell receptor alpha chain	**W**GK**FQ**FG**A**	7014	Adaptive immunity (Latour, 2016)
CSMD1	**W**LLFQTDGSGSSLGF**K**A**S**	8803	Maturation of neurons (Gutierrez et al., 2019)

Table 4.1: Human proteins aligned with motif 1 in human C16orf72. Protein alignment was performed with BlastP. Amino acid residues that aligned with the queried motif are indicated in bold.

Protein	Aligned sequence	E-value	Example(s) of Function(s)
CCG1	**W**KS**K**DRP**RRIR**M**E**	42	Unknown
TFIID subunit 1	**W**KS**K**D**R**P**R**RI**R**M**E**	42	Initiates transcription (Papai et al., 2011)
CDP/cut	**W**FHNY**R**S**R**-**IRRE**	223	Represses gene transcription (Snyder et al., 2001)
HUWE1	**IRRE**V**L**QNQ**L**-**G**IRP**P**	515	Partakes in the DDR, the replication stress response, and has a plethora of other functions (Choe et al., 2016; Hall et al., 2007; Kao et al., 2018; Mandemaker et al., 2017; Parsons et al., 2009; Sander et al., 2017; Zhong et al., 2005)
SHF isoform o	**W**RSTT**R**L**RIIR**L**R**DR**L**	588	Regulates apoptosis (Lindholm et al., 2000)

Table 4.2: Human proteins aligned with motif 2 in human C16orf72. Protein alignment was performed with BlastP. Amino acid residues that aligned with the queried motif are indicated in bold.

4.2.5 Loss of C16orf72 further sensitises U2OS cells to HU, APH, WEE1i and ATRi

HUWE1 has a well characterised role in the DNA replication stress response (Choe et al., 2016). Given that C16orf72 has a highly conserved motif that has similar amino acid sequence to parts of HUWE1, I hypothesised that C16orf72 may function in the DNA replication stress response. Loss of numerous replication stress response proteins such as Ring Finger Protein 8 (RNF8), ETAA1, Zinc Finger Protein 161 homolog (ZFP161), BRCA1, BOD1L, Translocated promoter region (Tpr), EXD2, HUWE1, RIF1 and Fanconi Anemia Group J (FANCJ) can sensitise cells to hydroxyurea (HU) and/or aphidicolin (APH) (Choe et al., 2016; Daza-Martin et al., 2019; Higgs et al., 2015; Kim et al., 2019; Kosar et al., 2021; Lee et al., 2016; Nieminuszczy et al., 2019; Schwab et al., 2013; Sy et al., 2011; Xu et al., 2010). HU induces DNA replication stress by suppressing the activity of ribonucleotide reductase, which reduces the cellular dNTP pool and consequently induces fork stalling (Bianchi et al., 1986; Petermann et al., 2010). APH induces DNA replication stress by inhibiting DNA polymerase α and ε (Ikegami et al., 1978). Loss of DNA replication stress response genes such as *FANCM* can sensitise cells to WEE1 inhibitor (WEE1i) (Aarts et al., 2015). The cell-killing mechanisms of WEE1i often depends on the genetic background of cells and the majority of these mechanisms are ill-defined. Therefore, I hypothesised that if loss of C16orf72 further sensitises U2OS cells to HU and/or APH and/or WEE1i, then these findings will support the notion that C16orf72 may participate in the DNA replication stress response. Loss of proteins that function in the DNA replication stress response, such as BRCA2, PALB2, ATM and ERCC1 can further sensitise cells to ATR inhibitor (ATRi) (Bétous et al., 2018; Hustedt et al., 2019; Kwok et al., 2016; Mohni et al., 2014; Wang et al., 2019). However, the exact

mechanism of ATRi-induced cell death is unclear. Additionally, publications that used a genome-wide CRISPR dropout screen approach demonstrated that loss of C16orf72 further sensitises a range of cell lines (excluding U2OS cells which were not included in the screen) to ATRi, which suggests that C16orf72 may function in the DNA replication stress response (Hustedt et al., 2019; Wang, et al., 2019). Therefore, if loss of C16orf72 further sensitises U2OS cells to ATRi, then this finding will strengthen the argument that C16orf72 may function in the DNA replication stress response. In order to determine whether loss of C16orf72 further sensitises cells to one or more of these reagents, *C16orf72Δ* U2OS knockout cell lines were required.

Dr Khairul Ramlee generated two independent CRISPR-Cas9-mediated *C16orf72Δ* clones, *C16orf72Δ*.1 and *C16orf72Δ*.2 in the U2OS cell line, which were validated via western blot (Figure 4.8 a). Exon 1 of *C16orf72* was targeted by two independent gRNAs. C16orf72 could only be visualised in wild type U2OS cells treated with vehicle (DMSO) following long exposure, as evidenced by a faint band at ~37 kDa. Therefore, proteasome inhibition via MG-132 treatment was required to validate the two *C16orf72Δ* knockout clones via immunoblotting, which also indicated that endogenous C16orf72 undergoes rapid turnover in cells via the ubiquitin-proteasome system (UPS) (Bhattacharyya et al., 2014; Lee & Goldberg, 1998). Given that the CRISPR gRNAs used to generate these cell lines targeted exon 1, which is found in both isoforms, it was assumed that loss of the ~37 kDa band indicated that both C16orf72 isoforms were knocked out in the two *C16orf72Δ* clones. Furthermore, empty vector FLAG-HA (EV) or FLAG-HA-C16orf72 was over-expressed in wild type U2OS, *C16orf72Δ*.1 and *C16orf72Δ*.2 cells via lentiviral transduction (Figure 4.8 b). These cell lines were generated in order to assess whether any observed phenotypes were due to loss of

C16orf72 rather than due to CRISPR-Cas9-induced off target mutations, as well as to study the recruitment of C16orf72 to chromatin in response to exogenous DNA replication stress (see 5.2.2). FLAG-HA-C16orf72 overexpression was validated via western blot, with a ~45 kDa protein product observed in the U2OS + FLAG-HA-C16orf72, *C16orf72Δ*.1 + FLAG-HA-C16orf72 and *C16orf72Δ*.2 + FLAG-HA-C16orf72 cell lines. The ~45 kDa protein product likely represented the FLAG-HA-tagged long isoform of C16orf72, since the U2OS + FLAG-HA-C16orf72, *C16orf72Δ*.1 + FLAG-HA-C16orf72 and *C16orf72Δ*.2 + FLAG-HA-C16orf72 cell lines expressed complementary DNA encoding all four exons of FLAG-HA-C16orf72.

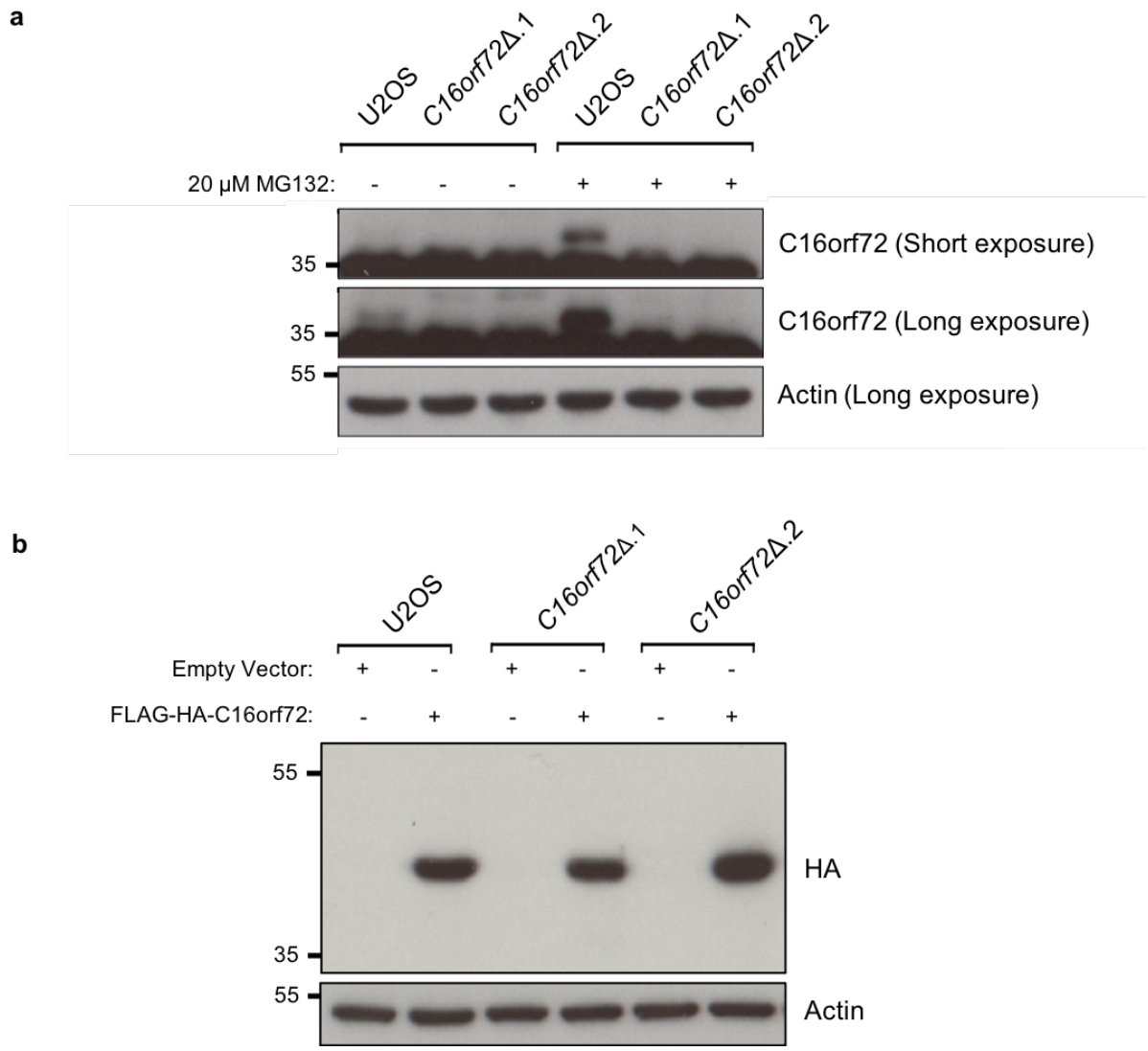


Figure 4.8: Validation of C16orf72 knockout and FLAG-HA-C16orf72-overexpressing cell lines. (a) Wild type U2OS, *C16orf72Δ*.1 and *C16orf72Δ*.2 cell lines were treated with DMSO or 20μM MG132 for 1 h and whole cell lysates were visualised with the indicated antibodies via western blot. Generation of the indicated cell lines and validation via western blot was performed by Dr Khairul Ramlee. **(b)** Whole cell lysates of untreated wild type U2OS, *C16orf72Δ*.1 and *C16orf72Δ*.2 cells expressing empty vector or FLAG-HA-C16orf72 were prepared and were visualised with the indicated antibodies via western blot. Generation of the indicated cell lines and validation via western blot was performed by Dr Khairul Ramlee.

Following generation of the required cell lines, Dr Khairul Ramlee and I first investigated the potential involvement of C16orf72 in the DNA replication stress response by assessing the ability of cells lacking C16orf72 to form colonies following exposure to HU and APH via clonogenic survival assay (Figure 4.9 a-c). I exposed U2OS + EV, *C16orf72Δ*.1 + EV and *C16orf72Δ*.1 + FLAG-HA-C16orf72 cells to HU for 24 h and observed that the *C16orf72Δ*.1 + EV clone was further sensitised to HU relative to wild type U2OS + EV cells ($p < 0.0001$). Furthermore, overexpressing FLAG-HA-C16orf72 in *C16orf72Δ*.1 cells almost completely rescued the sensitivity of *C16orf72Δ*.1 + EV cells to HU, since *C16orf72Δ*.1 + FLAG-HA-C16orf72 cells exhibited decreased sensitivity to HU relative to *C16orf72Δ*.1 + EV cells ($p < 0.0001$), and had nearly the same sensitivity to HU relative to U2OS + EV cells, although this small difference was statistically significant ($p = 0.0017$). Furthermore, Dr Khairul Ramlee performed the same clonogenic survival assay with *C16orf72Δ*.2 + EV and *C16orf72Δ*.2 + FLAG-HA-C16orf72 cells instead and observed that the *C16orf72Δ*.2 + EV clone was further sensitised to HU relative to wild type U2OS + EV cells (p =

0.0050). Additionally, overexpression of FLAG-HA-C16orf72 in *C16orf72Δ*.2 cells fully rescued the sensitivity of *C16orf72Δ*.2 + EV cells to HU, since a decreased sensitivity of *C16orf72Δ*.2 + FLAG-HA-C16orf72 cells to HU was observed relative to *C16orf72Δ*.2 + EV cells ($p = 0.0036$), and *C16orf72Δ*.2 + FLAG-HA-C16orf72 cells had the same sensitivity to HU relative to U2OS + EV cells ($p = 0.9895$). Therefore, the observed sensitivity to HU in both empty vector-expressing *C16orf72Δ* clones is not due to off-target CRISPR-Cas9-mediated mutation and is specifically caused by loss of C16orf72 (Fu et al., 2013). Dr Khairul Ramlee also exposed wild type U2OS, *C16orf72Δ*.1 and *C16orf72Δ*.2 cells to APH for 24 h and assessed the ability of these cells to form colonies via clonogenic survival assay. *C16orf72Δ*.1 ($p < 0.0001$) and *C16orf72Δ*.2 ($p = 0.0004$) cells were further sensitised to APH relative to wild type U2OS cells.

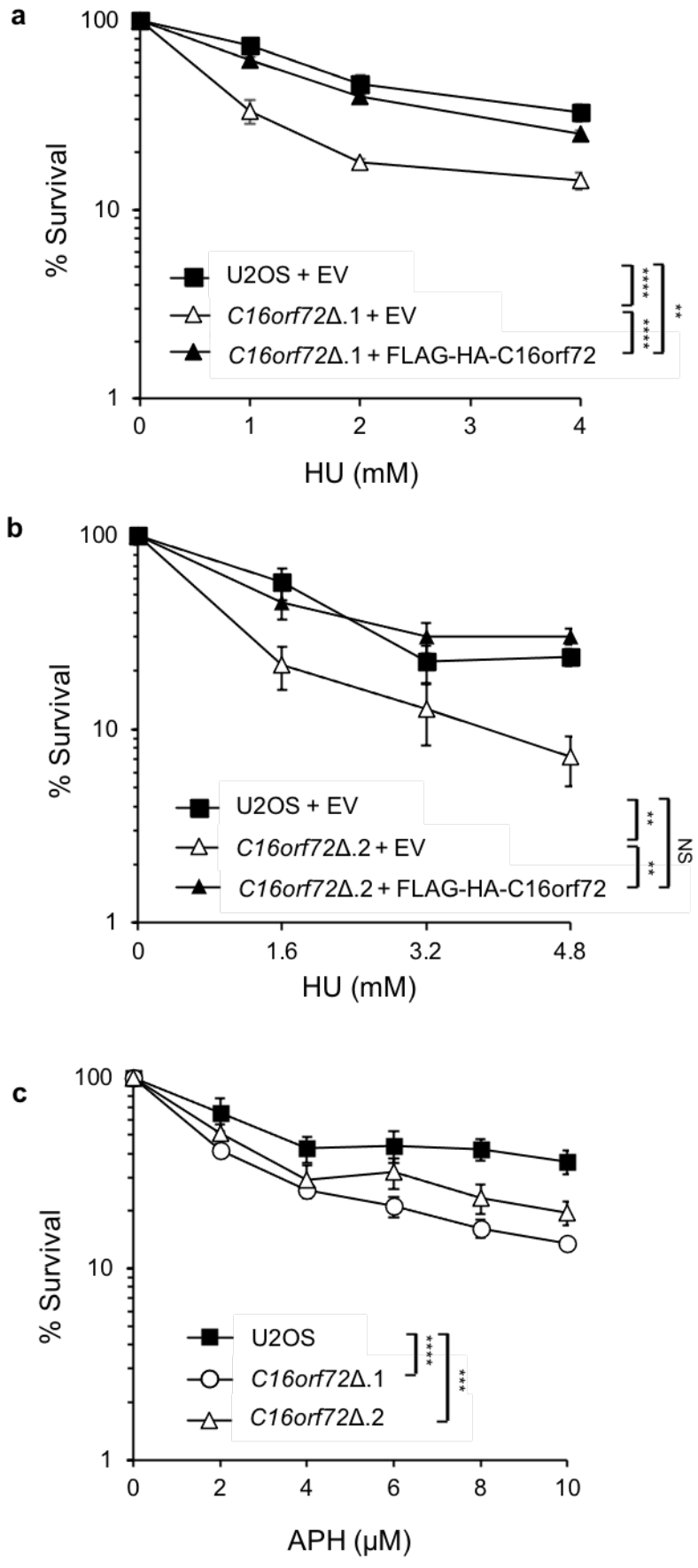

a
100
10
1
% Survival
U2OS + EV
C16orf72Δ.1 + EV
C16orf72Δ.1 + FLAG-HA-C16orf72
****
****
**
0
1
2
3
4
HU (mM)
b
100
10
1
% Survival
U2OS + EV
C16orf72Δ.2 + EV
C16orf72Δ.2 + FLAG-HA-C16orf72
**
**
NS
0
1.6
3.2
4.8
HU (mM)
c
100
10
1
% Survival
U2OS
C16orf72Δ.1
C16orf72Δ.2
****
***
0
2
4
6
8
10
APH (μM)

Figure 4.9: Loss of C16orf72 further sensitises U2OS cells to HU and APH. (a) U2OS + EV, *C16orf72Δ*.1 + EV and *C16orf72Δ*.1 + FLAG-HA-C16orf72 cells were treated with HU and their ability to form colonies was analysed via clonogenic survival assay. **(b)** U2OS + EV, *C16orf72Δ*.2 + EV and *C16orf72Δ*.2 + FLAG-HA-C16orf72 cells were treated with HU and their ability to form colonies was analysed via clonogenic survival assay. **(c)** U2OS, *C16orf72Δ*.1 and *C16orf72Δ*.2 FLAG-HA-C16orf72 cells were treated with APH and their ability to form colonies was analysed via clonogenic survival assay. Error bars at each data point represent the SEM from three separate biological replicates. A two-way ANOVA with Tukey's post hoc analysis was used to determine the statistical significance between conditions. The experiments presented in **(b)** and **(c)** were performed by Dr Khairul Ramlee. For all statistical tests performed, ns, not significant; ** $p < 0.01$; *** $p < 0.001$; **** $p < 0.0001$.

To provide additional evidence that C16orf72 functions in the replication stress response, my colleagues and I assessed the ability of *C16orf72*-deficient cells to form colonies following exposure to WEE1i and ATRi via clonogenic survival assay (Figure 4.10, 4.11 and Appendices Figure 3). Firstly, I exposed U2OS + EV, *C16orf72Δ*.1 + EV, *C16orf72Δ*.1 + FLAG-HA-C16orf72, *C16orf72Δ*.2 + EV and *C16orf72Δ*.2 + FLAG-HA-C16orf72 cells to WEE1i for 24 h and observed the following. *C16orf72Δ*.1 + EV ($p < 0.0001$) and *C16orf72Δ*.2 + EV ($p = 0.0003$) cells were further sensitised to WEE1i relative to wild type U2OS + EV cells. Additionally, overexpression of FLAG-HA-

C16orf72 in the *C16orf72Δ*.1 cell line partially rescued the sensitivity of *C16orf72Δ*.1 + EV cells to WEE1i, since *C16orf72Δ*.1 + FLAG-HA-C16orf72 cells exhibited decreased sensitivity to WEE1i relative to *C16orf72Δ*.1 + EV cells ($p = 0.0355$) and had similar sensitivity to WEE1i (especially at the 1000 nM concentration) relative to U2OS + EV cells ($p = 0.0272$). Furthermore, overexpression of FLAG-HA-C16orf72 in *C16orf72Δ*.2 cells fully rescued the sensitivity of *C16orf72Δ*.1 + EV cells to WEE1i, since *C16orf72Δ*.1 + FLAG-HA-C16orf72 cells exhibited increased survival following WEE1i treatment compared to *C16orf72Δ*.1 + EV cells ($p = 0.0144$), and *C16orf72Δ*.1 + FLAG-HA-C16orf72 cells had the same sensitivity to WEE1i relative to U2OS + EV cells ($p = 0.3258$). Given that both EV-expressing *C16orf72Δ* cell lines exhibited similar sensitivity to WEE1i relative to EV-expressing U2OS cells, I propose that the partial rescue of this sensitivity in FLAG-HA-C16orf72-overexpressing *C16orf72Δ*.1 cells is due to a problem with this specific complemented cell line. Therefore, it is probable that the increased sensitivity of both empty vector-expressing *C16orf72Δ* clones to WEE1i relative to empty vector-expressing U2OS cells is not due to off-target CRISPR-Cas9-induced mutation and occurs as a consequence of C16orf72 loss (Fu et al., 2013). Next, I exposed wild type U2OS cells transfected with non-targeting control siRNA or C16orf72-targeting SMARTpool siRNA to ATRi for 48 h and observed that C16orf72 depletion further sensitises wild type U2OS cells to ATRi, which is consistent with previous findings ($p = 0.0162$) (Hustedt et al., 2019; Wang, et al., 2019). In parallel, Dr Khairul Ramlee and Amy Wolstenholme in the Lakin lab exposed U2OS + EV, *C16orf72Δ*.1 + EV and *C16orf72Δ*.1 + FLAG-HA-C16orf72 cells to ATRi for 9 days. They observed that *C16orf72Δ*.1 + EV cells were further sensitised to ATRi relative to wild type U2OS + EV cells ($p < 0.0001$). Additionally, they observed that overexpression of FLAG-HA-C16orf72 in *C16orf72Δ*.1 cells partially rescued the

sensitivity of *C16orf72Δ*.1+EV cells to ATRi, since *C16orf72Δ*.1 + FLAG-HA-C16orf72 cells exhibited decreased sensitivity to ATRi relative to *C16orf72Δ*.1 + EV cells ($p < 0.0001$), and displayed increased sensitivity to ATRi relative to U2OS + EV cells ($p = 0.0001$). Following completion of the bioinformatic analysis, two research groups demonstrated that C16orf72 deletion sensitises a variety of cell lines (although none of the screens were performed in U2OS cells) to ATRi (Hustedt et al. 2019b; Wang, et al., 2019). Given these reports and the observation that siRNA-mediated C16orf72 depletion also further sensitises U2OS cells to ATRi, it is assumed that the partial, rather than complete rescue of the ATRi sensitivity that was observed in FLAG-HA-C16orf72-overexpressing *C16orf72Δ*.1 cells is due to an issue with this complemented cell line. Therefore, it is assumed that the increased sensitivity of *C16orf72Δ*.1 cells to ATRi relative to empty vector-expressing U2OS cells occurs due to C16orf72 loss and does not arise as result of off-target CRISPR-Cas9-dependent mutation (Fu et al., 2013).

Overall, these findings suggest that loss of C16orf72 further sensitises U2OS cells to HU, APH, WEE1i and ATRi, which support the notion that C16orf72 may participate in the DNA replication stress response.

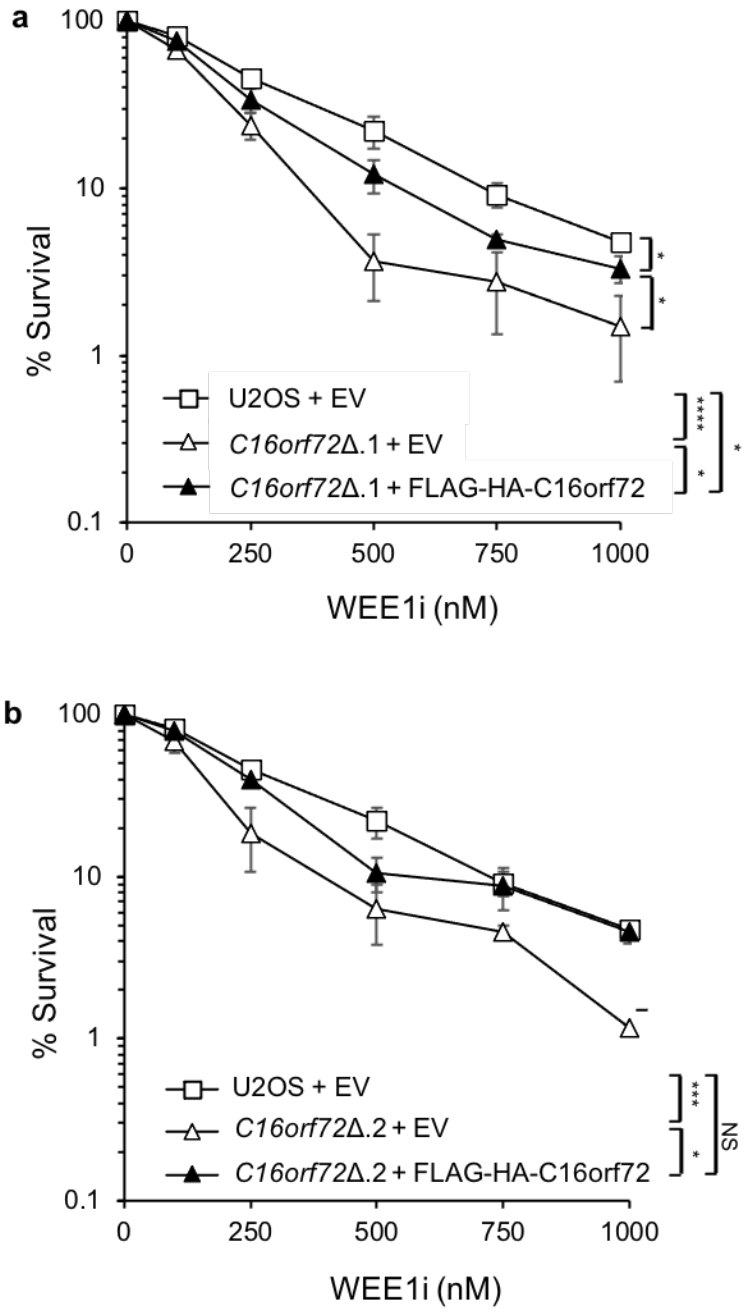


Figure 4.10: Loss of C16orf72 sensitises further sensitises U2OS cells to WEE1i

(a) U2OS + EV, *C16orf72Δ*.1 + EV and *C16orf72Δ*.1 + FLAG-HA-C16orf72 cells were treated with WEE1i and their ability to form colonies was analysed via clonogenic survival assay. **(b)** U2OS + EV, *C16orf72Δ*.2 + EV and *C16orf72Δ*.2 + FLAG-HA-C16orf72 cells were treated with WEE1i and their ability to form colonies was analysed via clonogenic survival assay. Error bars at each data point represent the standard

error of the mean from three separate biological replicates. A two-way ANOVA with Tukey's post hoc analysis was used to determine the statistical significance between conditions. **(a)** and **(b)** were performed in parallel, but are presented separately for ease of visualisation. Error bars at each data point represent the SEM from three separate biological replicates. For all statistical tests performed, ns, not significant; * $p < 0.05$; *** $p < 0.001$; **** $p < 0.0001$.

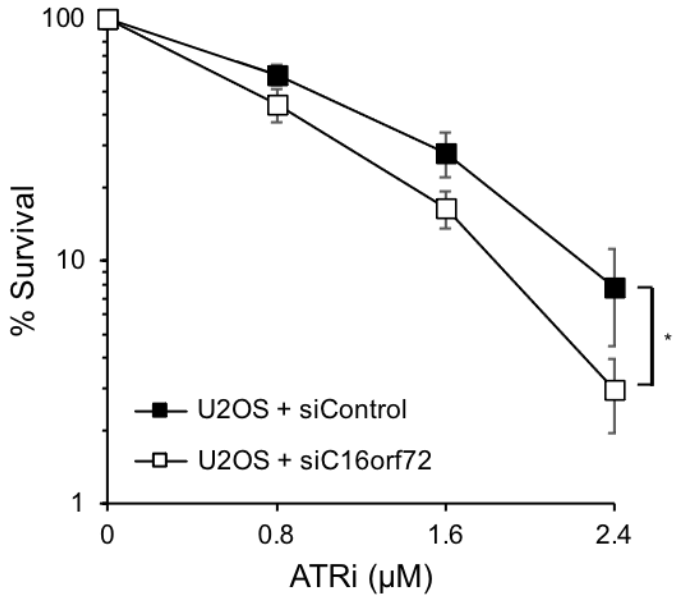


Figure 4.11: C16orf72 depletion sensitises U2OS cells to ATRi. Wild type U2OS cells were transfected with non-targeting control siRNA or C16orf72-targeting SMARTpool siRNA, treated with ATRi for 48 h, and recovered in fresh growth media. A two-way ANOVA was used to determine the statistical significance between conditions. Error bars at each data point represent the standard error of the mean from three separate biological replicates. * $p < 0.05$.

4.2.6 Loss of C16orf72 further sensitises U2OS cells to ATRi-ATMi combinations

Individual loss of DNA replication stress response proteins, such as ATM, can further sensitise a range of cell lines to ATRi (Balmus et al., 2019; Hustedt et al., 2019; Kwok et al., 2016; Wang, et al., 2019). I hypothesised that if *C16orf72Δ* cells are further sensitised to ATRi-ATMi combinations relative to U2OS cells, then this finding would support the notion that C16orf72 may function in the DNA replication stress response. This hypothesis is based on the assumption that combined disruption (deletion or inhibition) in the function of two DNA replication stress response proteins may further sensitise (by a cytostatic or cytotoxic sensitisation) U2OS cells to ATRi compared to U2OS cells in which the function of a single DNA replication stress response factor has been disrupted.

To test this hypothesis, I performed a high throughput combination screen, which enables researchers to investigate the individual and combined effects of two separate treatments on cell growth and survival. In the screen, U2OS + EV, *C16orf72Δ*.1 + EV and *C16orf72Δ*.1 + FLAG-HA-C16orf72 cells were seeded into individual 384-well plates and treated with a variety of ATRi-ATMi combination concentrations using a liquid handler. Five days post-treatment, the wells of the 384-well plates were treated with Cell-Titre Glo 2.0 and cell viability was measured with a plate reader. The Cell-Titre Glo 2.0 assay is a luciferin-based assay that can measure the amount of ATP present in wells. The amount of luminescence produced per well correlated to the number of live cells per well (Figure 4.12). The output of these screens can provide a wealth of information. The effect of drug combinations in each cell line is summarised in experimental activity heatmaps. For a given combination treatment, cytostatic

activity is indicated with an experimental activity score of 0-100, whereas cytotoxic activity is indicated with a score of 101-200. I considered an experimental activity score of ≥ 20 for a particular concentration combination to be a sensitisation. In rare instances, a negative experimental activity score can be observed which, for the purpose of these screens is considered to indicate a combination treatment that promotes cell viability. These screens can also be used to identify combination treatments that have synergistic experimental activities in specific cancers cell lines – the findings of which can be used to develop effective and targeted treatments for cancers in the clinic (Fok et al., 2019; Lloyd et al., 2020). Synergy occurs when the collective activity of multiple compounds supersedes the predicted additive activity of the compounds (Greco et al., 1996). The discovery of synergistic treatments is advantageous as they have the potential to reduce the concentration of each of the drugs within the combination that is administered to a patient, which may mitigate adverse effects (Tallarida, 2011). The highest single agent (HSA) model was used to predict the expected activity for all of the ATRi-ATMi combination concentrations in each of the cell lines. This model estimates that the effect of a given combination will be the highest effect that is observed from a single agent. Therefore, for a given ATRi-ATMi concentration combination, experimental activity that exceeded the predicted experimental activity by the HSA model (activity in excess) is indicative of synergistic activity. A synergy score was calculated based on the activity in excess observed from each treatment. If a synergy score was > 5, the effect of the combination was considered to be synergistic, but if a synergy score was between 0 and 5, then a combination was considered to have an additive effect (Fok et al., 2019). The synergy scores have been included for completion but will not be analysed in this study, since I only sought to determine whether specific concentration combinations further

sensitised *C16orf72Δ*.1 + EV cells relative to U2OS + EV cells. For ease of visualisation, the difference in sensitivities between indicated cell lines is signified by differential activity units in the lower set of panels. The differential activity scores in the panels labelled '*C16orf72Δ*.1 + EV vs U2OS + EV' was calculated by subtracting the experimental activities of U2OS + EV cells from the experimental activities of *C16orf72Δ*.1 + EV cells for each equivalent treatment. Therefore, in this panel, the greater the differential activity, the more sensitive *C16orf72Δ*.1 + EV cells are to a particular treatment relative to U2OS + EV cells. The differential activity scores in the panels identified as '*C16orf72Δ*.1 + FLAG-HA-C16orf72 vs *C16orf72Δ*.1 + EV' were computed by subtracting, for a given combination treatment, the experimental activity score in *C16orf72Δ*.1 + EV cells from the experimental activity score in *C16orf72Δ*.1 + FLAG-HA-C16orf72 cells. Therefore, the higher the differential activity score for each given combination treatment, the more convincing the rescue of any potential sensitivity phenotype relative to U2OS + EV cells. Complete rescue of any potential sensitivity phenotypes observed in *C16orf72Δ*.1 + EV cells would be indicated when the differential activity scores in the *C16orf72Δ*.1 + EV vs U2OS + EV panel and the *C16orf72Δ*.1 + FLAG-HA-C16orf72 vs *C16orf72Δ*.1 + EV panel are identical. Three biological replicates were performed of this high throughput combination screen and a single representative biological replicate for this screen is presented and analysed in this chapter. The two additional biological replicates for this screen can be found in the appendices (Appendices Figure 4 a and b). Given the breadth of data provided from the high throughput combination screen, only relevant findings will be mentioned. Please refer to Table 4.3 below for a summary of all of the findings from these screens.

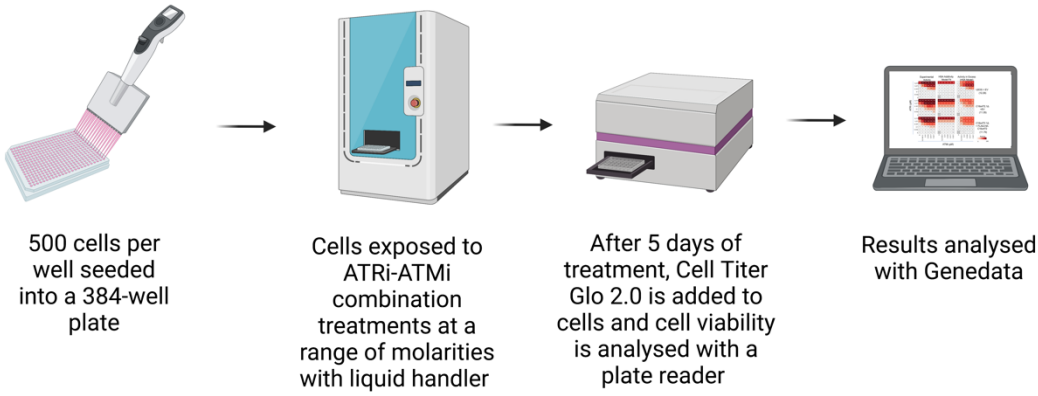


Figure 4.12: Schematic of high-throughput ATRi-ATMi combination screen. 384-well microplates were seeded with U2OS + EV, *C16orf72Δ*.1 + EV and *C16orf72Δ*.1 + FLAG-HA-C16orf72 cells (500 cells per well). Using a liquid hander, cells were exposed to a variety of concentration combinations of ATRi and ATMi. 5 days post-treatment, CellTitre Glo 2.0 was added to the microplates; cell viability was analysed with a plate reader; and Genedata was used to analyse the results. Produced with BioRender.

C16orf72Δ.1 + EV cells were further sensitised to ATRi (especially following 1 μM treatment) relative to U2OS + EV cells (Figure 4.13, green box). This sensitivity was partially rescued in *C16orf72Δ*.1 + FLAG-HA-C16orf72 cells (Figure 4.13, yellow box). Surprisingly, this sensitivity phenotype was due to a cytostatic effect rather than an expected cytotoxic effect (Hustedt et al., 2019; Wang, et al., 2019). U2OS + EV and *C16orf72Δ*.1 + EV cells were both sensitised to ATRi-ATMi combinations, although in both cell lines, at most concentration combinations, the sensitisation was due to a cytostatic effect rather than a cytotoxic effect (Figure 4.13). However, interestingly, *C16orf72Δ*.1 + EV cells were further sensitised to ATRi-ATMi combinations relative to U2OS + EV cells at a range of concentration combinations (Figure 4.13, red box). Additionally, overexpression of FLAG-HA-C16orf72 in the *C16orf72Δ*.1 cell line partially rescued this sensitivity (Figure 4.13, purple box). The partial rescue of the sensitivity phenotypes described above was likely due to a problem with the *C16orf72Δ*.1 + FLAG-HA-C16orf72 cell line, as this cell line has never been able to completely rescue any sensitivity phenotypes observed in the *C16orf72Δ*.1 clone, or to completely rescue sensitivity phenotypes that have been previously reported in C16orf72-deficient cells (Hustedt et al., 2019; Wang, et al., 2019). Therefore, it is assumed that both of the sensitivity phenotypes observed in the *C16orf72Δ*.1 + EV cell line within this screen arose as a consequence of C16orf72 loss, and did not arise as a result of CRISPR-Cas9-mediated off-target mutations (Fu et al., 2013). Overall, the results from this screen suggest that loss of C16orf72 further sensitises U2OS cells to ATRi alone, and in combination with ATMi, which supports the notion that C16orf72 may function in the DNA replication stress response.

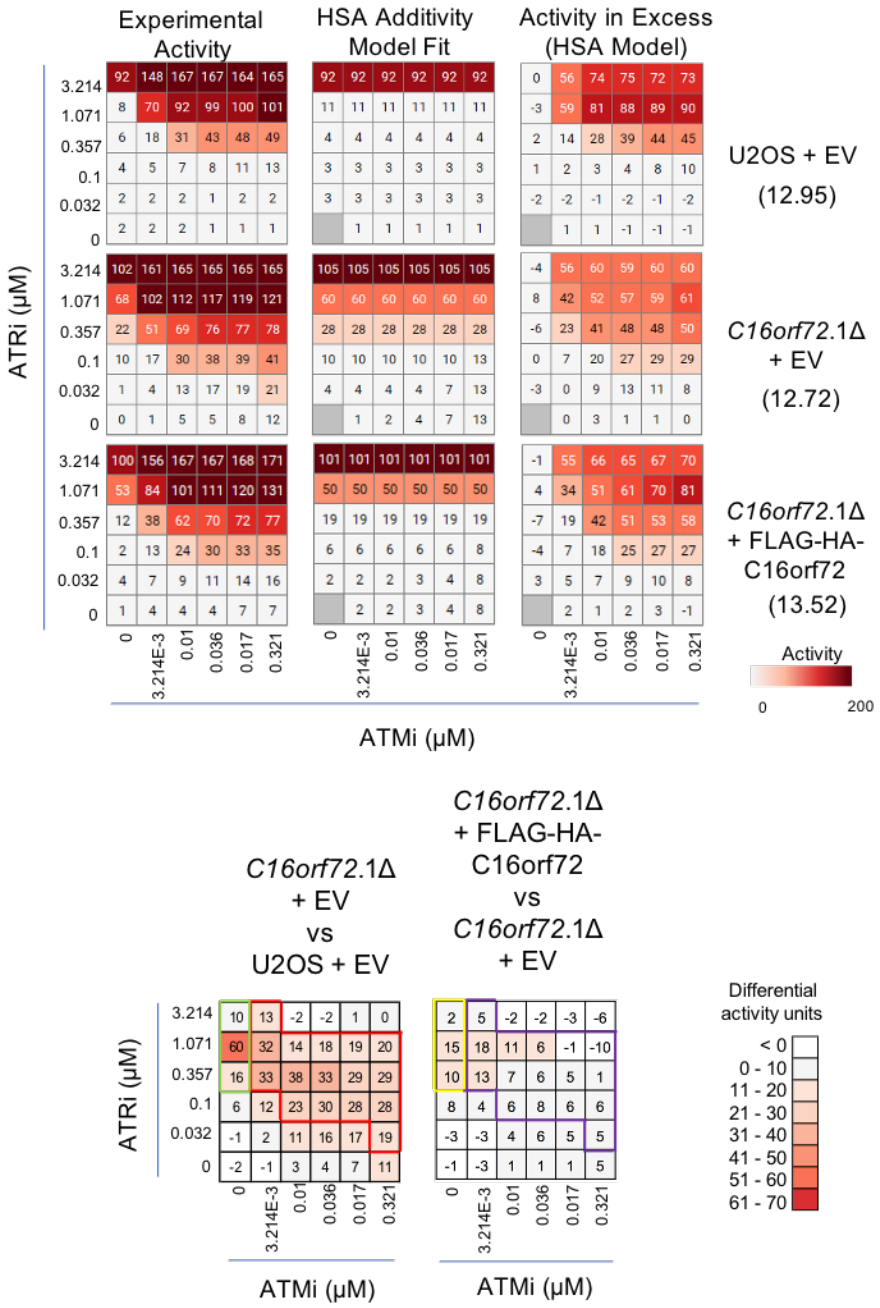


Figure 4.13: *C16orf72* deletion further sensitises U2OS cells to ATRi-ATMi combinations. Heatmap of U2OS + EV, *C16orf72Δ*.1 + EV and *C16orf72Δ*.1 + FLAG-HA-C16orf72 cells exposed to a 6x6 ATRi-ATMi combination matrix for 5 days. Experimental activity signifies extent of growth inhibition or cytotoxicity for a given concentration combination. An experimental activity of < 0 indicates that a treatment promotes the growth of cells. An experimental activity of 0 – 100 indicates that a

treatment causes a cytostatic effect. An experimental activity of 101-200 indicates that a treatment causes a cytotoxic effect. Activity in excess signifies the excess experimental activity observed compared to the highest single agent (HSA) additivity model. For each cell line, activity in excess was used to calculate a synergy score (in brackets). Differences in experimental activity between indicated cell lines is signified with differential activity scores. Green box indicates further sensitisation of *C16orf72Δ*.1 + EV cells to ATRi relative to U2OS + EV cells. Red box indicates further sensitisation of *C16orf72Δ*.1 + EV cells to ATRi-ATMi combinations relative to U2OS + EV cells. Yellow box indicates partial rescue of ATRi sensitivity in *C16orf72Δ*.1 + FLAG-HA-C16orf72 cells relative to U2OS + EV cells. Purple box indicates partial rescue of ATRi-ATMi sensitivity observed in *C16orf72Δ*.1 + FLAG-HA-C16orf72 relative to U2OS + EV cells. Three independent biological repeats of this screen were performed. This figure is a representative biological repeat of this experiment.

	ATRi	ATMi
Sensitises U2OS + EV cells?	Yes	No
Further Sensitises U2OS + EV cells to ATRi?	N/A	Yes
Further sensitises *C16orf72Δ*.1 + EV cells relative to U2OS + EV cells / Further sensitisation rescued in *C16orf72Δ*.1 + FLAG-HA-C16orf72 relative to U2OS + EV cells?	Yes / Partial rescue	No / N/A

Further sensitises *C16orf72Δ*.1 + EV cells to ATRi relative to U2OS + EV cells / Further sensitisation rescued in *C16orf72Δ*.1 + FLAG-HA-C16orf72 cells relative to *C16orf72Δ*.1 + EV cells?	N/A	Yes / Partial rescue
Synergistic with ATRi in U2OS + EV cells?	N/A	Yes
Synergistic with ATRi in *C16orf72Δ*.1 + EV cells?	N/A	Yes
Synergistic with ATRi in *C16orf72Δ*.1 + FLAG-HA-C16orf72 cells	N/A	Yes

Table 4.3. Summary of findings from the high-throughput combination screens.

4.3 Discussion

In this chapter, I sought to identify novel synthetic lethal interactions with combined loss of PARP1 and PARP2. PARP1 and PARP2 participate in the DDR in numerous ways (Sousa et al., 2012). Therefore, a key reason for pursuing this screen was to identify novel DNA damage repair proteins, as it has been proposed that synthetic lethal interactions can occur between genes that are redundant in function (Nijman, 2011; Ashworth & Lord, 2018). To address this question a forward genetics approach was taken by employing a genome-wide CRISPR dropout screen in wild type U2OS and *PARP1ΔPARP2Δ* cells. The screen was performed with the Toronto Knockout CRISPR Library (TKOv3) – consisting of 70,948 guide RNAs – which was introduced into the cell lines via lentiviral transduction (Hart et al., 2017; Olivieri & Durocher, 2021). Through this screen, the effect of individually disrupting 18,053 protein-coding genes on the viability of each of these cell lines was assessed (Figure 4.1). Analysis of the screen hits identified 10 genes which, when individually disrupted, uniquely reduced the viability of *PARP1ΔPARP2Δ* cells, but not wild type U2OS cells, which represent 10 synthetic lethal interactions with combined loss of PARP1 and PARP2. Furthermore, individual disruption of 193 genes reduced the viability of wild type U2OS cells only, and individual disruption of 49 genes reduced the viability of both cell lines (Figure 4.2). Interestingly, there were some shared gene hits between those that were unique to *PARP1ΔPARP2Δ* cells in our screen and those that sensitise cells to olaparib (in a variety of cell lines) that were uncovered in a separate genome-wide CRISPR dropout screen, such as RNASEH2A and FANCF (Zimmermann et al., 2018). FANCF is a protein within the FA core complex that contributes to the resolution of ICLs via the Fanconi anaemia pathway (Walden & Deans, 2014). RNASEH2A forms part of the RNASEH2 protein trimer and acts as the catalytic subunit of this complex.

As DNA replication is performed, RNASEH2 eliminates incorrectly incorporated ribonucleotides from DNA and contributes to R-loop resolution (Chon et al., 2013; Crow et al., 2006; Hiller et al., 2012; Jeong et al., 2004; Pizzi et al., 2015; Williams et al., 2017). This may suggest that loss of PARP1 and PARP2 catalytic function, with or without trapping of PARP1 and PARP2 to DNA, can induce these synthetic lethal interactions. This finding is particularly surprising in the case of RNASEH2A, as RNASEH2-deficient cells are thought to be synthetic lethal with olaparib almost entirely as a consequence of cytotoxic trapping of PARP1 to DNA (Murai et al., 2012; Zimmermann et al., 2018). It has been proposed that loss of the *RNASEH2A*, *RNASEH2B* and *RNASEH2C* genes results in the accumulation of aberrantly incorporated ribonucleotides. These lesions are channelled down a TOP1-dependent pathway that results in the generation of DNA damage that acts as PARP1 substrate. Therefore, olaparib treatment in *RNASEH2*-deficient cells results in elevated levels of PARP1 trapping to DNA, which may explain the mechanistic basis of the hypersensitisation of these cells to olaparib (Huang et al., 2017; Kim et al., 2011; Sekiguchi & Shuman, 1997; Sparks & Burgers, 2015; Williams et al., 2013; Zimmermann et al., 2018). Further investigation will be required to understand why RNASEH2A is also synthetic lethal with combined loss of PARP1 and PARP2, which is independent of PARP1 trapping. It is important to note that other than RNASEH2A and FANCF, the top-ranking gene hits in the Lakin screen (*DNAJC*9, *NVL*, *SARS*, *RPL36*, *MRPS34*, *ABCC6*, *PTBP1* and *C16orf72*) and the top-ranking gene hits in the screen performed by Zimmermann et al., 2018 shared no similarity, which suggests that the remaining synthetic lethal interactions identified in the Lakin screen occur due to mechanisms that are independent of trapping of PARP1 and PARP2 to DNA. For a summary of the known cellular functions (when applicable) of these genes, refer to

4.2.1. Importantly, the presence of the DDR factors RNASEH2A and FANCF as high-ranking hits in the Lakin screen suggests that the remaining high-ranking hits may also function in the DDR. Therefore, these findings underline the value of this screen as we have demonstrated that this screen was a valid experimental approach for identifying potential novel DDR factors.

Excitingly, one of the high-ranking gene hits identified in our genome-wide CRISPR dropout screen was C16orf72. At the time when this gene was identified through the genome-wide CRISPR dropout screen, its function was poorly defined, which made it an ideal candidate to take forward for further characterisation. Therefore, as an initial step after analysis of the genome-wide CRISPR dropout screen was performed, I validated the synthetic lethal interaction between C16orf72 and combined loss of PARP1 and PARP2 with three independent C16orf72-targeting siRNAs. In addition to confirming that C16orf72 depletion is synthetic lethal with combined *PARP1* and *PARP2* deletion (Figure 4.3 a and b), by depleting C16orf72 in U2OS, *PARP1Δ*, *PARP2Δ* and *PARP1ΔPARP2Δ* cells, I was able to show that PARP1 and PARP2 are both key determinants of this synthetic lethal interaction. Interestingly, PARP1 and PARP2 were not high-ranking gene hits in a genome-wide CRISPR dropout screen to identify synthetic lethal interactions with C16orf72 loss in NALM-6 cells – a pre-B acute lymphoblastic leukaemia cell line – which further supports the finding that both PARP1 and PARP2 are key determinants of this synthetic lethal interaction (Benslimane et al., 2021; Hurwitz et al., 1979). The synthetic lethal interaction between C16orf72 and combined loss of PARP1 and PARP2 differs from other well-characterised PARP-dependent synthetic lethal interactions, in which the key determinant is often PARP1 alone. For example, simultaneous depletion of BRCA2 and PARP1, but not BRCA2

and PARP2 results in a large reduction in cell viability. However, combined depletion of PARP1 and PARP2 does not result in further reduction of cell viability when BRCA2 is also depleted (Bryant et al., 2005). In a separate example, cells lacking PARP1, but not cells lacking PARP2, are sensitised to the HR inhibitor B02 relative to wild type U2OS cells. Additionally, combined loss of PARP1 and PARP2 does not result in additional sensitisation to B02 relative to cells lacking PARP1 (Huang et al., 2012; Ronson et al., 2018).

Moving forward, it will be important to further validate the novel synthetic lethal interaction between C16orf72 and combined loss of PARP1 and PARP2 using a high-quality antibody to assess the knockdown efficiency of C16orf72-targeting siRNA via western blot, as none of the commercially available or custom antibodies that I assessed were of sufficient quality for robust assessment of endogenous C16orf72 depletion. Instead, Reverse transcription quantitative real-time PCR (RT-qPCR) was used to assess the knockdown efficiency of the C16orf72-targeting siRNAs in wild type U2OS and *PARP1ΔPARP2Δ* cells, which encouragingly showed that the severity of the synthetic lethal interaction positively correlated with knockdown efficiency (Appendices Figure 1). However, this RT-qPCR validation did not include all of the siRNAs that were used in the initial validation experiments. To increase the certainty that this synthetic lethal interaction is due to C16orf72 depletion and not off-target depletion, at least three independent biological replicates of the RT-qPCR knockdown analysis should be performed which includes all of the C16orf72-targeting siRNAs used in these experiments. Alternatively, validation of C16orf72 knockdown efficiency can be assessed by western blot with a high quality antibody that was used in a recently published study (Amici et al., 2022). Alternatively, this novel synthetic lethal

interaction could be validated by siRNA-mediated depletion of PARP1 and PARP2 in cells lacking C16orf72.

In order to understand more about the cellular functions of C16orf72 and to reveal other characteristics of this protein, I performed a bioinformatic analysis of C16orf72. I found that C16orf72 encodes a short and a long protein isoform that each contain a DUF4588 domain that spans the majority of the protein (Jones et al., 2014) (Figure 4.5). Consistent with this, in a recent study both of these isoforms have been detected in cells by western blot (Amici et al., 2022). I also found that this protein is highly conserved in the chordates and arthropods, but not in ascomycetes (Figure 4.6 and Appendices Figure 2). Furthermore, I identified numerous sites of ubiquitination and phosphorylation in human C16orf72, but the importance of these PTMs to the function of this protein is not clear and requires further investigation (Figure 4.5). Additionally, the predicted structures of vertebrate C16orf72 were highly conserved, whereas the predicted structure of ascomycete C16orf72 only shared slight similarity with the predicted structure of vertebrate C16orf72 (Figure 4.7 a). Within the DUF4588 domain, I found two motifs (motif 1 and motif 2) that are highly conserved in chordate and arthropod C16orf72 (Figure 4.6 and 4.7 b). Refer to Table 4.1 and Table 4.2 for summaries of human proteins that contain similar motifs to motif 1 and motif 2, respectively. It was intriguing to find that motif 1 had high sequence similarity with the UBM1 domain of the ubiquitin ligase HUWE1 (Hunkeler et al., 2021). HUWE1 diminishes DNA replication stress; participates in other DDR pathways; functions in the UPS; and also performs a plethora of other functions within the cell (Choe et al., 2016; Gong et al., 2016; Hall et al., 2007; Hunkeler et al., 2021; Kao et al., 2018; Mandemaker et al., 2017; Noy et al., 2012; Parsons et al., 2009; Sander et al., 2017;

Zhong et al., 2005). Furthermore, protein-protein interactions between HUWE1 and C16orf72 have been demonstrated in cells via co-immunoprecipitation, affinity purification combined with mass spectrometry, and BioID protein proximity labelling (Amici et al., 2022; Benslimane et al., 2021; Sears et al., 2019). Therefore, this suggests that C16orf72 may have similar cellular functions to HUWE1.

To further study the cellular functions of C16orf72, two independent *C16orf72Δ* clones were generated using the CRISPR-Cas9 system. Treatment of wild type U2OS, *C16orf72Δ*.1 and *C16orf72Δ*.2 cells with the proteasome inhibitor MG132 was necessary for the clear detection, by western blot, of a single band that was present in the wild type U2OS cells but absent in both *C16orf72Δ* clones (Figure 4.8 a). This suggests that both C16orf72 isoforms were lost in the *C16orf72Δ*.1 and *C16orf72Δ*.2 cells. Furthermore, this also provides additional evidence to support the notion that this protein may be involved in UPS pathways (Gong et al., 2016). Indeed, a recent study reported that C16orf72 forms homodimers which is crucial for preventing its degradation by the proteasome. This interaction is dependent on its highly conserved Gly119 residue, which when mutated, results in its proteasomal degradation. Furthermore, this group revealed that C16orf72 degradation is dependent on HUWE1-dependent Lys48-linked ubiquitination (Amici et al., 2022). Importantly, as mentioned earlier, a research group recently demonstrated by western blot that C16orf72 could be robustly detected with a commercially available antibody in unperturbed cells. In the future, using this high-quality antibody, the *C16orf72Δ* clones should also be validated in unperturbed conditions by western blot. Additionally, wild type U2OS, *C16orf72Δ*.1 and *C16orf72Δ*.2 cell lines overexpressing empty vector or the long isoform of FLAG-HA-tagged C16orf72 were generated and validated by western blot

via lentiviral transduction, and these cell lines were used as an additional tool to study the cellular function of C16orf72 (Figure 4.8 b).

By exposing wild type U2OS, *C16orf72Δ*.1 and *C16orf72Δ*.2 cells; EV-expressing U2OS, *C16orf72Δ*.1 and *C16orf72Δ*.2 cells; FLAG-HA-C16orf72-overexpressing *C16orf72Δ*.1 and *C16orf72Δ*.2 cells; and U2OS cells transfected with control siRNA or C16orf72-targeting SMARTpool siRNA to a variety of chemical agents my colleagues and I made the following observations via clonogenic survival assay. Firstly, *C16orf72Δ*.1 and *C16orf72Δ*.2 cells were further sensitised to APH relative to U2OS cells (Figure 4.9 c). Secondly, *C16orf72Δ*.1 + EV and *C16orf72Δ*.2 + EV cells were further sensitised to HU and WEE1i relative to U2OS + EV cells. Overexpression of FLAG-HA-C16orf72 completely rescued, or almost completely rescued these sensitivity phenotypes in *C16orf72Δ*.1 and *C16orf72Δ*.2 cells, respectively (Figure 4.9 a-b and 4.10 a-b). Thirdly, EV-expressing *C16orf72Δ*.1 cells were further sensitised to ATRi relative to EV-expressing U2OS cells. Overexpression of FLAG-HA-C16orf72 partially rescued this sensitivity phenotype in the *C16orf72Δ*.1 cells (Appendices Figure 3). Fourthly, depletion of C16orf72 further sensitised U2OS cells to ATRi (Figure 4.11). Interestingly, following completion of the work in this chapter, in a study that performed multiple genome-wide CRISPR dropout screens to identify genes which confer resistance to a range of genotoxic stresses, C16orf72 loss was predicted to sensitise cells to HU (Olivieri et al., 2020). Furthermore, in many instances, loss of proteins that function in the DNA replication stress response, such as HUWE1, ETAA1, ZFP161, BRCA1, BOD1L, Tpr, EXD2, RNF8, RIF1 and FANCJ further sensitise cells to APH and/or HU (Choe et al., 2016; Daza-Martin et al., 2019; Higgs et al., 2015; Kim et al., 2019; Kosar et al., 2021; Lee et al., 2016; Nieminuszczy et al.,

2019; Schwab et al., 2013; Sy et al., 2011; Xu et al., 2010). Additionally, loss of the DNA replication stress response proteins such as FANCM, can sensitise cells to WEE1i (Aarts et al., 2015). Moreover, loss of DNA replication stress response proteins (e.g. ATM, ERCC1, BRCA2 and PALB2) can further sensitises cells to ATRi (Bétous et al., 2018; Hustedt et al., 2019a; Kwok et al., 2016; Mohni et al., 2014; Wang et al., 2019). Importantly, genome-wide CRISPR dropout screens have demonstrated that C16orf72 loss sensitises MCF10A, HCT116 and hTERT-immortalised p53-null RPE-1 cells, but not HEK293A cells to ATRi (Hustedt et al., 2019; Wang, et al., 2019). MCF10A cells are a cell model for regular breast epithelial cells (Soule et al., 1990). RPE-1 cells are a cell model for normal human retinal pigment epithelial cells which can be immortalised via transfection with telomerase (Bodnar et al., 1998). HEK293A cells are used to produce recombinant adenovirus and are derived from HEK293, which are a model for embryonic kidney cells (Yuan et al., 2018). However, it is not clear why C16orf72 loss further sensitises some, but not all cell lines to ATRi. Overall, these findings suggest that loss of C16orf72 further sensitises U2OS cells to HU, APH, WEE1i and ATRi, which supports the notion that C16orf72 may function in the DNA replication stress response.

By performing a high-throughput ATRi-ATMi combination screen with EV-expressing U2OS cells, EV-expressing *C16orf72Δ*.1 cells and FLAG-HA-C16orf72-overexpressing *C16orf72Δ*.1 cells (see 4.2.6 for rationale), I made the following key observations. Firstly, EV-expressing *C16orf72Δ*.1 cells were further sensitised to ATRi relative to EV-expressing U2OS cells, and overexpression of FLAG-HA-C16orf72 in the *C16orf72Δ*.1 cell line partially rescued this sensitivity phenotype. Secondly, EV-expressing *C16orf72Δ*.1 cells were further sensitised to ATRi-ATMi combinations

relative to EV-expressing U2OS cells, and this further sensitisation was partially rescued by overexpressing FLAG-HA-C16orf72 in *C16orf72Δ*.1 cells (Figure 4.13). Refer to Table 4.3 for a summary of all of the findings from this screen. Together, these findings suggest that loss of C16orf72 further sensitises U2OS cells to ATRi and ATRi-ATMi combinations, which support the notion that C16orf72 may function in the DNA replication stress response (Hustedt et al., 2019; Wang, et al., 2019)

In summary, in this chapter, we have identified C16orf72 – a highly conserved protein that may have a diverse range of cellular functions. Interestingly, our findings suggest that C16orf72 may participate in the DNA replication stress response, in other DDR pathways, and in UPS pathways. While a recent report has confirmed the role of C16orf72 in UPS pathways, additional experimental evidence is required to confirm the involvement of C16orf72 in the DNA replication stress response and other DDR pathways. Additionally, C16orf72 has numerous predicted sites of phosphorylation and ubiquitination. However, it is not clear how these PTMs regulate the function of this protein.

Chapter 5. Investigating the function of C16orf72 in the DNA replication stress response

5.1 Introduction

5.1.1 C16orf72 may be a novel DNA replication stress response factor

In the previous chapter, through a whole-genome CRISPR dropout screen I identified and validated a novel synthetic lethal interaction between C16orf72 loss and combined loss of PARP1 and PARP2. This finding suggested that C16orf72 may be a novel DDR factor (Nijman, 2011). Notably, I identified that C16orf72-deficient cells are sensitised to HU and APH, which suggested that C16orf72 may function in the DNA replication stress response (Choe et al., 2016; Daza-Martin et al., 2019; Higgs et al., 2015; Lee et al., 2016; Schwab et al., 2013). However, additional experimental evidence is required in order to confirm that C16orf72 functions in the DNA replication stress response.

5.1.2 Aims

The participation of C16orf72 in the DNA replication stress response has not yet been confirmed. Therefore, the aims of this chapter are:

1. To seek multiple lines of evidence that confirm the participation of C16orf72 in the DNA replication stress response.

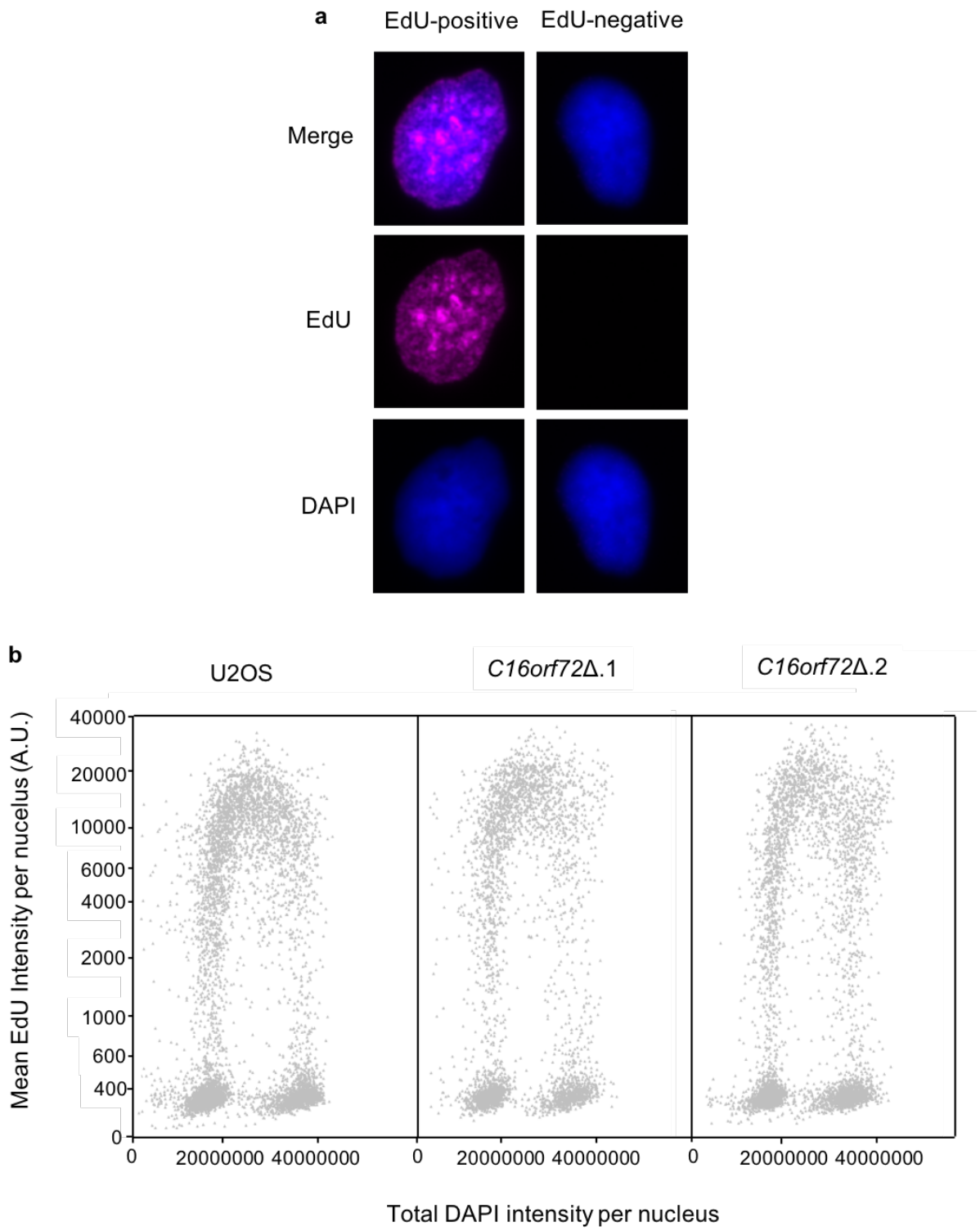
2. To determine the DNA replication stress response pathway(s) that C16orf72 functions within.

5.2 Results

5.2.1 QIBC analysis of cell cycle distribution in *C16orf72Δ* cells

Loss of DNA replication stress response genes can, in some cases, alter the cell cycle distribution of unperturbed cells (Bass et al., 2016; Kim et al., 2019). However, it should be noted that there are also instances where loss of DNA replication stress response genes does not notably alter the cell cycle distribution of unperturbed cells (Higgs et al., 2015). Therefore, I hypothesised that if loss of C16orf72 alters the cell cycle distribution in unperturbed cells, then this would support the notion that C16orf72 may function in the DNA replication stress response, but if loss of C16orf72 does not alter the cell cycle distribution in unperturbed cells then this finding would neither support nor refute the notion that C16orf72 may function in the DNA replication stress response. To assess this hypothesis, I treated wild type U2OS, *C16orf72Δ*.1 and *C16orf72Δ*.2 cells with a 30-minute pulse of EdU before fixation. After performing the azide click reaction and staining the DNA with DAPI, the cell cycle distribution of the cells was analysed by quantitative image-based cytometry (QIBC), a single-cell high content microscopy approach that can quantitatively and unbiasedly monitor the dynamics of cellular responses at an unprecedented level of detail and in a fully automated fashion (Figure 1 a, b). Therefore, it is a more powerful technique than standard immunofluorescence microscopy or western blot analysis (Toledo et al., 2017; Toledo et al., 2013). Using this approach, I evaluated whether *C16orf72Δ* cells had a different cell cycle profile to wild type U2OS cells (Figure 1 c). S-phase cells were identified as EdU-positive, as they were integrating the thymidine analogue into their actively replicating DNA during the EdU pulse treatment. The percentage of U2OS, *C16orf72Δ*.1 and *C16orf72Δ*.2 cells in G_1-phase was 35.5%, 30.8% and

36.1%, respectively, although the differences in mean proportion of G_1-phase cells in *C16orf72Δ*.1 ($p > 0.9999$) and *C16orf72Δ*.2 ($p > 0.9999$) cells relative to U2OS cells were not statistically significant. The percentage of unperturbed U2OS, *C16orf72Δ*.1 and *C16orf72Δ*.2 cells in S-phase was 45.3%, 47.8%, and 37.7%, respectively, although the differences in percentage of S-phase cells in *C16orf72Δ*.1 ($p > 0.9999$) and *C16orf72Δ*.2 ($p = 0.5409$) cells relative to U2OS cells were not statistically significant. The percentage of unperturbed U2OS, *C16orf72Δ*.1 and *C16orf72Δ*.2 cells in G_2/M-phase was 19.2%, 21.4%, and 26.2%, respectively, but the differences in mean proportion of G_2/M-phase cells in *C16orf72Δ*.1 ($p > 0.9999$) and *C16orf72Δ*.2 ($p = 0.6716$) cells relative to U2OS cells were not statistically significant. Therefore, these data suggest that C16orf72 deletion does not alter cell cycle distribution in unperturbed cells, which neither supports nor negates the notion that C16orf72 may participate in the DNA replication stress response.


a
EdU-positive
EdU-negative
Merge
EdU
DAPI
b
U2OS
C16orf72Δ.1
C16orf72Δ.2
Mean EdU Intensity per nucelus (A.U.)
40000
20000
10000
6000
4000
2000
1000
600
400
0
0
20000000
40000000
Total DAPI intensity per nucleus

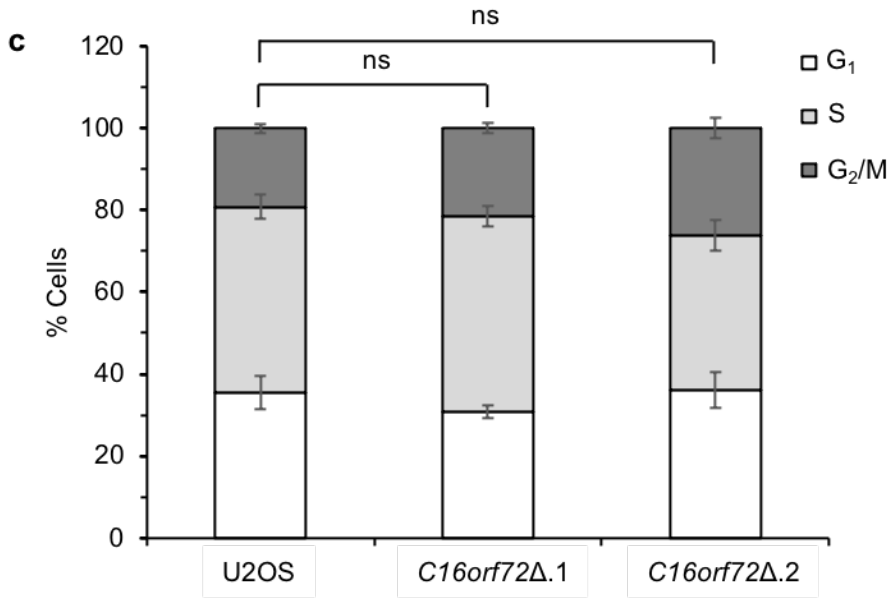


Figure 5.1: Cell cycle distribution is not altered in *C16orf72Δ* cells. (a) Wild type U2OS, *C16orf72Δ*.1 and *C16orf72Δ*.2 cells were treated with a 10 μM EdU pulse for 30 min, fixed and analysed by QIBC. Representative images of EdU-positive (S-phase) and EdU-negative (G_1-, G_2- and M-phase) DAPI-stained nuclei are presented. **(b)** QIBC analysis of mean EdU intensity per nucleus and total DAPI intensity per nucleus. Each experiment was performed with three independent biological repeats and at least 1300 cells were analysed per condition. Each scatter plot is a representative biological repeat for the indicated cell line. **(c)** Bar chart summarising cell cycle distribution of wild type U2OS, *C16orf72Δ*.1 and *C16orf72Δ*.2 cells. Three independent biological replicates of the experiment described in **(a)** were performed and error bars indicate the SEM. Statistical significance between the percentage of G_1, S and G_2/M cells in *C16orf72Δ* cells relative to wild type U2OS cells was evaluated by a One-way ANOVA and a Bonferroni post-hoc test. ns, not significant.

5.2.2 C16orf72 is recruited to chromatin in response to exogenous replication stress in an ATR-independent manner

Proteins involved in the DNA replication stress response are often recruited to chromatin in response to exogenous replication stress (Choe et al., 2016; Gao et al., 2021; Lossaint et al., 2013; Murai et al., 2018; Schlacher et al., 2012; Schubert et al., 2017). Therefore, I hypothesised that if C16orf72 participates in the DNA replication stress response, then it may be recruited to chromatin in response to HU treatment. To assess this, I treated U2OS cells overexpressing FLAG-HA-C16orf72 with vehicle or 2 mM HU for 24 h and prepared chromatin extracts, as well as whole cell extracts (Figure 2 a). FLAG-HA-C16orf72 recruitment was analysed via western blot using an anti-FLAG antibody. Following treatment with vehicle, I did not observe any recruitment of FLAG-HA-C16orf72 to chromatin. However, I observed a striking increase in the recruitment of FLAG-HA-C16orf72 to chromatin in response to 24 h 2 mM HU treatment. Importantly, FLAG-HA-C16orf72 protein levels remained the same in vehicle-treated and HU-treated whole cell extracts, suggesting that C16of72 is recruited to chromatin in response to HU (Figure 2 a).

Proteins that participate in the DNA replication stress response can be recruited to chromatin under conditions of exogenous replication stress in an ATR-dependent manner (Gao et al., 2021). However, it is important to note that there are instances where proteins involved in the DNA replication stress response are not recruited to chromatin by ATR under conditions of exogenous replication stress, such as RPA (Toledo et al., 2013). Therefore, I hypothesised that if C16orf72 is recruited to chromatin under conditions of exogenous replication stress in an ATR-dependent manner then this would support the notion that C16orf72 may participate in the DNA

replication stress response, but if C16orf72 is recruited to chromatin under conditions of exogenous replication stress in an ATR-independent manner then this would neither support nor negate the notion that C16orf72 may participate in the DNA replication stress response. To test this hypothesis, I treated *C16orf72Δ*.2 cells overexpressing FLAG-HA-C16orf72 with vehicle (DMSO), 1 μM of the ATR inhibitor (ATRi) AZD6738, 2 mM HU, or a combination of both treatments for 24 h (Foote et al., 2018) (Figure 2 b). Chromatin extracts were prepared and analysed via western blot and an anti-HA antibody was used to assess FLAG-HA-C16orf72 recruitment in response to the different treatments. Following treatment with vehicle, I observed low levels, but not complete absence of FLAG-HA-C16orf72 chromatin recruitment. Additionally, I observed clear recruitment of FLAG-HA-C16orf72 to chromatin in response to HU treatment. For reasons that are not clear, I also observed recruitment of FLAG-HA-C16orf72 in response to ATRi, but to a lesser extent than HU-mediated FLAG-HA-C16orf72 recruitment. Importantly, ATRi treatment did not prevent HU-induced recruitment of C16orf72 to chromatin. Overall, these data demonstrate that FLAG-HA-C16orf72 is recruited to chromatin in response to HU, but its HU-dependent recruitment is not mediated by ATR. Therefore, two conclusions can be drawn from these data. Firstly, FLAG-HA-C16orf72 is recruited to chromatin in response to exogenous replication stress, which supports the notion that C16orf72 participates in the DNA replication stress response. Secondly, FLAG-HA-C16orf72 is recruited to chromatin in response to exogenous replication stress independently of ATR which neither supports nor negates the notion that C16orf72 may participate in the DNA replication stress response.

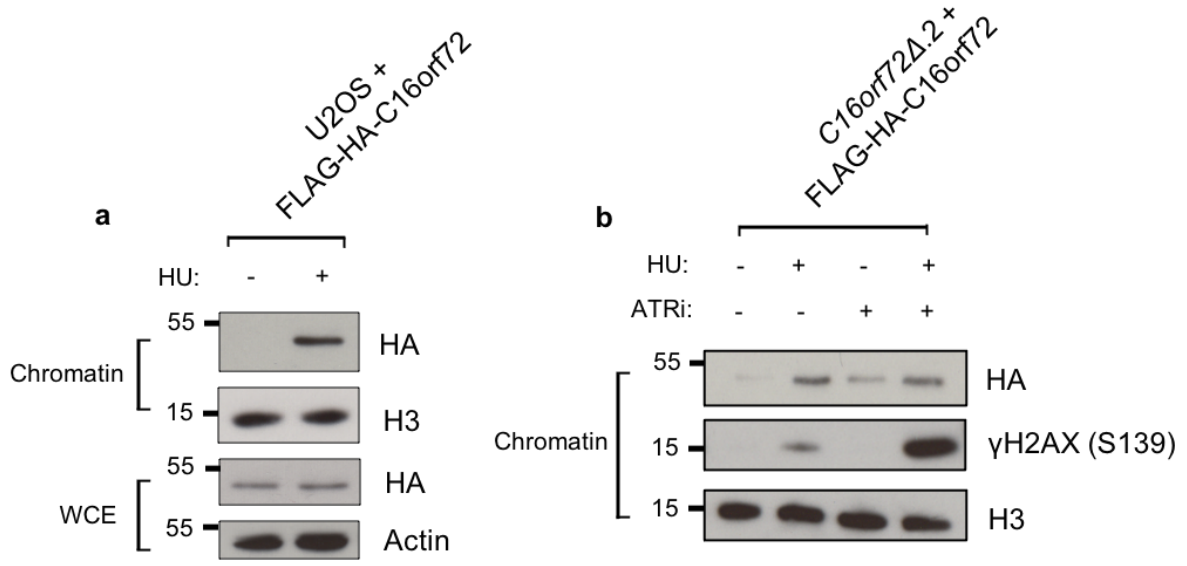


Figure 5.2: FLAG-HA-C16orf72 is recruited to chromatin in response to HU treatment but independently of ATR. (a) U2OS + FLAG-HA-C16orf72 cells were treated with vehicle (Milli-Q) for 0 h or with 2 mM HU for 24 h, and chromatin preparations and whole cell extracts were prepared. The samples were analysed with the indicated antibodies by western blot. Histone H3 and actin acted as loading controls for whole cell extracts and chromatin extracts, respectively. **(b)** *C16orf72Δ*.2 + FLAG-HA-C16orf72 cells were treated with vehicle, 2 mM HU, 1 μM ATRi, or a combination of both for 24 h. Chromatin preparations of each condition were prepared, and the samples were analysed with the indicated antibodies by western blot. Histone H3 acted as a loading control for the chromatin extracts.

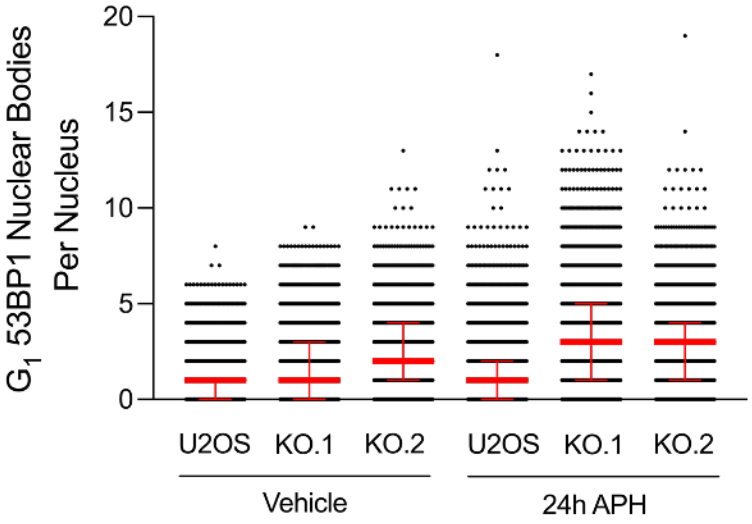
5.2.3 QIBC analysis of G_1-phase 53BP1 nuclear body formation in *C16orf72Δ* cells in the absence and presence of exogenous replication stress

It has been proposed that replication stress can induce permanent stalling of a pair of approaching replication forks (double fork stall) which can result in under-replicated DNA (Moreno et al., 2016; Wilson et al., 2015). Following the accumulation of endogenous replication stress-induced double fork stalls in parent cells, in the subsequent cell cycle, G_1-phase 53BP1 nuclear bodies form at sites of DNA damage within daughter cell that arise from the resulting under-replicated DNA (Fernandez-Vidal et al., 2017; Harrigan et al., 2011; Lukas et al., 2011; Moreno et al., 2016). The G_1-phase 53BP1 nuclear bodies repress deleterious RAD51-mediated repair of the inherited DNA damage, and promote the repair of the sites of DNA damage by a RAD52-dependent pathway (Spies et al., 2019). APH supresses the function of DNA polymerase α and ε, and therefore induces replication stress (Ikegami et al., 1978). In unperturbed conditions, loss of DNA replication stress response genes can result in elevated G_1-phase 53BP1 nuclear body formation relative to wild type cells and this phenotype can be exacerbated following treatment with APH (Lukas et al., 2011). In rare cases, loss of DNA replication stress response genes results in elevated G_1-phase 53BP1 nuclear body formation relative to wild type cells following exposure to APH, but has no effect on the formation of G_1-phase 53BP1 nuclear bodies in unperturbed conditions relative to wild type cells (Kosar et al., 2021). Therefore, I hypothesised that if C16orf72 may participate in the DNA replication stress response, then loss of C16orf72 will result in either of the observations described above. To test this hypothesis, I treated wild type U2OS, *C16orf72Δ*.1 and *C16orf72Δ*.2 cells with vehicle or 0.2 μM APH for 24 h and processed the cells for QIBC (Figure 3 a, b).

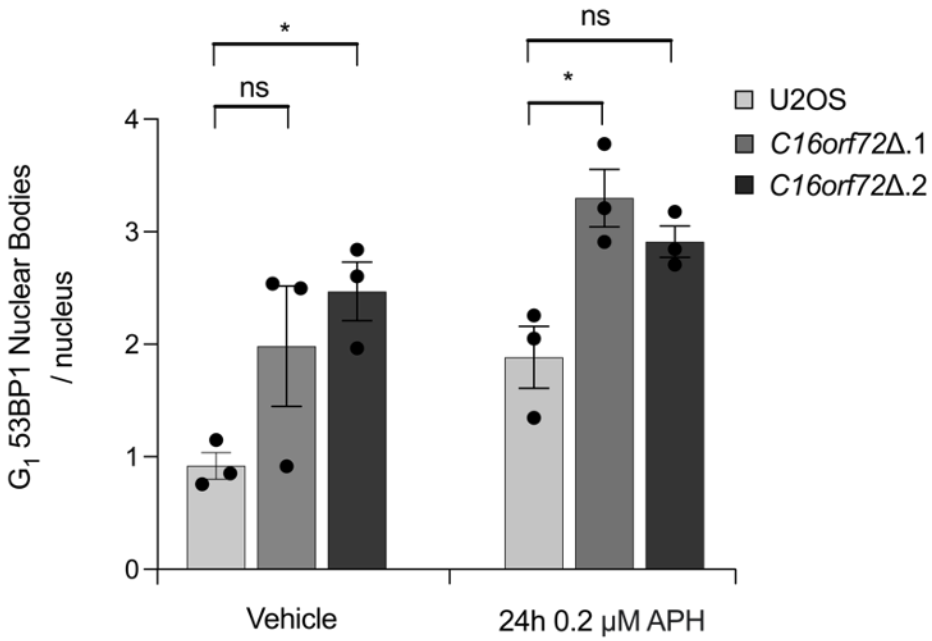
Subsequently, individual nuclei were stained with DAPI. In these samples, mean cyclin A intensity per nucleus and mean G_1-phase 53BP1 nuclear bodies per nucleus were analysed by QIBC. The presence of cyclin A is an indicator of cells in S- and G_2 -phase (Lukas et al., 2011). Therefore, cyclin A-negative cells are in G_1- or G_2/M-phase. Cyclin A-negative G_1-phase cells were distinguished from cyclin A-negative G_2/M-phase cells by their 2N and 4N DNA content, respectively. Given that there is no universally accepted method of analysing the statistical significance of observed differences in nuclear foci (or in this case G_1-phase 53BP1 nuclear bodies per nucleus) between experimental conditions in data collected via QIBC, I followed two approaches to analyse the data. In the first approach, for each experimental condition, I amalgamated the individual cell data from three independent biological replicates and calculated the median frequency of G_1-phase 53BP1 nuclear bodies per nucleus. In the second approach, I calculated the mean frequency of G_1-phase 53BP1 nuclear bodies per nucleus across the three biological replicates. Subsequently, a one-way ANOVA with a Bonferroni post hoc to test was performed to assess the statistical significance of differences in mean G_1 -phase 53BP1 bodies per nucleus between indicated experimental conditions. I chose to analyse this experiment using the second method of statistical analysis because it represented the full range of individual cell data from all three biological repeats while also assessing the variation in each experimental condition between biological repeats. For reasons that are not clear, following treatment with vehicle, there was no difference in mean G_1 -phase 53BP1 bodies per nucleus in *C16orf72Δ*.1 cells relative to wild type U2OS cells ($p = 0.1049$), whereas there was a ~2.7-fold increase in mean G_1 -phase 53BP1 bodies per nucleus in *C16orf72Δ*.2 cells relative to wild type U2OS cells ($p = 0.0123$). Additionally, for reasons that are not clear, following treatment with 0.2 μM APH for 24 h, there was a

~1.8-fold increase in mean G_1 -phase 53BP1 bodies per nucleus in *C16orf72Δ*.1 cells relative to wild type U2OS cells ($p = 0.0223$), whereas there was no difference in mean G_1 -phase 53BP1 bodies per nucleus in *C16orf72Δ*.2 cells relative to wild type U2OS cells ($p = 0.1234$). Therefore, it is not clear from these data whether C16orf72 may participate in the DNA replication stress response.

a


G1 53BP1 Nuclear Bodies Per Nucleus
20
15
10
5
0
U2OS
KO.1
KO.2
U2OS
KO.1
KO.2
Vehicle
24h APH

b


G1 53BP1 Nuclear Bodies / nucleus
*
ns
ns
*
4
3
2
1
0
U2OS
C16orf72Δ.1
C16orf72Δ.2
Vehicle
24h 0.2 μM APH

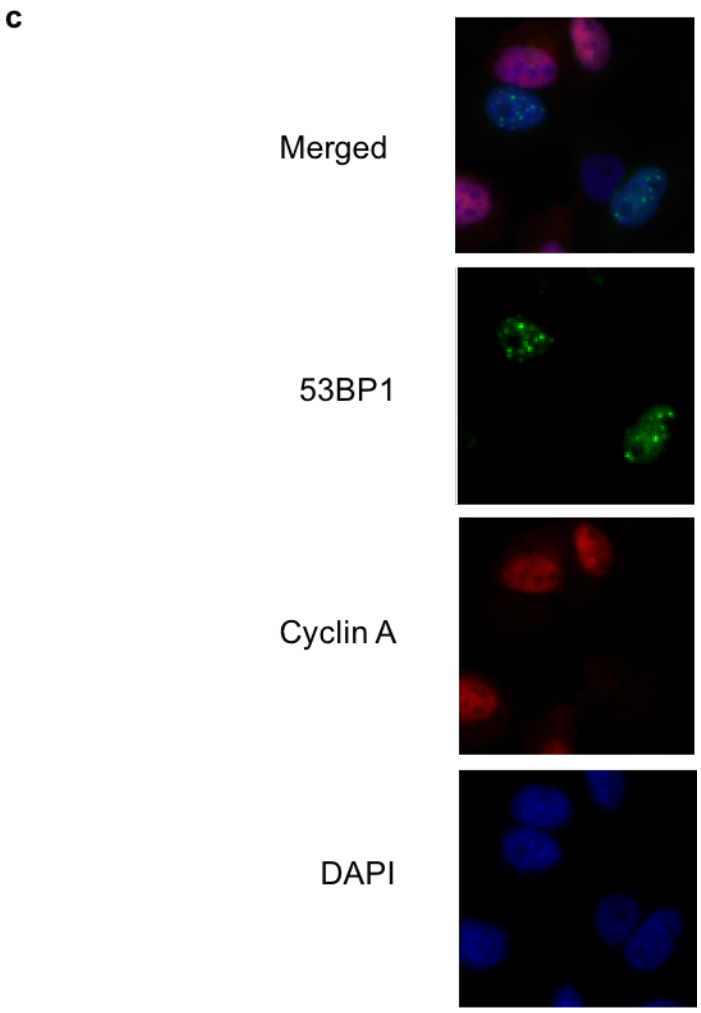


Figure 5.3: G_1-phase 53BP1 nuclear body formation in *C16orf72Δ* cells in the absence and presence of APH. (a) U2OS, *C16orf72Δ*.1 (KO.1) and *C16orf72Δ*.2 (KO.2) cells were treated with vehicle or 0.2 μM APH for 24h before fixation. Cells were imaged and analysed by QIBC. The data points within each condition (black dots) of the scatter plot represents the frequency of G_1-phase 53BP1 nuclear bodies per nucleus, amalgamated from three independent biological replicates. Within each independent biological replicate, at least 500 G_1-phase (cyclin A-negative) cells were analysed per condition. For each condition, the red line represents the median, and the lower and upper whiskers represent the 25th and 75th percentile, respectively. **(b)** The data points within each condition represent the mean quantity of nuclear G1-phase 53BP1 bodies per biological repeat. Error bars represent the SEM. Statistical

significance was evaluated by a one-way ANOVA with a Bonferroni post hoc test. ns, not significant; * $p < 0.05$. **(c)** Example images of G_1-phase 53BP1 nuclear body formation in unperturbed *C16orf72Δ*.2 cells.

5.2.4 Western blot analysis of pRPA, pDNA-PK$_{CS}$, pCHK1 and γH2AX levels in *C16orf72Δ* cells in the absence and/or presence of exogenous replication stress

pRPA32 (Ser4/Ser8) is a marker of broken replication forks that are formed as a consequence of exogenous replication stress (Chanut et al., 2016; Toledo et al., 2013). This posttranslational modification is thought to be mediated mostly via DNA-PK$_{CS}$-dependent kinase activity (Anantha et al., 2007; Liaw et al., 2011; Liu et al., 2012; Shiotani et al., 2013). DNA-PK$_{CS}$ can be phosphorylated by another DNA-PK$_{CS}$ protein at Ser2056 (Meek et al., 2007). It is thought that pDNA-PK$_{CS}$ (Ser2056) signalling occurs due to an accumulation of stalled replication forks that have not undergone end resection, as HU-induced pDNA-PK$_{CS}$ (Ser2056) and RPA foci rarely overlap (Ying et al., 2016). ATM restrains the NHEJ-mediated repair of broken replication forks that are induced by exogenous replication stress (Britton et al., 2020). In cells treated with ATMi, pDNA-PK$_{CS}$ (Ser2056) is also thought to occur when broken replication forks that arise due to exogenous replication stress are repaired by c-NHEJ (Britton et al., 2020; Roy et al., 2015). γH2AX (Ser139) can be an indicator of stalled and collapsed replication forks under conditions of exogenous replication stress (Gagou et al., 2010; Sirbu et al., 2011). Replication fork collapse is defined as replication forks that no longer possess the ability to replicate DNA. Examples of collapsed fork structures are broken replication forks and stalled forks in which replisome disassembly has occurred

(Carr et al., 2011; Cortez, 2015; Zeman & Cimprich, 2014). pCHK1 (Ser317) can be induced in response to replication stress in an ATR-dependent manner (Zhao & Piwnica-Worms, 2001). Therefore, pCHK1 signalling is a marker for proficient ATR signalling in response to replication stress. In unperturbed conditions, loss of DNA replication stress response proteins can result in an increase in γH2AX (Ser139) levels relative to wild type cells, although this is not always the case (Higgs et al., 2015; Schwab et al., 2015). For the purpose of this assay and other assays that detect this biomarker in this chapter, an increase in γH2AX (Ser139) levels in unperturbed cells is assumed to indicate an increase in accumulated stalled and collapsed replication forks within cells that arise due to endogenous replication stress. I hypothesised that if *C16orf72Δ* cells exhibit elevated levels of γH2AX (Ser139) in the absence and/or presence of exogenous replication stress relative to wild type U2OS cells, then C16orf72 may participate in the DNA replication stress response to prevent the accumulation of stalled and/or collapsed replication forks under conditions of endogenous or exogenous replication stress. Additionally, I hypothesised that if *C16orf72Δ* cells exhibit elevated levels of pRPA (S4/S8) in the presence of exogenous replication stress relative to wild type U2OS cells, then C16orf72 may participate in the DNA replication stress response to prevent the accumulation of broken replication forks under these conditions. Furthermore, I hypothesised that if *C16orf72Δ* cells exhibit elevated levels of pDNA-PK_{CS} (Ser2056) in the presence of exogenous replication stress relative to wild type U2OS cells, then C16orf72 may function in the DNA replication stress response to prevent the accumulation of stalled and/or broken replication forks. I also hypothesised that if C16orf72 functions within the ATR pathway of the DNA replication stress response then pCHK1 (Ser317) signalling will be impaired in *C16orf72Δ* cells treated with exogenous replication stress relative wild type

U2OS cells. To investigate these hypotheses, I performed a 2 mM HU time course in wild type U2OS, *C16orf72Δ*.1 and *C16orf72Δ*.2 cells and prepared whole cell extracts of these cell lines at 2 h, 8 h and 24 h post-HU treatment (Figure 4). Vehicle treated whole cell extracts of each cell line were also prepared almost immediately after treatment. The vehicle-treated wild type U2OS cells acted as a negative control. Samples were analysed via western blot for pCHK1 (Ser317), CHK1, pRPA32 (Ser4/Ser8), RPA32, pDNA-PK_{CS} (Ser2056), DNA-PK_{CS}, γH2AX (Ser139) and vinculin (Figure 4).

As expected, low levels of γH2AX (Ser139) were observed in vehicle-treated U2OS cells and following treatment with 2 mM HU, γH2AX (Ser139) levels continued to increase in a time-dependent manner (Petermann et al., 2010). This indicates that the assay worked as expected. Following treatment with vehicle, *C16orf72Δ*.1 cells exhibited similar levels of γH2AX (Ser139) relative to wild type U2OS cells, whereas *C16orf72Δ*.2 cells exhibited elevated levels of γH2AX (Ser139) relative to U2OS wild type cells. Therefore, it is not clear from these data whether C16orf72 participates in the DNA replication stress response to prevent the accumulation of stalled and/or collapsed forks that arise as a consequence of endogenous replication stress. Following treatment with 2 mM HU for 2 and 24 h, *C16orf72Δ*.1 and *C16orf72Δ*.2 cells exhibited elevated γH2AX (Ser139) levels relative to wild type U2OS cells. Following 8 h of 2 mM HU treatment, wild type U2OS cells and *C16orf72Δ*.1 cells exhibited similar levels of γH2AX (Ser139), whereas elevated levels of γH2AX (Ser139) were observed in *C16orf72Δ*.2 cells relative to wild type U2OS cells. Therefore, these findings support the notion that C16orf72 may participate in the DNA replication stress response by preventing the accumulation of stalled and/or collapsed forks under

conditions of short (2 h) and prolonged (24 h) exposure to exogenous replication stress. However, it is not clear from these observations whether C16orf72 participates in the DNA replication stress response to prevent the accumulation of stalled and/or collapsed forks following intermediate (8 h) exposure to exogenous replication stress.

In response to 2, 8 and 24 h of HU treatment, pCHK1 (Ser317) levels were similar in *C16orf72Δ*.1 cells relative to wild type U2OS cells. However, at these time points of HU exposure, *C16orf72Δ*.2 cells exhibited reduced levels of pCHK1 (Ser317) relative to wild type U2OS cells. This is likely due to the presence of less total CHK1 in *C16orf72Δ*.2 cells relative to wild type U2OS and *C16orf72Δ*.1 cells. Therefore, it is not clear from these data whether C16orf72 functions within the ATR pathway of the DNA replication stress response.

In response to 2 h of HU treatment, elevated levels of pRPA32 (Ser4/Ser8) were observed in *C16orf72Δ*.1 and *C16orf72Δ*.2 cells relative to wild type U2OS cells. Furthermore, similar levels of RPA32 were present in vehicle-treated *C16orf72Δ*.1 and *C16orf72Δ*.2 cells relative to wild type U2OS cells, indicating that this phenotype was not due to increased levels of RPA32 in *C16orf72Δ* cells. Following treatment of wild type U2OS, *C16orf72Δ*.1 and *C16orf72Δ*.2 cells to 2 mM HU for 8 and 24 h, *C16orf72Δ*.1 and *C16orf72Δ*.2 cells exhibited similar levels of pRPA32 (Ser4/Ser8) relative to wild type U2OS cells. Therefore, these findings support the following. Firstly, C16orf72 may participate in the DNA replication stress response to prevent the accumulation of broken replication forks under conditions of short (2 h) exposure to exogenous replication stress. Secondly, C16orf72 may not participate in the DNA replication stress response to prevent the accumulation of broken replication forks

under conditions of intermediate (8 h) and prolonged (24 h) exposure to exogenous replication stress.

Wild type U2OS, *C16orf72Δ*.1 and *C16orf72Δ*.2 cells treated with 2 mM HU for 2 and 8 h displayed similar levels of pDNA-PK_{CS} (Ser2056). However, following exposure of these cell lines to HU for 24 h, *C16orf72Δ*.1 and *C16orf72Δ*.2 cells exhibited elevated levels of pDNA-PK_{CS} (Ser2056) relative to wild type U2OS cells. Furthermore, all prepared samples of U2OS, *C16orf72Δ*.1 and *C16orf72Δ*.2 cells in this experiment contained similar levels of total DNA-PK_{CS}, indicating that the increase in pDNA-PK_{CS} (Ser2056) levels was not due to increased levels of total DNA-PK_{CS} in *C16orf72Δ* cells. Therefore, these data suggest the following. Firstly, C16orf72 may participate in the DNA replication stress response to prevent the accumulation of stalled and/or broken replication forks under conditions of prolonged (24 h) exposure to exogenous DNA replication stress. Secondly, C16orf72 may not participate in the DNA replication stress response to prevent the accumulation of stalled and/or broken replication forks under conditions of short (2 h) and intermediate (8 h) exposure to exogenous replication stress.

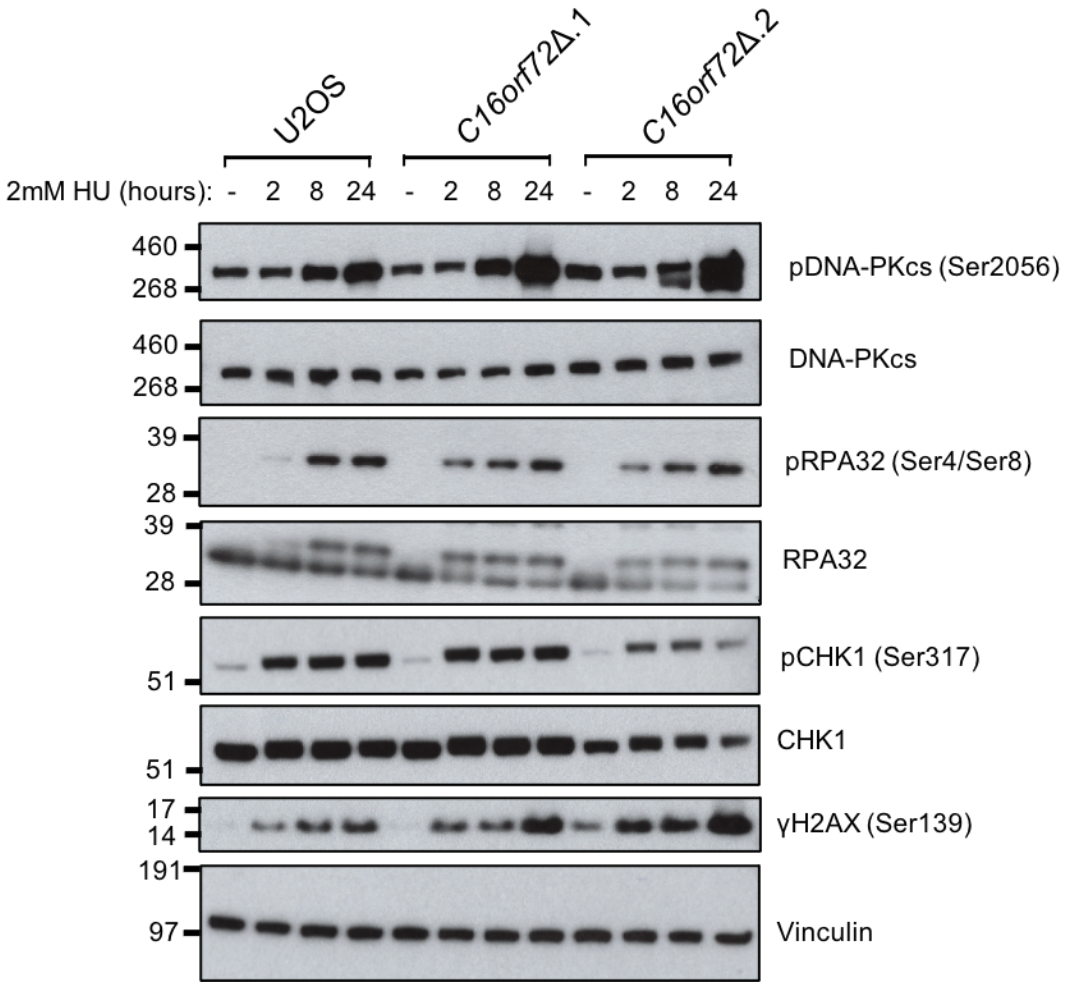


Figure 5.4: Western blot analysis of pRPA, pDNA-PK$_{CS}$, pCHK1 and γH2AX levels in *C16orf72Δ* cells in the absence and presence of HU. U2OS, *C16orf72Δ*.1 and *C16orf72Δ*.2 cells were treated with vehicle (-), or with HU for 2 h, 8 h or 24 h. Whole cell extracts were prepared, and samples were analysed by western blot with the indicated antibodies. Vinculin acted as a loading control for the whole cell extracts.

5.2.5 QIBC analysis of γH2AX and RPA70 levels in *C16orf72Δ* cells in the absence and presence of exogenous replication stress

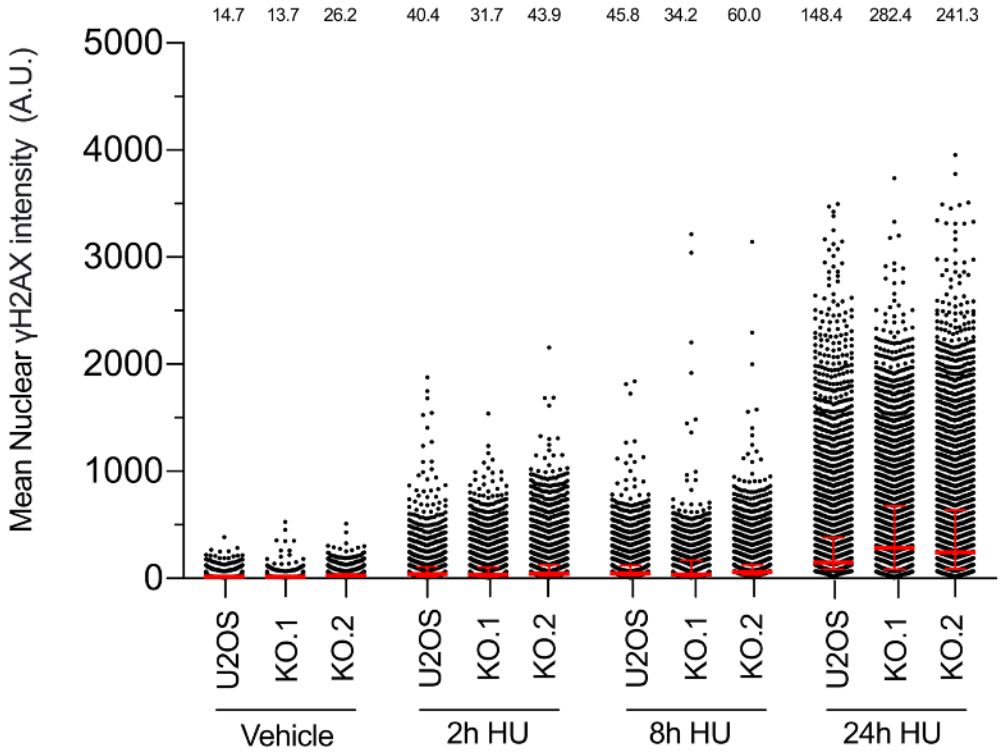
RPA intensity per nucleus or RPA foci per nucleus can be used as a proxy for cellular ssDNA accumulation (Bass et al., 2016; Raderschall et al., 1999). Loss of DNA replication stress response proteins can result in elevated ssDNA within cells (Toledo et al., 2013). Therefore, I hypothesised that if loss of C16orf72 results in an increase in nuclear RPA intensity in unperturbed cells and/or in cells treated with exogenous replication stress when analysed by QIBC, then C16orf72 may participate in the DNA replication stress response to prevent the accumulation of replication stress-induced ssDNA (Toledo et al., 2013). Additionally, given that I observed elevated γH2AX (Ser139) levels in *C16orf72Δ* cells in response to HU treatment at certain time points (Figure 4), I hypothesised that these findings should be reproduceable when analysed by QIBC. To test these hypotheses, I performed a 2 mM HU time course in U2OS, *C16orf72Δ*.1 and *C16orf72Δ*.2 cells and fixed the cells at 2, 8 and 24 h post-HU treatment. Vehicle-treated samples of each cell line were also fixed almost immediately after treatment. Samples were pre-extracted and stained with DAPI to identify individual nuclei. Mean nuclear γH2AX (Ser139) intensity (Figure 5 a and b) and mean nuclear RPA70 (Figure 6a and b) intensity were analysed in the same set of samples. Analysis of this experiment rests on the assumptions that mean RPA intensity per nucleus in unperturbed cells only increases as a consequence of elevated levels of replication stress-induced ssDNA. There is no universally accepted method of analysing the statistical significance of observed differences in nuclear intensity between experimental conditions in data collected via QIBC, and there are instances where research groups have presented nuclear intensity data that was collected by QIBC data without performing any statistical analyses (Toledo et al., 2013; Tromans-

Coia et al., 2021). For the reasons outlined previously (see 5.2.3), for each experimental condition, I calculated the median of mean nuclear RPA70/γH2AX intensity (median nuclear RPA70/γH2AX intensity) by combining the individual cell data from three independent biological replicates, and also calculated the mean nuclear RPA70/γH2AX intensity across the three biological replicates. Subsequently, a one-way ANOVA with a Bonferroni post hoc to test was performed to assess the statistical significance of differences in mean nuclear RPA70/γH2AX intensity between indicated experimental conditions. I chose to analyse this experiments using the second method of statistical analysis because it represented the full range of individual cell data from all three biological repeats while also assessing the variation in each experimental condition between biological repeats.

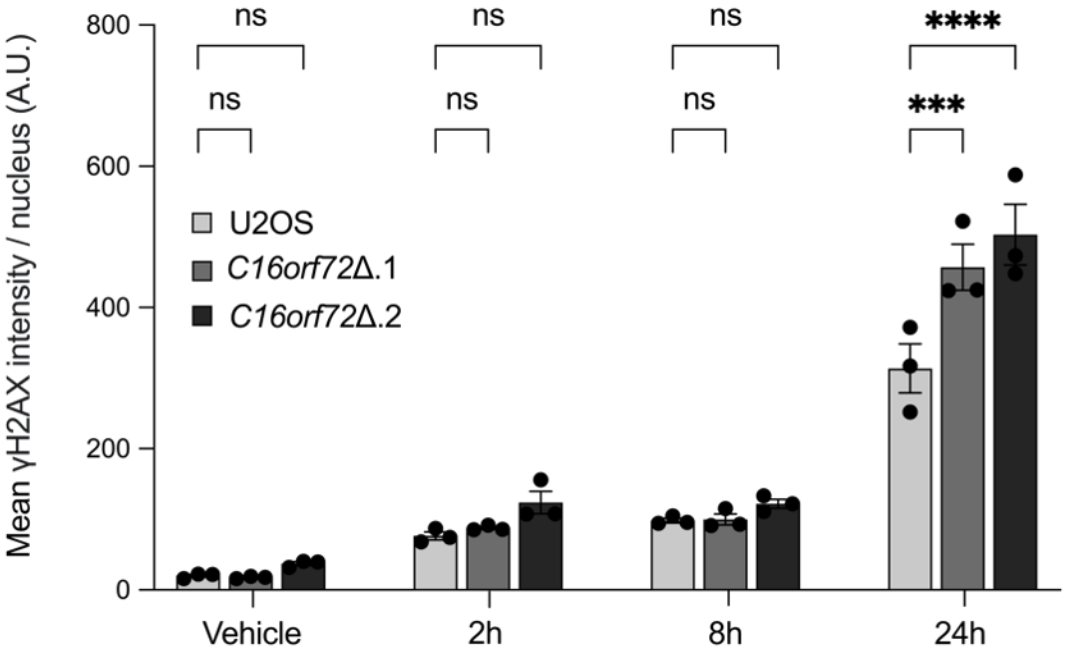
Following treatment with vehicle, *C16orf72Δ*.1 cells ($p > 0.9999$) and *C16orf72Δ*.2 ($p > 0.9999$) cells exhibited the same mean nuclear γH2AX (Ser139) intensity relative to wild type U2OS cells. After exposure to 2 mM HU for 2 h *C16orf72Δ*.1 cells ($p > 0.9999$) and *C16orf72Δ*.2 ($p > 0.7900$) cells exhibited the same mean nuclear γH2AX (Ser139) intensity relative to wild type U2OS cells. Following treatment with 2 mM HU for 24 h, *C16orf72Δ*.1 and *C16orf72Δ*.2 cells exhibited a ~1.5-fold and a ~1.6-fold increase in mean nuclear γH2AX (Ser139) intensity relative to wild type U2OS cells, respectively. Therefore, these data suggest the following. Firstly, C16orf72 may not participate in the DNA replication stress response to prevent the accumulation of stalled and/or collapsed replication forks under conditions of endogenous replication stress. Secondly, C16orf72 may not participate in the DNA replication stress response to prevent the accumulation of stalled and/or collapsed replication forks under conditions of short (2 h) or intermediate (8 h) exposure to exogenous replication

stress. Finally, C16orf72 may participate in the DNA replication stress response to prevent the accumulation of stalled and/or collapsed replication forks under conditions of prolonged exposure (24 h) to exogenous replication stress.

a


14.7
13.7
26.2
40.4
31.7
43.9
45.8
34.2
60.0
148.4
282.4
241.3
Mean Nuclear γH2AX intensity (A.U.)
5000
4000
3000
2000
1000
0
U2OS
KO.1
KO.2
Vehicle
2h HU
8h HU
24h HU

b


Mean γH2AX intensity / nucleus (A.U.)
800
600
400
200
0
ns
****
***
U2OS
C16orf72Δ.1
C16orf72Δ.2
Vehicle
2h
8h
24h

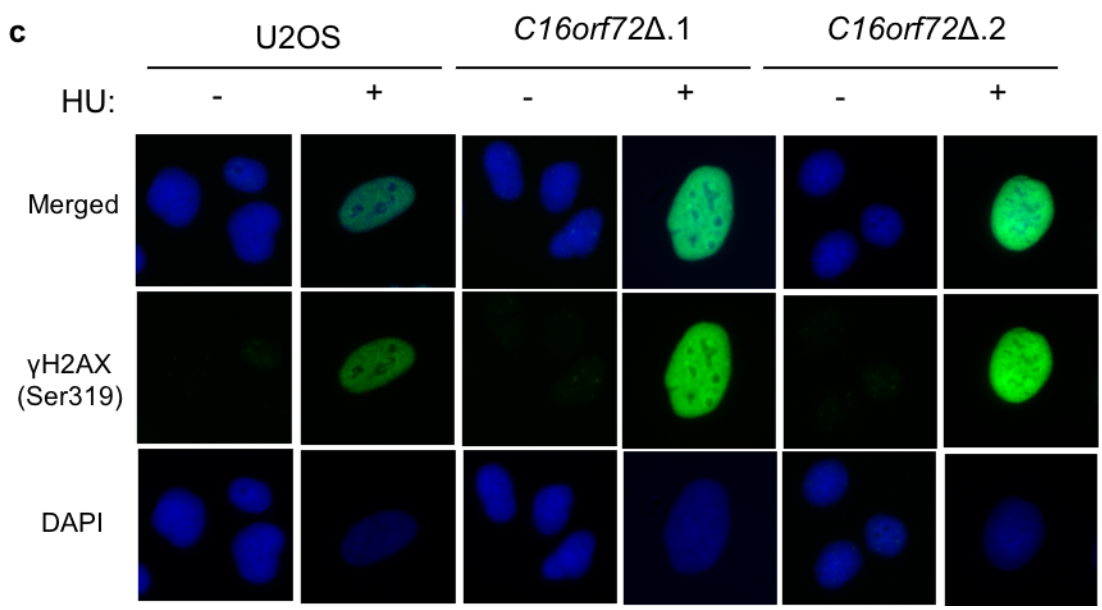
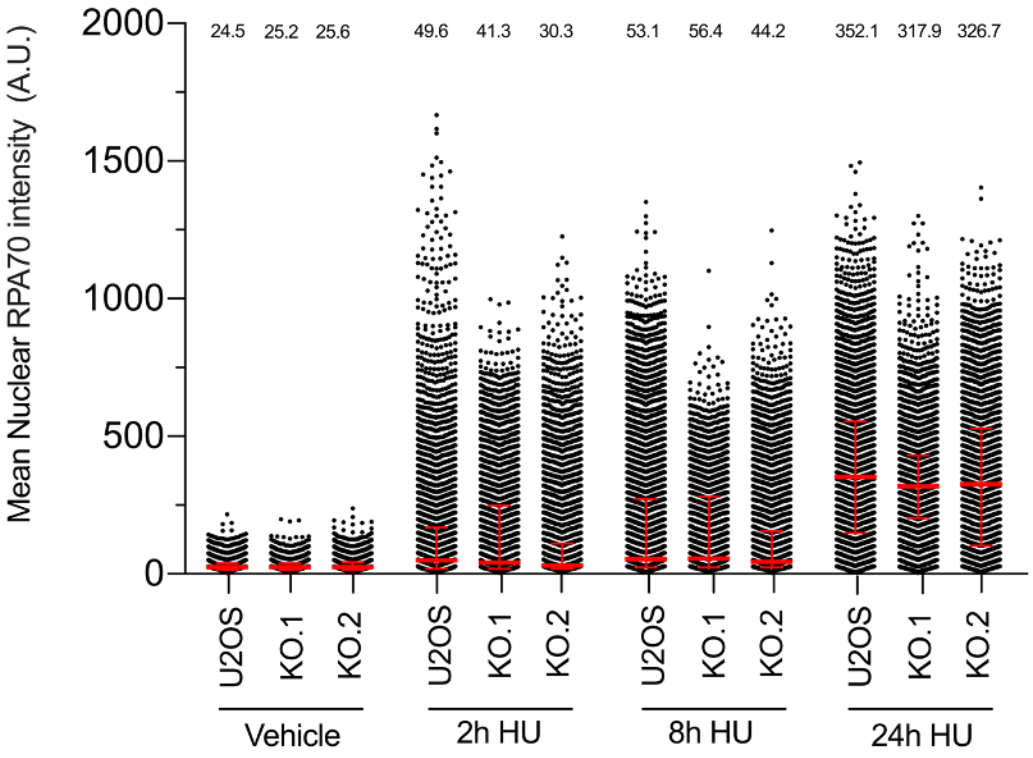


Figure 5.5: QIBC analysis of nuclear γH2AX intensity in *C16orf72Δ* cells in the absence and presence of HU. (a) U2OS, *C16orf72Δ*.1 (KO.1) and *C16orf72Δ*.2 (KO.2) cells were treated with vehicle or with 2 mM HU for 2, 8, or 24 h, before fixation. Mean nuclear γH2AX (Ser139) fluorescence was analysed by QIBC. The data points (black dots) within each condition of the scatter plot represent mean nuclear γH2AX fluorescence, amalgamated from three independent biological replicates. Within each biological replicate, at least 500 cells were analysed per condition. For each condition, the red line represents the median, and the lower and upper whiskers represent the 25th and 75th percentile, respectively. **(b)** The data points within each condition represent the mean nuclear γH2AX fluorescence per biological repeat. Error bars represent the SEM. Statistical significance was evaluated by a one-way ANOVA with a Bonferroni post hoc test. ns, not significant; *** $p < 0.001$; **** $p < 0.0001$. **(c)** Representative images of γH2AX (Ser139) levels in wild type U2OS, *C16orf72Δ*.1 and *C16orf72Δ*.2 cells treated with vehicle for (-) or with 2 mM HU for 24 h.

Following treatment with vehicle, no significant difference in mean RPA70 intensity per nucleus was observed in *C16orf72Δ*.1 ($p > 0.9999$) and *C16orf72Δ*.2 ($p > 0.9999$) cells relative to wild type U2OS cells. Additionally, following treatment with 2 mM HU for 2 h, no significant difference in mean RPA70 intensity per nucleus was observed in *C16orf72Δ*.1 ($p > 0.9999$) and *C16orf72Δ*.2 ($p > 0.9999$) cells relative to wild type U2OS cells. Furthermore, following treatment with 2 mM HU for 8 h, no significant difference in mean RPA70 intensity per nucleus was observed in *C16orf72Δ*.1 ($p > 0.9999$) and *C16orf72Δ*.2 ($p > 0.9999$) cells relative to wild type U2OS cells. Finally, following treatment with 2 mM HU for 24 h, no significant difference in mean RPA70 intensity per nucleus was observed in *C16orf72Δ*.1 ($p = 0.4985$) and *C16orf72Δ*.2 ($p = 0.7736$) cells relative to wild type U2OS cells. Therefore, these data suggest that C16orf72 may not participate in the DNA replication stress response to prevent the accumulation of ssDNA under conditions of endogenous replication stress, or following exposure to short (2 h), intermediate (8 h) or prolonged (24 h) replication stress.

a


Mean Nuclear RPA70 intensity (A.U.)
2000
1500
1000
500
0
24.5 25.2 25.6 49.6 41.3 30.3 53.1 56.4 44.2 352.1 317.9 326.7
U2OS KO.1 KO.2 U2OS KO.1 KO.2 U2OS KO.1 KO.2 U2OS KO.1 KO.2
Vehicle
2h HU
8h HU
24h HU

b

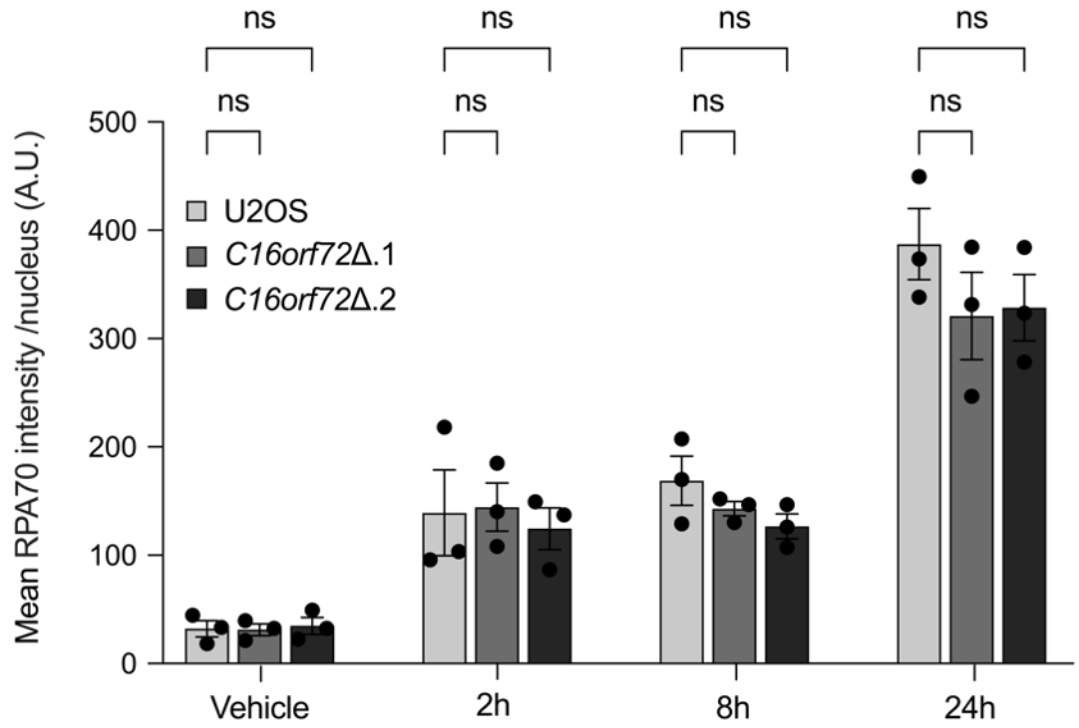

Mean RPA70 intensity /nucleus (A.U.)
ns
ns
ns
ns
ns
ns
ns
ns
500
400
300
200
100
0
U2OS
C16orf72Δ.1
C16orf72Δ.2
Vehicle
2h
8h
24h

Figure 5.6: QIBC analysis of RPA70 levels in *C16orf72Δ* cells in the absence and presence of HU. (a) U2OS, *C16orf72Δ*.1 (KO.1) and *C16orf72Δ*.2 (KO.2) cells were treated with 2 mM HU for the indicated time points. Mean nuclear RPA70 intensity was analysed by QIBC. At least 500 cells were analysed per condition. The data points (black dots) within each condition of the scatter plot represent mean nuclear RPA70 fluorescence, amalgamated from three independent biological replicates. Within each biological replicate, at least 500 cells were analysed per condition. For each condition, the red line represents the median, and the lower and upper whiskers represent the 25th and 75th percentile, respectively. **(b)** The data points within each condition represent the mean nuclear RPA70 fluorescence per biological repeat. Error bars represent the SEM. Statistical significance was evaluated by a one-way ANOVA with a Bonferroni post hoc test. ns, not significant.

5.2.6 QIBC analysis of RPA-γH2AX-positive cells in the absence and presence of exogenous replication stress

Following prolonged exposure (24 h) to exogenous replication stress, cells can accumulate excessive tracts of ssDNA, which sequesters all of the available RPA in the cell, and ultimately results in an abundance of fork breakage events across the nucleus - a phenomenon which has been referred to as replication catastrophe (Toledo et al., 2013). Cells undergoing replication catastrophe are identifiable as cells with nuclei in which high mean nuclear intensities of γH2AX (Ser139) and RPA70 colocalise, or 'RPA70-γH2AX-positive cells' (Toledo et al., 2013). Loss of DNA replication stress response genes can increase the percentage of cells that undergo replication catastrophe under conditions of prolonged exogenous replication stress. Under these conditions, ATR is thought to prevent replication catastrophe by

repressing inappropriate firing of dormant origins (Toledo et al., 2013). Therefore, I hypothesised that if *C16orf72Δ* cells exhibit a higher percentage of RPA70-γH2AX-positive cells under conditions of prolonged replication stress relative to wild type U2OS cells, then this would support the notion that C16orf72 may participate in the DNA replication stress response to limit replication catastrophe under these conditions (Toledo et al., 2013). I assessed this hypothesis by re-analysing the co-stained RPA70 and γH2AX (Ser139) time course data via QIBC (Figures 5 a and 6) and measured the percentage of RPA70-γH2AX-positive wild type U2OS, *C16orf72Δ*.1 and *C16orf72Δ*.2 cells that accumulate in response to vehicle treatment or to 2 mM HU for 24 h (Figure 7 b). The cells that fell within the indicated red squares were deemed RPA70-γH2AX-positive cells (Figure 7 a). As expected, there were no RPA70-γH2AX-positive cells in vehicle-treated wild type U2OS cells, and exposure of wild type U2OS cells to 2mM HU for 24 h resulted in an increase in RPA70-γH2AX-positive cells relative to vehicle-treated wild type U2OS cells. Together, these observations demonstrate that the assay was working as expected (Toledo et al., 2013). Following treatment with vehicle, there was no significant difference in the percentage of RPA70-γH2AX-positive *C16orf72Δ*.1 ($p > 0.9999$) and *C16orf72Δ*.2 ($p > 0.9999$) cells relative to wild type U2OS cells. However, after exposure to 2 mM HU for 24 h, the percentage of the U2OS, *C16orf72Δ*.1 and *C16orf72Δ*.2 cells that were considered RPA70-γH2AX positive was 33.9%, 53.8% and 47.2%, respectively. Therefore, under these conditions, a statistically significant increase in the percentage of RPA70-γH2AX positive cells was observed in *C16orf72*.1Δ ($p = 0.0003$) and *C16orf72*.2Δ ($p = 0.0081$) cells relative wild type U2OS cells. Taken together, these data suggest that C16orf72 may participate in the DNA replication stress response to limit replication catastrophe under conditions of prolonged (24 h) exposure to exogenous replication stress.

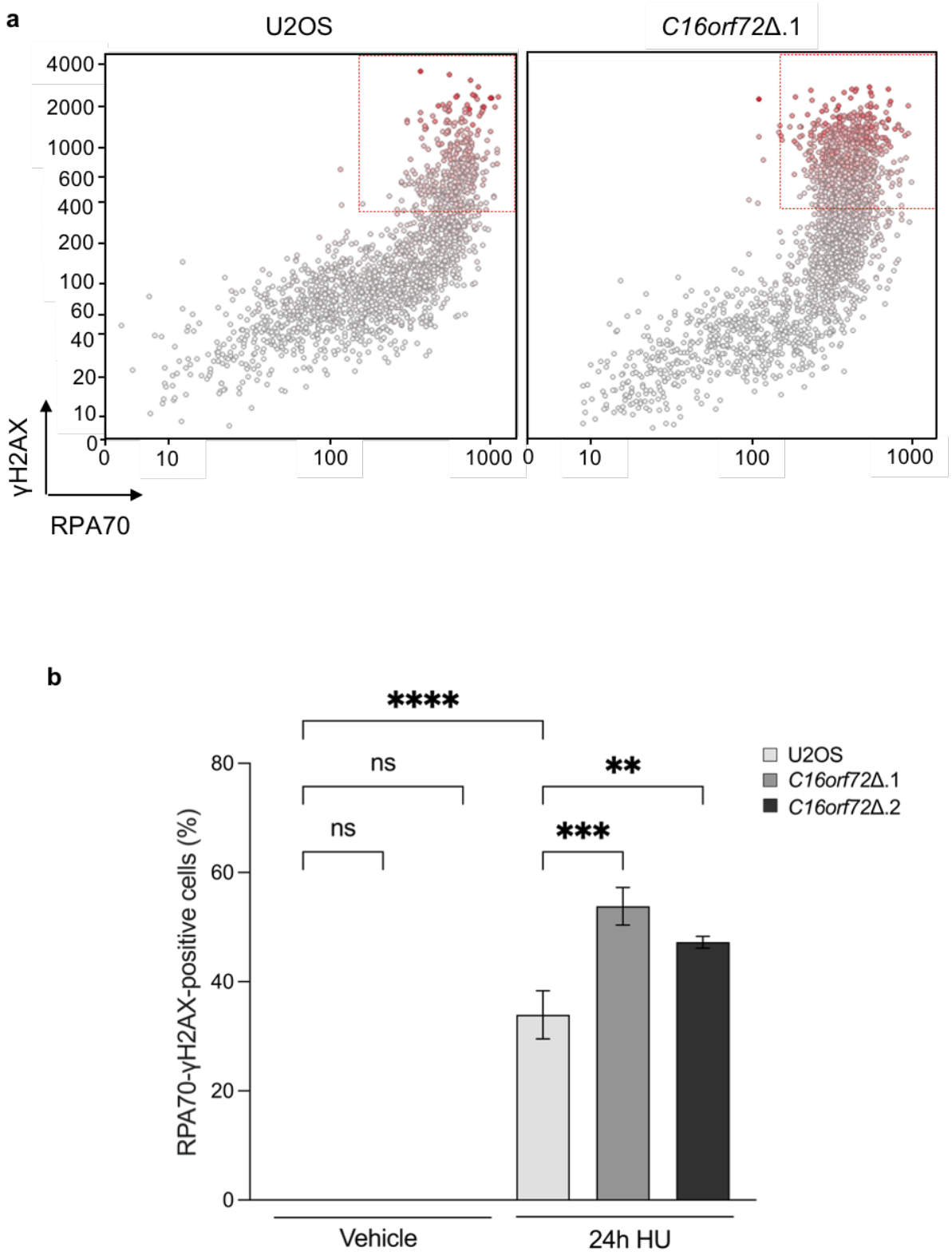


Figure 5.7: QIBC analysis of RPA70-γH2AX-positive cells in the absence and presence of HU. (a) U2OS, *C16orf72Δ*.1 and *C16orf72Δ*.2 cells were treated vehicle or with 2 mM HU for 24 h before fixation. Mean RPA70 intensity per nucleus and mean

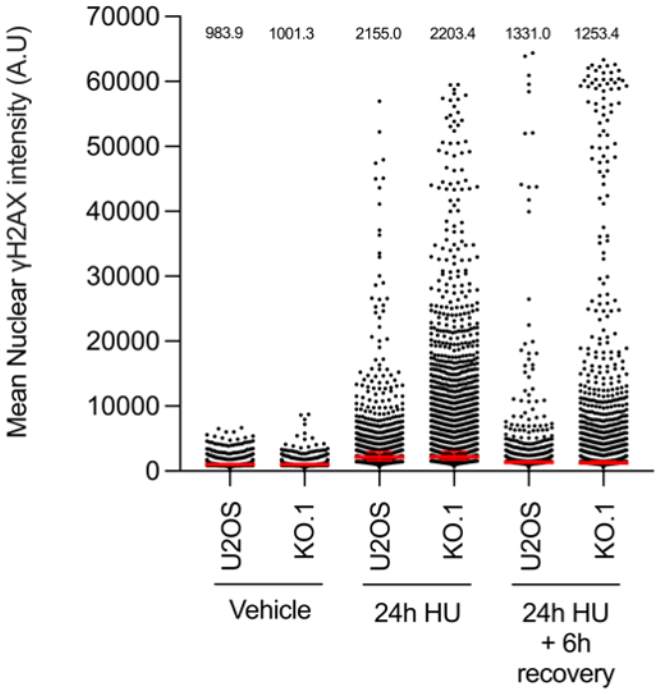
nuclear γH2AX (Ser319) intensity were imaged and analysed by QIBC. Each scatter plot is a representative biological repeat for wild type U2OS (cell number = 1835) and *C16orf72Δ*.1 (cell number = 2347) cells treated with 2 mM HU for 24 h. The percentage of RPA-γH2AX positive cells were calculated by quantifying the percentage of the cells that fall within the red square. **(b)** Bar chart summarising the experiment as described in **(a)**. Three independent biological replicates of this experiment were performed. Error bars represent the SEM. A one-way ANOVA with a Bonferroni post-hoc analysis was used to determine the statistical significance between the indicated conditions. **** $p < 0.0001$; *** $p < 0.001$; ** $p < 0.01$; and ns, not significant.

5.2.7 QIBC analysis of recovery of γH2AX levels in *C16orf72Δ* cells following removal of exogenous replication stress

Finally, I investigated whether C16orf72 may participate in the DNA replication stress response to prevent the accumulation of stalled forks and/or collapsed forks following the removal of exogenous replication stress. I hypothesised that if this is the case, then a delay in the reduction of γH2AX levels would be observed in *C16orf72Δ* cells relative to wild type U2OS cells following removal of HU treatment. To assess this possibility, U2OS and *C16orf72Δ*.1 cells were treated with 200 μM HU for 24 h and fixed, or cells were treated with 200 μM HU for 24 h; allowed to recover in fresh growth media for 6 h; and processed for QIBC. In these samples, mean nuclear γH2AX (Ser139) intensity was analysed by QIBC. As before, and for the reasons described above (see 5.2.3), I calculated the median of mean nuclear γH2AX intensity (median nuclear γH2AX intensity) by combining the individual cell data from three independent biological replicates (Figure 8 a), and also calculated the mean nuclear γH2AX

intensity across the three biological replicates (Figure 8 b). Subsequently, a one-way ANOVA with a Bonferroni post hoc to test was performed to assess the statistical significance of differences in mean nuclear γH2AX intensity between indicated experimental conditions. An assumption of this assay was that exposure of wild type U2OS and *C16orf72Δ* cells to 200 μM HU for 24 h induced resolvable stalled and collapsed forks in these cell lines but did not induce replication catastrophe in these cell lines. Following treatment with vehicle, no difference in mean nuclear γH2AX (Ser319) intensity was observed in *C16orf72Δ.*1 cells relative to wild type U2OS cells ($p = 0.7551$). Following exposure to 200 μM HU for 24 h, no difference in mean nuclear γH2AX (Ser319) intensity was observed in *C16orf72Δ.*1 cells relative to wild type U2OS cells ($p = 0.3076$). However, after treatment with 200 μM HU for 24 h followed by recovery in fresh media for 6 h, a ~1.5-fold increase in mean nuclear γH2AX (Ser319) intensity was observed in *C16orf72Δ.*1 cells relative to wild type U2OS cells (0.0267). Therefore, the following conclusions can be drawn from these data. Firstly, C16orf72 may not participate in the DNA replication stress response to prevent the accumulation of stalled and/or collapsed forks under conditions of endogenous replication stress. Secondly, C16orf72 may not participate in the DNA replication stress response to prevent the accumulation of stalled and/or collapsed forks under conditions of prolonged exposure to mild exogenous replication stress (24 h, 200 μM HU). Thirdly, C16orf72 may participate in the DNA replication stress response to prevent the accumulation of stalled and/or collapsed forks following removal of prolonged, mild exogenous replication stress (24 h, 200 μM HU).

a


Mean Nuclear γH2AX intensity (A.U)
70000
60000
50000
40000
30000
20000
10000
0
983.9
1001.3
2155.0
2203.4
1331.0
1253.4
U2OS
KO.1
U2OS
KO.1
U2OS
KO.1
Vehicle
24h HU
24h HU + 6h recovery

b

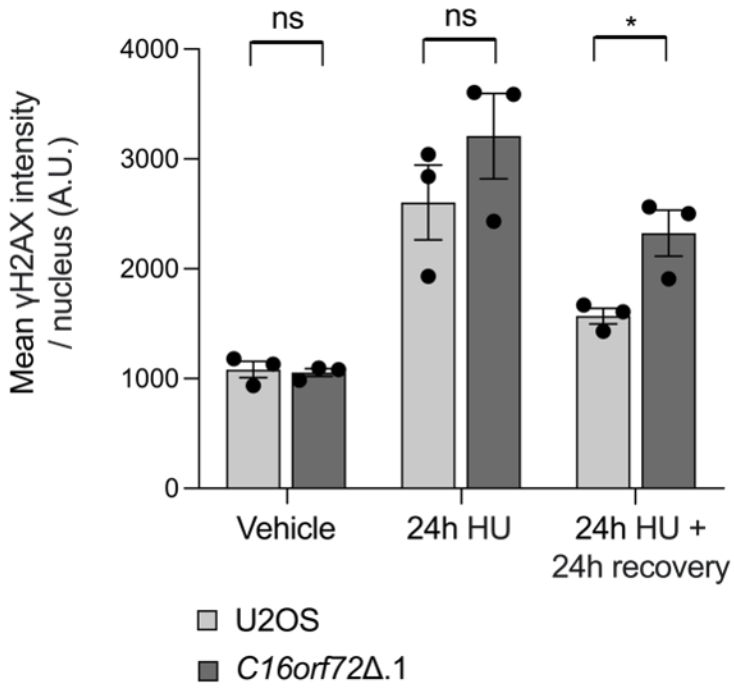

Mean γH2AX intensity / nucleus (A.U.)
4000
3000
2000
1000
0
ns
ns
*
Vehicle
24h HU
24h HU + 24h recovery
U2OS
C16orf72Δ.1

Figure 5.8: QIBC analysis of recovery of γH2AX levels in *C16orf72Δ* cells following removal of HU. (a) U2OS, *C16orf72Δ*.1 (KO.1) cells were treated with 200 μM HU for 24h, or with 200 μM HU for 24h and recovered in fresh growth media for 6 h, before fixation. Mean nuclear γH2AX (S319) fluorescence was analysed by QIBC. The data points (black dots) within each condition of the scatter plot represent mean nuclear γH2AX fluorescence, amalgamated from three independent biological replicates. Within each biological replicate, at least 1500 cells were analysed per condition. For each condition, the red line represents the median, and the lower and upper whiskers represent the 25th and 75th percentile, respectively. **(b)** The data points within each condition represent the mean nuclear γH2AX fluorescence per biological repeat. Error bars represent the SEM. Statistical significance was evaluated by unpaired t-tests. ns, not significant; * $p < 0.05$.

5.3 Discussion

In this chapter, I investigated the potential involvement of C16orf72 in the DNA replication stress response through a number of different experimental approaches. Firstly, I demonstrated via western blot that FLAG-HA-C16orf72 is recruited to chromatin in response to exogenous replication stress (Figure 2 a). This supports the notion that C16orf72 may participate in the DNA replication stress response. Indeed, numerous DNA replication stress response proteins such as BRCA1, BRCA2, HUWE1, SLFN11 and DOCK7 are also recruited to chromatin under the same conditions (Choe et al., 2016; Gao et al., 2021; Lossaint et al., 2013; Murai et al., 2018; Schlacher et al., 2012; Schubert et al., 2017). However, given that FLAG-HA-C16orf72 was not detected in chromatin by western blot in unperturbed FLAG-HA-C16orf72-

overexpressing wild type U2OS cells, but low levels of FLAG-HA-C16orf72 were detected in chromatin in unperturbed FLAG-HA-C16orf72-overexpressing *C16orf72Δ*.2 cells, it is not clear whether C16orf72 is recruited to chromatin under these conditions (Figure 2 b). I have also shown that the recruitment of FLAG-HA-C16orf72 to chromatin in response to exogenous replication stress is not disrupted by ATRi treatment (Figure 2 b). This suggests that the recruitment of FLAG-HA-C16orf72 to chromatin in response to exogenous replication stress is ATR-independent. Given that the ssDNA-binding replication stress response factor RPA is recruited to chromatin independently of ATR, this finding neither support nor refutes the notion that C16orf72 may participate in the DNA replication stress response (Blackwell & Borowiec, 1994; Toledo et al., 2013). Intriguingly, FLAG-HA-C16orf72 was also recruited to chromatin in response to ATRi treatment alone (Figure 2 b). Given that ATRi treatment can induce ssDNA accumulation, which can arise due to replication fork stalling, perhaps FLAG-HA-C16or72 is recruited to chromatin in response to ATRi-induced replication stress (Buisson et al., 2015; Zeman & Cimprich, 2014). However, further studies on the cellular effects of ATRi on replication fork progression are required to confirm whether this is the case. A recent publication reported that two isoforms of C16orf72 are expressed by cells: a long, higher molecular weight isoform and a short, lower molecular weight isoform (Amici et al., 2022). However, I observed that overexpressed FLAG-HA-C16orf72 was detected as a single product in chromatin extracts and whole cell extracts via western blot (Figure 2 a and b). This is because the FLAG-HA-C16orf72 overexpressing cell lines were expressing C16orf72 complementary DNA, which only produces the unspliced, long isoform. It is possible that FLAG-HA-C16orf72 is recruited stalled/damaged replication forks in chromatin. Yet surprisingly, mass spectrometry-based isolation of proteins on nascent DNA

(iPOND) studies have not identified C16orf72 as a protein that is present at replication forks under conditions of HU-induced replication stress (Dungrawala et al., 2015; Nakamura et al., 2021; Sirbu et al., 2011). However, perhaps C16orf72 is present at stalled replication forks, but its cellular abundance is too low to be detected by iPOND (Han et al., 2008). If this is the case, then the proximity ligation assay (PLA)-based in situ protein interactions at nascent and stalled replication forks (SIRF) technique may be able to detect interactions of C16orf72 with HU-induced stalled replication forks (Roy, Luzwick, et al., 2018).

Through QIBC analysis, I observed there was no significant difference in the percentage of G_1-, S- and G_2/M-phase *C16orf72Δ*.1 and *C16orf72Δ*.2 cells relative to wild type U2OS cells (Figure 1 c). This suggests that loss of C16orf72 does not alter the cell cycle distribution of unperturbed U2OS cells. Since both wild type cells and cells lacking DNA replication stress response factors (e.g. BOD1L) can exhibit this phenotype, this observation neither supports nor negates the notion that C16orf72 may participate in the DNA replication stress response (Higgs et al., 2015).

Through QIBC analysis, I determined that following vehicle treatment, *C16orf72Δ*.2 cells, but not *C16orf72Δ*.1 cells exhibited an increase in mean G_1-phase 53BP1 nuclear bodies per nucleus (Figure 3 b). Furthermore, following treatment with 0.2 μM APH for 24 h, *C16orf72Δ*.1 cells, but not *C16orf72Δ*.2 cells exhibited an increase in mean G_1-phase 53BP1 bodies per nucleus relative to wild type U2OS cells (Figure 3 b). Exactly why inconsistent phenotypes were observed between clones under these conditions is not clear. Therefore, it is not clear from these data whether C16orf72 participates in the DNA replication stress response.

Following vehicle treatment, increased γH2AX (Ser319) levels were observed in *C16orf72Δ*.2 cells relative to wild type U2OS, but no notable difference in γH2AX (Ser319) levels was observed in *C16orf72Δ*.1 cells relative to wild type U2OS cells, when analysed by western blot (Figure 4). However, under the same conditions *C16orf72Δ*.1 cells and *C16orf72Δ*.2 cells had the same mean nuclear γH2AX (Ser319) intensity relative to wild type U2OS cells, when analysed by QIBC (Figure 5 b). When analysed by western blot, after treatment with 2 mM HU for 2 h, *C16orf72Δ*.1 and *C16orf72Δ*.2 cells exhibited an increase in γH2AX (Ser319) levels relative to wild type U2OS cells (Figure 4). However, QIBC analysis at the same HU timepoint showed that *C16orf72Δ*.1 cells and *C16orf72Δ*.2 cells exhibited the same mean nuclear γH2AX (Ser319) intensity relative to wild type U2OS cells (Figure 5 b). When analysed by western blot, following exposure to 2 mM HU for 8 h, no difference in γH2AX (Ser 319) levels was observed in *C16orf72Δ*.1 cells relative to wild type U2OS cells (Figure 4). Yet, when analysed by western blot, an increase in γH2AX levels was observed in *C16orf72Δ*.2 cells relative to wild type U2OS cells (Figure 4). However, QIBC analysis at the same HU timepoint showed that *C16orf72Δ*.1 cells and *C16orf72Δ*.2 cells exhibited the same mean nuclear γH2AX (Ser319) intensity relative to wild type U2OS cells (Figure 5 b). Following 2 mM HU treatment for 24 h, an increase in γH2AX (Ser319) levels were observed in *C16orf72Δ*.1 and *C16orf72Δ*.2 cells relative to wild type U2OS cells, when analysed by western blot (Figure 4). Consistent with these findings, under the same conditions, an increase in mean nuclear γH2AX (Ser319) intensity was observed in *C16orf72Δ*.1 and *C16orf72Δ*.2 cells relative to wild type U2OS cells, when analysed by QIBC (Figure 5 b). A possible explanation for the observed differences in the western blot and QIBC analyses is that the western blot

timecourse was only performed once and provided semi-quantitative data, whereas three independent biological replicates of the QIBC timecourse were performed, which provided quantitative data. Therefore, given the increased reliability of the QIBC analysis compared to the western blot analysis, conclusions from this timecourse will be drawn from the QIBC data and are as follows: Firstly, C16orf72 may not participate in the DNA replication stress response to prevent the accumulation of stalled and/or collapsed replication forks under conditions of endogenous replication stress (Gagou et al., 2010; Sirbu et al., 2011). However, a recent publication claimed that siRNA-mediated C16orf72 depletion in unperturbed U2OS cells results in elevated γH2AX (Ser319) levels (Amici et al., 2022). Why this phenotype in was not observed in the *C16orf72Δ*.1 and *C16orf72Δ*.2 cells under these conditions is not clear. Secondly, C16orf72 does not participate in the DNA replication stress response to prevent the accumulation of stalled and/or collapsed replication forks under conditions of short (2 h) and intermediate (8 h) exposure to exogenous replication stress (Gagou et al., 2010; Sirbu et al., 2011). Finally, C16orf72 may participate in the DNA replication stress response to prevent the accumulation of stalled and/or collapsed replication forks under conditions of prolonged (24 h) exposure to exogenous replication stress (Gagou et al., 2010; Sirbu et al., 2011).

Interestingly, following treatment with 2 mM HU for 24 h, an increase in the percentage of RPA70-γH2AX-positive cells – an indicator of cells undergoing replication catastrophe – was observed in two independent *C16orf72Δ* clones relative to wild type U2OS cells (Toledo et al., 2013) (Figure 7 b). These data suggest that C16orf72 may participate in the DNA damage response by limiting replication catastrophe under conditions of prolonged (24 h) exposure to exogenous replication stress (Toledo et al.,

2013). However, exactly how C16orf72 may execute this function remains unclear. ATR is thought to participate in the DNA replication stress response to repress atypical new origin firing under conditions of exogenous replication stress in order to limit replication catastrophe (Toledo et al., 2013). Therefore, perhaps C16orf72 may also contribute to the suppression of new origin firing under similar conditions (Toledo et al., 2013). In order to determine whether this is the case, a DNA fibre assay should be performed (Nieminuszczy et al., 2016).

When analysed by QIBC, following treatment with vehicle, there was no observed difference in mean nuclear RPA70 intensity in *C16orf72Δ*.1 and *C16orf72Δ*.2 cells relative to wild type U2OS cells (Figure 6). This suggests that C16orf72 may not participate in the DNA replication stress response to prevent the accumulation of ssDNA under conditions of endogenous replication stress (Bass et al., 2016; Raderschall et al., 1999). Following treatment with 2 mM HU for 2 h, there was no observed difference in mean nuclear RPA70 intensity in *C16orf72Δ*.1 cells and *C16orf72Δ*.2 cells relative to wild type U2OS cells, when analysed by QIBC (Figure 6). This suggests that C16orf72 may not participate in the DNA replication stress response to prevent the accumulation of ssDNA under under these conditions (Bass et al., 2016; Raderschall et al., 1999). Following exposure to 2 mM HU for 8 h, QIBC analysis did not reveal a difference in mean nuclear RPA70 intensity in *C16orf72Δ*.1 cells and *C16orf72Δ*.2 cells relative to wild type U2OS cells (Figure 6). Therefore, these data suggest that C16orf72 may not participate in the DNA replication stress response to prevent the accumulation of ssDNA under these conditions (Bass et al., 2016; Raderschall et al., 1999). Following treatment with 2 mM HU for 24 h, when analysed by QIBC, wild type *C16orf72Δ*.1 and *C16orf72Δ*.2 cells displayed the same

mean nuclear RPA70 intensity relative to wild type U2OS cells, which suggests that C16orf72 may not participate in the DNA replication stress response to prevent the accumulation of ssDNA under conditions of prolonged (24 h) exposure to exogenous replication stress (Bass et al., 2016; Raderschall et al., 1999) (Figure 6). This is a surprising observation, given that under the same conditions, a higher percentage of *C16orf72Δ* cells undergo replication catastrophe relative to wild type U2OS cells (Figure 7 b). A feasible explanation for these inconsistent findings is that under these conditions, *C16orf72Δ* cells only exhibit a small increase in the percentage of cells undergoing replication catastrophe relative to wild type U2OS cells, which does not lead to a detectable difference in ssDNA accumulation when analysed via QIBC. A native 5-bromo-2'-deoxyuridine (BrdU) labelling assay should be performed to determine whether under conditions of prolonged (24 h) exogenous replication stress, *C16orf72Δ* cells accumulate more ssDNA relative to wild type U2OS cells (Kilgas et al., 2021).

Following treatment with 2 mM HU for 24 h, both *C16orf72Δ* clones exhibited increased pDNA-PK_{CS} (Ser2056) levels relative to wild type U2OS cells, suggesting that C16orf72 may participate in the DNA replication stress response to prevent accumulation of stalled and/or broken replication forks under conditions of prolonged (24 h) exogenous replication stress (Britton et al., 2020; Roy et al., 2015; Ying et al., 2016) (Figure 4). Given that wild type U2OS and *C16orf72Δ* cells exhibited replication catastrophe when subjected to these conditions, the high levels of pDNA-PK_{CS} (Ser2056) that are observed in all of these cell lines may suggest that following nuclear-wide replication fork breakage, cells still attempt to repair the broken forks via c-NHEJ (Britton et al., 2020) (Figures 4 and 7 b). If this is found to be the case, this

finding would challenge the notion that all replication forks that break as a consequence of replication catastrophe are irreparable (Toledo et al., 2017; Toledo et al., 2013).

Following treatment with 2 mM HU for 2 h, *C16orf72Δ* cells displayed elevated pRPA (S4/S8) levels relative to wild type U2OS cells when analysed via western blot (Figure 4). This supports that notion that C16orf72 may participate in the DNA replication stress response to prevent the accumulation of broken replication forks under conditions of short (2 h) exogenous replication stress (Chanut et al., 2016; Toledo et al., 2013). However, it is not clear why, under the same conditions, similar median nuclear γH2AX (Ser319) intensity, rather than an expected increase in median nuclear γH2AX (Ser319) intensity, was observed in *C16orf72Δ*.1 and *C16orf72Δ*.2 cells relative to wild type U2OS cells, when analysed by QIBC (Higgs et al., 2015; Toledo et al., 2013) (Figure 5 a). After exposure to 2 mM HU for 8 h and 24 h, *C16orf72Δ* cells exhibited similar levels of pRPA (Ser4/Ser8) when analysed via western blot, relative to wild type U2OS cells, which, suggests that C16orf72 may not participate in the DNA replication stress response to prevent the accumulation of broken replication forks under conditions of intermediate (8 h) and prolonged (24 h) exposure to exogenous replication stress (Chanut et al., 2016; Toledo et al., 2013) (Figure 4). However, this is a surprising observation given that a greater percentage of *C16orf72Δ* cells undergo replication catastrophe in response to 2 mM HU treatment for 24 h, relative to wild type U2OS cells (Toledo et al., 2013) (Figure 7 b). A plausible explanation for these contradictory findings is that following exposure to 2 mM HU for 24 h, loss of C16orf72 only results in a slight increase in the percentage of cells undergoing replication catastrophe relative to wild type U2OS cells, and therefore differences in the

accumulation of broken replication forks may not be detectable under these conditions in *C16orf72Δ* cells relative to wild type U2OS cells, when pRPA (Ser4/Ser8) is analysed by western blot (Chanut et al., 2016; Toledo et al., 2013). To confirm whether an increase in fork breakage occurs in *C16orf72Δ* cells relative to wild type U2OS cell following exposure to 2 mM HU for 2 and 24 h, a PFGE assay should be performed (Saintigny et al., 2001).

Following exposure to 200 μM HU for 24 h, a difference in mean nuclear γH2AX (Ser319) intensity was not detected in *C16orf72Δ*.1 cells relative to wild type U2OS cells (Figure 8 b). This suggests that C16orf72 may not participate in the DNA replication stress response to prevent the accumulation of stalled and/or collapsed forks under conditions of prolonged exposure to mild replication stress (24 h HU, 200 μM) (Gagou et al., 2010; Sirbu et al., 2011). It is important to note that when individual cell data is analysed from this experiment, upon an initial glance, it appears as if an increase in mean nuclear γH2AX (Ser319) intensity may be apparent in *C16orf72Δ*.1 cells relative to wild type U2OS cells (Figure 8 a). However, the range of mean nuclear γH2AX (Ser319) intensity is the same across both cell lines, and any misinterpretation of the data is due to more cells being analysed from *C16orf72Δ*.1 cells compared to wild type U2OS cells under these conditions. 6 h post-removal of 200 μM 24h HU treatment, an increase in mean nuclear γH2AX (S319) intensity was observed in *C16orf72Δ*.1 cells relative to wild type U2OS cells (Figure 8 b). This suggests that C16orf72 may function in the DNA replication stress response to prevent the accumulation of stalled and/or collapsed forks following removal of prolonged, mild replication stress (24 h HU, 200 μM) (Gagou et al., 2010; Sirbu et al., 2011). Therefore, these findings also indicate that C16orf72 may participate in the DNA replication stress

response to restart stalled forks following removal of prolonged, mild replication stress (24 h HU, 200 μM), which could be confirmed by DNA fibre analysis in the future (Gagou et al., 2010; Nieminuszczy et al., 2016; Sirbu et al., 2011; Zeman & Cimprich, 2014). Furthermore, these observations suggest that C16orf72 may participate in the DNA replication stress response to repair collapsed forks following removal of prolonged, mild replication stress (24 h HU, 200 μM), which could be confirmed with a GFP-based BIR reporter (Costantino et al., 2014; Sirbu et al., 2011).

From the data presented in this chapter, it was not possible to identify the DNA replication stress response pathway(s) that C16orf72 functions within. When subjected to 2 mM HU for 2, 8 and 24h, *C16orf72Δ*.1 cells exhibited the same levels of pCHK1 (Ser317) relative to wild type U2OS cells, when analysed via western blot (Figure 4). However, following exposure to 2 mM HU for 2, 8 and 24 h, *C16orf72Δ*.2 exhibited lower pCHK1 (Ser317) levels relative to wild type U2OS cells when analysed via western blot, although this is likely due to the lower abundance of total CHK1 that was observed in *C16orf72Δ*.2 cells (Figure 4). The cause of the different levels of total CHK1 present in the *C16orf72Δ*.1 and *C16orf72Δ*.2 clones is not clear, but it is possible that these differences may have arisen due to clonal variation. Therefore, it is not clear from these data whether C16orf72 functions within the ATR pathway of the DNA replication stress response (Zhao & Piwnica-Worms, 2001). Intriguingly, in a recent set of publications, C16orf72 was found to reduce the stability of p53 in unperturbed cells and reduce p53 abundance in cells treated with the replication stress-inducing agent cyclophosphamide, which can induce interstrand crosslinks (Amici et al., 2022; Benslimane et al., 2021; Crook et al., 1986; Lü et al., 2022). By showing that telomerase-inhibited or telomerase-deficient cells are sensitive to

C16orf72 loss, Benslimane et al., 2021 argue that C16orf72 functions to moderate the p53-dependent induction of senescence when telomeres are severely shortened (Herbig et al., 2004). It has been hypothesised that oxidative DNA damage that arises due to a plethora of cellular operations can exacerbate telomere shortening (Panieri & Santoro, 2016; von Zglinicki, 2002). However, this notion has been challenged by the recent claim that DNA damage that is induced by oxidative stress can trigger senescence without shortening telomeres (Barnes et al., 2022). While repressing permanent exit from the cell cycle may theoretically increase the ability of cell to finish DNA replication during or following exposure to DNA replication stress, it is not clear how most non-cancerous somatic cell types, which lack telomere maintenance mechanisms, could overcome the end-replication problem when cells accrue critically short telomeres, or why subverting this response would be beneficial to non-cancerous cells (Hiyama & Hiyama, 2007; Levy et al., 1992). Further research is required to determine whether this new-found role of C16orf72 in regulating the p53 response to telomere shortening also implicates this protein in the DNA replication stress response. The C16orf72 yeast orthologue (YJR056C) interacts with the yeast orthologue of the human ubiquitin ligase HUWE1 (Tom1) in the absence of exogenous replication stress, as demonstrated by a mass spectrometry-based study (Sung et al., 2016; Zhong et al., 2005). Consistent with this finding, C16orf72 interacts with and is ubiquitinated by HUWE1 in unperturbed cells. In so doing, HUWE1 ubiquitinates C16orf72, which targets C16orf72 for proteasomal degradation (Amici et al., 2022). HUWE1 localises DNA replication stress response factors to stalled forks and stimulates fork restart (Choe et al., 2016). Furthermore, an interaction between C16orf72 and the deubiquitinating enzyme Ubiquitin Specific Peptidate 7 (USP7) has been demonstrated via co-immunoprecipitation (Li et al., 2002; Lü et al., 2022).

Additionally, USP7 and HUWE1 interact to modulate p53 stability in response to DNA damage (Khoronenkova et al., 2013; Chen et al., 2005). USP7 also promotes localisation of the TLS DNA polymerase η to sites of fork stalling (Zlatanou et al., 2016). A recent study showed that p53 represses ill-defined and mutagenic RAD52- and Polθ-dependent stalled fork restart/collapsed fork repair pathways following removal of mild exogenous replication stress. In so doing, p53 is thought to stimulate MRE11-dependent restart of stalled forks/repair of collapsed forks (Bryant et al., 2009; Roy, Tomaszowski, et al., 2018; Trenz et al., 2006). In light of recent findings, it is possible that the RAD52- and Polθ-dependent pathways that are repressed by p53 may be the collapsed fork repair pathways BIR and alt-NHEJ, respectively (Llorens-Agost et al., 2021; Sotiriou et al., 2016). Recently, p53 and Polı have been shown to collaborate in a homology-directed DDT pathway that functions to overcome challenging lesions faced by progressing replication forks (Biber et al., 2020; Hampp et al., 2016). Given that HUWE1, USP7 and C16orf72 regulate p53 stability; HUWE1, USP7 and p53 are implicated in the DNA replication stress response; and C16orf72 interacts with or regulates these proteins, perhaps C16orf72 participates in a DNA replication stress response pathway that consists of these proteins. Co-immunoprecipitation should be performed to determine whether C16orf72 interacts with HUWE1, USP7 and p53 under conditions of exogenous replication stress.

Interestingly, through a transcriptomics approach, Amici et al. 2022 demonstrated that C16orf72 down-regulates the transcription of genes involved in the DNA replication stress response under conditions of exogenous replication stress. However, it is not clear from these data whether C16orf72 functions within the DNA replication stress response, as it is uncertain how down-regulation of DNA replication stress response

genes would promote complete DNA replication under these conditions. Furthermore, through a transcriptomic approach this research group also demonstrated that C16orf72 acts as a cellular nerve centre that modulates the transcriptional response to a multitude of cellular stressors (Amici et al., 2022).

In conclusion, in this chapter, as well as in the previous chapter, numerous pieces of evidence have been presented that support the notion that C16orf72 may function within the DNA replication stress response. Therefore, collectively, I propose that these findings demonstrate that C16orf72 is a novel DNA replication stress response factor. However, the precise molecular mechanisms of how C16orf72 functions within the DNA replication stress response remain to be elucidated and should be subject to investigation in future studies.

6. General Discussion

Previous work from the Lakin lab demonstrated that PARPi (olaparib) exposure results in the additional sensitisation of *PARP1ΔPARP2Δ* cells to base alkylating agent MMS. This raised the possibility that another PARP family member participates in the repair of MMS-induced DNA damage in cells that are deficient in PARP1 and PARP2 (Ronson, 2017). Therefore, in this thesis, I first aimed to reveal the identity of this PARP.

By following a chemical proteomics-based approach, it was not possible to determine any potential PARP candidates that may participate in the repair of MMS-induced DNA damage, as wild-type PARP1 and PARP2 was detected in the *PARP1ΔPARP2Δ* cell lysates (Médard et al., 2015). It is not clear why this was the case, but it is possible that these lysates were contaminated with wild-type cell lysates.

I also performed clonogenic survival assay-based PARP depletion screens in *PARP1ΔPARP2Δ* cells to identify the PARP in question. Overall, when evaluated by two-way ANOVA the key observations from the PARP depletion screens were as follows. Firstly, *PARP1ΔPARP2Δ* cells were not further sensitised to MMS following depletion of PARP6 or PARP14. Secondly, PARPi did not further sensitise *PARP1ΔPARP2Δ* cells to MMS following PARP6 or PARP14 depletion. Together, these findings suggest that either of these PARPs may be trapped to DNA by olaparib via a mechanism that is independent of their catalytic inhibition, which indicates that either of these PARPs may participate in the repair of MMS-induced DNA damage in *PARP1ΔPARP2Δ* cells (Murai et al., 2012; Ronson et al., 2018). However, given that this observation was reproduceable following PARP6 depletion but not PARP14

depletion in these cells, it is more likely that PARP6, rather than PARP14 performs this role in response to MMS-induced DNA damage. It is not clear how either of these PARPs may be trapped to DNA by olaparib, but it is conceivable that olaparib may bind to PARP6 or PARP14 in a manner that does not inhibit catalysis but induces allosteric changes that mediate trapping. Indeed, recent work has revealed a mode of PARPi-induced PARP2 trapping that does not require catalytic inhibition of PARP2 (Lin et al., 2022). PARP6 regulates mitosic cell division, the development of neurones, and the Wnt signalling pathway (Huang et al., 2016; Tang et al., 2020; Wang et al., 2018; Vermehren-Schmaedick et al., 2021; Tuncel et al., 2012). PARP14 regulates HR; the nucleolytic processing of reversed replication forks; and also performs other cellular roles (Dhoonmoon et al., 2022; Nicolae et al., 2015). However, it remains unclear precisely how PARP6 or PARP14 may participate in the repair of MMS-induced DNA damage in cells lacking PARP1 and PARP2. As noted in section 3.3, a number of key experimental approaches could be taken to explore the potential role of PARP6 or PARP14 in the repair of this DNA damage in more mechanistic detail.

It is important to note that following evaluation of the PARP-depletion screens by two-way ANOVA with Tukey's post hoc analysis, it was not possible determine whether these conclusions still apply, as the above observations were not statistically significant in any of the experiments. However, this may have occurred because two-way ANOVA with Tukey's post hoc analysis is a more conservative approach of statistical analysis compared to two-way ANOVA. In order to determine whether these conclusions still apply when evaluated by two-way ANOVA with Tukey's post hoc analysis, it is likely that statistical power of these experiments must be increased. A possible method of achieving this is by carrying out additional biological repeats of

these assays. Therefore, while evaluation of the PARP depletion screens by two-way ANOVA suggest that PARP6 or PARP14 may participate in the repair of MMS-induced DNA damage in cells lacking PARP1 and PARP2, further investigation is required to confirm that these PARPs perform this function when evaluated by two-way ANOVA with Tukey's post hoc analysis.

The second aim of this thesis was to identify novel DDR factors by identifying genes that are synthetic lethal with combined loss of PARP1 and PARP2 (Nijman, 2011; Ashworth & Lord, 2018). Through a genome-wide CRISPR dropout screen, we identified 10 genes (*DNAJC9*, *RNASEH2A*, *NVL*, *SARS*, *RPL36*, *FANCF*, *MRPS3*4, *ABBC6*, *PTBP1* and *C16orf7*2) which when disrupted, reduced the viability of *PARP1ΔPARP2Δ* cells, but not wild type U2OS cells, and were therefore synthetic lethal with combined loss of PARP1 and PARP2. Of these genes*, RNASEH2A* and *FANCF* were known DDR factors (Hiller et al., 2012; Walden & Deans, 2014). However, we chose to study the potential role of C16orf72 in the DDR, as it was largely unstudied when this screen was performed. In light of this, the synthetic lethal interaction between C16orf72 and combined loss of PARP1 and PARP2, was validated with 3 independent C16orf72-targeting siRNAs as well as well as with C16orf72-targeting SMARTpool siRNA. Additionally, while not subject to further investigation in this thesis, the other 7 genes may also represent novel DDR genes, but additional work is required to confirm the role of these proteins in the DDR.

I also investigated whether this synthetic lethal interaction is dependent on individual loss of PARP1 or PARP2 or combined loss of these PARPs. C16orf72 depletion did not significantly reduce the viability of *PARP1Δ* or *PARP2Δ* cells, but significantly

reduced the viability of *PARP1ΔPARP2Δ* cells. Therefore, both PARP1 and PARP2 may be the key determinants of this synthetic lethal interaction. This is in contrast to the synthetic lethal interaction between PARP1 loss and *BRCA2*-deficiency (Bryant et al., 2005). Indeed, as far as I am aware, this appears to be the first example of a synthetic lethal interaction in which both PARP1 and PARP2 may be key determinants. However, the mechanism by which C16orf72 loss induces selective-killing in *PARP1ΔPARP2Δ* and not wild type cells is yet to be determined.

The third aim of this thesis was to learn more about the cellular function(s) of C16orf72 and about other characteristics of this protein. A variety of experimental approaches have been used to study proteins involved in the DNA replication stress response (Balmus et al., 2019; Britton et al., 2020; Chanut et al., 2016; Choe et al., 2016; Daza-Martin et al., 2019; Gagou et al., 2010; Higgs et al., 2015; Hustedt et al., 2019; Kim et al., 2019, Kosar et al., 2021; Kwok et al., 2016; Lee et al., 2016; Nieminuszczy et al., 2019 Olivieri et al., 2020; Roy et al., 2015; Schwab et al., 2013; Sirbu et al., 2011; Sy et al., 2011; Toledo et al., 2013; Wang et al., 2019; Xu et al., 2010; Ying et al., 2016). Through a variety of experimental approaches, I made the following key observations: (1) *C16orf72Δ* cells were further sensitised to the replication-stress inducing agents HU and APH. This suggests that C16orf72 responds to DNA damage that is induced by these agents. Consistent with these sensitivity phenotypes, recent genome-wide CRISPR dropout screens in the literature have also revealed that loss of C16orf72 reduces the viability of cells exposed to HU and APH. (2) Under conditions of exogenous replication stress, C16orf72 was recruited to chromatin. (3) Under conditions of exogenous replication stress, *C16orf72Δ* cells exhibited increased levels of γH2AX (Ser139), pRPA (S4/S8) and pDNA-PK (Ser2056). This suggests that

C16orf72 prevents the accumulation of stalled and/or collapsed replication forks under these conditions. (4) Loss of C16orf72 resulted in the increased accumulation of RPA70-γH2AX-positive cells under conditions of prolonged exogenous replication stress (HU). This suggests that C16orf72 limits replication catastrophe under these conditions (Figure 1). While it is not clear how C16orf72 performs this function, it is conceivable that this protein may repress aberrant dormant origin firing under conditions of prolonged replication stress (HU) in a manner that is analogous to ATR. (5) Loss of C16orf72 resulted in increased levels of γH2AX (Ser139) following removal of prolonged, mild exogenous replication stress (HU). This suggests that C16orf72 prevents the accumulation of stalled and/or collapsed forks under these conditions. While it is not clear how C16orf72 performs this function, it is possible this protein may promote the restart of stalled forks or repair collapsed forks following removal of prolonged, mild replication stress. Together these observations demonstrate that C16orf72 is a novel DDR factor that functions in the DNA replication stress response.

I also considered whether C16orf72 functions in the ATR pathway of the DNA replication stress response. However, given that under conditions of exogenous replication stress (HU), reduced pCHK1 (S317) levels were observed in one, but not both *C16orf72Δ* clones, it was not possible to determine whether C16orf72 functions in this pathway (Zhao & Piwnica-Worms, 2001). Yet, recent studies have revealed that in unperturbed conditions, C16orf72 interacts with HUWE1 and USP7 (Amici et al., 2022; Benslimane et al., 2021; Lü et al., 2022). Additionally, C16orf72, HUWE1 and USP7 function to modulate p53 stability under a range of cellular conditions (Chen et al., 2005; Khoronenkova & Dianov, 2013; Lü et al., 2022). Furthermore, HUWE1, USP7 and p53 have all been implicated in the DNA replication stress response (Biber

et al., 2020; Choe et al., 2016; Hampp et al., 2016; Roy et al., 2018; Zlatanou et al., 2016). While speculative, given these observations, perhaps C16orf72 participates in a DNA replication stress response pathway that consists of HUWE1, USP7 and p53 (Figure 1). As noted in section 5.3, a number of key experimental approaches could be taken to explore the role of C16orf72 within the DNA replication stress response in more mechanistic detail.

Bioinformatic analysis of C16orf72 also provided the following key insights: (1) C16orf72 contains motifs of unknown function that are highly conserved in the chordates and arthropods, and the protein structure of C16orf72 is highly conserved in the vertebrates. This underscores the importance of C16orf72 function within cells. (2) A domain of unknown function (DUF4588) spans the majority of the protein and the DUF4588 has a number of predicted ubiquitination and phosphorylation sites. While the importance of these PTMs in the regulation of C16orf72 function is not clear, perhaps HUWE1 regulates C16orf72 stability by ubiquitinating one of these predicted sites of ubiquitination. Indeed, a recent study confirmed that HUWE1-mediated polyubiquitination of C16orf72 reduces the stability of C16orf72, although it remains to be determined whether this polyubiquitination is applied at the ubiquitination sites revealed in my bioinformatic analysis (Amici et al., 2022).

In addition to the newly identified role for C16orf72 in the DNA replication stress response presented in this thesis, recent work has also revealed further cellular roles for C16orf72. Indeed, C16orf72 represses the p53-mediated initiation of senescence following severe shortening of telomeres (Benslimane et al., 2021). For this reason,

Benslimane et al., 2021 named C16orf72 Telomere Attrition and p53 Response 1 (TAPR1). Furthermore, C16orf72 acts to fine-tune gene transcription in response to a

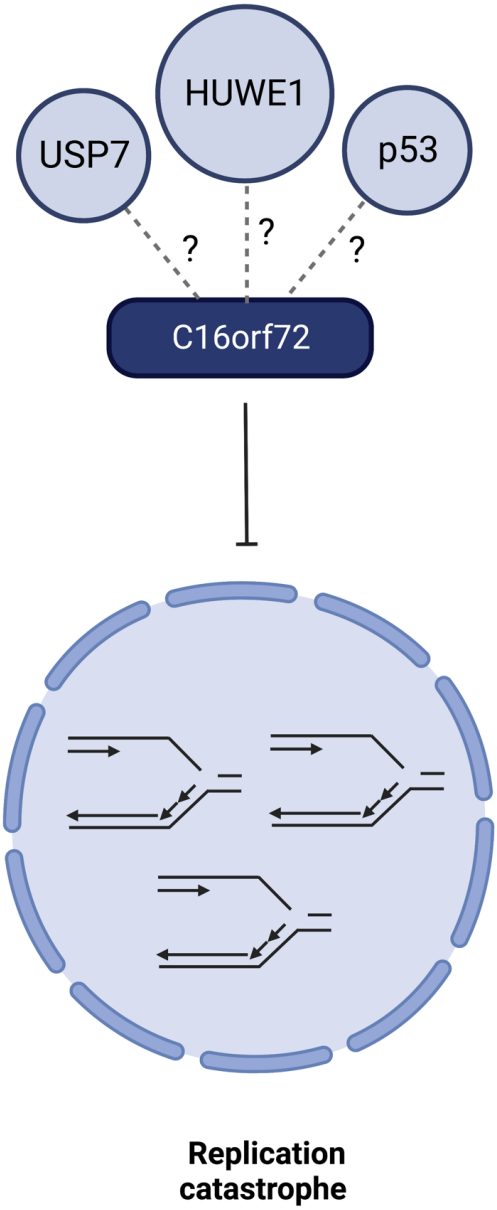


Figure 6.1: Proposed model of C16orf72 function within the DNA replication stress response. Under conditions of exogenous replication stress, C16orf72 performs a number of roles. Importantly, C16orf72 limits replication catastrophe under these conditions. The precise mechanism by which C16orf72 performs this role is yet

to be defined, although it may mediate this function by preventing aberrant firing of dormant replication origins under conditions of prolonged exposure to replication stress. The DNA replication stress response pathway that C16orf72 functions within is not clear, although it may participate in a pathway consisting of USP7, HUWE1 and p53. Produced with BioRender.

variety of stress conditions such as nutrient stress, hypoxia and DNA damage. Importantly, C16orf72 represses the transcription of DNA replication stress response genes in unperturbed conditions and under conditions of exogenous replication stress (Amici et al., 2022). Given that many of the observed functions of C16orf72 are dependent on a physical interaction between HUWE1 and C16orf72, Amici et al., 2022 named this protein HUWE1-associated protein modifying stress responses (HAPSTR1). Whether the findings from these publications support the notion that C16orf72 functions within the DNA replication stress response is yet to be determined as it is not clear how repressing the response to telomere shortening or repressing the transcription of genes in response to replication stress would promote the replication of DNA during or following replication stress.

In summary, two important findings are presented in this thesis. Firstly, I have determined that PARP6 or PARP14 may participate in the repair of MMS-induced DNA damage in cells that lack PARP1 and PARP2. Secondly, I have determined that C16orf72 is a novel DDR factor that participates in the DNA replication stress response. Overall, my work has provided new insight into PARP biology and the DNA replication stress response, which both represent critical facets of the DDR.

7. References

Aarts, M., Bajrami, I., Herrera-Abreu, M. T., Elliott, R., Brough, R., Ashworth, A., Lord, C. J., & Turner, N. C. (2015). Functional genetic screen identifies increased sensitivity to WEE1 inhibition in cells with defects in Fanconi Anaemia and HR pathways. Molecular Cancer Therapeutics, 14(4), 865–876.

Abbotts, R., & Wilson, D. M. (2017). Coordination of DNA Single Strand Break Repair. Free Radical Biology & Medicine, 107, 228–244.

Abplanalp, J., Leutert, M., Frugier, E., Nowak, K., Feurer, R., Kato, J., Kistemaker, H. V. A., Filippov, D. V., Moss, J., Caflisch, A., & Hottiger, M. O. (2017). Proteomic analyses identify ARH3 as a serine mono-ADP-ribosylhydrolase. Nature Communications, 8(1), Article 1. 1

Adar, S., Izhar, L., Hendel, A., Geacintov, N., & Livneh, Z. (2009). Repair of gaps opposite lesions by homologous recombination in mammalian cells. Nucleic Acids Research, 37(17), 5737–5748.

Aguiar, R. C. T., Takeyama, K., He, C., Kreinbrink, K., & Shipp, M. A. (2005). B-aggressive Lymphoma Family Proteins Have Unique Domains That Modulate Transcription and Exhibit Poly(ADP-ribose) Polymerase Activity. Journal of Biological Chemistry, 280(40), 33756–33765.

Ahel, I., Rass, U., El-Khamisy, S. F., Katyal, S., Clements, P. M., McKinnon, P. J., Caldecott, K. W., & West, S. C. (2006). The neurodegenerative disease protein aprataxin resolves abortive DNA ligation intermediates. Nature, 443(7112), Article 7112.

Ahel, D., Horejsí, Z., Wiechens, N., Polo, S. E., Garcia-Wilson, E., Ahel, I., Flynn, H., Skehel, M., West, S. C., Jackson, S. P., Owen-Hughes, T., & Boulton, S. J. (2009). Poly(ADP-ribose)-dependent regulation of DNA repair by the chromatin remodeling enzyme ALC1. *Science (New York, N.Y.)*, *325*(5945), 1240–1243.

Ahmad, A., Robinson, A. R., Duensing, A., van Drunen, E., Beverloo, H. B., Weisberg, D. B., Hasty, P., Hoeijmakers, J. H. J., & Niedernhofer, L. J. (2008). ERCC1-XPF endonuclease facilitates DNA double-strand break repair. Molecular and Cellular Biology, 28(16), 5082–5092.

Ahnesorg, P., Smith, P., & Jackson, S. P. (2006). XLF interacts with the XRCC4-DNA ligase IV complex to promote DNA nonhomologous end-joining. Cell, 124(2), 301–313.

Akamatsu, Y., & Jasin, M. (2010). Role for the Mammalian Swi5-Sfr1 Complex in DNA Strand Break Repair through Homologous Recombination. PLoS Genetics, 6(10), e1001160.

Alvarez-Gonzalez, R., & Althaus, F. R. (1989). Poly(ADP-ribose) catabolism in mammalian cells exposed to DNA-damaging agents. Mutation Research, 218(2), 67–74.

Amé, J.-C., Rolli, V., Schreiber, V., Niedergang, C., Apiou, F., Decker, P., Muller, S., Höger, T., Murcia, J. M., & de Murcia, G. (1999). PARP-2, A Novel Mammalian DNA Damage-dependent Poly(ADP-ribose) Polymerase*. Journal of Biological Chemistry, 274(25), 17860–17868.

Amé, J.-C., Spenlehauer, C., & de Murcia, G. (2004). The PARP superfamily. BioEssays, 26(8), 882–893.

Amici, D. R., Ansel, D. J., Metz, K. A., Smith, R. S., Phoumyvong, C. M., Gayatri, S., Chamera, T., Edwards, S. L., O'Hara, B. P., Srivastava, S., Brockway, S., Takagishi, S. R., Cho, B.-K., Goo, Y. A., Kelleher, N. L., Ben-Sahra, I., Foltz, D. R., Li, J., & Mendillo, M. L. (2022). C16orf72/HAPSTR1 is a molecular rheostat in an integrated network of stress response pathways. Proceedings of the National Academy of Sciences, 119(27), e2111262119.

Anand, R., Ranjha, L., Cannavo, E., & Cejka, P. (2016). Phosphorylated CtIP Functions as a Co-factor of the MRE11-RAD50-NBS1 Endonuclease in DNA End Resection. Molecular Cell, 64(5), 940–950.

Anantha, R. W., Vassin, V. M., & Borowiec, J. A. (2007). Sequential and Synergistic Modification of Human RPA Stimulates Chromosomal DNA Repair *. Journal of Biological Chemistry, 282(49), 35910–35923.

Anderson, P., & Kedersha, N. (2008). Stress granules: The Tao of RNA triage. Trends in Biochemical Sciences, 33(3), 141–150.

Arana, M. E., Seki, M., Wood, R. D., Rogozin, I. B., & Kunkel, T. A. (2008). Low-fidelity DNA synthesis by human DNA polymerase theta. Nucleic Acids Research, 36(11), 3847–3856.

Ashour, M. E., & Mosammaparast, N. (2021). Mechanisms of damage tolerance and repair during DNA replication. Nucleic Acids Research, 49(6), 3033–3047.

Ashworth, A., & Lord, C. J. (2018). Synthetic lethal therapies for cancer: What's next after PARP inhibitors? Nature Reviews Clinical Oncology, 15(9), Article 9.

Ashworth, A., Lord, C. J., & Reis-Filho, J. S. (2011). Genetic interactions in cancer progression and treatment. Cell, 145(1), 30–38.

Audebert, M., Salles, B., & Calsou, P. (2004). Involvement of poly(ADP-ribose) polymerase-1 and XRCC1/DNA ligase III in an alternative route for DNA double-strand breaks rejoining. The Journal of Biological Chemistry, 279(53), 55117–55126.

Aylon, Y., Liefshitz, B., & Kupiec, M. (2004). The CDK regulates repair of double-strand breaks by homologous recombination during the cell cycle. The EMBO Journal, 23(24), 4868–4875.

Baba, T. W., Giroir, B. P., & Humphries, E. H. (1985). Cell lines derived from avian lymphomas exhibit two distinct phenotypes. Virology, 144(1), 139–151.

Bai, G., Kermi, C., Stoy, H., Schiltz, C. J., Bacal, J., Zaino, A. M., Hadden, M. K., Eichman, B. F., Lopes, M., & Cimprich, K. A. (2020). HLTF Promotes Fork Reversal, Limiting Replication Stress Resistance and Preventing Multiple Mechanisms of Unrestrained DNA Synthesis. Molecular Cell, 78(6), 1237-1251.e7.

Bai, P., Canto, C., Brunyánszki, A., Huber, A., Szántó, M., Cen, Y., Yamamoto, H., Houten, S. M., Kiss, B., Oudart, H., Gergely, P., Menissier-de Murcia, J., Schreiber, V., Sauve, A. A., & Auwerx, J. (2011). PARP-2 regulates SIRT1 expression and whole-body energy expenditure. Cell Metabolism, 13(4), 450–460.

Bakkenist, C. J., & Kastan, M. B. (2003). DNA damage activates ATM through intermolecular autophosphorylation and dimer dissociation. Nature, 421(6922), Article 6922.

Balmus, G., Pilger, D., Coates, J., Demir, M., Sczaniecka-Clift, M., Barros, A. C., Woods, M., Fu, B., Yang, F., Chen, E., Ostermaier, M., Stankovic, T., Ponstingl, H., Herzog, M., Yusa, K., Martinez, F. M., Durant, S. T., Galanty, Y., Beli, P., … Jackson, S. P. (2019). ATM orchestrates the DNA-damage response to counter toxic non-homologous end-joining at broken replication forks. Nature Communications, 10(1), 87.

Baretić, D., Pollard, H. K., Fisher, D. I., Johnson, C. M., Santhanam, B., Truman, C. M., Kouba, T., Fersht, A. R., Phillips, C., & Williams, R. L. (2017). Structures of closed and open conformations of dimeric human ATM. *Science Advances*, *3*(5), e1700933.

Barkauskaite, E., Brassington, A., Tan, E. S., Warwicker, J., Dunstan, M. S., Banos, B., Lafite, P., Ahel, M., Mitchison, T. J., Ahel, I., & Leys, D. (2013). Visualization of poly(ADP-ribose) bound to PARG reveals inherent balance between exo- and endo-glycohydrolase activities. Nature Communications, 4(1), Article 1.

Barkauskaite, E., Jankevicius, G., & Ahel, I. (2015). Structures and Mechanisms of Enzymes Employed in the Synthesis and Degradation of PARP-Dependent Protein ADP-Ribosylation. Molecular Cell, 58(6), 935–946.

Barnes, R. P., de Rosa, M., Thosar, S. A., Detwiler, A. C., Roginskaya, V., Van Houten, B., Bruchez, M. P., Stewart-Ornstein, J., & Opresko, P. L. (2022). Telomeric 8-oxo-guanine drives rapid premature senescence in the absence of telomere shortening. Nature Structural & Molecular Biology, 29(7), Article 7.

Barrangou, R., Fremaux, C., Deveau, H., Richards, M., Boyaval, P., Moineau, S., Romero, D. A., & Horvath, P. (2007). CRISPR provides acquired resistance against viruses in prokaryotes. Science (New York, N.Y.), 315(5819), 1709–1712.

Bartlett, E., Bonfiglio, J. J., Prokhorova, E., Colby, T., Zobel, F., Ahel, I., & Matic, I. (2018). Interplay of Histone Marks with Serine ADP-Ribosylation. Cell Reports, 24(13), 3488-3502.e5.

Bass, T. E., Luzwick, J. W., Kavanaugh, G., Carroll, C., Dungrawala, H., Glick, G. G., Feldkamp, M. D., Putney, R., Chazin, W. J., & Cortez, D. (2016). ETAA1 acts at stalled replication forks to maintain genome integrity. Nature Cell Biology, 18(11), 1185–1195.

Baumann, C., Körner, R., Hofmann, K., & Nigg, E. A. (2007). PICH, a centromere-associated SNF2 family ATPase, is regulated by Plk1 and required for the spindle checkpoint. Cell, 128(1), 101–114.

Beck, C., Boehler, C., Guirouilh Barbat, J., Bonnet, M.-E., Illuzzi, G., Ronde, P., Gauthier, L. R., Magroun, N., Rajendran, A., Lopez, B. S., Scully, R., Boussin, F. D., Schreiber, V., & Dantzer, F. (2014). PARP3 affects the relative contribution of homologous recombination and nonhomologous end-joining pathways. Nucleic Acids Research, 42(9), 5616–5632.

Beck, H., Nähse-Kumpf, V., Larsen, M. S. Y., O'Hanlon, K. A., Patzke, S., Holmberg, C., Mejlvang, J., Groth, A., Nielsen, O., Syljuåsen, R. G., & Sørensen, C. S. (2012). Cyclin-dependent kinase suppression by WEE1 kinase protects the genome through control of replication initiation and nucleotide consumption. Molecular and Cellular Biology, 32(20), 4226–4236.

Bennett, L. G., Wilkie, A. M., Antonopoulou, E., Ceppi, I., Sanchez, A., Vernon, E. G., Gamble, A., Myers, K. N., Collis, S. J., Cejka, P., & Staples, C. J. (2020). MRNIP is a replication fork protection factor. Science Advances, 6(28), eaba5974.

Bennett, R. A., Wilson, D. M., Wong, D., & Demple, B. (1997). Interaction of human apurinic endonuclease and DNA polymerase beta in the base excision repair pathway. Proceedings of the National Academy of Sciences of the United States of America, 94(14), 7166–7169.

Bensimon, A., Schmidt, A., Ziv, Y., Elkon, R., Wang, S.-Y., Chen, D. J., Aebersold, R., & Shiloh, Y. (2010). ATM-dependent and -independent dynamics of the nuclear phosphoproteome after DNA damage. Science Signaling, 3(151), rs3.

Benslimane, Y., Sánchez-Osuna, M., Coulombe-Huntington, J., Bertomeu, T., Henry, D., Huard, C., Bonneil, É., Thibault, P., Tyers, M., & Harrington, L. (2021). A novel p53 regulator, C16ORF72/TAPR1, buffers against telomerase inhibition. Aging Cell, 20(4), e13331.

Bermudez, V. P., Lindsey-Boltz, L. A., Cesare, A. J., Maniwa, Y., Griffith, J. D., Hurwitz, J., & Sancar, A. (2003). Loading of the human 9-1-1 checkpoint complex onto DNA by the checkpoint clamp loader hRad17-replication factor C complex in vitro. Proceedings of the National Academy of Sciences of the United States of America, 100(4), 1633–1638.

Berti, M., Chaudhuri, A. R., Thangavel, S., Gomathinayagam, S., Kenig, S., Vujanovic, M., Odreman, F., Glatter, T., Graziano, S., Mendoza-Maldonado, R., Marino, F., Lucic, B., Biasin, V., Gstaiger, M., Aebersold, R., Sidorova, J. M., Jr, R. J. M., Lopes, M., & Vindigni, A. (2013). Human RECQ1 promotes restart of replication forks reversed by DNA topoisomerase I inhibition. Nature Structural & Molecular Biology, 20(3), 347–354.

Berti, M., Cortez, D., & Lopes, M. (2020). The plasticity of DNA replication forks in response to clinically relevant genotoxic stress. Nature Reviews Molecular Cell Biology, 21(10), Article 10.

Berti, M., Teloni, F., Mijic, S., Ursich, S., Fuchs, J., Palumbieri, M. D., Krietsch, J., Schmid, J. A., Garcin, E. B., Gon, S., Modesti, M., Altmeyer, M., & Lopes, M. (2020). Sequential role of RAD51 paralog complexes in replication fork remodeling and restart. Nature Communications, 11(1), Article 1.

Bétous, R., Couch, F. B., Mason, A. C., Eichman, B. F., Manosas, M., & Cortez, D. (2013). Substrate-selective repair and restart of replication forks by DNA translocases. Cell Reports, 3(6), 1958–1969.

Bétous, R., Goullet de Rugy, T., Pelegrini, A. L., Queille, S., de Villartay, J.-P., & Hoffmann, J.-S. (2018). DNA replication stress triggers rapid DNA replication fork breakage by Artemis and XPF. PLoS Genetics, 14(7), e1007541.

Bétous, R., Mason, A. C., Rambo, R. P., Bansbach, C. E., Badu-Nkansah, A., Sirbu, B. M., Eichman, B. F., & Cortez, D. (2012). SMARCAL1 catalyzes fork regression and Holliday junction migration to maintain genome stability during DNA replication. Genes & Development, 26(2), 151–162.

Bhat, K. P., Krishnamoorthy, A., Dungrawala, H., Garcin, E. B., Modesti, M., & Cortez, D. (2018). RADX Modulates RAD51 Activity to Control Replication Fork Protection. Cell Reports, 24(3), 538–545.

Bhattacharyya, S., Yu, H., Mim, C., & Matouschek, A. (2014). Regulated protein turnover: Snapshots of the proteasome in action. Nature Reviews. Molecular Cell Biology, 15(2), 122–133.

Bhowmick, R., Minocherhomji, S., & Hickson, I. D. (2016). RAD52 Facilitates Mitotic DNA Synthesis Following Replication Stress. Molecular Cell, 64(6), 1117–1126.

Bianchi, J., Rudd, S. G., Jozwiakowski, S. K., Bailey, L. J., Soura, V., Taylor, E., Stevanovic, I., Green, A. J., Stracker, T. H., Lindsay, H. D., & Doherty, A. J. (2013). PrimPol Bypasses UV Photoproducts during Eukaryotic Chromosomal DNA Replication. Molecular Cell, 52(4), 566–573.

Bianchi, V., Pontis, E., & Reichard, P. (1986). Changes of deoxyribonucleoside triphosphate pools induced by hydroxyurea and their relation to DNA synthesis. The Journal of Biological Chemistry, 261(34), 16037–16042.

Biber, S., Pospiech, H., Gottifredi, V., & Wiesmüller, L. (2020). Multiple biochemical properties of the p53 molecule contribute to activation of polymerase iota-dependent DNA damage tolerance. Nucleic Acids Research, 48(21), 12188–12203.

Bitler, B. G., Watson, Z. L., Wheeler, L. J., & Behbakht, K. (2017). PARP inhibitors: Clinical utility and possibilities of overcoming resistance. Gynecologic Oncology, 147(3), 695–704.

Blackford, A. N., & Jackson, S. P. (2017). ATM, ATR, and DNA-PK: The Trinity at the Heart of the DNA Damage Response. Molecular Cell, 66(6), 801–817.

Blackwell, L. J., & Borowiec, J. A. (1994). Human replication protein A binds single-stranded DNA in two distinct complexes. Molecular and Cellular Biology, 14(6), 3993–4001.

Blastyák, A., Hajdú, I., Unk, I., & Haracska, L. (2010). Role of double-stranded DNA translocase activity of human HLTF in replication of damaged DNA. Molecular and Cellular Biology, 30(3), 684–693.

Blastyák, A., Pintér, L., Unk, I., Prakash, L., Prakash, S., & Haracska, L. (2007). Yeast Rad5 protein required for postreplication repair has a DNA helicase activity specific for replication fork regression. Molecular Cell, 28(1), 167–175.

Bledau, A. S., Schmidt, K., Neumann, K., Hill, U., Ciotta, G., Gupta, A., Torres, D. C., Fu, J., Kranz, A., Stewart, A. F., & Anastassiadis, K. (2014). The H3K4 methyltransferase Setd1a is first required at the epiblast stage, whereas Setd1b becomes essential after gastrulation. Development (Cambridge, England), 141(5), 1022–1035.

Boboila, C., Oksenych, V., Gostissa, M., Wang, J. H., Zha, S., Zhang, Y., Chai, H., Lee, C.-S., Jankovic, M., Saez, L.-M. A., Nussenzweig, M. C., McKinnon, P. J., Alt, F. W., & Schwer, B. (2012). Robust chromosomal DNA repair via alternative end-joining in the absence of X-ray repair cross-

complementing protein 1 (XRCC1). Proceedings of the National Academy of Sciences of the United States of America, 109(7), 2473–2478.

Bodnar, A. G., Ouellette, M., Frolkis, M., Holt, S. E., Chiu, C.-P., Morin, G. B., Harley, C. B., Shay, J. W., Lichtsteiner, S., & Wright, W. E. (1998). Extension of Life-Span by Introduction of Telomerase into Normal Human Cells. Science, 279(5349), 349–352.

Bonfiglio, J. J., Fontana, P., Zhang, Q., Colby, T., Gibbs-Seymour, I., Atanassov, I., Bartlett, E., Zaja, R., Ahel, I., & Matic, I. (2017). Serine ADP-Ribosylation Depends on HPF1. Molecular Cell, 65(5), 932-940.e6.

Boulton, S. J., & Jackson, S. P. (1996). Saccharomyces cerevisiae Ku70 potentiates illegitimate DNA double-strand break repair and serves as a barrier to error-prone DNA repair pathways. The EMBO Journal, 15(18), 5093–5103.

Bouwman, P., Aly, A., Escandell, J. M., Pieterse, M., Bartkova, J., van der Gulden, H., Hiddingh, S., Thanasoula, M., Kulkarni, A., Yang, Q., Haffty, B. G., Tommiska, J., Blomqvist, C., Drapkin, R., Adams, D. J., Nevanlinna, H., Bartek, J., Tarsounas, M., Ganesan, S., & Jonkers, J. (2010). 53BP1 loss rescues BRCA1 deficiency and is associated with triple-negative and BRCA-mutated breast cancers. Nature Structural & Molecular Biology, 17(6), 688–695.

Breslin, C., Hornyak, P., Ridley, A., Rulten, S. L., Hanzlikova, H., Oliver, A. W., & Caldecott, K. W. (2015). The XRCC1 phosphate-binding pocket binds poly (ADP-ribose) and is required for XRCC1 function. Nucleic Acids Research, 43(14), 6934–6944.

Bridges, C. B. (1922). The Origin of Variations in Sexual and Sex-Limited Characters. The American Naturalist, 56(642), 51–63.

Britton, S., Chanut, P., Delteil, C., Barboule, N., Frit, P., & Calsou, P. (2020). ATM antagonizes NHEJ proteins assembly and DNA-ends synapsis at single-ended DNA double strand breaks. Nucleic Acids Research, 48(17), 9710–9723.

Britton, S., Coates, J., & Jackson, S. P. (2013). A new method for high-resolution imaging of Ku foci to decipher mechanisms of DNA double-strand break repair. The Journal of Cell Biology, 202(3), 579–595.

Broderick, R., Nieminuszczy, J., Baddock, H. T., Deshpande, R., Gileadi, O., Paull, T. T., McHugh, P. J., & Niedzwiedz, W. (2016). EXD2 promotes homologous recombination by facilitating DNA end resection. Nature Cell Biology, 18(3), 271–280.

Brouwer, I., Sitters, G., Candelli, A., Heerema, S. J., Heller, I., Melo de, A. J., Zhang, H., Normanno, D., Modesti, M., Peterman, E. J. G., & Wuite, G. J. L. (2016). Sliding sleeves of XRCC4–XLF bridge DNA and connect fragments of broken DNA. Nature, 535(7613), Article 7613.

Brown, J. S., Lukashchuk, N., Sczaniecka-Clift, M., Britton, S., le Sage, C., Calsou, P., Beli, P., Galanty, Y., & Jackson, S. P. (2015). Neddylation Promotes Ubiquitylation and Release of Ku from DNA-Damage Sites. Cell Reports, 11(5), 704–714.

Bryant, H. E., Petermann, E., Schultz, N., Jemth, A.-S., Loseva, O., Issaeva, N., Johansson, F., Fernandez, S., McGlynn, P., & Helleday, T. (2009). PARP is activated at stalled forks to mediate Mre11-dependent replication restart and recombination. The EMBO Journal, 28(17), 2601–2615.

Bryant, H. E., Schultz, N., Thomas, H. D., Parker, K. M., Flower, D., Lopez, E., Kyle, S., Meuth, M., Curtin, N. J., & Helleday, T. (2005). Specific killing of BRCA2-deficient tumours with inhibitors of poly(ADP-ribose) polymerase. Nature, 434(7035), 913–917.

Bugreev, D. V., Rossi, M. J., & Mazin, A. V. (2011). Cooperation of RAD51 and RAD54 in regression of a model replication fork. Nucleic Acids Research, 39(6), 2153–2164.

Buisson, R., Boisvert, J. L., Benes, C. H., & Zou, L. (2015). Distinct but Concerted Roles of ATR, DNA-PK, and Chk1 in Countering Replication Stress during S Phase. Molecular Cell, 59(6), 1011–1024.

Bunting, S. F., Callén, E., Wong, N., Chen, H.-T., Polato, F., Gunn, A., Bothmer, A., Feldhahn, N., Fernandez-Capetillo, O., Cao, L., Xu, X., Deng, C.-X., Finkel, T., Nussenzweig, M., Stark, J. M., & Nussenzweig, A. (2010). 53BP1 inhibits homologous recombination in Brca1-deficient cells by blocking resection of DNA breaks. Cell, 141(2), 243–254.

Burma, S., Chen, B. P., Murphy, M., Kurimasa, A., & Chen, D. J. (2001). ATM phosphorylates histone H2AX in response to DNA double-strand breaks. The Journal of Biological Chemistry, 276(45), 42462–42467.

Butler, A. J., & Ordahl, C. P. (1999). Poly(ADP-ribose) polymerase binds with transcription enhancer factor 1 to MCAT1 elements to regulate muscle-specific transcription. Molecular and Cellular Biology, 19(1), 296–306.

Byun, T. S., Pacek, M., Yee, M., Walter, J. C., & Cimprich, K. A. (2005). Functional uncoupling of MCM helicase and DNA polymerase activities activates the ATR-dependent checkpoint. Genes & Development, 19(9), 1040–1052.

Caldecott, K. W. (2008). Single-strand break repair and genetic disease. Nature Reviews. Genetics, 9(8), 619–631.

Caldecott, K. W. (2019). XRCC1 protein; Form and function. DNA Repair, 81, 102664.

Caldecott, K. W. (2020). Mammalian DNA base excision repair: Dancing in the moonlight. DNA Repair, 93, 102921.

Caldecott, K. W. (2022). DNA single-strand break repair and human genetic disease. Trends in Cell Biology, 32(9), 733–745.

Caldecott, K. W., Aoufouchi, S., Johnson, P., & Shall, S. (1996). XRCC1 polypeptide interacts with DNA polymerase beta and possibly poly (ADP-ribose) polymerase, and DNA ligase III is a novel molecular “nick-sensor” in vitro. Nucleic Acids Research, 24(22), 4387–4394.

Caldecott, K. W., McKeown, C. K., Tucker, J. D., Ljungquist, S., & Thompson, L. H. (1994). An interaction between the mammalian DNA repair protein XRCC1 and DNA ligase III. Molecular and Cellular Biology, 14(1), 68–76.

Cannan, W. J., & Pederson, D. S. (2016). Mechanisms and Consequences of Double-strand DNA Break Formation in Chromatin. Journal of Cellular Physiology, 231(1), 3–14.

Cao, X., Khitun, A., Luo, Y., Na, Z., Phoodokmai, T., Sappakhaw, K., Olatunji, E., Uttamapinant, C., & Slavoff, S. A. (2021). Alt-RPL36 downregulates the PI3K-AKT-mTOR signaling pathway by interacting with TMEM24. Nature Communications, 12(1), 508.

Carr, A. M., Paek, A. L., & Weinert, T. (2011). DNA replication: Failures and inverted fusions. Seminars in Cell & Developmental Biology, 22(8), 866–874.

Carreira, A., Hilario, J., Amitani, I., Baskin, R. J., Shivji, M. K. K., Venkitaraman, A. R., & Kowalczykowski, S. C. (2009). The BRC repeats of BRCA2 modulate the DNA-binding selectivity of RAD51. Cell, 136(6), 1032–1043.

Carvajal-Garcia, J., Cho, J.-E., Carvajal-Garcia, P., Feng, W., Wood, R. D., Sekelsky, J., Gupta, G. P., Roberts, S. A., & Ramsden, D. A. (2020). Mechanistic basis for microhomology identification and genome scarring by polymerase theta. Proceedings of the National Academy of Sciences, 117(15), 8476–8485.

Catara, G., Grimaldi, G., Schembri, L., Spano, D., Turacchio, G., Lo Monte, M., Beccari, A. R., Valente, C., & Corda, D. (2017). PARP1-produced poly-ADP-ribose causes the PARP12 translocation to stress granules and impairment of Golgi complex functions. Scientific Reports, 7(1), Article 1.

Ceccaldi, R., Liu, J. C., Amunugama, R., Hajdu, I., Primack, B., Petalcorin, M. I. R., O'Connor, K. W., Konstantinopoulos, P. A., Elledge, S. J., Boulton, S. J., Yusufzai, T., & D'Andrea, A. D. (2015). Homologous-recombination-deficient tumours are dependent on Polθ-mediated repair. Nature, 518(7538), 258–262.

Cejka, P., Cannavo, E., Polaczek, P., Masuda-Sasa, T., Pokharel, S., Campbell, J. L., & Kowalczykowski, S. C. (2010). DNA end resection by Dna2–Sgs1–RPA and its stimulation by Top3–Rmi1 and Mre11–Rad50–Xrs2. Nature, 467(7311), Article 7311.

Chambon, P., Weill, J. D., & Mandel, P. (1963). Nicotinamide mononucleotide activation of a new DNA-dependent polyadenylic acid synthesizing nuclear enzyme. Biochemical and Biophysical Research Communications, 11(1), 39–43.

Chang, P., Coughlin, M., & Mitchison, T. J. (2005). Tankyrase-1 polymerization of poly(ADP-ribose) is required for spindle structure and function. Nature Cell Biology, 7(11), 1133–1139.

Chang, W., Dynek, J. N., & Smith, S. (2005). NuMA is a major acceptor of poly(ADP-ribosyl)ation by tankyrase 1 in mitosis. The Biochemical Journal, 391(Pt 2), 177–184.

Chang, H. H. Y., Pannunzio, N. R., Adachi, N., & Lieber, M. R. (2017). Non-homologous DNA end joining and alternative pathways to double-strand break repair. *Nature Reviews Molecular Cell Biology*, *18*(8), Article 8.

Chanut, P., Britton, S., Coates, J., Jackson, S. P., & Calsou, P. (2016). Coordinated nuclease activities counteract Ku at single-ended DNA double-strand breaks. Nature Communications, 7, 12889.

Chaplin, A. K., Hardwick, S. W., Liang, S., Kefala Stavridi, A., Hnizda, A., Cooper, L. R., De Oliveira, T. M., Chirgadze, D. Y., & Blundell, T. L. (2021). Dimers of DNA-PK create a stage for DNA double-strand break repair. Nature Structural & Molecular Biology, 28(1), Article 1.

Chapman, J. R., & Jackson, S. P. (2008). Phospho-dependent interactions between NBS1 and MDC1 mediate chromatin retention of the MRN complex at sites of DNA damage. EMBO Reports, 9(8), 795–801.

Chapman, J. R., Taylor, M. R. G., & Boulton, S. J. (2012). Playing the End Game: DNA Double-Strand Break Repair Pathway Choice. Molecular Cell, 47(4), 497–510.

Chatterjee, N., & Walker, G. C. (2017). Mechanisms of DNA damage, repair and mutagenesis. Environmental and Molecular Mutagenesis, 58(5), 235–263.

Chaudhuri, A. R., & Nussenzweig, A. (2017). The multifaceted roles of PARP1 in DNA repair and chromatin remodelling. Nature Reviews Molecular Cell Biology, 18(10), 610.

Chellappan, S. P., Hiebert, S., Mudryj, M., Horowitz, J. M., & Nevins, J. R. (1991). The E2F transcription factor is a cellular target for the RB protein. Cell, 65(6), 1053–1061.

Chen, L., Nievera, C. J., Lee, A. Y.-L., & Wu, X. (2008). Cell Cycle-dependent Complex Formation of BRCA1·CtIP·MRN Is Important for DNA Double-strand Break Repair *. Journal of Biological Chemistry, 283(12), 7713–7720.

Chen, D., Kon, N., Li, M., Zhang, W., Qin, J., & Gu, W. (2005). ARF-BP1/Mule is a critical mediator of the ARF tumor suppressor. Cell, 121(7), 1071–1083.

Chen, Q., Kassab, M. A., Dantzer, F., & Yu, X. (2018). PARP2 mediates branched poly ADP-ribosylation in response to DNA damage. Nature Communications, 9(1), 3233.

Chen, X.-B., Melchionna, R., Denis, C.-M., Gaillard, P.-H. L., Blasina, A., Weyer, I. V. de, Boddy, M. N., Russell, P., Vialard, J., & McGowan, C. H. (2001). Human Mus81-Associated Endonuclease Cleaves Holliday Junctions In Vitro. Molecular Cell, 8(5), 1117–1127.

Cheng, C. H., & Kuchta, R. D. (1993). DNA polymerase epsilon: Aphidicolin inhibition and the relationship between polymerase and exonuclease activity. Biochemistry, 32(33), 8568–8574.

Chiang, Y. J., Hsiao, S. J., Yver, D., Cushman, S. W., Tessarollo, L., Smith, S., & Hodes, R. J. (2008). Tankyrase 1 and Tankyrase 2 Are Essential but Redundant for Mouse Embryonic Development. PLoS ONE, 3(7).

Cho, Y.-W., Hong, T., Hong, S., Guo, H., Yu, H., Kim, D., Guszczynski, T., Dressler, G. R., Copeland, T. D., Kalkum, M., & Ge, K. (2007). PTIP associates with MLL3- and MLL4-containing histone H3 lysine 4 methyltransferase complex. The Journal of Biological Chemistry, 282(28), 20395–20406.

Choe, K. N., Nicolae, C. M., Constantin, D., Imamura Kawasawa, Y., Delgado-Diaz, M. R., De, S., Freire, R., Smits, V. A., & Moldovan, G.-L. (2016). HUWE1 interacts with PCNA to alleviate replication stress. EMBO Reports, 17(6), 874–886.

Chon, H., Sparks, J. L., Rychlik, M., Nowotny, M., Burgers, P. M., Crouch, R. J., & Cerritelli, S. M. (2013). RNase H2 roles in genome integrity revealed by unlinking its activities. Nucleic Acids Research, 41(5), 3130–3143.

Chu, W. K., Payne, M. J., Beli, P., Hanada, K., Choudhary, C., & Hickson, I. D. (2015). FBH1 influences DNA replication fork stability and homologous recombination through ubiquitylation of RAD51. Nature Communications, 6(1), 5931.

Ciccia, A., Constantinou, A., & West, S. C. (2003). Identification and Characterization of the Human Mus81-Eme1 Endonuclease *. Journal of Biological Chemistry, 278(27), 25172–25178.

Ciccia, A., Nimonkar, A. V., Hu, Y., Hajdu, I., Achar, Y. J., Izhar, L., Petit, S. A., Adamson, B., Yoon, J. C., Kowalczykowski, S. C., Livingston, D. M., Haracska, L., & Elledge, S. J. (2012). Polyubiquitinated PCNA recruits the ZRANB3 translocase to maintain genomic integrity after replication stress. Molecular Cell, 47(3), 396–409.

Cimprich, K. A., Shin, T. B., Keith, C. T., & Schreiber, S. L. (1996). CDNA cloning and gene mapping of a candidate human cell cycle checkpoint protein. Proceedings of the National Academy of Sciences of the United States of America, 93(7), 2850–2855.

Cistulli, C., Lavrik, O. I., Prasad, R., Hou, E., & Wilson, S. H. (2004). AP endonuclease and poly(ADP-ribose) polymerase-1 interact with the same base excision repair intermediate. DNA Repair, 3(6), 581–591.

Clements, P. M., Breslin, C., Deeks, E. D., Byrd, P. J., Ju, L., Bieganowski, P., Brenner, C., Moreira, M.-C., Taylor, A. M. R., & Caldecott, K. W. (2004). The ataxia-oculomotor apraxia 1 gene product has a role distinct from ATM and interacts with the DNA strand break repair proteins XRCC1 and XRCC4. DNA Repair, 3(11), 1493–1502.

Collins, N., Poot, R. A., Kukimoto, I., García-Jiménez, C., Dellaire, G., & Varga-Weisz, P. D. (2002). An ACF1-ISWI chromatin-remodeling complex is required for DNA replication through heterochromatin. Nature Genetics, 32(4), 627–632.

Cong, K., & Cantor, S. B. (2022). Exploiting replication gaps for cancer therapy. Molecular Cell, 82(13), 2363–2369.

Cong, K., Peng, M., Kousholt, A. N., Lee, W. T. C., Lee, S., Nayak, S., Krais, J., VanderVere-Carozza, P. S., Pawelczak, K. S., Calvo, J., Panzarino, N. J., Turchi, J. J., Johnson, N., Jonkers, J., Rothenberg, E., & Cantor, S. B. (2021a). Replication gaps are a key determinant of PARP inhibitor synthetic lethality with BRCA deficiency. Molecular Cell, 81(15), 3128-3144.e7.

Cong, K., Peng, M., Kousholt, A. N., Lee, W. T. C., Lee, S., Nayak, S., Krais, J., VanderVere-Carozza, P. S., Pawelczak, K. S., Calvo, J., Panzarino, N. J., Turchi, J. J., Johnson, N., Jonkers, J., Rothenberg, E., & Cantor, S. B. (2021b). Replication gaps are a key determinant of PARP inhibitor synthetic lethality with BRCA deficiency. Molecular Cell, 81(15), 3128-3144.e7.

Cong, L., Ran, F. A., Cox, D., Lin, S., Barretto, R., Habib, N., Hsu, P. D., Wu, X., Jiang, W., Marraffini, L. A., & Zhang, F. (2013). Multiplex genome engineering using CRISPR/Cas systems. Science (New York, N.Y.), 339(6121), 819–823.

Conibear, A. C. (2020). Deciphering protein post-translational modifications using chemical biology tools. Nature Reviews Chemistry, 4(12), Article 12.

Cortez, D. (2015). Preventing Replication Fork Collapse to Maintain Genome Integrity. DNA Repair, 32, 149–157.

Cortez, D., Guntuku, S., Qin, J., & Elledge, S. J. (2001). ATR and ATRIP: Partners in checkpoint signaling. Science (New York, N.Y.), 294(5547), 1713–1716.

Costantino, L., Sotiriou, S. K., Rantala, J. K., Magin, S., Mladenov, E., Helleday, T., Haber, J. E., Iliakis, G., Kallioniemi, O., & Halazonetis, T. D. (2014). Break-induced replication repair of damaged forks induces genomic duplications in human cells. Science (New York, N.Y.), 343(6166), 88–91.

Cotta-Ramusino, C., McDonald, E. R., Hurov, K., Sowa, M. E., Harper, J. W., & Elledge, S. J. (2011). A DNA damage response screen identifies RHINO, a 9-1-1 and TopBP1 interacting protein required for ATR signaling. Science (New York, N.Y.), 332(6035), 1313–1317.

Couch, F. B., Bansbach, C. E., Driscoll, R., Luzwick, J. W., Glick, G. G., Bétous, R., Carroll, C. M., Jung, S. Y., Qin, J., Cimprich, K. A., & Cortez, D. (2013). ATR phosphorylates SMARCAL1 to prevent replication fork collapse. Genes & Development, 27(14), 1610–1623.

Cox, J. S., Shamu, C. E., & Walter, P. (1993). Transcriptional induction of genes encoding endoplasmic reticulum resident proteins requires a transmembrane protein kinase. Cell, 73(6), 1197–1206.

Crawford, K., Bonfiglio, J. J., Mikoč, A., Matic, I., & Ahel, I. (2018). Specificity of reversible ADP-ribosylation and regulation of cellular processes. Critical Reviews in Biochemistry and Molecular Biology, 53(1), 64–82.

Crook, T. R., Souhami, R. L., & McLean, A. E. (1986). Cytotoxicity, DNA cross-linking, and single strand breaks induced by activated cyclophosphamide and acrolein in human leukemia cells. Cancer Research, 46(10), 5029–5034.

Crow, Y. J., Leitch, A., Hayward, B. E., Garner, A., Parmar, R., Griffith, E., Ali, M., Semple, C., Aicardi, J., Babul-Hirji, R., Baumann, C., Baxter, P., Bertini, E., Chandler, K. E., Chitayat, D., Cau, D., Déry, C., Fazzi, E., Goizet, C., … Jackson, A. P. (2006). Mutations in genes encoding ribonuclease H2 subunits cause Aicardi-Goutières syndrome and mimic congenital viral brain infection. Nature Genetics, 38(8), 910–916.

Cunningham, F., Allen, J. E., Allen, J., Alvarez-Jarreta, J., Amode, M. R., Armean, I. M., Austine-Orimoloye, O., Azov, A. G., Barnes, I., Bennett, R., Berry, A., Bhai, J., Bignell, A., Billis, K., Boddu, S., Brooks, L., Charkhchi, M., Cummins, C., Da Rin Fioretto, L., … Flicek, P. (2022). Ensembl 2022. Nucleic Acids Research, 50(D1), D988–D995.

Dantzer, F., Giraud-Panis, M.-J., Jaco, I., Amé, J.-C., Schultz, I., Blasco, M., Koering, C.-E., Gilson, E., Ménissier-de Murcia, J., de Murcia, G., & Schreiber, V. (2004). Functional interaction between poly(ADP-Ribose) polymerase 2 (PARP-2) and TRF2: PARP activity negatively regulates TRF2. Molecular and Cellular Biology, 24(4), 1595–1607.

Das, B. B., Huang, S. N., Murai, J., Rehman, I., Amé, J.-C., Sengupta, S., Das, S. K., Majumdar, P., Zhang, H., Biard, D., Majumder, H. K., Schreiber, V., & Pommier, Y. (2014). PARP1–TDP1 coupling for the repair of topoisomerase I–induced DNA damage. Nucleic Acids Research, 42(7), 4435–4449.

Dawicki-McKenna, J. M., Langelier, M.-F., DeNizio, J. E., Riccio, A. A., Cao, C. D., Karch, K. R., McCauley, M., Steffen, J. D., Black, B. E., & Pascal, J. M. (2015). PARP-1 Activation Requires Local Unfolding of an Autoinhibitory Domain. Molecular Cell, 60(5), 755–768.

Daza-Martin, M., Starowicz, K., Jamshad, M., Tye, S., Ronson, G. E., MacKay, H. L., Chauhan, A. S., Walker, A. K., Stone, H. R., Beesley, J. F. J., Coles, J. L., Garvin, A. J., Stewart, G. S., McCorvie, T. J., Zhang, X., Densham, R. M., & Morris, J. R. (2019). Isomerization of BRCA1–BARD1 promotes replication fork protection. Nature, 571(7766), 521–527.

de Massy, B. (2013). Initiation of Meiotic Recombination: How and Where? Conservation and Specificities Among Eukaryotes. Annual Review of Genetics, 47(1), 563–599.

De Rycker, M., & Price, C. M. (2004). Tankyrase polymerization is controlled by its sterile alpha motif and poly(ADP-ribose) polymerase domains. Molecular and Cellular Biology, 24(22), 9802–9812.

De Rycker, M., Venkatesan, R. N., Wei, C., & Price, C. M. (2003). Vertebrate tankyrase domain structure and sterile alpha motif (SAM)-mediated multimerization. Biochemical Journal, 372(Pt 1), 87–96.

Delacroix, S., Wagner, J. M., Kobayashi, M., Yamamoto, K., & Karnitz, L. M. (2007). The Rad9-Hus1-Rad1 (9-1-1) clamp activates checkpoint signaling via TopBP1. Genes & Development, 21(12), 1472–1477.

Demin, A. A., Hirota, K., Tsuda, M., Adamowicz, M., Hailstone, R., Brazina, J., Gittens, W., Kalasova, I., Shao, Z., Zha, S., Sasanuma, H., Hanzlikova, H., Takeda, S., & Caldecott, K. W. (2021). XRCC1 prevents toxic PARP1 trapping during DNA base excision repair. Molecular Cell, 81(14), 3018-3030.e5.

DeMott, M. S., Beyret, E., Wong, D., Bales, B. C., Hwang, J.-T., Greenberg, M. M., & Demple, B. (2002). Covalent trapping of human DNA polymerase beta by the oxidative DNA lesion 2-deoxyribonolactone. The Journal of Biological Chemistry, 277(10), 7637–7640.

Demple, B., & DeMott, M. S. (2002). Dynamics and diversions in base excision DNA repair of oxidized abasic lesions. Oncogene, 21(58), Article 58.

Demple, B., Herman, T., & Chen, D. S. (1991). Cloning and expression of APE, the cDNA encoding the major human apurinic endonuclease: Definition of a family of DNA repair enzymes. Proceedings of the National Academy of Sciences of the United States of America, 88(24), 11450–11454.

Deriano, L., & Roth, D. B. (2013). Modernizing the Nonhomologous End-Joining Repertoire: Alternative and Classical NHEJ Share the Stage. Annual Review of Genetics, 47(1), 433–455.

Deshpande, R. A., Lee, J.-H., Arora, S., & Paull, T. T. (2016). Nbs1 Converts the Human Mre11/Rad50 Nuclease Complex into an Endo/Exonuclease Machine Specific for Protein-DNA Adducts. Molecular Cell, 64(3), 593–606.

Dev, H., Chiang, T.-W. W., Lescale, C., de Krijger, I., Martin, A. G., Pilger, D., Coates, J., Sczaniecka-Clift, M., Wei, W., Ostermaier, M., Herzog, M., Lam, J., Shea, A., Demir, M., Wu, Q., Yang, F., Fu, B., Lai, Z., Balmus, G., … Jackson, S. P. (2018). Shieldin complex promotes DNA end-joining and counters homologous recombination in BRCA1-null cells. Nature Cell Biology, 20(8), 954–965.

Dhoonmoon, A., Nicolae, C. M., & Moldovan, G.-L. (2022). The KU-PARP14 axis differentially regulates DNA resection at stalled replication forks by MRE11 and EXO1. Nature Communications, 13(1), Article 1.

Di Marco, S., Hasanova, Z., Kanagaraj, R., Chappidi, N., Altmannova, V., Menon, S., Sedlackova, H., Langhoff, J., Surendranath, K., Hühn, D., Bhowmick, R., Marini, V., Ferrari, S., Hickson, I. D., Krejci, L., & Janscak, P. (2017). RECQ5 Helicase Cooperates with MUS81 Endonuclease in Processing Stalled Replication Forks at Common Fragile Sites during Mitosis. Molecular Cell, 66(5), 658-671.e8.

Di Virgilio, M., Callen, E., Yamane, A., Zhang, W., Jankovic, M., Gitlin, A. D., Feldhahn, N., Resch, W., Oliveira, T. Y., Chait, B. T., Nussenzweig, A., Casellas, R., Robbiani, D. F., & Nussenzweig, M. C. (2013). Rif1 prevents resection of DNA breaks and promotes immunoglobulin class switching. Science (New York, N.Y.), 339(6120), 711–715.

Dianov, G. L., & Hübscher, U. (2013). Mammalian base excision repair: The forgotten archangel. Nucleic Acids Research, 41(6), 3483–3490.

Dias, M. P., Moser, S. C., Ganesan, S., & Jonkers, J. (2021). Understanding and overcoming resistance to PARP inhibitors in cancer therapy. Nature Reviews Clinical Oncology, 1–19.

Dibitetto, D., Marshall, S., Sanchi, A., Liptay, M., Badar, J., Lopes, M., Rottenberg, S., & Smolka, M. B. (2022). DNA-PKcs promotes fork reversal and chemoresistance. Molecular Cell, 82(20), 3932-3942.e6.

Ding, Q., Reddy, Y. V. R., Wang, W., Woods, T., Douglas, P., Ramsden, D. A., Lees-Miller, S. P., & Meek, K. (2003). Autophosphorylation of the catalytic subunit of the DNA-dependent protein kinase is required for efficient end processing during DNA double-strand break repair. Molecular and Cellular Biology, 23(16), 5836–5848.

Dobzhansky, Th. (1946). Genetics of Natural Populations. Xiii. Recombination and Variability in Populations of Drosophila Pseudoobscura. Genetics, 31(3), 269–290.

Doench, J. G. (2018). Am I ready for CRISPR? A user's guide to genetic screens. Nature Reviews Genetics, 19(2), 67–80.

Domínguez-Kelly, R., Martín, Y., Koundrioukoff, S., Tanenbaum, M. E., Smits, V. A. J., Medema, R. H., Debatisse, M., & Freire, R. (2011). Wee1 controls genomic stability during replication by regulating the Mus81-Eme1 endonuclease. The Journal of Cell Biology, 194(4), 567–579.

Donnianni, R. A., & Symington, L. S. (2013). Break-induced replication occurs by conservative DNA synthesis. Proceedings of the National Academy of Sciences, 110(33), 13475–13480.

Dungrawala, H., Bhat, K. P., Le Meur, R., Chazin, W. J., Ding, X., Sharan, S. K., Wessel, S. R., Sathe, A. A., Zhao, R., & Cortez, D. (2017). RADX Promotes Genome Stability and Modulates Chemosensitivity by Regulating RAD51 at Replication Forks. Molecular Cell, 67(3), 374-386.e5.

Dungrawala, H., Rose, K. L., Bhat, K. P., Mohni, K. N., Glick, G. G., Couch, F. B., & Cortez, D. (2015). The Replication Checkpoint Prevents Two Types of Fork Collapse without Regulating Replisome Stability. Molecular Cell, 59(6), 998–1010.

Dunstan, M. S., Barkauskaite, E., Lafite, P., Knezevic, C. E., Brassington, A., Ahel, M., Hergenrother, P. J., Leys, D., & Ahel, I. (2012). Structure and mechanism of a canonical poly(ADP-ribose) glycohydrolase. Nature Communications, 3(1), Article 1.

Duro, E., Lundin, C., Ask, K., Sanchez-Pulido, L., MacArtney, T. J., Toth, R., Ponting, C. P., Groth, A., Helleday, T., & Rouse, J. (2010). Identification of the MMS22L-TONSL complex that promotes homologous recombination. Molecular Cell, 40(4), 632–644.

Duursma, A. M., Driscoll, R., Elias, J. E., & Cimprich, K. A. (2013). A role for the MRN complex in ATR activation via TOPBP1 recruitment. Molecular Cell, 50(1), 116–122.

Edwards, S. L., Brough, R., Lord, C. J., Natrajan, R., Vatcheva, R., Levine, D. A., Boyd, J., Reis-Filho, J. S., & Ashworth, A. (2008). Resistance to therapy caused by intragenic deletion in BRCA2. Nature, 451(7182), Article 7182.

Eggler, A. L., Inman, R. B., & Cox, M. M. (2002). The Rad51-dependent Pairing of Long DNA Substrates Is Stabilized by Replication Protein A*. Journal of Biological Chemistry, 277(42), 39280–39288.

Elbæk, C. R., Petrosius, V., Benada, J., Erichsen, L., Damgaard, R. B., & Sørensen, C. S. (2022). WEE1 kinase protects the stability of stalled DNA replication forks by limiting CDK2 activity. Cell Reports, 38(3), 110261.

El-Khamisy, S. F., Masutani, M., Suzuki, H., & Caldecott, K. W. (2003). A requirement for PARP-1 for the assembly or stability of XRCC1 nuclear foci at sites of oxidative DNA damage. Nucleic Acids Research, 31(19), 5526–5533.

Ellison, V., & Stillman, B. (2003). Biochemical Characterization of DNA Damage Checkpoint Complexes: Clamp Loader and Clamp Complexes with Specificity for 5′ Recessed DNA. PLOS Biology, 1(2), e33.

Ensminger, M., Iloff, L., Ebel, C., Nikolova, T., Kaina, B., & Löbrich, M. (2014). DNA breaks and chromosomal aberrations arise when replication meets base excision repair. J Cell Biol, 206(1), 29–43.

Epum, E. A., & Haber, J. E. (2022). DNA replication: The recombination connection. Trends in Cell Biology, 32(1), 45–57.

Escribano-Díaz, C., Orthwein, A., Fradet-Turcotte, A., Xing, M., Young, J. T. F., Tkáč, J., Cook, M. A., Rosebrock, A. P., Munro, M., Canny, M. D., Xu, D., & Durocher, D. (2013). A cell cycle-dependent regulatory circuit composed of 53BP1-RIF1 and BRCA1-CtIP controls DNA repair pathway choice. Molecular Cell, 49(5), 872–883.

Esteller, M., Silva, J. M., Dominguez, G., Bonilla, F., Matias-Guiu, X., Lerma, E., Bussaglia, E., Prat, J., Harkes, I. C., Repasky, E. A., Gabrielson, E., Schutte, M., Baylin, S. B., & Herman, J. G. (2000). Promoter hypermethylation and BRCA1 inactivation in sporadic breast and ovarian tumors. Journal of the National Cancer Institute, 92(7), 564–569.

Eustermann, S., Videler, H., Yang, J.-C., Cole, P. T., Gruszka, D., Veprintsev, D., & Neuhaus, D. (2011). The DNA-binding domain of human PARP-1 interacts with DNA single-strand breaks as a monomer through its second zinc finger. Journal of Molecular Biology, 407(1), 149–170.

Eustermann, S., Wu, W.-F., Langelier, M.-F., Yang, J.-C., Easton, L. E., Riccio, A. A., Pascal, J. M., & Neuhaus, D. (2015). Structural Basis of Detection and Signaling of DNA Single-Strand Breaks by Human PARP-1. Molecular Cell, 60(5), 742–754.

Farmer, H., McCabe, N., Lord, C. J., Tutt, A. N. J., Johnson, D. A., Richardson, T. B., Santarosa, M., Dillon, K. J., Hickson, I., Knights, C., Martin, N. M. B., Jackson, S. P., Smith, G. C. M., & Ashworth, A. (2005). Targeting the DNA repair defect in BRCA mutant cells as a therapeutic strategy. Nature, 434(7035), Article 7035.

Fekairi, S., Scaglione, S., Chahwan, C., Taylor, E. R., Tissier, A., Coulon, S., Dong, M.-Q., Ruse, C., Yates, J. R., Russell, P., Fuchs, R. P., McGowan, C. H., & Gaillard, P.-H. L. (2009). Human SLX4 is a Holliday Junction Resolvase Subunit that Binds Multiple DNA Repair/Recombination Endonucleases. Cell, 138(1), 78–89.

Feng, W., Simpson, D. A., Carvajal-Garcia, J., Price, B. A., Kumar, R. J., Mose, L. E., Wood, R. D., Rashid, N., Purvis, J. E., Parker, J. S., Ramsden, D. A., & Gupta, G. P. (2019). Genetic determinants of cellular addiction to DNA polymerase theta. Nature Communications, 10(1), Article 1.

Fisher, A. E. O., Hochegger, H., Takeda, S., & Caldecott, K. W. (2007). Poly(ADP-Ribose) Polymerase 1 Accelerates Single-Strand Break Repair in Concert with Poly(ADP-Ribose) Glycohydrolase. Molecular and Cellular Biology, 27(15), 5597–5605.

Fernandez-Vidal, A., Vignard, J., & Mirey, G. (2017). Around and beyond 53BP1 Nuclear Bodies. International Journal of Molecular Sciences, 18(12), E2611.

Flaus, A., Martin, D. M. A., Barton, G. J., & Owen-Hughes, T. (2006). Identification of multiple distinct Snf2 subfamilies with conserved structural motifs. Nucleic Acids Research, 34(10), 2887–2905.

Fok, J. H. L., Ramos-Montoya, A., Vazquez-Chantada, M., Wijnhoven, P. W. G., Follia, V., James, N., Farrington, P. M., Karmokar, A., Willis, S. E., Cairns, J., Nikkilä, J., Beattie, D., Lamont, G. M., Finlay, M. R. V., Wilson, J., Smith, A., O'Connor, L. O., Ling, S., Fawell, S. E., … Cadogan, E. B. (2019). AZD7648 is a potent and selective DNA-PK inhibitor that enhances radiation, chemotherapy and olaparib activity. Nature Communications, 10(1), 5065.

Fontana, P., Bonfiglio, J. J., Palazzo, L., Bartlett, E., Matic, I., & Ahel, I. (2017). Serine ADP-ribosylation reversal by the hydrolase ARH3. ELife, 6, e28533.

Frattini, C., Promonet, A., Alghoul, E., Vidal-Eychenie, S., Lamarque, M., Blanchard, M.-P., Urbach, S., Basbous, J., & Constantinou, A. (2021). TopBP1 assembles nuclear condensates to switch on ATR signaling. Molecular Cell, 81(6), 1231-1245.e8.

Frosina, G., Fortini, P., Rossi, O., Carrozzino, F., Raspaglio, G., Cox, L. S., Lane, D. P., Abbondandolo, A., & Dogliotti, E. (1996). Two pathways for base excision repair in mammalian cells. The Journal of Biological Chemistry, 271(16), 9573–9578.

Fu, Y., Foden, J. A., Khayter, C., Maeder, M. L., Reyon, D., Joung, J. K., & Sander, J. D. (2013). High-frequency off-target mutagenesis induced by CRISPR-Cas nucleases in human cells. Nature Biotechnology, 31(9),

Fugger, K., Mistrik, M., Danielsen, J. R., Dinant, C., Falck, J., Bartek, J., Lukas, J., & Mailand, N. (2009). Human Fbh1 helicase contributes to genome maintenance via pro- and anti-recombinase activities. Journal of Cell Biology, 186(5), 655–663.

Fujimoto, M., Takii, R., Takaki, E., Katiyar, A., Nakato, R., Shirahige, K., & Nakai, A. (2017). The HSF1–PARP13–PARP1 complex facilitates DNA repair and promotes mammary tumorigenesis. Nature Communications, 8(1), 1–16.

Gagné, J.-P., Isabelle, M., Lo, K. S., Bourassa, S., Hendzel, M. J., Dawson, V. L., Dawson, T. M., & Poirier, G. G. (2008). Proteome-wide identification of poly(ADP-ribose) binding proteins and poly(ADP-ribose)-associated protein complexes. Nucleic Acids Research, 36(22), 6959–6976.

Gagou, M. E., Zuazua-Villar, P., & Meuth, M. (2010). Enhanced H2AX Phosphorylation, DNA Replication Fork Arrest, and Cell Death in the Absence of Chk1. Molecular Biology of the Cell, 21(5), 739.

Gaillard, H., García-Muse, T., & Aguilera, A. (2015). Replication stress and cancer. Nature Reviews Cancer, 15(5), 276–289.

Gao, F., Kwon, S. W., Zhao, Y., & Jin, Y. (2009). PARP1 poly(ADP-ribosyl)ates Sox2 to control Sox2 protein levels and FGF4 expression during embryonic stem cell differentiation. The Journal of Biological Chemistry, 284(33), 22263–22273.

Gao, M., Guo, G., Huang, J., Hou, X., Ham, H., Kim, W., Zhao, F., Tu, X., Zhou, Q., Zhang, C., Zhu, Q., Liu, J., Yan, Y., Xu, Z., Yin, P., Luo, K., Weroha, J., Deng, M., Billadeau, D. D., & Lou, Z. (2021). DOCK7 protects against replication stress by promoting RPA stability on chromatin. Nucleic Acids Research, 49(6), 3322–3337.

Gao, S., Feng, S., Ning, S., Liu, J., Zhao, H., Xu, Y., Shang, J., Li, K., Li, Q., Guo, R., & Xu, D. (2018). An OB-fold complex controls the repair pathways for DNA double-strand breaks. Nature Communications, 9(1), Article 1.

Gao, Y., Katyal, S., Lee, Y., Zhao, J., Rehg, J. E., Russell, H. R., & McKinnon, P. J. (2011). DNA ligase III is critical for mtDNA integrity but not Xrcc1-mediated nuclear DNA repair. Nature, 471(7337), Article 7337.

García-Gómez, S., Reyes, A., Martínez-Jiménez, M. I., Chocrón, E. S., Mourón, S., Terrados, G., Powell, C., Salido, E., Méndez, J., Holt, I. J., & Blanco, L. (2013). PrimPol, an Archaic Primase/Polymerase Operating in Human Cells. Molecular Cell, 52(4), 541–553.

Gari, K., Décaillet, C., Delannoy, M., Wu, L., & Constantinou, A. (2008). Remodeling of DNA replication structures by the branch point translocase FANCM. Proceedings of the National Academy of Sciences, 105(42), 16107–16112.

Garneau, J. E., Dupuis, M.-È., Villion, M., Romero, D. A., Barrangou, R., Boyaval, P., Fremaux, C., Horvath, P., Magadán, A. H., & Moineau, S. (2010). The CRISPR/Cas bacterial immune system cleaves bacteriophage and plasmid DNA. Nature, 468(7320), 67–71.

Gavet, O., & Pines, J. (2010). Progressive activation of CyclinB1-Cdk1 coordinates entry to mitosis. Developmental Cell, 18(4), 533–543.

Ge, X. Q., Jackson, D. A., & Blow, J. J. (2007). Dormant origins licensed by excess Mcm2–7 are required for human cells to survive replicative stress. Genes & Development, 21(24), 3331–3341.

Geley, S., Kramer, E., Gieffers, C., Gannon, J., Peters, J. M., & Hunt, T. (2001). Anaphase-promoting complex/cyclosome-dependent proteolysis of human cyclin A starts at the beginning of mitosis and is not subject to the spindle assembly checkpoint. The Journal of Cell Biology, 153(1), 137–148.

Genois, M.-M., Gagné, J.-P., Yasuhara, T., Jackson, J., Saxena, S., Langelier, M.-F., Ahel, I., Bedford, M. T., Pascal, J. M., Vindigni, A., Poirier, G. G., & Zou, L. (2021). CARM1 regulates replication fork speed and stress response by stimulating PARP1. Molecular Cell, 81(4), 784-800.e8.

Ghezraoui, H., Oliveira, C., Becker, J. R., Bilham, K., Moralli, D., Anzilotti, C., Fischer, R., Deobagkar-Lele, M., Sanchiz-Calvo, M., Fueyo-Marcos, E., Bonham, S., Kessler, B. M., Rottenberg, S., Cornall, R. J., Green, C. M., & Chapman, J. R. (2018). 53BP1 cooperation with the REV7-shieldin complex underpins DNA structure-specific NHEJ. Nature, 560(7716), 122–127. h

Giannattasio, M., Zwicky, K., Follonier, C., Foiani, M., Lopes, M., & Branzei, D. (2014). Visualization of recombination–mediated damage-bypass by template switching. Nature Structural & Molecular Biology, 21(10), 884–892.

Giansanti, C., Manzini, V., Dickmanns, A., Dickmanns, A., Palumbieri, M. D., Sanchi, A., Kienle, S. M., Rieth, S., Scheffner, M., Lopes, M., & Dobbelstein, M. (2022). MDM2 binds and ubiquitinates PARP1 to enhance DNA replication fork progression. Cell Reports, 39(9), 110879.

Gibbs, P. E. M., McGregor, W. G., Maher, V. M., Nisson, P., & Lawrence, C. W. (1998). A human homolog of the Saccharomyces cerevisiae REV3 gene, which encodes the catalytic subunit of DNA polymerase ζ. Proceedings of the National Academy of Sciences of the United States of America, 95(12), 6876–6880.

Gibbs-Seymour, I., Fontana, P., Rack, J. G. M., & Ahel, I. (2016). HPF1/C4orf27 Is a PARP-1-Interacting Protein that Regulates PARP-1 ADP-Ribosylation Activity. Molecular Cell, 62(3), 432–442.

Goenka, S., Cho, S. H., & Boothby, M. (2007). Collaborator of Stat6 (CoaSt6)-associated Poly(ADP-ribose) Polymerase Activity Modulates Stat6-dependent Gene Transcription *. Journal of Biological Chemistry, 282(26), 18732–18739.

Gong, B., Radulovic, M., Figueiredo-Pereira, M. E., & Cardozo, C. (2016). The Ubiquitin-Proteasome System: Potential Therapeutic Targets for Alzheimer's Disease and Spinal Cord Injury. Frontiers in Molecular Neuroscience, 9, 4.

Gong, D., & Ferrell, J. E. (2010). The Roles of Cyclin A2, B1, and B2 in Early and Late Mitotic Events. Molecular Biology of the Cell, 21(18), 3149–3161.

Goodarzi, A. A., Yu, Y., Riballo, E., Douglas, P., Walker, S. A., Ye, R., Härer, C., Marchetti, C., Morrice, N., Jeggo, P. A., & Lees-Miller, S. P. (2006). DNA-PK autophosphorylation facilitates Artemis endonuclease activity. The EMBO Journal, 25(16), 3880–3889.

Gottipati, P., Vischioni, B., Schultz, N., Solomons, J., Bryant, H. E., Djureinovic, T., Issaeva, N., Sleeth, K., Sharma, R. A., & Helleday, T. (2010). Poly(ADP-Ribose) Polymerase Is Hyperactivated in Homologous Recombination–Defective Cells. Cancer Research, 70(13), 5389–5398.

Gottlieb, T. M., & Jackson, S. P. (1993). The DNA-dependent protein kinase: Requirement for DNA ends and association with Ku antigen. Cell, 72(1), 131–142.

Goulian, M., Richards, S. H., Heard, C. J., & Bigsby, B. M. (1990). Discontinuous DNA synthesis by purified mammalian proteins. The Journal of Biological Chemistry, 265(30), 18461–18471.

Greco, W. R., Faessel, H., & Levasseur, L. (1996). The Search for Cytotoxic Synergy Between Anticancer Agents: A Case of Dorothy and the Ruby Slippers? JNCI: Journal of the National Cancer Institute, 88(11), 699–700.

Grimaldi, G., Filograna, A., Schembri, L., Lo Monte, M., Di Martino, R., Pirozzi, M., Spano, D., Beccari, A. R., Parashuraman, S., Luini, A., Valente, C., & Corda, D. (2022). PKD-dependent PARP12-catalyzed mono-ADP-ribosylation of Golgin-97 is required for E-cadherin transport from Golgi to plasma membrane. Proceedings of the National Academy of Sciences, 119(1), e2026494119.

Groelly, F. J., Dagg, R. A., Petropoulos, M., Rossetti, G. G., Prasad, B., Panagopoulos, A., Paulsen, T., Karamichali, A., Jones, S. E., Ochs, F., Dionellis, V. S., Puig Lombardi, E., Miossec, M. J., Lockstone, H., Legube, G., Blackford, A. N., Altmeyer, M., Halazonetis, T. D., & Tarsounas, M. (2022). Mitotic DNA synthesis is caused by transcription-replication conflicts in BRCA2-deficient cells. Molecular Cell, 82(18), 3382-3397.e7.

Grundy, G. J., Polo, L. M., Zeng, Z., Rulten, S. L., Hoch, N. C., Paomephan, P., Xu, Y., Sweet, S. M., Thorne, A. W., Oliver, A. W., Matthews, S. J., Pearl, L. H., & Caldecott, K. W. (2016). PARP3 is a sensor of nicked nucleosomes and monoribosylates histone H2BGlu2. *Nature Communications*, *7*(1), Article 1.

Gu, Y., Rosenblatt, J., & Morgan, D. O. (1992). Cell cycle regulation of CDK2 activity by phosphorylation of Thr160 and Tyr15. The EMBO Journal, 11(11), 3995–4005.

Guettler, S., LaRose, J., Petsalaki, E., Gish, G., Scotter, A., Pawson, T., Rottapel, R., & Sicheri, F. (2011). Structural basis and sequence rules for substrate recognition by Tankyrase explain the basis for cherubism disease. Cell, 147(6), 1340–1354.

Guilliam, T. A., Jozwiakowski, S. K., Ehlinger, A., Barnes, R. P., Rudd, S. G., Bailey, L. J., Skehel, J. M., Eckert, K. A., Chazin, W. J., & Doherty, A. J. (2015). Human PrimPol is a highly error-prone polymerase regulated by single-stranded DNA binding proteins. Nucleic Acids Research, 43(2), 1056–1068.

Guo, H.-L., Zhang, C., Liu, Q., Li, Q., Lian, G., Wu, D., Li, X., Zhang, W., Shen, Y., Ye, Z., Lin, S.-Y., & Lin, S.-C. (2012). The Axin/TNKS complex interacts with KIF3A and is required for insulin-stimulated GLUT4 translocation. Cell Research, 22(8), Article 8.

Guo, T., Zuo, Y., Qian, L., Liu, J., Yuan, Y., Xu, K., Miao, Y., Feng, Q., Chen, X., Jin, L., Zhang, L., Dong, C., Xiong, S., & Zheng, H. (2019). ADP-ribosyltransferase PARP11 modulates the interferon antiviral response by mono-ADP-ribosylating the ubiquitin E3 ligase β-TrCP. Nature Microbiology, 4(11), Article 11.

Guo, X., Carroll, J.-W. N., Macdonald, M. R., Goff, S. P., & Gao, G. (2004). The zinc finger antiviral protein directly binds to specific viral mRNAs through the CCCH zinc finger motifs. Journal of Virology, 78(23), 12781–12787.

Gupta, R., Somyajit, K., Narita, T., Maskey, E., Stanlie, A., Kremer, M., Typas, D., Lammers, M., Mailand, N., Nussenzweig, A., Lukas, J., & Choudhary, C. (2018). DNA Repair Network Analysis Reveals Shieldin as a Key Regulator of NHEJ and PARP Inhibitor Sensitivity. Cell, 173(4), 972-988.e23.

Haahr, P., Hoffmann, S., Tollenaere, M. A. X., Ho, T., Toledo, L. I., Mann, M., Bekker-Jensen, S., Räschle, M., & Mailand, N. (2016). Activation of the ATR kinase by the RPA-binding protein ETAA1. Nature Cell Biology, 18(11), 1196–1207.

Haince, J.-F., McDonald, D., Rodrigue, A., Déry, U., Masson, J.-Y., Hendzel, M. J., & Poirier, G. G. (2008). PARP1-dependent Kinetics of Recruitment of MRE11 and NBS1 Proteins to Multiple DNA Damage Sites *. Journal of Biological Chemistry, 283(2), 1197–1208.

Halder, S., Ranjha, L., Taglialatela, A., Ciccia, A., & Cejka, P. (2022). Strand annealing and motor driven activities of SMARCAL1 and ZRANB3 are stimulated by RAD51 and the paralog complex. Nucleic Acids Research, 50(14), 8008–8022.

Hall, J. R., Kow, E., Nevis, K. R., Lu, C. K., Luce, K. S., Zhong, Q., & Cook, J. G. (2007). Cdc6 Stability Is Regulated by the Huwe1 Ubiquitin Ligase after DNA Damage. Molecular Biology of the Cell, 18(9), 3340–3350.

Hammond, C. M., Bao, H., Hendriks, I. A., Carraro, M., García-Nieto, A., Liu, Y., Reverón-Gómez, N., Spanos, C., Chen, L., Rappsilber, J., Nielsen, M. L., Patel, D. J., Huang, H., & Groth, A. (2021). DNAJC9 integrates heat shock molecular chaperones into the histone chaperone network. Molecular Cell, 81(12), 2533-2548.e9.

Hampp, S., Kiessling, T., Buechle, K., Mansilla, S. F., Thomale, J., Rall, M., Ahn, J., Pospiech, H., Gottifredi, V., & Wiesmüller, L. (2016). DNA damage tolerance pathway involving DNA polymerase ι and the tumor suppressor p53 regulates DNA replication fork progression. Proceedings of the National Academy of Sciences, 113(30), E4311–E4319.

Han, X., Aslanian, A., & Yates, J. R. (2008). Mass Spectrometry for Proteomics. Current Opinion in Chemical Biology, 12(5), 483–490.

Hanada, K., Budzowska, M., Davies, S. L., van Drunen, E., Onizawa, H., Beverloo, H. B., Maas, A., Essers, J., Hickson, I. D., & Kanaar, R. (2007). The structure-specific endonuclease Mus81 contributes to replication restart by generating double-strand DNA breaks. Nature Structural & Molecular Biology, 14(11), 1096–1104.

Hanada, K., Budzowska, M., Modesti, M., Maas, A., Wyman, C., Essers, J., & Kanaar, R. (2006). The structure-specific endonuclease Mus81–Eme1 promotes conversion of interstrand DNA crosslinks into double-strands breaks. The EMBO Journal, 25(20), 4921–4932.

Hanzlikova, H., Gittens, W., Krejcikova, K., Zeng, Z., & Caldecott, K. W. (2017). Overlapping roles for PARP1 and PARP2 in the recruitment of endogenous XRCC1 and PNKP into oxidized chromatin. Nucleic Acids Research, 45(5), 2546–2557.

Hanzlikova, H., Kalasova, I., Demin, A. A., Pennicott, L. E., Cihlarova, Z., & Caldecott, K. W. (2018). The Importance of Poly(ADP-Ribose) Polymerase as a Sensor of Unligated Okazaki Fragments during DNA Replication. Molecular Cell, 71(2), 319-331.e3.

Hanzlikova, H., Prokhorova, E., Krejcikova, K., Cihlarova, Z., Kalasova, I., Kubovciak, J., Sachova, J., Hailstone, R., Brazina, J., Ghosh, S., Cirak, S., Gleeson, J. G., Ahel, I., & Caldecott, K. W. (2020). Pathogenic ARH3 mutations result in ADP-ribose chromatin scars during DNA strand break repair. Nature Communications, 11(1), Article 1.

Harding, H. P., Zhang, Y., & Ron, D. (1999). Protein translation and folding are coupled by an endoplasmic-reticulum-resident kinase. Nature, 397(6716), 271–274.

Harper, J. W., Adami, G. R., Wei, N., Keyomarsi, K., & Elledge, S. J. (1993). The p21 Cdk-interacting protein Cip1 is a potent inhibitor of G1 cyclin-dependent kinases. Cell, 75(4), 805–816.

Harrigan, J. A., Belotserkovskaya, R., Coates, J., Dimitrova, D. S., Polo, S. E., Bradshaw, C. R., Fraser, P., & Jackson, S. P. (2011). Replication stress induces 53BP1-containing OPT domains in G1 cells. The Journal of Cell Biology, 193(1), 97–108.

Harrington, J. J., & Lieber, M. R. (1994). The characterization of a mammalian DNA structure-specific endonuclease. The EMBO Journal, 13(5), 1235–1246.

Hart, T., Tong, A. H. Y., Chan, K., Van Leeuwen, J., Seetharaman, A., Aregger, M., Chandrashekhar, M., Hustedt, N., Seth, S., Noonan, A., Habsid, A., Sizova, O., Nedyalkova, L., Climie, R., Tworzyanski, L., Lawson, K., Sartori, M. A., Alibeh, S., Tieu, D., … Moffat, J. (2017). Evaluation and Design of Genome-Wide CRISPR/SpCas9 Knockout Screens. G3: Genes|Genomes|Genetics, 7(8), 2719–2727.

Hartley, K. O., Gell, D., Smith, G. C., Zhang, H., Divecha, N., Connelly, M. A., Admon, A., Lees-Miller, S. P., Anderson, C. W., & Jackson, S. P. (1995). DNA-dependent protein kinase catalytic subunit: A relative of phosphatidylinositol 3-kinase and the ataxia telangiectasia gene product. Cell, 82(5), 849–856.

Hashimoto, Y., Ray Chaudhuri, A., Lopes, M., & Costanzo, V. (2010). Rad51 protects nascent DNA from Mre11-dependent degradation and promotes continuous DNA synthesis. Nature Structural & Molecular Biology, 17(11), 1305–1311.

Hatakeyama, K., Nemoto, Y., Ueda, K., & Hayaishi, O. (1986). Purification and characterization of poly(ADP-ribose) glycohydrolase. Different modes of action on large and small poly(ADP-ribose). The Journal of Biological Chemistry, 261(32), 14902–14911.

Haupt, Y., Maya, R., Kazaz, A., & Oren, M. (1997). Mdm2 promotes the rapid degradation of p53. Nature, 387(6630), Article 6630.

He, P., & Yang, W. (2018). Template and primer requirements for DNA Pol θ-mediated end joining. Proceedings of the National Academy of Sciences of the United States of America, 115(30), 7747–7752.

Hegde, M. L., Hazra, T. K., & Mitra, S. (2008). Early steps in the DNA base excision/single-strand interruption repair pathway in mammalian cells. Cell Research, 18(1), 27–47.

Hegde, M. L., Izumi, T., & Mitra, S. (2012). Oxidized base damage and single-strand break repair in mammalian genomes: Role of disordered regions and posttranslational modifications in early enzymes. Progress in Molecular Biology and Translational Science, 110, 123–153.

Hendriks, I. A., Larsen, S. C., & Nielsen, M. L. (2019). An Advanced Strategy for Comprehensive Profiling of ADP-ribosylation Sites Using Mass Spectrometry-based Proteomics. Molecular & Cellular Proteomics: MCP, 18(5), 1010–1026.

Herbig, U., Jobling, W. A., Chen, B. P. C., Chen, D. J., & Sedivy, J. M. (2004). Telomere Shortening Triggers Senescence of Human Cells through a Pathway Involving ATM, p53, and p21CIP1, but Not p16INK4a. Molecular Cell, 14(4), 501–513.

Hicks, W. M., Kim, M., & Haber, J. E. (2010). Increased mutagenesis and unique mutation signature associated with mitotic gene conversion. Science (New York, N.Y.), 329(5987), 82–85.

Higgs, M. R., Reynolds, J. J., Winczura, A., Blackford, A. N., Borel, V., Miller, E. S., Zlatanou, A., Nieminuszczy, J., Ryan, E. L., Davies, N. J., Stankovic, T., Boulton, S. J., Niedzwiedz, W., & Stewart, G. S. (2015). BOD1L Is Required to Suppress Deleterious Resection of Stressed Replication Forks. Molecular Cell, 59(3), 462–477.

Higgs, M. R., Sato, K., Reynolds, J. J., Begum, S., Bayley, R., Goula, A., Vernet, A., Paquin, K. L., Skalnik, D. G., Kobayashi, W., Takata, M., Howlett, N. G., Kurumizaka, H., Kimura, H., & Stewart, G. S. (2018). Histone Methylation by SETD1A Protects Nascent DNA through the Nucleosome Chaperone Activity of FANCD2. *Molecular Cell*, *71*(1), 25-41.e6.

Hiller, B., Achleitner, M., Glage, S., Naumann, R., Behrendt, R., & Roers, A. (2012). Mammalian RNase H2 removes ribonucleotides from DNA to maintain genome integrity. The Journal of Experimental Medicine, 209(8), 1419–1426.

Hiyama, E., & Hiyama, K. (2007). Telomere and telomerase in stem cells. British Journal of Cancer, 96(7), 1020–1024.

Ho, Y.-C., Ku, C.-S., Tsai, S.-S., Shiu, J.-L., Jiang, Y.-Z., Miriam, H. E., Zhang, H.-W., Chen, Y.-T., Chiu, W.-T., Chang, S.-B., Shen, C.-H., Myung, K., Chi, P., & Liaw, H. (2022). PARP1 recruits DNA translocases to restrain DNA replication and facilitate DNA repair. *PLOS Genetics*, *18*(12), e1010545.

Hoege, C., Pfander, B., Moldovan, G.-L., Pyrowolakis, G., & Jentsch, S. (2002). RAD6-dependent DNA repair is linked to modification of PCNA by ubiquitin and SUMO. Nature, 419(6903), Article 6903.

Hornbeck, P. V., Zhang, B., Murray, B., Kornhauser, J. M., Latham, V., & Skrzypek, E. (2015). PhosphoSitePlus, 2014: Mutations, PTMs and recalibrations. Nucleic Acids Research, 43(Database issue), D512–D520.

Hottiger, M. O., Hassa, P. O., Lüscher, B., Schüler, H., & Koch-Nolte, F. (2010). Toward a unified nomenclature for mammalian ADP-ribosyltransferases. Trends in Biochemical Sciences, 35(4), 208–219.

Hsiang, Y. H., Lihou, M. G., & Liu, L. F. (1989). Arrest of replication forks by drug-stabilized topoisomerase I-DNA cleavable complexes as a mechanism of cell killing by camptothecin. Cancer Research, 49(18), 5077–5082.

Hu, Y., Raynard, S., Sehorn, M. G., Lu, X., Bussen, W., Zheng, L., Stark, J. M., Barnes, E. L., Chi, P., Janscak, P., Jasin, M., Vogel, H., Sung, P., & Luo, G. (2007). RECQL5/Recql5 helicase regulates homologous recombination and suppresses tumor formation via disruption of Rad51 presynaptic filaments. Genes & Development, 21(23), 3073–3084.

Huang, F., Mazina, O. M., Zentner, I. J., Cocklin, S., & Mazin, A. V. (2012). Inhibition of homologous recombination in human cells by targeting RAD51 recombinase. Journal of Medicinal Chemistry, 55(7), 3011–3020.

Huang, J. Y., Wang, K., Vermehren-Schmaedick, A., Adelman, J. P., & Cohen, M. S. (2016). PARP6 is a Regulator of Hippocampal Dendritic Morphogenesis. Scientific Reports, 6(1), 18512.

Huang, S. N., Williams, J. S., Arana, M. E., Kunkel, T. A., & Pommier, Y. (2017). Topoisomerase I-mediated cleavage at unrepaired ribonucleotides generates DNA double-strand breaks. The EMBO Journal, 36(3), 361–373.

Huang, S.-M. A., Mishina, Y. M., Liu, S., Cheung, A., Stegmeier, F., Michaud, G. A., Charlat, O., Wiellette, E., Zhang, Y., Wiessner, S., Hild, M., Shi, X., Wilson, C. J., Mickanin, C., Myer, V., Fazal, A., Tomlinson, R., Serluca, F., Shao, W., … Cong, F. (2009). Tankyrase inhibition stabilizes axin and antagonizes Wnt signalling. Nature, 461(7264), 614–620.

Huertas, P., & Jackson, S. P. (2009). Human CtIP mediates cell cycle control of DNA end resection and double strand break repair. The Journal of Biological Chemistry, 284(14), 9558–9565.

Hunkeler, M., Jin, C. Y., Ma, M. W., Monda, J. K., Overwijn, D., Bennett, E. J., & Fischer, E. S. (2021). Solenoid architecture of HUWE1 contributes to ligase activity and substrate recognition. Molecular Cell, 81(17), 3468-3480.e7.

Hurwitz, R., Hozier, J., Lebien, T., Minowada, J., Gajl-Peczalska, K., Kubonishi, I., & Kersey, J. (1979). Characterization of a leukemic cell line of the pre-B phenotype. International Journal of Cancer, 23(2), 174–180.

Hustedt, N., Álvarez-Quilón, A., McEwan, A., Yuan, J. Y., Cho, T., Koob, L., Hart, T., & Durocher, D. (2019). A consensus set of genetic vulnerabilities to ATR inhibition. *Open Biology*, *9*(9), 190156.

Hustedt, N., Saito, Y., Zimmermann, M., Álvarez-Quilón, A., Setiaputra, D., Adam, S., McEwan, A., Yuan, J. Y., Olivieri, M., Zhao, Y., Kanemaki, M. T., Jurisicova, A., & Durocher, D. (2019). Control of homologous recombination by the HROB–MCM8–MCM9 pathway. Genes & Development.

Ikegami, S., Taguchi, T., Ohashi, M., Oguro, M., Nagano, H., & Mano, Y. (1978). Aphidicolin prevents mitotic cell division by interfering with the activity of DNA polymerase-α. Nature, 275(5679), 458–460.

Ikejima, M., Noguchi, S., Yamashita, R., Ogura, T., Sugimura, T., Gill, D. M., & Miwa, M. (1990). The zinc fingers of human poly(ADP-ribose) polymerase are differentially required for the recognition of DNA breaks and nicks and the consequent enzyme activation. Other structures recognize intact DNA. The Journal of Biological Chemistry, 265(35), 21907–21913.

Iliás, A., Urbán, Z., Seidl, T. L., Saux, O. L., Sinkó, E., Boyd, C. D., Sarkadi, B., & Váradi, A. (2002). Loss of ATP-dependent Transport Activity in Pseudoxanthoma Elasticum-associated Mutants of Human ABCC6 (MRP6) *. Journal of Biological Chemistry, 277(19), 16860–16867.

Ip, S. C. Y., Rass, U., Blanco, M. G., Flynn, H. R., Skehel, J. M., & West, S. C. (2008). Identification of Holliday junction resolvases from humans and yeast. Nature, 456(7220), 357–361.

Ira, G., Pellicioli, A., Balijja, A., Wang, X., Fiorani, S., Carotenuto, W., Liberi, G., Bressan, D., Wan, L., Hollingsworth, N. M., Haber, J. E., & Foiani, M. (2004). DNA end resection, homologous recombination and DNA damage checkpoint activation require CDK1. Nature, 431(7011), 1011–1017.

Ishimi, Y., Claude, A., Bullock, P., & Hurwitz, J. (1988). Complete enzymatic synthesis of DNA containing the SV40 origin of replication. The Journal of Biological Chemistry, 263(36), 19723–19733.

Iwata, H., Goettsch, C., Sharma, A., Ricchiuto, P., Goh, W. W. B., Halu, A., Yamada, I., Yoshida, H., Hara, T., Wei, M., Inoue, N., Fukuda, D., Mojcher, A., Mattson, P. C., Barabási, A.-L., Boothby, M., Aikawa, E., Singh, S. A., & Aikawa, M. (2016). PARP9 and PARP14 cross-regulate macrophage activation via STAT1 ADP-ribosylation. Nature Communications, 7(1), Article 1.

Iyer, L. M., Babu, M. M., & Aravind, L. (2006). The HIRAN domain and recruitment of chromatin remodeling and repair activities to damaged DNA. Cell Cycle (Georgetown, Tex.), 5(7), 775–782.

Jackson, S. P. (2002). Sensing and repairing DNA double-strand breaks. Carcinogenesis, 23(5), 687–696.

Jacobs, A. L., & Schär, P. (2012). DNA glycosylases: In DNA repair and beyond. Chromosoma, 121(1), 1–20.

Jankevicius, G., Ariza, A., Ahel, M., & Ahel, I. (2016). The Toxin-Antitoxin System DarTG Catalyzes Reversible ADP-Ribosylation of DNA. Molecular Cell, 64(6), 1109–1116.

Jankevicius, G., Hassler, M., Golia, B., Rybin, V., Zacharias, M., Timinszky, G., & Ladurner, A. G. (2013). A family of macrodomain proteins reverses cellular mono-ADP-ribosylation. Nature Structural & Molecular Biology, 20(4), Article 4.

Jaspers, J. E., Sol, W., Kersbergen, A., Schlicker, A., Guyader, C., Xu, G., Wessels, L., Borst, P., Jonkers, J., & Rottenberg, S. (2015). BRCA2-Deficient Sarcomatoid Mammary Tumors Exhibit Multidrug Resistance. Cancer Research, 75(4), 732–741.

Jeffrey, P. D., Tong, L., & Pavletich, N. P. (2000). Structural basis of inhibition of CDK-cyclin complexes by INK4 inhibitors. Genes & Development, 14(24), 3115–3125.

Jensen, R. B., Carreira, A., & Kowalczykowski, S. C. (2010). Purified human BRCA2 stimulates RAD51-mediated recombination. Nature, 467(7316), 678–683.

Jeong, H.-S., Backlund, P. S., Chen, H.-C., Karavanov, A. A., & Crouch, R. J. (2004). RNase H2 of Saccharomyces cerevisiae is a complex of three proteins. Nucleic Acids Research, 32(2), 407–414.

Jinek, M., Chylinski, K., Fonfara, I., Hauer, M., Doudna, J. A., & Charpentier, E. (2012). A programmable dual RNA-guided DNA endonuclease in adaptive bacterial immunity. Science (New York, N.Y.), 337(6096), 816–821.

Johnson, R. E., Prakash, S., & Prakash, L. (1999). Efficient bypass of a thymine-thymine dimer by yeast DNA polymerase, Poleta. Science (New York, N.Y.), 283(5404), 1001–1004.

Jones, P., Binns, D., Chang, H.-Y., Fraser, M., Li, W., McAnulla, C., McWilliam, H., Maslen, J., Mitchell, A., Nuka, G., Pesseat, S., Quinn, A. F., Sangrador-Vegas, A., Scheremetjew, M., Yong, S.-Y., Lopez, R., & Hunter, S. (2014). InterProScan 5: Genome-scale protein function classification. Bioinformatics, 30(9), 1236–1240.

Jumper, J., Evans, R., Pritzel, A., Green, T., Figurnov, M., Ronneberger, O., Tunyasuvunakool, K., Bates, R., Žídek, A., Potapenko, A., Bridgland, A., Meyer, C., Kohl, S. A. A., Ballard, A. J., Cowie, A., Romera-Paredes, B., Nikolov, S., Jain, R., Adler, J., … Hassabis, D. (2021). Highly accurate protein structure prediction with AlphaFold. Nature, 596(7873), 583–589.

Jungmichel, S., Clapperton, J. A., Lloyd, J., Hari, F. J., Spycher, C., Pavic, L., Li, J., Haire, L. F., Bonalli, M., Larsen, D. H., Lukas, C., Lukas, J., MacMillan, D., Nielsen, M. L., Stucki, M., & Smerdon, S. J. (2012). The molecular basis of ATM-dependent dimerization of the Mdc1 DNA damage checkpoint mediator. Nucleic Acids Research, 40(9), 3913–3928.

Jwa, M., & Chang, P. (2012). PARP16 is a tail-anchored endoplasmic reticulum protein required for the PERK and IRE1α-mediated unfolded protein response. Nature Cell Biology, 14(11), 1223–1230.

Kabotyanski, E. B., Gomelsky, L., Han, J. O., Stamato, T. D., & Roth, D. B. (1998). Double-strand break repair in Ku86- and XRCC4-deficient cells. Nucleic Acids Research, 26(23), 5333–5342.

Kais, Z., Rondinelli, B., Holmes, A., O'Leary, C., Kozono, D., D'Andrea, A. D., & Ceccaldi, R. (2016). FANCD2 maintains fork stability in BRCA1/2-deficient tumors and promotes alternative end-joining DNA repair. Cell Reports, 15(11), 2488–2499.

Kamine, J., Elangovan, B., Subramanian, T., Coleman, D., & Chinnadurai, G. (1996). Identification of a Cellular Protein That Specifically Interacts with the Essential Cysteine Region of the HIV-1 Tat Transactivator. Virology, 216(2), 357–366.

Kanagaraj, R., Saydam, N., Garcia, P. L., Zheng, L., & Janscak, P. (2006). Human RECQ5β helicase promotes strand exchange on synthetic DNA structures resembling a stalled replication fork. Nucleic Acids Research, 34(18), 5217–5231.

Kanai, M., Tong, W.-M., Sugihara, E., Wang, Z.-Q., Fukasawa, K., & Miwa, M. (2003). Involvement of Poly(ADP-Ribose) Polymerase 1 and Poly(ADP-Ribosyl)ation in Regulation of Centrosome Function. Molecular and Cellular Biology, 23(7), 2451–2462.

Kannouche, P. L., Wing, J., & Lehmann, A. R. (2004). Interaction of human DNA polymerase eta with monoubiquitinated PCNA: A possible mechanism for the polymerase switch in response to DNA damage. Molecular Cell, 14(4), 491–500.

Kao, S.-H., Wu, H.-T., & Wu, K.-J. (2018). Ubiquitination by HUWE1 in tumorigenesis and beyond. Journal of Biomedical Science, 25(1), 67.

Karlberg, T., Klepsch, M., Thorsell, A.-G., Andersson, C. D., Linusson, A., & Schüler, H. (2015). Structural Basis for Lack of ADP-ribosyltransferase Activity in Poly(ADP-ribose) Polymerase-13/Zinc Finger Antiviral Protein. Journal of Biological Chemistry, 290(12), 7336–7344.

Karras, G. I., Kustatscher, G., Buhecha, H. R., Allen, M. D., Pugieux, C., Sait, F., Bycroft, M., & Ladurner, A. G. (2005). The macro domain is an ADP-ribose binding module. The EMBO Journal, 24(11), 1911–1920.

Kato, J., Matsushime, H., Hiebert, S. W., Ewen, M. E., & Sherr, C. J. (1993). Direct binding of cyclin D to the retinoblastoma gene product (pRb) and pRb phosphorylation by the cyclin D-dependent kinase CDK4. Genes & Development, 7(3), 331–342.

Kaufman, B., Shapira-Frommer, R., Schmutzler, R. K., Audeh, M. W., Friedlander, M., Balmaña, J., Mitchell, G., Fried, G., Stemmer, S. M., Hubert, A., Rosengarten, O., Steiner, M., Loman, N., Bowen, K., Fielding, A., & Domchek, S. M. (2015). Olaparib monotherapy in patients with advanced cancer and a germline BRCA1/2 mutation. Journal of Clinical Oncology: Official Journal of the American Society of Clinical Oncology, 33(3), 244–250.

Kedersha, N. L., & Rome, L. H. (1986). Isolation and characterization of a novel ribonucleoprotein particle: Large structures contain a single species of small RNA. The Journal of Cell Biology, 103(3), 699–709.

Kickhoefer, V. A., Siva, A. C., Kedersha, N. L., Inman, E. M., Ruland, C., Streuli, M., & Rome, L. H. (1999). The 193-Kd Vault Protein, Vparp, Is a Novel Poly(Adp-Ribose) Polymerase. The Journal of Cell Biology, 146(5), 917–928.

Kiehlbauch, C. C., Aboul-Ela, N., Jacobson, E. L., Ringer, D. P., & Jacobson, M. K. (1993). High resolution fractionation and characterization of ADP-ribose polymers. Analytical Biochemistry, 208(1), 26–34.

Kile, A. C., Chavez, D. A., Bacal, J., Eldirany, S., Korzhnev, D. M., Bezsonova, I., Eichman, B. F., & Cimprich, K. A. (2015). HLTF's Ancient HIRAN Domain Binds 3' DNA Ends to Drive Replication Fork Reversal. Molecular Cell, 58(6), 1090–1100.

Kilgas, S., Kiltie, A. E., & Ramadan, K. (2021). Immunofluorescence microscopy-based detection of ssDNA foci by BrdU in mammalian cells. STAR Protocols, 2(4), 100978.

Kim, J., Kim, J.-H., Lee, S.-H., Kim, D.-H., Kang, H.-Y., Bae, S.-H., Pan, Z.-Q., & Seo, Y.-S. (2002). The novel human DNA helicase hFBH1 is an F-box protein. The Journal of Biological Chemistry, 277(27), 24530–24537.

Kim, J.-H., Kim, J., Kim, D.-H., Ryu, G.-H., Bae, S.-H., & Seo, Y.-S. (2004). SCFhFBH1 can act as helicase and E3 ubiquitin ligase. Nucleic Acids Research, 32(8), 2287–2297.

Kim, M. K., Dudognon, C., & Smith, S. (2012). Tankyrase 1 regulates centrosome function by controlling CPAP stability. EMBO Reports, 13(8), 724–732.

Kim, N., Huang, S. N., Williams, J., Li, Y. C., Clark, A. B., Cho, J.-E., Kunkel, T. A., Pommier, Y., & Jinks-Robertson, S. (2011). Mutagenic processing of ribonucleotides in DNA by yeast topoisomerase 1. Science (New York, N.y.), 332(6037), 1561–1564.

Kim, S. T., Lim, D. S., Canman, C. E., & Kastan, M. B. (1999). Substrate specificities and identification of putative substrates of ATM kinase family members. The Journal of Biological Chemistry, 274(53), 37538–37543.

Kim, W., Zhao, F., Wu, R., Qin, S., Nowsheen, S., Huang, J., Zhou, Q., Chen, Y., Deng, M., Guo, G., Luo, K., Lou, Z., & Yuan, J. (2019). ZFP161 regulates replication fork stability and maintenance of genomic stability by recruiting the ATR/ATRIP complex. Nature Communications, 10(1), 1–11.

Kleine, H., Poreba, E., Lesniewicz, K., Hassa, P. O., Hottiger, M. O., Litchfield, D. W., Shilton, B. H., & Lüscher, B. (2008). Substrate-Assisted Catalysis by PARP10 Limits Its Activity to Mono-ADP-Ribosylation. Molecular Cell, 32(1), 57–69.

Klungland, A., & Lindahl, T. (1997). Second pathway for completion of human DNA base excision-repair: Reconstitution with purified proteins and requirement for DNase IV (FEN1). The EMBO Journal, 16(11), 3341–3348.

Knezevic, C. E., Wright, G., Rix, L. L. R., Kim, W., Kuenzi, B. M., Luo, Y., Watters, J. M., Koomen, J. M., Haura, E. B., Monteiro, A. N., Radu, C., Lawrence, H. R., & Rix, U. (2016). Proteome-wide Profiling of Clinical PARP Inhibitors Reveals Compound-Specific Secondary Targets. Cell Chemical Biology, 23(12), 1490–1503.

Koc, E. C., Burkhart, W., Blackburn, K., Moseley, A., & Spremulli, L. L. (2001). The Small Subunit of the Mammalian Mitochondrial Ribosome: IDENTIFICATION OF THE FULL COMPLEMENT OF RIBOSOMAL PROTEINS PRESENT *. Journal of Biological Chemistry, 276(22), 19363–19374.

Koh, D. W., Lawler, A. M., Poitras, M. F., Sasaki, M., Wattler, S., Nehls, M. C., Stöger, T., Poirier, G. G., Dawson, V. L., & Dawson, T. M. (2004). Failure to degrade poly(ADP-ribose) causes increased sensitivity to cytotoxicity and early embryonic lethality. Proceedings of the National Academy of Sciences of the United States of America, 101(51), 17699–17704.

Kojima, Y., Machida, Y., Palani, S., Caulfield, T. R., Radisky, E. S., Kaufmann, S. H., & Machida, Y. J. (2020). FAM111A protects replication forks from protein obstacles via its trypsin-like domain. Nature Communications, 11(1), Article 1.

Kolinjivadi, A. M., Sannino, V., De Antoni, A., Zadorozhny, K., Kilkenny, M., Técher, H., Baldi, G., Shen, R., Ciccia, A., Pellegrini, L., Krejci, L., & Costanzo, V. (2017). Smarcal1-Mediated Fork Reversal Triggers Mre11-Dependent Degradation of Nascent DNA in the Absence of Brca2 and Stable Rad51 Nucleofilaments. Molecular Cell, 67(5), 867-881.e7.

Khoronenkova, S. V., & Dianov, G. L. (2013). USP7S-dependent inactivation of Mule regulates DNA damage signalling and repair. Nucleic Acids Research, 41(3), 1750–1756.

Kosar, M., Giannattasio, M., Piccini, D., Maya-Mendoza, A., García-Benítez, F., Bartkova, J., Barroso, S. I., Gaillard, H., Martini, E., Restuccia, U., Ramirez-Otero, M. A., Garre, M., Verga, E., Andújar-Sánchez, M., Maynard, S., Hodny, Z., Costanzo, V., Kumar, A., Bachi, A., … Foiani, M. (2021). The human nucleoporin Tpr protects cells from RNA-mediated replication stress. Nature Communications, 12(1), Article 1.

Koundrioukoff, S., Carignon, S., Técher, H., Letessier, A., Brison, O., & Debatisse, M. (2013). Stepwise Activation of the ATR Signaling Pathway upon Increasing Replication Stress Impacts Fragile Site Integrity. PLOS Genetics, 9(7), e1003643.

Kramara, J., Osia, B., & Malkova, A. (2018). Break-Induced Replication: The Where, The Why, and The How. Trends in Genetics: TIG, 34(7), 518–531.

Krastev, D. B., Li, S., Sun, Y., Wicks, A. J., Hoslett, G., Weekes, D., Badder, L. M., Knight, E. G., Marlow, R., Pardo, M. C., Yu, L., Talele, T. T., Bartek, J., Choudhary, J. S., Pommier, Y., Pettitt, S. J., Tutt, A. N. J., Ramadan, K., & Lord, C. J. (2022). The ubiquitin-dependent ATPase p97 removes cytotoxic trapped PARP1 from chromatin. Nature Cell Biology, 24(1), Article 1.

Krishnakumar, R., Gamble, M. J., Frizzell, K. M., Berrocal, J. G., Kininis, M., & Kraus, W. L. (2008). Reciprocal binding of PARP-1 and histone H1 at promoters specifies transcriptional outcomes. Science (New York, N.Y.), 319(5864), 819–821.

Krishnakumar, R., & Kraus, W. L. (2010). PARP-1 regulates chromatin structure and transcription through a KDM5B-dependent pathway. Molecular Cell, 39(5), 736–749.

Krokan, H. E., & Bjørås, M. (2013). Base excision repair. Cold Spring Harbor Perspectives in Biology, 5(4), a012583.

Kubbutat, M. H. G., Jones, S. N., & Vousden, K. H. (1997). Regulation of p53 stability by Mdm2. Nature, 387(6630), Article 6630.

Kuzminov, A. (2001). Single-strand interruptions in replicating chromosomes cause double-strand breaks. Proceedings of the National Academy of Sciences of the United States of America, 98(15), 8241–8246.

Kwok, M., Davies, N., Agathanggelou, A., Smith, E., Oldreive, C., Petermann, E., Stewart, G., Brown, J., Lau, A., Pratt, G., Parry, H., Taylor, M., Moss, P., Hillmen, P., & Stankovic, T. (2016). ATR inhibition induces synthetic lethality and overcomes chemoresistance in TP53- or ATM-defective chronic lymphocytic leukemia cells. Blood, 127(5), 582–595.

Lambert, S., Mizuno, K., Blaisonneau, J., Martineau, S., Chanet, R., Fréon, K., Murray, J. M., Carr, A. M., & Baldacci, G. (2010). Homologous recombination restarts blocked replication forks at the expense of genome rearrangements by template exchange. Molecular Cell, 39(3), 346–359.

Lange, S. S., Takata, K., & Wood, R. D. (2011). DNA polymerases and cancer. Nature Reviews. Cancer, 11(2), 96–110.

Langelier, M.-F., Billur, R., Sverzhinsky, A., Black, B. E., & Pascal, J. M. (2021). HPF1 dynamically controls the PARP1/2 balance between initiating and elongating ADP-ribose modifications. Nature Communications, 12(1), Article 1.

Langelier, M.-F., Planck, J. L., Roy, S., & Pascal, J. M. (2012). Structural basis for DNA damage-dependent poly(ADP-ribosyl)ation by human PARP-1. Science (New York, N.Y.), 336(6082), 728–732.

Langelier, M.-F., Riccio, A. A., & Pascal, J. M. (2014). PARP-2 and PARP-3 are selectively activated by 5' phosphorylated DNA breaks through an allosteric regulatory mechanism shared with PARP-1. Nucleic Acids Research, 42(12), 7762–7775.

Langelier, M.-F., Zandarashvili, L., Aguiar, P. M., Black, B. E., & Pascal, J. M. (2018). NAD+ analog reveals PARP-1 substrate-blocking mechanism and allosteric communication from catalytic center to DNA-binding domains. Nature Communications, 9.

Larsen, S. C., Hendriks, I. A., Lyon, D., Jensen, L. J., & Nielsen, M. L. (2018). Systems-wide Analysis of Serine ADP-Ribosylation Reveals Widespread Occurrence and Site-Specific Overlap with Phosphorylation. Cell Reports, 24(9), 2493-2505.e4.

Layer, J. V., Debaize, L., Van Scoyk, A., House, N. C., Brown, A. J., Liu, Y., Stevenson, K. E., Hemann, M., Roberts, S. A., Price, B. D., Weinstock, D. M., & Day, T. A. (2020). Polymerase δ promotes chromosomal rearrangements and imprecise double-strand break repair. Proceedings of the National Academy of Sciences, 117(44), 27566–27577.

Lee, D. H., & Goldberg, A. L. (1998). Proteasome inhibitors: Valuable new tools for cell biologists. Trends in Cell Biology, 8(10), 397–403.

Lee, J., Kumagai, A., & Dunphy, W. G. (2007). The Rad9-Hus1-Rad1 Checkpoint Clamp Regulates Interaction of TopBP1 with ATR*. Journal of Biological Chemistry, 282(38), 28036–28044.

Lee, J.-H., & Paull, T. T. (2004). Direct activation of the ATM protein kinase by the Mre11/Rad50/Nbs1 complex. Science (New York, N.Y.), 304(5667), 93–96.

Lee, J.-H., & Paull, T. T. (2005). ATM activation by DNA double-strand breaks through the Mre11-Rad50-Nbs1 complex. Science (New York, N.Y.), 308(5721), 551–554.

Lee, Y.-C., Zhou, Q., Chen, J., & Yuan, J. (2016). RPA-Binding Protein ETAA1 Is an ATR Activator Involved in DNA Replication Stress Response. Current Biology, 26(24), 3257–3268.

Lee-Theilen, M., Matthews, A. J., Kelly, D., Zheng, S., & Chaudhuri, J. (2011). CtIP promotes microhomology-mediated alternative end joining during class-switch recombination. Nature Structural & Molecular Biology, 18(1), 75–79.

Leidecker, O., Bonfiglio, J. J., Colby, T., Zhang, Q., Atanassov, I., Zaja, R., Palazzo, L., Stockum, A., Ahel, I., & Matic, I. (2016). Serine is a new target residue for endogenous ADP-ribosylation on histones. Nature Chemical Biology, 12(12), 998–1000.

Lemaçon, D., Jackson, J., Quinet, A., Brickner, J. R., Li, S., Yazinski, S., You, Z., Ira, G., Zou, L., Mosammaparast, N., & Vindigni, A. (2017). MRE11 and EXO1 nucleases degrade reversed forks and elicit MUS81-dependent fork rescue in BRCA2-deficient cells. Nature Communications, 8(1), Article 1.

Leung, A. K. L., Vyas, S., Rood, J. E., Bhutkar, A., Sharp, P. A., & Chang, P. (2011). Poly(ADP-Ribose) Regulates Stress Responses and MicroRNA Activity in the Cytoplasm. Molecular Cell, 42(4), 489–499.

Levin, D. S., McKenna, A. E., Motycka, T. A., Matsumoto, Y., & Tomkinson, A. E. (2000). Interaction between PCNA and DNA ligase I is critical for joining of Okazaki fragments and long-patch base-excision repair. Current Biology: CB, 10(15), 919–922.

Levin, J. D., & Demple, B. (1990). Analysis of class II (hydrolytic) and class I (beta-lyase) apurinic/apyrimidinic endonucleases with a synthetic DNA substrate. Nucleic Acids Research, 18(17), 5069–5075.

Levy, M. Z., Allsopp, R. C., Futcher, A. B., Greider, C. W., & Harley, C. B. (1992). Telomere end-replication problem and cell aging. Journal of Molecular Biology, 225(4), 951–960.

Lezaja, A., Panagopoulos, A., Wen, Y., Carvalho, E., Imhof, R., & Altmeyer, M. (2021). RPA shields inherited DNA lesions for post-mitotic DNA synthesis. Nature Communications, 12(1), Article 1.

Li, M., Chen, D., Shiloh, A., Luo, J., Nikolaev, A. Y., Qin, J., & Gu, W. (2002). Deubiquitination of p53 by HAUSP is an important pathway for p53 stabilization. Nature, 416(6881), 648–653.

Li, M., Lu, L.-Y., Yang, C.-Y., Wang, S., & Yu, X. (2013). The FHA and BRCT domains recognize ADP-ribosylation during DNA damage response. Genes & Development, 27(16), 1752–1768.

Li, M., & Yu, X. (2013). Function of BRCA1 in the DNA Damage Response Is Mediated by ADP-Ribosylation. Cancer Cell, 23(5), 693–704.

Li, S., Kanno, S., Watanabe, R., Ogiwara, H., Kohno, T., Watanabe, G., Yasui, A., & Lieber, M. R. (2011). Polynucleotide kinase and aprataxin-like forkhead-associated protein (PALF) acts as both a single-stranded DNA endonuclease and a single-stranded DNA 3' exonuclease and can participate in DNA end joining in a biochemical system. The Journal of Biological Chemistry, 286(42), 36368–36377.

Li, W., Xu, H., Xiao, T., Cong, L., Love, M. I., Zhang, F., Irizarry, R. A., Liu, J. S., Brown, M., & Liu, X. S. (2014). MAGeCK enables robust identification of essential genes from genome-scale CRISPR/Cas9 knockout screens. Genome Biology, 15(12), 554.

Li, X., Stith, C. M., Burgers, P. M., & Heyer, W.-D. (2009). PCNA is required for initiation of recombination-associated DNA synthesis by DNA polymerase δ. Molecular Cell, 36(4), 704–713.

Li, Y., Mao, P., Basenko, E. Y., Lewis, Z., Smerdon, M. J., & Czaja, W. (2021). Versatile cell-based assay for measuring DNA alkylation damage and its repair. Scientific Reports, 11(1), Article 1.

Liang, F., & Jasin, M. (1996). Ku80-deficient Cells Exhibit Excess Degradation of Extrachromosomal DNA *. Journal of Biological Chemistry, 271(24), 14405–14411.

Liaw, H., Lee, D., & Myung, K. (2011). DNA-PK-Dependent RPA2 Hyperphosphorylation Facilitates DNA Repair and Suppresses Sister Chromatid Exchange. PLOS ONE, 6(6), e21424.

Lin, W., Xin, H., Zhang, Y., Wu, X., Yuan, F., & Wang, Z. (1999). The human REV1 gene codes for a DNA template-dependent dCMP transferase. Nucleic Acids Research, 27(22), 4468–4475.

Lin, X., Jiang, W., Rudolph, J., Lee, B. J., Luger, K., & Zha, S. (2022). PARP inhibitors trap PARP2 and alter the mode of recruitment of PARP2 at DNA damage sites. Nucleic Acids Research, 50(7), 3958–3973.

Lindahl, T., & Wood, R. D. (1999). Quality control by DNA repair. Science (New York, N.Y.), 286(5446), 1897–1905.

Lindsey-Boltz, L. A., Kemp, M. G., Capp, C., & Sancar, A. (2015). RHINO forms a stoichiometric complex with the 9-1-1 checkpoint clamp and mediates ATR-Chk1 signaling. Cell Cycle (Georgetown, Tex.), 14(1), 99–108.

Liu, C., Vyas, A., Kassab, M. A., Singh, A. K., & Yu, X. (2017). The role of poly ADP-ribosylation in the first wave of DNA damage response. Nucleic Acids Research, 45(14), 8129–8141.

Liu, J., Luo, S., Zhao, H., Liao, J., Li, J., Yang, C., Xu, B., Stern, D. F., Xu, X., & Ye, K. (2012). Structural mechanism of the phosphorylation-dependent dimerization of the MDC1 forkhead-associated domain. Nucleic Acids Research, 40(9), 3898–3912.

Liu, L., Sandow, J. J., Leslie Pedrioli, D. M., Samson, A. L., Silke, N., Kratina, T., Ambrose, R. L., Doerflinger, M., Hu, Z., Morrish, E., Chau, D., Kueh, A. J., Fitzibbon, C., Pellegrini, M., Pearson, J. S., Hottiger, M. O., Webb, A. I., Lalaoui, N., & Silke, J. (2022). Tankyrase-mediated ADP-ribosylation is a regulator of TNF-induced death. Science Advances, 8(19), eabh2332.

Liu, P., Barkley, L. R., Day, T., Bi, X., Slater, D. M., Alexandrow, M. G., Nasheuer, H.-P., & Vaziri, C. (2006). The Chk1-mediated S-phase checkpoint targets initiation factor Cdc45 via a Cdc25A/Cdk2-independent mechanism. The Journal of Biological Chemistry, 281(41), 30631–30644.

Liu, Q., Guntuku, S., Cui, X. S., Matsuoka, S., Cortez, D., Tamai, K., Luo, G., Carattini-Rivera, S., DeMayo, F., Bradley, A., Donehower, L. A., & Elledge, S. J. (2000). Chk1 is an essential kinase that is regulated by Atr and required for the G(2)/M DNA damage checkpoint. Genes & Development, 14(12), 1448–1459.

Liu, S., Opiyo, S. O., Manthey, K., Glanzer, J. G., Ashley, A. K., Amerin, C., Troksa, K., Shrivastav, M., Nickoloff, J. A., & Oakley, G. G. (2012). Distinct roles for DNA-PK, ATM and ATR in RPA phosphorylation and checkpoint activation in response to replication stress. Nucleic Acids Research, 40(21), 10780–10794.

Llorens-Agost, M., Ensminger, M., Le, H. P., Gawai, A., Liu, J., Cruz-García, A., Bhetawal, S., Wood, R. D., Heyer, W.-D., & Löbrich, M. (2021). POLθ-mediated end joining is restricted by RAD52 and BRCA2 until the onset of mitosis. Nature Cell Biology, 23(10), Article 10.

Lloyd, R. L., Wijnhoven, P. W. G., Ramos-Montoya, A., Wilson, Z., Illuzzi, G., Falenta, K., Jones, G. N., James, N., Chabbert, C. D., Stott, J., Dean, E., Lau, A., & Young, L. A. (2020). Combined PARP and ATR inhibition potentiates genome instability and cell death in ATM-deficient cancer cells. Oncogene, 39(25), Article 25.

Loizou, J. I., El-Khamisy, S. F., Zlatanou, A., Moore, D. J., Chan, D. W., Qin, J., Sarno, S., Meggio, F., Pinna, L. A., & Caldecott, K. W. (2004). The protein kinase CK2 facilitates repair of chromosomal DNA single-strand breaks. Cell, 117(1), 17–28.

Lopes, M., Foiani, M., & Sogo, J. M. (2006). Multiple Mechanisms Control Chromosome Integrity after Replication Fork Uncoupling and Restart at Irreparable UV Lesions. Molecular Cell, 21(1), 15–27.

Lord, C. J., & Ashworth, A. (2017a). PARP inhibitors: Synthetic lethality in the clinic. Science, 355(6330), 1152–1158.

Lossaint, G., Larroque, M., Ribeyre, C., Bec, N., Larroque, C., Décaillet, C., Gari, K., & Constantinou, A. (2013). FANCD2 Binds MCM Proteins and Controls Replisome Function upon Activation of S Phase Checkpoint Signaling. Molecular Cell, 51(5), 678–690.

Lü, Y., Cho, T., Mukherjee, S., Malik, A., Gonzalez-Foutel, N. S., Oh, R., Langille, E., Al-Zahrani, K. N., Lin, Z. Y., Rotter, V., Ashton-Prolla, P., Chemes, L. B., Moffat, J., Gingras, A.-C., Oren, M., Durocher, D., & Schramek, D. (2022). Genome-wide CRISPR screens identify novel regulators of wild-type and mutant p53 stability (p. 2022.03.13.483372). bioRxiv.

Luedeman, M. E., Stroik, S., Feng, W., Luthman, A. J., Gupta, G. P., & Ramsden, D. A. (2022). Poly(ADP) ribose polymerase promotes DNA polymerase theta-mediated end joining by activation of end resection. Nature Communications, 13(1), Article 1.

Luijsterburg, M. S., de Krijger, I., Wiegant, W. W., Shah, R. G., Smeenk, G., de Groot, A. J. L., Pines, A., Vertegaal, A. C. O., Jacobs, J. J. L., Shah, G. M., & van Attikum, H. (2016). PARP1 Links CHD2-Mediated Chromatin Expansion and H3.3 Deposition to DNA Repair by Non-homologous End-Joining. Molecular Cell, 61(4), 547–562.

Luijsterburg, M. S., Typas, D., Caron, M.-C., Wiegant, W. W., van den Heuvel, D., Boonen, R. A., Couturier, A. M., Mullenders, L. H., Masson, J.-Y., & van Attikum, H. (n.d.). A PALB2-interacting domain in RNF168 couples homologous recombination to DNA break-induced chromatin ubiquitylation. ELife, 6, e20922.

Lukas, C., Savic, V., Bekker-Jensen, S., Doil, C., Neumann, B., Sølvhøj Pedersen, R., Grøfte, M., Chan, K. L., Hickson, I. D., Bartek, J., & Lukas, J. (2011). 53BP1 nuclear bodies form around DNA lesions generated by mitotic transmission of chromosomes under replication stress. Nature Cell Biology, 13(3), 243–253.

Lüscher, B., Ahel, I., Altmeyer, M., Ashworth, A., Bai, P., Chang, P., Cohen, M., Corda, D., Dantzer, F., Daugherty, M. D., Dawson, T. M., Dawson, V. L., Deindl, S., Fehr, A. R., Feijs, K. L. H., Filippov, D. V., Gagné, J.-P., Grimaldi, G., Guettler, S., … Ziegler, M. (2022). ADP-ribosyltransferases, an update on function and nomenclature. The FEBS Journal, 289(23), 7399–7410.

Ma, J.-L., Kim, E. M., Haber, J. E., & Lee, S. E. (2003). Yeast Mre11 and Rad1 proteins define a Ku-independent mechanism to repair double-strand breaks lacking overlapping end sequences. Molecular and Cellular Biology, 23(23), 8820–8828.

Ma, Y., Lu, H., Tippin, B., Goodman, M. F., Shimazaki, N., Koiwai, O., Hsieh, C.-L., Schwarz, K., & Lieber, M. R. (2004). A biochemically defined system for mammalian nonhomologous DNA end joining. Molecular Cell, 16(5), 701–713.

Machwe, A., Xiao, L., Groden, J., & Orren, D. K. (2006). The Werner and Bloom syndrome proteins catalyze regression of a model replication fork. Biochemistry, 45(47), 13939–13946.

MacPherson, L., Tamblyn, L., Rajendra, S., Bralha, F., McPherson, J. P., & Matthews, J. (2013). 2,3,7,8-Tetrachlorodibenzo-p-dioxin poly(ADP-ribose) polymerase (TiPARP, ARTD14) is a mono-ADP-ribosyltransferase and repressor of aryl hydrocarbon receptor transactivation. Nucleic Acids Research, 41(3), 1604–1621.

Mailand, N., Falck, J., Lukas, C., Syljuâsen, R. G., Welcker, M., Bartek, J., & Lukas, J. (2000). Rapid destruction of human Cdc25A in response to DNA damage. Science (New York, N.Y.), 288(5470), 1425–1429.

Makarova, K. S., Grishin, N. V., Shabalina, S. A., Wolf, Y. I., & Koonin, E. V. (2006). A putative RNA-interference-based immune system in prokaryotes: Computational analysis of the predicted enzymatic machinery, functional analogies with eukaryotic RNAi, and hypothetical mechanisms of action. Biology Direct, 1(1), 7.

Makharashvili, N., Tubbs, A. T., Yang, S.-H., Wang, H., Barton, O., Zhou, Y., Deshpande, R. A., Lee, J.-H., Lobrich, M., Sleckman, B. P., Wu, X., & Paull, T. T. (2014). Catalytic and noncatalytic roles of the CtIP endonuclease in double-strand break end resection. Molecular Cell, 54(6), 1022–1033.

Malacaria, E., Pugliese, G. M., Honda, M., Marabitti, V., Aiello, F. A., Spies, M., Franchitto, A., & Pichierri, P. (2019). Rad52 prevents excessive replication fork reversal and protects from nascent strand degradation. Nature Communications, 10, 1412.

Mali, P., Yang, L., Esvelt, K. M., Aach, J., Guell, M., DiCarlo, J. E., Norville, J. E., & Church, G. M. (2013). RNA-Guided Human Genome Engineering via Cas9. Science (New York, N.Y.), 339(6121), 823–826.

Maloisel, L., Fabre, F., & Gangloff, S. (2008). DNA polymerase delta is preferentially recruited during homologous recombination to promote heteroduplex DNA extension. Molecular and Cellular Biology, 28(4), 1373–1382.

Mandemaker, I. K., van Cuijk, L., Janssens, R. C., Lans, H., Bezstarosti, K., Hoeijmakers, J. H., Demmers, J. A., Vermeulen, W., & Marteijn, J. A. (2017). DNA damage-induced histone H1 ubiquitylation is mediated by HUWE1 and stimulates the RNF8-RNF168 pathway. Scientific Reports, 7(1), 15353.

Mansour, W. Y., Rhein, T., & Dahm-Daphi, J. (2010). The alternative end-joining pathway for repair of DNA double-strand breaks requires PARP1 but is not dependent upon microhomologies. Nucleic Acids Research, 38(18), 6065–6077.

Mao, Z., Bozzella, M., Seluanov, A., & Gorbunova, V. (2008). DNA repair by nonhomologous end joining and homologous recombination during cell cycle in human cells. Cell Cycle (Georgetown, Tex.), 7(18), 2902–2906.

Marsischky, G. T., Wilson, B. A., & Collier, R. J. (1995). Role of glutamic acid 988 of human poly-ADP-ribose polymerase in polymer formation. Evidence for active site similarities to the ADP-ribosylating toxins. The Journal of Biological Chemistry, 270(7), 3247–3254.

Masani, S., Han, L., Meek, K., & Yu, K. (2016). Redundant function of DNA ligase 1 and 3 in alternative end-joining during immunoglobulin class switch recombination. Proceedings of the National Academy of Sciences, 113(5), 1261–1266.

Mason, J. M., Chan, Y.-L., Weichselbaum, R. W., & Bishop, D. K. (2019). Non-enzymatic roles of human RAD51 at stalled replication forks. Nature Communications, 10, 4410.

Mason, J. M., Dusad, K., Wright, W. D., Grubb, J., Budke, B., Heyer, W.-D., Connell, P. P., Weichselbaum, R. R., & Bishop, D. K. (2015). RAD54 family translocases counter genotoxic effects of RAD51 in human tumor cells. Nucleic Acids Research, 43(6), 3180–3196.

Masson, M., Niedergang, C., Schreiber, V., Muller, S., Menissier-de Murcia, J., & de Murcia, G. (1998). XRCC1 is specifically associated with poly(ADP-ribose) polymerase and negatively regulates its activity following DNA damage. Molecular and Cellular Biology, 18(6), 3563–3571.

Masson, J.-Y., Tarsounas, M. C., Stasiak, A. Z., Stasiak, A., Shah, R., McIlwraith, M. J., Benson, F. E., & West, S. C. (2001). Identification and purification of two distinct complexes containing the five RAD51 paralogs. Genes & Development, 15(24), 3296–3307.

Mateos-Gomez, P. A., Gong, F., Nair, N., Miller, K. M., Lazzerini-Denchi, E., & Sfeir, A. (2015). Mammalian polymerase θ promotes alternative NHEJ and suppresses recombination. Nature, 518(7538), 254–257.

Matsumoto, Y., & Kim, K. (1995). Excision of deoxyribose phosphate residues by DNA polymerase beta during DNA repair. Science (New York, N.Y.), 269(5224), 699–702.

Matsuoka, S., Ballif, B. A., Smogorzewska, A., McDonald, E. R., Hurov, K. E., Luo, J., Bakalarski, C. E., Zhao, Z., Solimini, N., Lerenthal, Y., Shiloh, Y., Gygi, S. P., & Elledge, S. J. (2007). ATM and ATR Substrate Analysis Reveals Extensive Protein Networks Responsive to DNA Damage. Science, 316(5828), 1160–1166.

Matthews, H. K., Bertoli, C., & de Bruin, R. A. M. (2022). Cell cycle control in cancer. Nature Reviews Molecular Cell Biology, 23(1), Article 1.

Maya-Mendoza, A., Moudry, P., Merchut-Maya, J. M., Lee, M., Strauss, R., & Bartek, J. (2018). High speed of fork progression induces DNA replication stress and genomic instability. Nature, 559(7713), 279–284.

McIntosh, D., & Blow, J. J. (2012). Dormant Origins, the Licensing Checkpoint, and the Response to Replicative Stresses. *Cold Spring Harbor Perspectives in Biology*, *4*(10), a012955.

Médard, G., Pachl, F., Ruprecht, B., Klaeger, S., Heinzlmeir, S., Helm, D., Qiao, H., Ku, X., Wilhelm, M., Kuehne, T., Wu, Z., Dittmann, A., Hopf, C., Kramer, K., & Kuster, B. (2015). Optimized Chemical Proteomics Assay for Kinase Inhibitor Profiling. Journal of Proteome Research, 14(3), 1574–1586.

Meek, K., Dang, V., & Lees-Miller, S. P. (2008). Chapter 2 DNA-PK: The Means to Justify the Ends? In Advances in Immunology (Vol. 99, pp. 33–58). Academic Press.

Meek, K., Douglas, P., Cui, X., Ding, Q., & Lees-Miller, S. P. (2007). Trans Autophosphorylation at DNA-Dependent Protein Kinase's Two Major Autophosphorylation Site Clusters Facilitates End Processing but Not End Joining. Molecular and Cellular Biology, 27(10), 3881–3890.

Mehrotra, P., Hollenbeck, A., Riley, J. P., Li, F., Patel, R. J., Akhtar, N., & Goenka, S. (2013). Poly (ADP-ribose) polymerase 14 and its enzyme activity regulates T(H)2 differentiation and allergic airway disease. The Journal of Allergy and Clinical Immunology, 131(2), 521-531.e1-12.

Mehrotra, P., Riley, J. P., Patel, R., Li, F., Voss, L., & Goenka, S. (2011). PARP-14 Functions as a Transcriptional Switch for Stat6-dependent Gene Activation. The Journal of Biological Chemistry, 286(3), 1767–1776.

Melander, F., Bekker-Jensen, S., Falck, J., Bartek, J., Mailand, N., & Lukas, J. (2008). Phosphorylation of SDT repeats in the MDC1 N terminus triggers retention of NBS1 at the DNA damage-modified chromatin. The Journal of Cell Biology, 181(2), 213–226.

Ménissier de Murcia, J., Ricoul, M., Tartier, L., Niedergang, C., Huber, A., Dantzer, F., Schreiber, V., Amé, J.-C., Dierich, A., LeMeur, M., Sabatier, L., Chambon, P., & de Murcia, G. (2003). Functional interaction between PARP-1 and PARP-2 in chromosome stability and embryonic development in mouse. The EMBO Journal, 22(9), 2255–2263.

Ménissier-de Murcia, J., Molinete, M., Gradwohl, G., Simonin, F., & de Murcia, G. (1989). Zinc-binding domain of poly(ADP-ribose)polymerase participates in the recognition of single strand breaks on DNA. Journal of Molecular Biology, 210(1), 229–233.

Meyer-Ficca, M. L., Ihara, M., Bader, J. J., Leu, N. A., Beneke, S., & Meyer, R. G. (2015). Spermatid head elongation with normal nuclear shaping requires ADP-ribosyltransferase PARP11 (ARTD11) in mice. Biology of Reproduction, 92(3), 80.

Mijic, S., Zellweger, R., Chappidi, N., Berti, M., Jacobs, K., Mutreja, K., Ursich, S., Ray Chaudhuri, A., Nussenzweig, A., Janscak, P., & Lopes, M. (2017). Replication fork reversal triggers fork degradation in BRCA2-defective cells. Nature Communications, 8(1), Article 1.

Mimori, T., Hardin, J. A., & Steitz, J. A. (1986). Characterization of the DNA-binding protein antigen Ku recognized by autoantibodies from patients with rheumatic disorders. The Journal of Biological Chemistry, 261(5), 2274–2278.

Minocherhomji, S., Ying, S., Bjerregaard, V. A., Bursomanno, S., Aleliunaite, A., Wu, W., Mankouri, H. W., Shen, H., Liu, Y., & Hickson, I. D. (2015). Replication stress activates DNA repair synthesis in mitosis. Nature, 528(7581), 286–290.

Mocanu, C., & Chan, K.-L. (2021). Mind the replication gap. Royal Society Open Science, 8(6), 201932.

Mochizuki, A. L., Katanaya, A., Hayashi, E., Hosokawa, M., Moribe, E., Motegi, A., Ishiai, M., Takata, M., Kondoh, G., Watanabe, H., Nakatsuji, N., & Chuma, S. (2017). PARI Regulates Stalled Replication Fork Processing To Maintain Genome Stability upon Replication Stress in Mice. Molecular and Cellular Biology, 37(23), e00117-17.

Mohiuddin, M., Evans, T. J., Rahman, M. M., Keka, I. S., Tsuda, M., Sasanuma, H., & Takeda, S. (2018). SUMOylation of PCNA by PIAS1 and PIAS4 promotes template switch in the chicken and human B cell lines. Proceedings of the National Academy of Sciences of the United States of America, 115(50), 12793–12798.

Mohni, K. N., Kavanaugh, G. M., & Cortez, D. (2014). ATR pathway inhibition is synthetically lethal in cancer cells with ERCC1 deficiency. Cancer Research, 74(10), 2835–2845.

Moldovan, G.-L., Dejsuphong, D., Petalcorin, M. I. R., Hofmann, K., Takeda, S., Boulton, S. J., & D'Andrea, A. D. (2012). Inhibition of homologous recombination by the PCNA-interacting protein PARI. Molecular Cell, 45(1), 75–86. h

Moreno, A., Carrington, J. T., Albergante, L., Mamun, M. A., Haagensen, E. J., Komseli, E.-S., Gorgoulis, V. G., Newman, T. J., & Blow, J. J. (2016). Unreplicated DNA remaining from unperturbed S phases passes through mitosis for resolution in daughter cells. Proceedings of the National Academy of Sciences, 113(39), E5757–E5764.

Mortusewicz, O., Amé, J.-C., Schreiber, V., & Leonhardt, H. (2007). Feedback-regulated poly(ADP-ribosyl)ation by PARP-1 is required for rapid response to DNA damage in living cells. *Nucleic Acids Research*, *35*(22), 7665–7675.

Motycka, T. A., Bessho, T., Post, S. M., Sung, P., & Tomkinson, A. E. (2004). Physical and functional interaction between the XPF/ERCC1 endonuclease and hRad52. The Journal of Biological Chemistry, 279(14), 13634–13639.

Mourón, S., Rodriguez-Acebes, S., Martínez-Jiménez, M. I., García-Gómez, S., Chocrón, S., Blanco, L., & Méndez, J. (2013). Repriming of DNA synthesis at stalled replication forks by human PrimPol. Nature Structural & Molecular Biology, 20(12), Article 12.

Mueller, P. R., Coleman, T. R., Kumagai, A., & Dunphy, W. G. (1995). Myt1: A membrane-associated inhibitory kinase that phosphorylates Cdc2 on both threonine-14 and tyrosine-15. Science (New York, N.Y.), 270(5233), 86–90.

Mueller-Dieckmann, C., Kernstock, S., Lisurek, M., von Kries, J. P., Haag, F., Weiss, M. S., & Koch-Nolte, F. (2006). The structure of human ADP-ribosylhydrolase 3 (ARH3) provides insights into the reversibility of protein ADP-ribosylation. Proceedings of the National Academy of Sciences, 103(41), 15026–15031.

Mukherjee, C., Tripathi, V., Manolika, E. M., Heijink, A. M., Ricci, G., Merzouk, S., de Boer, H. R., Demmers, J., van Vugt, M. A. T. M., & Ray Chaudhuri, A. (2019). RIF1 promotes replication fork protection and efficient restart to maintain genome stability. Nature Communications, 10(1), Article 1.

Munnur, D., Bartlett, E., Mikolčević, P., Kirby, I. T., Rack, J. G. M., Mikoč, A., Cohen, M. S., & Ahel, I. (2019). Reversible ADP-ribosylation of RNA. Nucleic Acids Research, 47(11), 5658–5669.

Muñoz, I. M., Hain, K., Déclais, A.-C., Gardiner, M., Toh, G. W., Sanchez-Pulido, L., Heuckmann, J. M., Toth, R., Macartney, T., Eppink, B., Kanaar, R., Ponting, C. P., Lilley, D. M. J., & Rouse, J. (2009). Coordination of Structure-Specific Nucleases by Human SLX4/BTBD12 Is Required for DNA Repair. Molecular Cell, 35(1), 116–127.

Murai, J., Huang, S. N., Das, B. B., Renaud, A., Zhang, Y., Doroshow, J. H., Ji, J., Takeda, S., & Pommier, Y. (2012). Differential trapping of PARP1 and PARP2 by clinical PARP inhibitors. Cancer Research, 72(21), 5588–5599.

Murai, J., Huang, S.-Y. N., Renaud, A., Zhang, Y., Ji, J., Takeda, S., Morris, J., Teicher, B., Doroshow, J. H., & Pommier, Y. (2014a). Stereospecific PARP trapping by BMN 673 and comparison with olaparib and rucaparib. Molecular Cancer Therapeutics, 13(2), 433–443.

Murai, J., Tang, S.-W., Leo, E., Baechler, S. A., Redon, C. E., Zhang, H., Al Abo, M., Rajapakse, V. N., Nakamura, E., Jenkins, L. M. M., Aladjem, M. I., & Pommier, Y. (2018). SLFN11 Blocks Stressed Replication Forks Independently of ATR. Molecular Cell, 69(3), 371-384.e6.

Murai, J., Zhang, Y., Morris, J., Ji, J., Takeda, S., Doroshow, J. H., & Pommier, Y. (2014b). Rationale for poly(ADP-ribose) polymerase (PARP) inhibitors in combination therapy with camptothecins or

temozolomide based on PARP trapping versus catalytic inhibition. The Journal of Pharmacology and Experimental Therapeutics, 349(3), 408–416.

Nagahama, M., Yamazoe, T., Hara, Y., Tani, K., Tsuji, A., & Tagaya, M. (2006). The AAA-ATPase NVL2 is a component of pre-ribosomal particles that interacts with the DExD/H-box RNA helicase DOB1. Biochemical and Biophysical Research Communications, 346(3), 1075–1082.

Nagy, Z., Kalousi, A., Furst, A., Koch, M., Fischer, B., & Soutoglou, E. (2016). Tankyrases Promote Homologous Recombination and Check Point Activation in Response to DSBs. PLOS Genetics, 12(2), e1005791.

Nakamura, K., Kustatscher, G., Alabert, C., Hödl, M., Forne, I., Völker-Albert, M., Satpathy, S., Beyer, T. E., Mailand, N., Choudhary, C., Imhof, A., Rappsilber, J., & Groth, A. (2021). Proteome dynamics at broken replication forks reveal a distinct ATM-directed repair response suppressing DNA double-strand break ubiquitination. Molecular Cell, 81(5), 1084-1099.e6.

Nakano, T., Takahashi-Nakaguchi, A., Yamamoto, M., & Watanabe, M. (2015). Pierisins and CARP-1: ADP-ribosylation of DNA by ARTCs in butterflies and shellfish. Current Topics in Microbiology and Immunology, 384, 127–149.

Newman, J. A., Cooper, C. D. O., Aitkenhead, H., & Gileadi, O. (2015). Structure of the Helicase Domain of DNA Polymerase Theta Reveals a Possible Role in the Microhomology-Mediated End-Joining Pathway. Structure(London, England:1993), 23(12), 2319–2330.

Nicolae, C. M., Aho, E. R., Choe, K. N., Constantin, D., Hu, H.-J., Lee, D., Myung, K., & Moldovan, G.-L. (2015). A novel role for the mono-ADP-ribosyltransferase PARP14/ARTD8 in promoting homologous recombination and protecting against replication stress. Nucleic Acids Research, 43(6), 3143–3153.

Nicolae, C. M., Aho, E. R., Vlahos, A. H. S., Choe, K. N., De, S., Karras, G. I., & Moldovan, G.-L. (2014). The ADP-ribosyltransferase PARP10/ARTD10 Interacts with Proliferating Cell Nuclear Antigen (PCNA) and Is Required for DNA Damage Tolerance. The Journal of Biological Chemistry, 289(19), 13627–13637.

Nieminuszczy, J., Broderick, R., Bellani, M. A., Smethurst, E., Schwab, R. A., Cherdyntseva, V., Evmorfopoulou, T., Lin, Y.-L., Minczuk, M., Pasero, P., Gagos, S., Seidman, M. M., & Niedzwiedz, W. (2019). EXD2 Protects Stressed Replication Forks and Is Required for Cell Viability in the Absence of BRCA1/2. Molecular Cell.

Nieminuszczy, J., Schwab, R. A., & Niedzwiedz, W. (2016). The DNA fibre technique – tracking helicases at work. Methods, 108, 92–98.

Niewolik, D., Pannicke, U., Lu, H., Ma, Y., Wang, L.-C. V., Kulesza, P., Zandi, E., Lieber, M. R., & Schwarz, K. (2006). DNA-PKcs dependence of Artemis endonucleolytic activity, differences between hairpins and 5' or 3' overhangs. The Journal of Biological Chemistry, 281(45), 33900–33909.

Nijman, S. M. B. (2011). Synthetic lethality: General principles, utility and detection using genetic screens in human cells. Febs Letters, 585(1), 1–6.

Nimonkar, A. V., Genschel, J., Kinoshita, E., Polaczek, P., Campbell, J. L., Wyman, C., Modrich, P., & Kowalczykowski, S. C. (2011). BLM-DNA2-RPA-MRN and EXO1-BLM-RPA-MRN constitute two DNA end resection machineries for human DNA break repair. Genes & Development, 25(4), 350–362.

Nimonkar, A. V., Ozsoy, A. Z., Genschel, J., Modrich, P., & Kowalczykowski, S. C. (2008). Human exonuclease 1 and BLM helicase interact to resect DNA and initiate DNA repair. Proceedings of the National Academy of Sciences of the United States of America, 105(44), 16906–16911.

Nitiss, J. L. (2009). DNA topoisomerase II and its growing repertoire of biological functions. Nature Reviews Cancer, 9(5), Article 5.

Niu, H., Chung, W.-H., Zhu, Z., Kwon, Y., Zhao, W., Chi, P., Prakash, R., Seong, C., Liu, D., Lu, L., Ira, G., & Sung, P. (2010). Mechanism of the ATP-dependent DNA end-resection machinery from Saccharomyces cerevisiae. Nature, 467(7311), Article 7311.

Noordermeer, S. M., Adam, S., Setiaputra, D., Barazas, M., Pettitt, S. J., Ling, A. K., Olivieri, M., Álvarez-Quilón, A., Moatti, N., Zimmermann, M., Annunziato, S., Krastev, D. B., Song, F., Brandsma, I., Frankum, J., Brough, R., Sherker, A., Landry, S., Szilard, R. K., … Durocher, D. (2018a). The Shieldin complex mediates 53BP1-dependent DNA repair. Nature, 560(7716), 117–121.

Nørregaard Jensen, O. (2004). Modification-specific proteomics: Characterization of post-translational modifications by mass spectrometry. Current Opinion in Chemical Biology, 8(1), 33–41.

Noy, T., Suad, O., Taglicht, D., & Ciechanover, A. (2012). HUWE1 ubiquitinates MyoD and targets it for proteasomal degradation. Biochemical and Biophysical Research Communications, 418(2), 408–413.

Ochi, T., Blackford, A. N., Coates, J., Jhujh, S., Mehmood, S., Tamura, N., Travers, J., Wu, Q., Draviam, V. M., Robinson, C. V., Blundell, T. L., & Jackson, S. P. (2015). DNA repair. PAXX, a paralog of XRCC4 and XLF, interacts with Ku to promote DNA double-strand break repair. Science (New York, N.Y.), 347(6218), 185–188.

O'Connell, M. J., Raleigh, J. M., Verkade, H. M., & Nurse, P. (1997). Chk1 is a wee1 kinase in the G2 DNA damage checkpoint inhibiting cdc2 by Y15 phosphorylation. The EMBO Journal, 16(3), 545–554.

O'Connor, P. J. (1981). Interaction of chemical carcinogens with macromolecules. Journal of Cancer Research and Clinical Oncology, 99(1–2), 167–186.

O'Connor, M. J., Thakar, T., Nicolae, C. M., & Moldovan, G.-L. (2021). PARP14 regulates cyclin D1 expression to promote cell-cycle progression. Oncogene, 40(30), 4872–4883.

O'Connor, T. R. (1993). Purification and characterization of human 3-methyladenine-DNA glycosylase. Nucleic Acids Research, 21(24), 5561–5569.

O'Donnell, L., Panier, S., Wildenhain, J., Tkach, J. M., Al-Hakim, A., Landry, M.-C., Escribano-Diaz, C., Szilard, R. K., Young, J. T. F., Munro, M., Canny, M. D., Kolas, N. K., Zhang, W., Harding, S. M., Ylanko, J., Mendez, M., Mullin, M., Sun, T., Habermann, B., … Durocher, D. (2010). The MMS22L-TONSL complex mediates recovery from replication stress and homologous recombination. Molecular Cell, 40(4), 619–631.

Ogata, N., Ueda, K., Kawaichi, M., & Hayaishi, O. (1981). Poly(ADP-ribose) synthetase, a main acceptor of poly(ADP-ribose) in isolated nuclei. *The Journal of Biological Chemistry*, *256*(9), 4135–4137.

Oka, S., Kato, J., & Moss, J. (2006). Identification and characterization of a mammalian 39-kDa poly(ADP-ribose) glycohydrolase. The Journal of Biological Chemistry, 281(2), 705–713.

Olivieri, M., & Durocher, D. (2021). Genome-scale chemogenomic CRISPR screens in human cells using the TKOv3 library. STAR Protocols, 2(1), 100321.

Orthwein, A., Fradet-Turcotte, A., Noordermeer, S. M., Canny, M. D., Brun, C. M., Strecker, J., Escribano-Diaz, C., & Durocher, D. (2014). Mitosis inhibits DNA double-strand break repair to guard against telomere fusions. *Science (New York, N.Y.)*, *344*(6180), 189–193.

Otto, H., Reche, P. A., Bazan, F., Dittmar, K., Haag, F., & Koch-Nolte, F. (2005). In silico characterization of the family of PARP-like poly(ADP-ribosyl)transferases (pARTs). BMC Genomics, 6, 139.

Otto, T., & Sicinski, P. (2017). Cell cycle proteins as promising targets in cancer therapy. Nature Reviews. Cancer, 17(2), 93–115.

Palazzo, L., Leidecker, O., Prokhorova, E., Dauben, H., Matic, I., & Ahel, I. (2018). Serine is the major residue for ADP-ribosylation upon DNA damage. ELife, 7.

Palazzo, L., Mikoč, A., & Ahel, I. (2017). ADP-ribosylation: New facets of an ancient modification. The Febs Journal, 284(18), 2932–2946.

Palazzo, L., Mikolčević, P., Mikoč, A., & Ahel, I. (2019). ADP-ribosylation signalling and human disease. Open Biology, 9(4), 190041.

Paniagua, I., Tayeh, Z., Falcone, M., Hernández Pérez, S., Cerutti, A., & Jacobs, J. J. L. (2022). MAD2L2 promotes replication fork protection and recovery in a shieldin-independent and REV3L-dependent manner. Nature Communications, 13(1), Article 1.

Panieri, E., & Santoro, M. M. (2016). ROS homeostasis and metabolism: A dangerous liason in cancer cells. Cell Death & Disease, 7(6), Article 6.

Panzarino, N. J., Krais, J. J., Cong, K., Peng, M., Mosqueda, M., Nayak, S. U., Bond, S. M., Calvo, J. A., Doshi, M. B., Bere, M., Ou, J., Deng, B., Zhu, L. J., Johnson, N., & Cantor, S. B. (2021). Replication Gaps Underlie BRCA Deficiency and Therapy Response. Cancer Research, 81(5), 1388–1397.

Park, S. H., Kang, N., Song, E., Wie, M., Lee, E. A., Hwang, S., Lee, D., Ra, J. S., Park, I. B., Park, J., Kang, S., Park, J. H., Hohng, S., Lee, K., & Myung, K. (2019). ATAD5 promotes replication restart by regulating RAD51 and PCNA in response to replication stress. Nature Communications, 10(1), 1–15.

Parker, L. L., & Piwnica-Worms, H. (1992). Inactivation of the p34cdc2-cyclin B complex by the human WEE1 tyrosine kinase. Science (New York, N.Y.), 257(5078), 1955–1957.

Parsons, J. L., Tait, P. S., Finch, D., Dianova, I. I., Edelmann, M. J., Khoronenkova, S. V., Kessler, B. M., Sharma, R. A., McKenna, W. G., & Dianov, G. L. (2009). Ubiquitin ligase ARF-BP1/Mule modulates base excision repair. The EMBO Journal, 28(20), 3207–3215.

Pascucci, B., Maga, G., Hübscher, U., Bjoras, M., Seeberg, E., Hickson, I. D., Villani, G., Giordano, C., Cellai, L., & Dogliotti, E. (2002). Reconstitution of the base excision repair pathway for 7,8-dihydro-8-oxoguanine with purified human proteins. *Nucleic Acids Research*, *30*(10), 2124–2130.

Patel, A. G., Sarkaria, J. N., & Kaufmann, S. H. (2011). Nonhomologous end joining drives poly(ADP-ribose) polymerase (PARP) inhibitor lethality in homologous recombination-deficient cells. Proceedings of the National Academy of Sciences of the United States of America, 108(8), 3406–3411.

Peng, C.-Y., Graves, P. R., Thoma, R. S., Wu, Z., Shaw, A. S., & Piwnica-Worms, H. (1997). Mitotic and G2 Checkpoint Control: Regulation of 14-3-3 Protein Binding by Phosphorylation of Cdc25C on Serine-216. Science, 277(5331), 1501–1505.

Petermann, E., & Helleday, T. (2010). Pathways of mammalian replication fork restart. Nature Reviews Molecular Cell Biology, 11(10), Article 10.

Petermann, E., Orta, M. L., Issaeva, N., Schultz, N., & Helleday, T. (2010). Hydroxyurea-Stalled Replication Forks Become Progressively Inactivated and Require Two Different RAD51-Mediated Pathways for Restart and Repair. Molecular Cell, 37(4), 492–502.

Pettitt, S. J., Krastev, D. B., Brandsma, I., Dréan, A., Song, F., Aleksandrov, R., Harrell, M. I., Menon, M., Brough, R., Campbell, J., Frankum, J., Ranes, M., Pemberton, H. N., Rafiq, R., Fenwick, K., Swain, A., Guettler, S., Lee, J.-M., Swisher, E. M., … Lord, C. J. (2018). Genome-wide and high-density CRISPR-Cas9 screens identify point mutations in PARP1 causing PARP inhibitor resistance. Nature Communications, 9(1),

Piberger, A. L., Bowry, A., Kelly, R. D. W., Walker, A. K., González-Acosta, D., Bailey, L. J., Doherty, A. J., Méndez, J., Morris, J. R., Bryant, H. E., & Petermann, E. (2020). PrimPol-dependent single-stranded gap formation mediates homologous recombination at bulky DNA adducts. Nature Communications, 11(1), Article 1.

Pickar-Oliver, A., & Gersbach, C. A. (2019). The next generation of CRISPR–Cas technologies and applications. Nature Reviews Molecular Cell Biology, 20(8), 490–507.

Pilié, P. G., Tang, C., Mills, G. B., & Yap, T. A. (2019). State-of-the-art strategies for targeting the DNA damage response in cancer. Nature Reviews Clinical Oncology, 16(2), Article 2.

Piwko, W., Mlejnkova, L. J., Mutreja, K., Ranjha, L., Stafa, D., Smirnov, A., Brodersen, M. M., Zellweger, R., Sturzenegger, A., Janscak, P., Lopes, M., Peter, M., & Cejka, P. (2016). The MMS22L-TONSL heterodimer directly promotes RAD51-dependent recombination upon replication stress. The EMBO Journal, 35(23), 2584–2601.

Pizzi, S., Sertic, S., Orcesi, S., Cereda, C., Bianchi, M., Jackson, A. P., Lazzaro, F., Plevani, P., & Muzi-Falconi, M. (2015). Reduction of hRNase H2 activity in Aicardi–Goutières syndrome cells leads to replication stress and genome instability. Human Molecular Genetics, 24(3), 649–658.

Pogozelski, W. K., & Tullius, T. D. (1998). Oxidative Strand Scission of Nucleic Acids: Routes Initiated by Hydrogen Abstraction from the Sugar Moiety. Chemical Reviews, 98(3), 1089–1108.

Poirier, G. G., de Murcia, G., Jongstra-Bilen, J., Niedergang, C., & Mandel, P. (1982). Poly(ADP-ribosyl)ation of polynucleosomes causes relaxation of chromatin structure. Proceedings of the National Academy of Sciences of the United States of America, 79(11), 3423–3427.

Polo, L. M., Xu, Y., Hornyak, P., Garces, F., Zeng, Z., Hailstone, R., Matthews, S. J., Caldecott, K. W., Oliver, A. W., & Pearl, L. H. (2019). Efficient Single-Strand Break Repair Requires Binding to Both Poly(ADP-Ribose) and DNA by the Central BRCT Domain of XRCC1. Cell Reports, 26(3), 573-581.e5.

Polyak, K., Kato, J. Y., Solomon, M. J., Sherr, C. J., Massague, J., Roberts, J. M., & Koff, A. (1994). P27Kip1, a cyclin-Cdk inhibitor, links transforming growth factor-beta and contact inhibition to cell cycle arrest. Genes & Development, 8(1), 9–22.

Pommier, Y., Redon, C., Rao, V. A., Seiler, J. A., Sordet, O., Takemura, H., Antony, S., Meng, L., Liao, Z., Kohlhagen, G., Zhang, H., & Kohn, K. W. (2003). Repair of and checkpoint response to topoisomerase I-mediated DNA damage. Mutation Research, 532(1–2), 173–203.

Postow, L., Ghenoiu, C., Woo, E. M., Krutchinsky, A. N., Chait, B. T., & Funabiki, H. (2008). Ku80 removal from DNA through double strand break–induced ubiquitylation. Journal of Cell Biology, 182(3), 467–479.

Povirk, L. F. (1996). DNA damage and mutagenesis by radiomimetic DNA-cleaving agents: Bleomycin, neocarzinostatin and other enediynes. Mutation Research/Fundamental and Molecular Mechanisms of Mutagenesis, 355(1), 71–89.

Povirk, L. F., Zhou, T., Zhou, R., Cowan, M. J., & Yannone, S. M. (2007). Processing of 3'-phosphoglycolate-terminated DNA double strand breaks by Artemis nuclease. The Journal of Biological Chemistry, 282(6), 3547–3558.

Pryor, J. M., Waters, C. A., Aza, A., Asagoshi, K., Strom, C., Mieczkowski, P. A., Blanco, L., & Ramsden, D. A. (2015). Essential role for polymerase specialization in cellular nonhomologous end joining. Proceedings of the National Academy of Sciences of the United States of America, 112(33), E4537-4545.

Przetocka, S., Porro, A., Bolck, H. A., Walker, C., Lezaja, A., Trenner, A., von Aesch, C., Himmels, S.-F., D'Andrea, A. D., Ceccaldi, R., Altmeyer, M., & Sartori, A. A. (2018). CtIP-Mediated Fork Protection Synergizes with BRCA1 to Suppress Genomic Instability upon DNA Replication Stress. Molecular Cell, 72(3), 568-582.e6.

Quénet, D., Gasser, V., Fouillen, L., Cammas, F., Sanglier-Cianferani, S., Losson, R., & Dantzer, F. (2008). The histone subcode: Poly(ADP-ribose) polymerase-1 (Parp-1) and Parp-2 control cell differentiation by regulating the transcriptional intermediary factor TIF1beta and the heterochromatin

protein HP1alpha. FASEB Journal: Official Publication of the Federation of American Societies for Experimental Biology, 22(11), 3853–3865.

Quinet, A., Tirman, S., Cybulla, E., Meroni, A., & Vindigni, A. (2021). To skip or not to skip: Choosing repriming to tolerate DNA damage. Molecular Cell, 81(4), 649–658.

Quinet, A., Tirman, S., Jackson, J., Šviković, S., Lemaçon, D., Carvajal-Maldonado, D., González-Acosta, D., Vessoni, A. T., Cybulla, E., Wood, M., Tavis, S., Batista, L. F. Z., Méndez, J., Sale, J. E., & Vindigni, A. (2020). PRIMPOL-Mediated Adaptive Response Suppresses Replication Fork Reversal in BRCA-Deficient Cells. Molecular Cell, 77(3), 461-474.e9.

Rack, J. G. M., Liu, Q., Zorzini, V., Voorneveld, J., Ariza, A., Honarmand Ebrahimi, K., Reber, J. M., Krassnig, S. C., Ahel, D., van der Marel, G. A., Mangerich, A., McCullagh, J. S. O., Filippov, D. V., & Ahel, I. (2021). Mechanistic insights into the three steps of poly(ADP-ribosylation) reversal. Nature Communications, 12(1), Article 1.

Raderschall, E., Golub, E. I., & Haaf, T. (1999). Nuclear foci of mammalian recombination proteins are located at single-stranded DNA regions formed after DNA damage. Proceedings of the National Academy of Sciences, 96(5), 1921–1926.

Radicella, J. P., Dherin, C., Desmaze, C., Fox, M. S., & Boiteux, S. (1997). Cloning and characterization of hOGG1, a human homolog of the OGG1 gene of Saccharomyces cerevisiae. Proceedings of the National Academy of Sciences of the United States of America, 94(15), 8010–8015.

Ramsden, D. A., Carvajal-Garcia, J., & Gupta, G. P. (2022). Mechanism, cellular functions and cancer roles of polymerase-theta-mediated DNA end joining. Nature Reviews Molecular Cell Biology, 23(2), Article 2.

Ranjha, L., Howard, S. M., & Cejka, P. (2018). Main steps in DNA double-strand break repair: An introduction to homologous recombination and related processes. Chromosoma, 127(2), 187–214.

Rao, Q., Liu, M., Tian, Y., Wu, Z., Hao, Y., Song, L., Qin, Z., Ding, C., Wang, H.-W., Wang, J., & Xu, Y. (2018). Cryo-EM structure of human ATR-ATRIP complex. Cell Research, 28(2), Article 2.

Rass, U., Compton, S. A., Matos, J., Singleton, M. R., Ip, S. C. Y., Blanco, M. G., Griffith, J. D., & West, S. C. (2010). Mechanism of Holliday junction resolution by the human GEN1 protein. Genes & Development, 24(14), 1559–1569.

Ray Chaudhuri, A., Callen, E., Ding, X., Gogola, E., Duarte, A. A., Lee, J.-E., Wong, N., Lafarga, V., Calvo, J. A., Panzarino, N. J., John, S., Day, A., Crespo, A. V., Shen, B., Starnes, L. M., Ruiter, J. R. de, Daniel, J. A., Konstantinopoulos, P. A., Cortez, D., … Nussenzweig, A. (2016). Replication fork stability confers chemoresistance in BRCA-deficient cells. Nature, 535(7612), 382–387.

Ray Chaudhuri, A., Hashimoto, Y., Herrador, R., Neelsen, K. J., Fachinetti, D., Bermejo, R., Cocito, A., Costanzo, V., & Lopes, M. (2012). Topoisomerase I poisoning results in PARP-mediated replication fork reversal. Nature Structural & Molecular Biology, 19(4), 417–423.

Reynolds, J. J., El-Khamisy, S. F., Katyal, S., Clements, P., McKinnon, P. J., & Caldecott, K. W. (2009). Defective DNA ligation during short-patch single-strand break repair in ataxia oculomotor apraxia 1. Molecular and Cellular Biology, 29(5), 1354–1362.

Richman, T. R., Ermer, J. A., Davies, S. M. K., Perks, K. L., Viola, H. M., Shearwood, A.-M. J., Hool, L. C., Rackham, O., & Filipovska, A. (2015). Mutation in MRPS34 Compromises Protein Synthesis and Causes Mitochondrial Dysfunction. PLOS Genetics, 11(3), e1005089.

Robert, X., & Gouet, P. (2014). Deciphering key features in protein structures with the new ENDscript server. Nucleic Acids Research, 42(Web Server issue), W320-324.

Rogakou, E. P., Pilch, D. R., Orr, A. H., Ivanova, V. S., & Bonner, W. M. (1998). DNA Double-stranded Breaks Induce Histone H2AX Phosphorylation on Serine 139 *. Journal of Biological Chemistry, 273(10), 5858–5868.

Rolli, V., O'Farrell, M., Ménissier-de Murcia, J., & de Murcia, G. (1997). Random mutagenesis of the poly(ADP-ribose) polymerase catalytic domain reveals amino acids involved in polymer branching. Biochemistry, 36(40), 12147–12154.

Rondinelli, B., Gogola, E., Yücel, H., Duarte, A. A., van de Ven, M., van der Sluijs, R., Konstantinopoulos, P. A., Jonkers, J., Ceccaldi, R., Rottenberg, S., & D'Andrea, A. D. (2017). EZH2 promotes degradation of stalled replication forks by recruiting MUS81 through histone H3 trimethylation. Nature Cell Biology, 19(11), 1371–1378.

Ronson, G. (2017). Investigation into the relationship between PARPs in DNA repair and synthetic lethality with homologous recombination deficiency, University of Oxford.

Ronson, G. E., Piberger, A. L., Higgs, M. R., Olsen, A. L., Stewart, G. S., McHugh, P. J., Petermann, E., & Lakin, N. D. (2018). PARP1 and PARP2 stabilise replication forks at base excision repair intermediates through Fbh1-dependent Rad51 regulation. Nature Communications, 9(1), 746.

Ropars, V., Drevet, P., Legrand, P., Baconnais, S., Amram, J., Faure, G., Márquez, J. A., Piétrement, O., Guerois, R., Callebaut, I., Le Cam, E., Revy, P., de Villartay, J.-P., & Charbonnier, J.-B. (2011). Structural characterization of filaments formed by human Xrcc4–Cernunnos/XLF complex involved in nonhomologous DNA end-joining. Proceedings of the National Academy of Sciences, 108(31), 12663–12668.

Rosenthal, F., Feijs, K. L. H., Frugier, E., Bonalli, M., Forst, A. H., Imhof, R., Winkler, H. C., Fischer, D., Caflisch, A., Hassa, P. O., Lüscher, B., & Hottiger, M. O. (2013). Macrodomain-containing proteins are new mono-ADP-ribosylhydrolases. Nature Structural & Molecular Biology, 20(4), Article 4.

Rothenberg, E., Grimme, J. M., Spies, M., & Ha, T. (2008). Human Rad52-mediated homology search and annealing occurs by continuous interactions between overlapping nucleoprotein complexes. Proceedings of the National Academy of Sciences, 105(51), 20274–20279.

Rottenberg, S., Jaspers, J. E., Kersbergen, A., van der Burg, E., Nygren, A. O. H., Zander, S. A. L., Derksen, P. W. B., de Bruin, M., Zevenhoven, J., Lau, A., Boulter, R., Cranston, A., O'Connor, M. J., Martin, N. M. B., Borst, P., & Jonkers, J. (2008). High sensitivity of BRCA1-deficient mammary tumors to the PARP inhibitor AZD2281 alone and in combination with platinum drugs. Proceedings of the National Academy of Sciences of the United States of America, 105(44), 17079–17084.

Rouleau, M., McDonald, D., Gagné, P., Ouellet, M.-E., Droit, A., Hunter, J. M., Dutertre, S., Prigent, C., Hendzel, M. J., & Poirier, G. G. (2007). PARP-3 associates with polycomb group bodies and with components of the DNA damage repair machinery. Journal of Cellular Biochemistry, 100(2), 385–401.

Roy, S., de Melo, A. J., Xu, Y., Tadi, S. K., Négrel, A., Hendrickson, E., Modesti, M., & Meek, K. (2015). XRCC4/XLF Interaction Is Variably Required for DNA Repair and Is Not Required for Ligase IV Stimulation. Molecular and Cellular Biology, 35(17), 3017–3028.

Roy, S., Luzwick, J. W., & Schlacher, K. (2018). SIRF: Quantitative in situ analysis of protein interactions at DNA replication forks. The Journal of Cell Biology, 217(4), 1521–1536.

Roy, S., Tomaszowski, K.-H., Luzwick, J. W., Park, S., Li, J., Murphy, M., & Schlacher, K. (2018a). P53 orchestrates DNA replication restart homeostasis by suppressing mutagenic RAD52 and POLθ pathways. ELife, 7, e31723.

Rudolph, J., Muthurajan, U. M., Palacio, M., Mahadevan, J., Roberts, G., Erbse, A. H., Dyer, P. N., & Luger, K. (2021). The BRCT domain of PARP1 binds intact DNA and mediates intrastrand transfer. Molecular Cell, 81(24), 4994-5006.e5.

Ruf, A., Rolli, V., de Murcia, G., & Schulz, G. E. (1998). The mechanism of the elongation and branching reaction of poly(ADP-ribose) polymerase as derived from crystal structures and mutagenesis. Journal of Molecular Biology, 278(1), 57–65.

Rulten, S. L., Fisher, A. E. O., Robert, I., Zuma, M. C., Rouleau, M., Ju, L., Poirier, G., Reina-San-Martin, B., & Caldecott, K. W. (2011). PARP-3 and APLF Function Together to Accelerate Nonhomologous End-Joining. Molecular Cell, 41(1), 33–45.

Ruscetti, T., Lehnert, B. E., Halbrook, J., Trong, H. L., Hoekstra, M. F., Chen, D. J., & Peterson, S. R. (1998). Stimulation of the DNA-dependent Protein Kinase by Poly(ADP-Ribose) Polymerase *. Journal of Biological Chemistry, 273(23), 14461–14467.

Russo, A. A., Tong, L., Lee, J. O., Jeffrey, P. D., & Pavletich, N. P. (1998). Structural basis for inhibition of the cyclin-dependent kinase Cdk6 by the tumour suppressor p16INK4a. Nature, 395(6699), 237–243.

Saha, L. K., Murai, Y., Saha, S., Jo, U., Tsuda, M., Takeda, S., & Pommier, Y. (2021). Replication-dependent cytotoxicity and Spartan-mediated repair of trapped PARP1–DNA complexes. Nucleic Acids Research, 49(18), 10493–10506.

Saini, N., Ramakrishnan, S., Elango, R., Ayyar, S., Zhang, Y., Deem, A., Ira, G., Haber, J. E., Lobachev, K. S., & Malkova, A. (2013). Migrating bubble during break-induced replication drives conservative DNA synthesis. Nature, 502(7471), Article 7471.

Saintigny, Y., Delacôte, F., Varès, G., Petitot, F., Lambert, S., Averbeck, D., & Lopez, B. S. (2001). Characterization of homologous recombination induced by replication inhibition in mammalian cells. The EMBO Journal, 20(14), 3861–3870.

Saldivar, J. C., Cortez, D., & Cimprich, K. A. (2017). The essential kinase ATR: Ensuring faithful duplication of a challenging genome. Nature Reviews Molecular Cell Biology, 18(10), 622–636.

Sanchez, Y., Wong, C., Thoma, R. S., Richman, R., Wu, Z., Piwnica-Worms, H., & Elledge, S. J. (1997). Conservation of the Chk1 Checkpoint Pathway in Mammals: Linkage of DNA Damage to Cdk Regulation Through Cdc25. Science, 277(5331), 1497–1501.

Sander, B., Xu, W., Eilers, M., Popov, N., & Lorenz, S. (2017). A conformational switch regulates the ubiquitin ligase HUWE1. ELife, 6, e21036.

Saredi, G., Huang, H., Hammond, C. M., Alabert, C., Bekker-Jensen, S., Forne, I., Reverón-Gómez, N., Foster, B. M., Mlejnkova, L., Bartke, T., Cejka, P., Mailand, N., Imhof, A., Patel, D. J., & Groth, A. (2016). H4K20me0 marks post-replicative chromatin and recruits the TONSL–MMS22L DNA repair complex. Nature, 534(7609), Article 7609.

Sassa, A., Yasui, M., & Honma, M. (2019). Current perspectives on mechanisms of ribonucleotide incorporation and processing in mammalian DNA. Genes and Environment, 41(1), 3.

Sato, K., Ishiai, M., Toda, K., Furukoshi, S., Osakabe, A., Tachiwana, H., Takizawa, Y., Kagawa, W., Kitao, H., Dohmae, N., Obuse, C., Kimura, H., Takata, M., & Kurumizaka, H. (2012). Histone chaperone activity of Fanconi anemia proteins, FANCD2 and FANCI, is required for DNA crosslink repair. The EMBO Journal, 31(17), 3524–3536.

Satoh, M. S., & Lindahl, T. (1992). Role of poly(ADP-ribose) formation in DNA repair. Nature, 356(6367), Article 6367.

Savitsky, K., Bar-Shira, A., Gilad, S., Rotman, G., Ziv, Y., Vanagaite, L., Tagle, D. A., Smith, S., Uziel, T., Sfez, S., Ashkenazi, M., Pecker, I., Frydman, M., Harnik, R., Patanjali, S. R., Simmons, A., Clines, G. A., Sartiel, A., Gatti, R. A., … Shiloh, Y. (1995). A single ataxia telangiectasia gene with a product similar to PI-3 kinase. Science (New York, N.Y.), 268(5218), 1749–1753.

Saxena, A., Wong, L. H., Kalitsis, P., Earle, E., Shaffer, L. G., & Choo, K. H. A. (2002). Poly(ADP-ribose) polymerase 2 localizes to mammalian active centromeres and interacts with PARP-1, Cenpa, Cenpb and Bub3, but not Cenpc. Human Molecular Genetics, 11(19), 2319–2329.

Sbodio, J. I., Lodish, H. F., & Chi, N.-W. (2002). Tankyrase-2 oligomerizes with tankyrase-1 and binds to both TRF1 (telomere-repeat-binding factor 1) and IRAP (insulin-responsive aminopeptidase). The Biochemical Journal, 361(Pt 3), 451–459.

Schlacher, K., Christ, N., Siaud, N., Egashira, A., Wu, H., & Jasin, M. (2011). Double-strand break repair-independent role for BRCA2 in blocking stalled replication fork degradation by MRE11. Cell, 145(4), 529–542.

Schlacher, K., Wu, H., & Jasin, M. (2012). A Distinct Replication Fork Protection Pathway Connects Fanconi Anemia Tumor Suppressors to RAD51-BRCA1/2. Cancer Cell, 22(1), 106–116.

Schleicher, E. M., Dhoonmoon, A., Jackson, L. M., Khatib, J. B., Nicolae, C. M., & Moldovan, G.-L. (2022). The TIP60-ATM axis regulates replication fork stability in BRCA-deficient cells. Oncogenesis, 11(1), Article 1.

Schleicher, E. M., Galvan, A. M., Imamura-Kawasawa, Y., Moldovan, G.-L., & Nicolae, C. M. (2018). PARP10 promotes cellular proliferation and tumorigenesis by alleviating replication stress. Nucleic Acids Research, 46(17), 8908–8916.

Schmid, J. A., Berti, M., Walser, F., Raso, M. C., Schmid, F., Krietsch, J., Stoy, H., Zwicky, K., Ursich, S., Freire, R., Lopes, M., & Penengo, L. (2018). Histone Ubiquitination by the DNA Damage Response Is Required for Efficient DNA Replication in Unperturbed S Phase. Molecular Cell, 71(6), 897-910.e8.

Schreiber, V., Amé, J.-C., Dollé, P., Schultz, I., Rinaldi, B., Fraulob, V., Murcia, J. M., & Murcia, G. de. (2002). Poly(ADP-ribose) Polymerase-2 (PARP-2) Is Required for Efficient Base Excision DNA Repair in Association with PARP-1 and XRCC1 *. *Journal of Biological Chemistry*, *277*(25), 23028–23036.

Schubert, L., Ho, T., Hoffmann, S., Haahr, P., Guérillon, C., & Mailand, N. (2017). RADX interacts with single-stranded DNA to promote replication fork stability. EMBO Reports, 18(11), 1991–2003.

Schultz, N., Lopez, E., Saleh-Gohari, N., & Helleday, T. (2003). Poly(ADP-ribose) polymerase (PARP-1) has a controlling role in homologous recombination. Nucleic Acids Research, 31(17), 4959–4964.

Schützenhofer, K., Rack, J. G. M., & Ahel, I. (2021). The Making and Breaking of Serine-ADP-Ribosylation in the DNA Damage Response. Frontiers in Cell and Developmental Biology, 9, 745922.

Schwab, R. A., Nieminuszczy, J., Shah, F., Langton, J., Lopez Martinez, D., Liang, C.-C., Cohn, M. A., Gibbons, R. J., Deans, A. J., & Niedzwiedz, W. (2015). The Fanconi Anemia Pathway Maintains Genome Stability by Coordinating Replication and Transcription. Molecular Cell, 60(3), 351–361.

Schwab, R. A., Nieminuszczy, J., Shin-ya, K., & Niedzwiedz, W. (2013). FANCJ couples replication past natural fork barriers with maintenance of chromatin structure. The Journal of Cell Biology, 201(1), 33–48.

Scully, R., Panday, A., Elango, R., & Willis, N. A. (2019). DNA double-strand break repair-pathway choice in somatic mammalian cells. Nature Reviews Molecular Cell Biology, 20(11), 698–714.

Sears, R. M., May, D. G., & Roux, K. J. (2019). BioID as a Tool for Protein-Proximity Labeling in Living Cells. Methods in Molecular Biology (Clifton, N.J.), 2012, 299–313.

Seimiya, H., & Smith, S. (2002). The telomeric poly(ADP-ribose) polymerase, tankyrase 1, contains multiple binding sites for telomeric repeat binding factor 1 (TRF1) and a novel acceptor, 182-kDa tankyrase-binding protein (TAB182). The Journal of Biological Chemistry, 277(16), 14116–14126.

Seki, M., Marini, F., & Wood, R. D. (2003). POLQ (Pol theta), a DNA polymerase and DNA-dependent ATPase in human cells. Nucleic Acids Research, 31(21), 6117–6126.

Sekiguchi, J., & Shuman, S. (1997). Site-specific ribonuclease activity of eukaryotic DNA topoisomerase I. Molecular Cell, 1(1), 89–97.

Seo, G. J., Kincaid, R. P., Phanaksri, T., Burke, J. M., Pare, J. M., Cox, J. E., Hsiang, T.-Y., Krug, R. M., & Sullivan, C. S. (2013). Reciprocal inhibition between intracellular antiviral signaling and the RNAi machinery in mammalian cells. Cell Host & Microbe, 14(4), 10.1016/j.chom.2013.09.002.

Serrano, M., Hannon, G. J., & Beach, D. (1993). A new regulatory motif in cell-cycle control causing specific inhibition of cyclin D/CDK4. Nature, 366(6456), Article 6456.

Shah Punatar, R., Martin, M. J., Wyatt, H. D. M., Chan, Y. W., & West, S. C. (2017). Resolution of single and double Holliday junction recombination intermediates by GEN1. Proceedings of the National Academy of Sciences of the United States of America, 114(3), 443–450.

Shahrour, M. A., Nicolae, C. M., Edvardson, S., Ashhab, M., Galvan, A. M., Constantin, D., Abu-Libdeh, B., Moldovan, G.-L., & Elpeleg, O. (2016). PARP10 deficiency manifests by infantile neurodegeneration and DNA repair defect. Neurogenetics, 17(4), 227–232.

Shalem, O., Sanjana, N. E., Hartenian, E., Shi, X., Scott, D. A., Mikkelson, T., Heckl, D., Ebert, B. L., Root, D. E., Doench, J. G., & Zhang, F. (2014). Genome-Scale CRISPR-Cas9 Knockout Screening in Human Cells. Science (New York, N.Y.), 343(6166), 84–87.

Shao, Z., Lee, B. J., Rouleau-Turcotte, É., Langelier, M.-F., Lin, X., Estes, V. M., Pascal, J. M., & Zha, S. (2020). Clinical PARP inhibitors do not abrogate PARP1 exchange at DNA damage sites in vivo. Nucleic Acids Research, 48(17), 9694–9709.

Sharifi, R., Morra, R., Appel, C. D., Tallis, M., Chioza, B., Jankevicius, G., Simpson, M. A., Matic, I., Ozkan, E., Golia, B., Schellenberg, M. J., Weston, R., Williams, J. G., Rossi, M. N., Galehdari, H., Krahn, J., Wan, A., Trembath, R. C., Crosby, A. H., … Ahel, I. (2013). Deficiency of terminal ADP-ribose protein glycohydrolase TARG1/C6orf130 in neurodegenerative disease. The EMBO Journal, 32(9), 1225–1237.

Shibata, A. (2017). Regulation of repair pathway choice at two-ended DNA double-strand breaks. Mutation Research/Fundamental and Molecular Mechanisms of Mutagenesis, 803–805, 51–55.

Shiloh, Y., & Ziv, Y. (2013). The ATM protein kinase: Regulating the cellular response to genotoxic stress, and more. Nature Reviews Molecular Cell Biology, 14(4), Article 4.

Shiotani, B., Nguyen, H. D., Håkansson, P., Maréchal, A., Tse, A., Tahara, H., & Zou, L. (2013). Two Distinct Modes of ATR Activation Orchestrated by Rad17 and Nbs1. Cell Reports, 3(5), 1651–1662.

Shorrocks, A.-M. K., Jones, S. E., Tsukada, K., Morrow, C. A., Belblidia, Z., Shen, J., Vendrell, I., Fischer, R., Kessler, B. M., & Blackford, A. N. (2021). The Bloom syndrome complex senses RPA-coated single-stranded DNA to restart stalled replication forks. Nature Communications, 12(1), Article 1.

Sievers, F., Barton, G. J., & Higgins, D. G. (2020). Multiple Sequence Alignments. In A. D. Baxevanis, G. D. Bader, & D. S. Wishart (Eds.), Bioinformatics (pp. 227–250). Wiley.

Sievers, F., & Higgins, D. G. (2018). Clustal Omega for making accurate alignments of many protein sequences. Protein Science: A Publication of the Protein Society, 27(1), 135–145.

Sievers, F., Wilm, A., Dineen, D., Gibson, T. J., Karplus, K., Li, W., Lopez, R., McWilliam, H., Remmert, M., Söding, J., Thompson, J. D., & Higgins, D. G. (2011). Fast, scalable generation of high-quality protein multiple sequence alignments using Clustal Omega. Molecular Systems Biology, 7, 539.

Sigurdsson, S., Van Komen, S., Bussen, W., Schild, D., Albala, J. S., & Sung, P. (2001). Mediator function of the human Rad51B–Rad51C complex in Rad51/RPA-catalyzed DNA strand exchange. Genes & Development, 15(24), 3308–3318.

Simandlova, J., Zagelbaum, J., Payne, M. J., Chu, W. K., Shevelev, I., Hanada, K., Chatterjee, S., Reid, D. A., Liu, Y., Janscak, P., Rothenberg, E., & Hickson, I. D. (2013). FBH1 Helicase Disrupts RAD51 Filaments in Vitro and Modulates Homologous Recombination in Mammalian Cells. The Journal of Biological Chemistry, 288(47), 34168–34180.

Simoneau, A., Xiong, R., & Zou, L. (2021). The trans cell cycle effects of PARP inhibitors underlie their selectivity toward BRCA1/2-deficient cells. Genes & Development, 35(17–18), 1271–1289.

Simsek, D., Brunet, E., Wong, S. Y.-W., Katyal, S., Gao, Y., McKinnon, P. J., Lou, J., Zhang, L., Li, J., Rebar, E. J., Gregory, P. D., Holmes, M. C., & Jasin, M. (2011). DNA Ligase III Promotes Alternative Nonhomologous End-Joining during Chromosomal Translocation Formation. PLOS Genetics, 7(6), e1002080.

Singh, J. K., Smith, R., Rother, M. B., de Groot, A. J. L., Wiegant, W. W., Vreeken, K., D'Augustin, O., Kim, R. Q., Qian, H., Krawczyk, P. M., González-Prieto, R., Vertegaal, A. C. O., Lamers, M., Huet, S., & van Attikum, H. (2021). Zinc finger protein ZNF384 is an adaptor of Ku to DNA during classical non-homologous end-joining. Nature Communications, 12(1), Article 1.

Singh, T. R., Ali, A. M., Busygina, V., Raynard, S., Fan, Q., Du, C., Andreassen, P. R., Sung, P., & Meetei, A. R. (2008). BLAP18/RMI2, a novel OB-fold-containing protein, is an essential component of the Bloom helicase-double Holliday junction dissolvasome. Genes & Development, 22(20), 2856–2868.

Sirbu, B. M., Couch, F. B., Feigerle, J. T., Bhaskara, S., Hiebert, S. W., & Cortez, D. (2011). Analysis of protein dynamics at active, stalled, and collapsed replication forks. Genes & Development, 25(12), 1320–1327.

Slade, D., Dunstan, M. S., Barkauskaite, E., Weston, R., Lafite, P., Dixon, N., Ahel, M., Leys, D., & Ahel, I. (2011). The structure and catalytic mechanism of a poly(ADP-ribose) glycohydrolase. Nature, 477(7366), Article 7366.

Smith, S., & de Lange, T. (2000). Tankyrase promotes telomere elongation in human cells. Current Biology: CB, 10(20), 1299–1302.

Smith, S., Giriat, I., Schmitt, A., & de Lange, T. (1998). Tankyrase, a poly(ADP-ribose) polymerase at human telomeres. Science (New York, N.Y.), 282(5393), 1484–1487.

Sogo, J. M., Lopes, M., & Foiani, M. (2002). Fork reversal and ssDNA accumulation at stalled replication forks owing to checkpoint defects. Science (New York, N.Y.), 297(5581), 599–602.

Solinger, J. A., Kiianitsa, K., & Heyer, W.-D. (2002). Rad54, a Swi2/Snf2-like Recombinational Repair Protein, Disassembles Rad51:dsDNA Filaments. Molecular Cell, 10(5), 1175–1188.

Somyajit, K., Saxena, S., Babu, S., Mishra, A., & Nagaraju, G. (2015). Mammalian RAD51 paralogs protect nascent DNA at stalled forks and mediate replication restart. Nucleic Acids Research, 43(20), 9835–9855.

Sørensen, C. S., Syljuåsen, R. G., Falck, J., Schroeder, T., Rönnstrand, L., Khanna, K. K., Zhou, B.-B., Bartek, J., & Lukas, J. (2003). Chk1 regulates the S phase checkpoint by coupling the physiological turnover and ionizing radiation-induced accelerated proteolysis of Cdc25A. Cancer Cell, 3(3), 247–258.

Sotiriou, S. K., Kamileri, I., Lugli, N., Evangelou, K., Da-Ré, C., Huber, F., Padayachy, L., Tardy, S., Nicati, N. L., Barriot, S., Ochs, F., Lukas, C., Lukas, J., Gorgoulis, V. G., Scapozza, L., & Halazonetis, T. D. (2016). Mammalian RAD52 Functions in Break-Induced Replication Repair of Collapsed DNA Replication Forks. Molecular Cell, 64(6), 1127–1134.

Soulas-Sprauel, P., Rivera-Munoz, P., Malivert, L., Le Guyader, G., Abramowski, V., Revy, P., & de Villartay, J.-P. (2007). V(D)J and immunoglobulin class switch recombinations: A paradigm to study the regulation of DNA end-joining. Oncogene, 26(56), Article 56.

Soule, H. D., Maloney, T. M., Wolman, S. R., Peterson, W. D., Brenz, R., McGrath, C. M., Russo, J., Pauley, R. J., Jones, R. F., & Brooks, S. C. (1990). Isolation and characterization of a spontaneously immortalized human breast epithelial cell line, MCF-10. Cancer Research, 50(18), 6075–6086.

Sousa, F. G., Matuo, R., Soares, D. G., Escargueil, A. E., Henriques, J. A. P., Larsen, A. K., & Saffi, J. (2012). PARPs and the DNA damage response. Carcinogenesis, 33(8), 1433–1440.

Soutoglou, E., Dorn, J. F., Sengupta, K., Jasin, M., Nussenzweig, A., Ried, T., Danuser, G., & Misteli, T. (2007). Positional stability of single double-strand breaks in mammalian cells. Nature Cell Biology, 9(6), 675–682.

Spagnolo, L., Barbeau, J., Curtin, N. J., Morris, E. P., & Pearl, L. H. (2012). Visualization of a DNA-PK/PARP1 complex. Nucleic Acids Research, 40(9), 4168–4177.

Sparks, J. L., & Burgers, P. M. (2015). Error-free and mutagenic processing of topoisomerase 1-provoked damage at genomic ribonucleotides. The EMBO Journal, 34(9), 1259–1269.

Spies, J., Lukas, C., Somyajit, K., Rask, M.-B., Lukas, J., & Neelsen, K. J. (2019). 53BP1 nuclear bodies enforce replication timing at under-replicated DNA to limit heritable DNA damage. Nature Cell Biology, 21(4), Article 4.

Spycher, C., Miller, E. S., Townsend, K., Pavic, L., Morrice, N. A., Janscak, P., Stewart, G. S., & Stucki, M. (2008). Constitutive phosphorylation of MDC1 physically links the MRE11-RAD50-NBS1 complex to damaged chromatin. The Journal of Cell Biology, 181(2), 227–240.

Steger, M., Murina, O., Hühn, D., Ferretti, L. P., Walser, R., Hänggi, K., Lafranchi, L., Neugebauer, C., Paliwal, S., Janscak, P., Gerrits, B., Del Sal, G., Zerbe, O., & Sartori, A. A. (2013). Prolyl isomerase PIN1 regulates DNA double-strand break repair by counteracting DNA end resection. Molecular Cell, 50(3), 333–343.

Ström, C. E., Johansson, F., Uhlén, M., Szigyarto, C. A.-K., Erixon, K., & Helleday, T. (2011). Poly (ADP-ribose) polymerase (PARP) is not involved in base excision repair but PARP inhibition traps a single-strand intermediate. Nucleic Acids Research, 39(8), 3166–3175.

Stucki, M., Clapperton, J. A., Mohammad, D., Yaffe, M. B., Smerdon, S. J., & Jackson, S. P. (2005). MDC1 directly binds phosphorylated histone H2AX to regulate cellular responses to DNA double-strand breaks. Cell, 123(7), 1213–1226.

Sun, F.-H., Zhao, P., Zhang, N., Kong, L.-L., Wong, C. C. L., & Yun, C.-H. (2021). HPF1 remodels the active site of PARP1 to enable the serine ADP-ribosylation of histones. Nature Communications, 12(1), Article 1.

Sung, M.-K., Porras-Yakushi, T. R., Reitsma, J. M., Huber, F. M., Sweredoski, M. J., Hoelz, A., Hess, S., & Deshaies, R. J. (2016). A conserved quality-control pathway that mediates degradation of unassembled ribosomal proteins. ELife, 5, e19105.

Suskiewicz, M. J., Zobel, F., Ogden, T. E. H., Fontana, P., Ariza, A., Yang, J.-C., Zhu, K., Bracken, L., Hawthorne, W. J., Ahel, D., Neuhaus, D., & Ahel, I. (2020). HPF1 completes the PARP active site for DNA damage-induced ADP-ribosylation. Nature, 579(7800), 598–602.

Suzuki, T., Terasaki, M., Takemoto-Hori, C., Hanada, T., Ueda, T., Wada, A., & Watanabe, K. (2001). Proteomic Analysis of the Mammalian Mitochondrial Ribosome: IDENTIFICATION OF PROTEIN COMPONENTS IN THE 28 S SMALL SUBUNIT *. Journal of Biological Chemistry, 276(35), 33181–33195.

Svendsen, J. M., Smogorzewska, A., Sowa, M. E., O'Connell, B. C., Gygi, S. P., Elledge, S. J., & Harper, J. W. (2009). Mammalian BTBD12/SLX4 assembles a Holliday junction resolvase and is required for DNA repair. Cell, 138(1), 63–77.

Svilar, D., Goellner, E. M., Almeida, K. H., & Sobol, R. W. (2011). Base excision repair and lesion-dependent subpathways for repair of oxidative DNA damage. Antioxidants & Redox Signaling, 14(12), 2491–2507.

Sy, S. M. H., Huen, M. S. Y., & Chen, J. (2009). PALB2 is an integral component of the BRCA complex required for homologous recombination repair. Proceedings of the National Academy of Sciences of the United States of America, 106(17), 7155–7160.

Sy, S. M.-H., Jiang, J., Dong, S., Lok, G. T. M., Wu, J., Cai, H., Yeung, E. S. L., Huang, J., Chen, J., Deng, Y., & Huen, M. S. Y. (2011). Critical Roles of Ring Finger Protein RNF8 in Replication Stress Responses *. Journal of Biological Chemistry, 286(25), 22355–22361.

Taglialatela, A., Alvarez, S., Leuzzi, G., Sannino, V., Ranjha, L., Huang, J.-W., Madubata, C., Anand, R., Levy, B., Rabadan, R., Cejka, P., Costanzo, V., & Ciccia, A. (2017). Restoration of replication fork stability in BRCA1- and BRCA2-deficient cells by inactivation of SNF2-family fork remodelers. Molecular Cell, 68(2), 414-430.e8.

Takata, M., Sasaki, M. S., Sonoda, E., Morrison, C., Hashimoto, M., Utsumi, H., Yamaguchi-Iwai, Y., Shinohara, A., & Takeda, S. (1998). Homologous recombination and non-homologous end-joining pathways of DNA double-strand break repair have overlapping roles in the maintenance of chromosomal integrity in vertebrate cells. The EMBO Journal, 17(18), 5497–5508.

Takeyama, K., Aguiar, R. C. T., Gu, L., He, C., Freeman, G. J., Kutok, J. L., Aster, J. C., & Shipp, M. A. (2003). The BAL-binding Protein BBAP and Related Deltex Family Members Exhibit Ubiquitin-Protein Isopeptide Ligase Activity *. Journal of Biological Chemistry, 278(24), 21930–21937.

Talhaoui, I., Lebedeva, N. A., Zarkovic, G., Saint-Pierre, C., Kutuzov, M. M., Sukhanova, M. V., Matkarimov, B. T., Gasparutto, D., Saparbaev, M. K., Lavrik, O. I., & Ishchenko, A. A. (2016). Poly(ADP-ribose) polymerases covalently modify strand break termini in DNA fragments in vitro. Nucleic Acids Research, 44(19), 9279–9295.

Tallarida, R. J. (2011). Quantitative Methods for Assessing Drug Synergism. Genes & Cancer, 2(11), 1003–1008.

Tao, Z., Gao, P., & Liu, H. (2009). Identification of the ADP-Ribosylation Sites in the PARP-1 Automodification Domain: Analysis and Implications. Journal of the American Chemical Society, 131(40), 14258–14260.

ter Brugge, P., Kristel, P., van der Burg, E., Boon, U., de Maaker, M., Lips, E., Mulder, L., de Ruiter, J., Moutinho, C., Gevensleben, H., Marangoni, E., Majewski, I., Jóźwiak, K., Kloosterman, W., van Roosmalen, M., Duran, K., Hogervorst, F., Turner, N., Esteller, M., … Jonkers, J. (2016). Mechanisms of Therapy Resistance in Patient-Derived Xenograft Models of BRCA1-Deficient Breast Cancer. JNCI: Journal of the National Cancer Institute, 108(11), djw148.

Thada, V., & Cortez, D. (2019). Common motifs in ETAA1 and TOPBP1 required for ATR kinase activation. The Journal of Biological Chemistry, 294(21), 8395–8402.

Thada, V., & Cortez, D. (2021). ATR activation is regulated by dimerization of ATR activating proteins. Journal of Biological Chemistry, 296.

Thangavel, S., Berti, M., Levikova, M., Pinto, C., Gomathinayagam, S., Vujanovic, M., Zellweger, R., Moore, H., Lee, E. H., Hendrickson, E. A., Cejka, P., Stewart, S., Lopes, M., & Vindigni, A. (2015). DNA2 drives processing and restart of reversed replication forks in human cells. The Journal of Cell Biology, 208(5), 545–562.

The Nobel Prize in Chemistry 2020. (2020). NobelPrize.Org.

The UniProt Consortium. (2021). UniProt: The universal protein knowledgebase in 2021. Nucleic Acids Research, 49(D1), D480–D489.

Thelander, L., & Reichard, P. (1979). Reduction of ribonucleotides. Annual Review of Biochemistry, 48, 133–158.

Thorsell, A.-G., Ekblad, T., Karlberg, T., Löw, M., Pinto, A. F., Trésaugues, L., Moche, M., Cohen, M. S., & Schüler, H. (2017). Structural Basis for Potency and Promiscuity in Poly(ADP-ribose) Polymerase (PARP) and Tankyrase Inhibitors. Journal of Medicinal Chemistry, 60(4), 1262–1271.

Tian, T., Bu, M., Chen, X., Ding, L., Yang, Y., Han, J., Feng, X.-H., Xu, P., Liu, T., Ying, S., Lei, Y., Li, Q., & Huang, J. (2020). The ZATT-TOP2A-PICH Axis Drives Extensive Replication Fork Reversal to Promote Genome Stability. Molecular Cell, 81, 198–211

Tillmar, L., Carlsson, C., & Welsh, N. (2002). Control of insulin mRNA stability in rat pancreatic islets. Regulatory role of a 3'-untranslated region pyrimidine-rich sequence. The Journal of Biological Chemistry, 277(2), 1099–1106.

Tillmar, L., & Welsh, N. (2002). Hypoxia may increase rat insulin mRNA levels by promoting binding of the polypyrimidine tract-binding protein (PTB) to the pyrimidine-rich insulin mRNA 3'-untranslated region. Molecular Medicine, 8(5), 263–272.

Todorova, T., Bock, F. J., & Chang, P. (2014). PARP13 regulates cellular mRNA post-transcriptionally and functions as a pro-apoptotic factor by destabilizing TRAILR4 transcript. Nature Communications, 5(1), Article 1.

Toledo, L. I., Altmeyer, M., Rask, M.-B., Lukas, C., Larsen, D. H., Povlsen, L. K., Bekker-Jensen, S., Mailand, N., Bartek, J., & Lukas, J. (2013). ATR Prohibits Replication Catastrophe by Preventing Global Exhaustion of RPA. Cell, 155(5), 1088–1103.

Toledo, L., Neelsen, K. J., & Lukas, J. (2017). Replication Catastrophe: When a Checkpoint Fails because of Exhaustion. Molecular Cell, 66(6), 735–749.

Tomida, J., Takata, K.-I., Bhetawal, S., Person, M. D., Chao, H.-P., Tang, D. G., & Wood, R. D. (2018). FAM35A associates with REV7 and modulates DNA damage responses of normal and BRCA1-defective cells. The EMBO Journal, 37(12), e99543.

Tomimatsu, N., Mukherjee, B., Catherine Hardebeck, M., Ilcheva, M., Vanessa Camacho, C., Louise Harris, J., Porteus, M., Llorente, B., Khanna, K. K., & Burma, S. (2014). Phosphorylation of EXO1 by CDKs 1 and 2 regulates DNA end resection and repair pathway choice. Nature Communications, 5, 3561.

Trenz, K., Smith, E., Smith, S., & Costanzo, V. (2006). ATM and ATR promote Mre11 dependent restart of collapsed replication forks and prevent accumulation of DNA breaks. The EMBO Journal, 25(8), 1764–1774.

Tripathi, V., Nagarjuna, T., & Sengupta, S. (2007). BLM helicase-dependent and -independent roles of 53BP1 during replication stress-mediated homologous recombination. The Journal of Cell Biology, 178(1), 9–14.

Tromans-Coia, C., Sanchi, A., Moeller, G. K., Timinszky, G., Lopes, M., & Ahel, I. (2021). TARG1 protects against toxic DNA ADP-ribosylation. Nucleic Acids Research, 49(18), 10477–10492.

Truong, L. N., Li, Y., Shi, L. Z., Hwang, P. Y.-H., He, J., Wang, H., Razavian, N., Berns, M. W., & Wu, X. (2013). Microhomology-mediated End Joining and Homologous Recombination share the initial end resection step to repair DNA double-strand breaks in mammalian cells. Proceedings of the National Academy of Sciences of the United States of America, 110(19), 7720–7725.

Tsai, S.-P., Su, G.-C., Lin, S.-W., Chung, C.-I., Xue, X., Dunlop, M. H., Akamatsu, Y., Jasin, M., Sung, P., & Chi, P. (2012). Rad51 presynaptic filament stabilization function of the mouse Swi5-Sfr1 heterodimeric complex. Nucleic Acids Research, 40(14), 6558–6569.

Tsodikov, O. V., Enzlin, J. H., Schärer, O. D., & Ellenberger, T. (2005). Crystal structure and DNA binding functions of ERCC1, a subunit of the DNA structure-specific endonuclease XPF–ERCC1. Proceedings of the National Academy of Sciences of the United States of America, 102(32), 11236–11241.

Tubbs, A., & Nussenzweig, A. (2017). Endogenous DNA Damage as a Source of Genomic Instability in Cancer. Cell, 168(4), 644–656.

Tucker, J. A., Bennett, N., Brassington, C., Durant, S. T., Hassall, G., Holdgate, G., McAlister, M., Nissink, J. W. M., Truman, C., & Watson, M. (2012). Structures of the Human Poly (ADP-Ribose) Glycohydrolase Catalytic Domain Confirm Catalytic Mechanism and Explain Inhibition by ADP-HPD Derivatives. PLoS ONE, 7(12), e50889.

Tuncel, H., Tanaka, S., Oka, S., Nakai, S., Fukutomi, R., Okamoto, M., Ota, T., Kaneko, H., Tatsuka, M., & Shimamoto, F. (2012). PARP6, a mono(ADP-ribosyl) transferase and a negative regulator of cell proliferation, is involved in colorectal cancer development. International Journal of Oncology, 41(6), 2079–2086.

Turner, N., Tutt, A., & Ashworth, A. (2004). Hallmarks of “BRCAness” in sporadic cancers. Nature Reviews. Cancer, 4(10), 814–819.

Uziel, T., Lerenthal, Y., Moyal, L., Andegeko, Y., Mittelman, L., & Shiloh, Y. (2003). Requirement of the MRN complex for ATM activation by DNA damage. The EMBO Journal, 22(20), 5612–5621.

Vaitsiankova, A., Burdova, K., Sobol, M., Gautam, A., Benada, O., Hanzlikova, H., & Caldecott, K. W. (2022). PARP inhibition impedes the maturation of nascent DNA strands during DNA replication. Nature Structural & Molecular Biology, 29(4), Article 4.

Vermehren-Schmaedick, A., Huang, J. Y., Levinson, M., Pomaville, M. B., Reed, S., Bellus, G. A., Gilbert, F., Keren, B., Heron, D., Haye, D., Janello, C., Makowski, C., Danhauser, K., Fedorov, L. M., Haack, T. B., Wright, K. M., & Cohen, M. S. (2021). Characterization of PARP6 Function in Knockout Mice and Patients with Developmental Delay. Cells, 10(6), Article 6.

von Zglinicki, T. (2002). Oxidative stress shortens telomeres. Trends in Biochemical Sciences, 27(7), 339–344.

Vrtis, K. B., Dewar, J. M., Chistol, G., Wu, R. A., Graham, T. G. W., & Walter, J. C. (2021). Single-strand DNA breaks cause replisome disassembly. *Molecular Cell*, *81*(6), 1309-1318.e6.

Vujanovic, M., Krietsch, J., Raso, M. C., Terraneo, N., Zellweger, R., Schmid, J. A., Taglialatela, A., Huang, J.-W., Holland, C. L., Zwicky, K., Herrador, R., Jacobs, H., Cortez, D., Ciccia, A., Penengo, L., & Lopes, M. (2017). Replication Fork Slowing and Reversal upon DNA Damage Require PCNA Polyubiquitination and ZRANB3 DNA Translocase Activity. Molecular Cell, 67(5), 882-890.e5.

Vyas, S., & Chang, P. (2014). New PARP targets for cancer therapy. Nature Reviews Cancer, 14(7), 502–509.

Vyas, S., Chesarone-Cataldo, M., Todorova, T., Huang, Y.-H., & Chang, P. (2013). A systematic analysis of the PARP protein family identifies new functions critical for cell physiology. Nature Communications, 4(1), 1–13.

Vyas, S., Matic, I., Uchima, L., Rood, J., Zaja, R., Hay, R. T., Ahel, I., & Chang, P. (2014). Family-wide analysis of poly(ADP-ribose) polymerase activity. Nature Communications, 5, 4426.

Waga, S., Bauer, G., & Stillman, B. (1994). Reconstitution of complete SV40 DNA replication with purified replication factors. The Journal of Biological Chemistry, 269(14), 10923–10934.

Wagner, E. J., & Garcia-Blanco, M. A. (2001). Polypyrimidine Tract Binding Protein Antagonizes Exon Definition. Molecular and Cellular Biology, 21(10), 3281–3288.

Wahlberg, E., Karlberg, T., Kouznetsova, E., Markova, N., Macchiarulo, A., Thorsell, A.-G., Pol, E., Frostell, Å., Ekblad, T., Öncü, D., Kull, B., Robertson, G. M., Pellicciari, R., Schüler, H., & Weigelt, J. (2012). Family-wide chemical profiling and structural analysis of PARP and tankyrase inhibitors. Nature Biotechnology, 30(3), 283–288.

Walden, H., & Deans, A. J. (2014). The Fanconi Anemia DNA Repair Pathway: Structural and Functional Insights into a Complex Disorder. Annual Review of Biophysics, 43(1), 257–278.

Walker, J. R., Corpina, R. A., & Goldberg, J. (2001). Structure of the Ku heterodimer bound to DNA and its implications for double-strand break repair. Nature, 412(6847), 607–614.

Wan, L., Lou, J., Xia, Y., Su, B., Liu, T., Cui, J., Sun, Y., Lou, H., & Huang, J. (2013). HPrimpol1/CCDC111 is a human DNA primase-polymerase required for the maintenance of genome integrity. EMBO Reports, 14(12), 1104–1112.

Wang, C., Chen, Z., Su, D., Tang, M., Nie, L., Zhang, H., Feng, X., Wang, R., Shen, X., Srivastava, M., McLaughlin, M. E., Hart, T., Li, L., & Chen, J. (2020). C17orf53 is identified as a novel gene involved in inter-strand crosslink repair. DNA Repair, 95, 102946.

Wang, C., Wang, G., Feng, X., Shepherd, P., Zhang, J., Tang, M., Chen, Z., Srivastava, M., McLaughlin, M. E., Navone, N. M., Hart, G. T., & Chen, J. (2019). Genome-wide CRISPR screens reveal synthetic lethality of RNASEH2 deficiency and ATR inhibition. Oncogene, 38(14), 2451–2463.

Wang, H., Li, Y., Truong, L. N., Shi, L. Z., Hwang, P. Y.-H., He, J., Do, J., Cho, M. J., Li, H., Negrete, A., Shiloach, J., Berns, M. W., Shen, B., Chen, L., & Wu, X. (2014). CtIP maintains stability at common fragile sites and inverted repeats by an end resection-independent endonuclease activity. Molecular Cell, 54(6), 1012–1021.

Wang, J. C. (2002). Cellular roles of DNA topoisomerases: A molecular perspective. Nature Reviews Molecular Cell Biology, 3(6), Article 6.

Wang, M., Wu, W., Wu, W., Rosidi, B., Zhang, L., Wang, H., & Iliakis, G. (2006). PARP-1 and Ku compete for repair of DNA double strand breaks by distinct NHEJ pathways. Nucleic Acids Research, 34(21), 6170–6182.

Wang, T., Wei, J. J., Sabatini, D. M., & Lander, E. S. (2014). Genetic screens in human cells using the CRISPR/Cas9 system. Science (New York, N.Y.), 343(6166), 80–84.

Wang, W., Li, N., Li, X., Tran, M. K., Han, X., & Chen, J. (2015). Tankyrase Inhibitors Target YAP by Stabilizing Angiomotin Family Proteins. Cell Reports, 13(3), 524–532.

Wang, Y.-C., Peterson, S. E., & Loring, J. F. (2014). Protein post-translational modifications and regulation of pluripotency in human stem cells. Cell Research, 24(2), 143.

Wang, Z., Grosskurth, S. E., Cheung, T., Petteruti, P., Zhang, J., Wang, X., Wang, W., Gharahdaghi, F., Wu, J., Su, N., Howard, R. T., Mayo, M., Widzowski, D., Scott, D. A., Johannes, J. W., Lamb, M. L., Lawson, D., Dry, J. R., Lyne, P. D., … Chen, H. (2018). Pharmacological Inhibition of PARP6 Triggers Multipolar Spindle Formation and Elicits Therapeutic Effects in Breast Cancer. Cancer Research, 78(23), 6691–6702.

Wang, Z., Song, Y., Li, S., Kurian, S., Xiang, R., Chiba, T., & Wu, X. (2019). DNA polymerase θ (POLQ) is important for repair of DNA double-strand breaks caused by fork collapse. The Journal of Biological Chemistry, 294(11), 3909–3919.

Wassing, I. E., & Esashi, F. (2021). RAD51: Beyond the break. Seminars in Cell & Developmental Biology, 113, 38–46.

Wassing, I. E., Graham, E., Saayman, X., Rampazzo, L., Ralf, C., Bassett, A., & Esashi, F. (2021). The RAD51 recombinase protects mitotic chromatin in human cells. Nature Communications, 12(1), Article 1.

Wattenberg, B., & Lithgow, T. (2001). Targeting of C-Terminal (Tail)-Anchored Proteins: Understanding how Cytoplasmic Activities are Anchored to Intracellular Membranes. Traffic, 2(1), 66–71.

Wei, H., & Yu, X. (2016). Functions of PARylation in DNA Damage Repair Pathways. Genomics, Proteomics & Bioinformatics, 14(3), 131–139.

Weinberg, R. A. (1995). The retinoblastoma protein and cell cycle control. Cell, 81(3), 323–330.

Weixler, L., Feijs, K. L. H., & Zaja, R. (2022). ADP-ribosylation of RNA in mammalian cells is mediated by TRPT1 and multiple PARPs. Nucleic Acids Research, 50(16), 9426–9441.

Welsby, I., Hutin, D., Gueydan, C., Kruys, V., Rongvaux, A., & Leo, O. (2014). PARP12, an Interferon-stimulated Gene Involved in the Control of Protein Translation and Inflammation. The Journal of Biological Chemistry, 289(38), 26642–26657.

Weston, R., Peeters, H., & Ahel, D. (2012). ZRANB3 is a structure-specific ATP-dependent endonuclease involved in replication stress response. Genes & Development, 26(14), 1558–1572.

Wiederhold, L., Leppard, J. B., Kedar, P., Karimi-Busheri, F., Rasouli-Nia, A., Weinfeld, M., Tomkinson, A. E., Izumi, T., Prasad, R., Wilson, S. H., Mitra, S., & Hazra, T. K. (2004). AP Endonuclease-Independent DNA Base Excision Repair in Human Cells. Molecular Cell, 15(2), 209–220.

Williams, J. S., Gehle, D. B., & Kunkel, T. A. (2017). The role of RNase H2 in processing ribonucleotides incorporated during DNA replication. DNA Repair, 53, 52–58.

Williams, J. S., Smith, D. J., Marjavaara, L., Lujan, S. A., Chabes, A., & Kunkel, T. A. (2013). Topoisomerase 1-mediated removal of ribonucleotides from nascent leading-strand DNA. Molecular Cell, 49(5), 1010–1015.

Wilson, T. E., Arlt, M. F., Park, S. H., Rajendran, S., Paulsen, M., Ljungman, M., & Glover, T. W. (2015). Large transcription units unify copy number variants and common fragile sites arising under replication stress. Genome Research, 25(2), 189–200.

Winding, P., & Berchtold, M. W. (2001). The chicken B cell line DT40: A novel tool for gene disruption experiments. Journal of Immunological Methods, 249(1), 1–16. 1

Wold, M. S. (1997). Replication protein A: A heterotrimeric, single-stranded DNA-binding protein required for eukaryotic DNA metabolism. Annual Review of Biochemistry, 66, 61–92.

Wolner, B., & Peterson, C. L. (2005). ATP-dependent and ATP-independent roles for the Rad54 chromatin remodeling enzyme during recombinational repair of a DNA double strand break. The Journal of Biological Chemistry, 280(11), 10855–10860.

Woodward, A. M., Göhler, T., Luciani, M. G., Oehlmann, M., Ge, X., Gartner, A., Jackson, D. A., & Blow, J. J. (2006). Excess Mcm2–7 license dormant origins of replication that can be used under conditions of replicative stress. The Journal of Cell Biology, 173(5), 673–683.

Wu, L., & Hickson, I. D. (2003). The Bloom's syndrome helicase suppresses crossing over during homologous recombination. Nature, 426(6968), 870–874.

Wyatt, D. W., Feng, W., Conlin, M. P., Yousefzadeh, M. J., Roberts, S. A., Mieczkowski, P., Wood, R. D., Gupta, G. P., & Ramsden, D. A. (2016). Essential Roles for Polymerase θ-Mediated End Joining in the Repair of Chromosome Breaks. Molecular Cell, 63(4), 662–673.

Wyatt, H. D. M., Sarbajna, S., Matos, J., & West, S. C. (2013). Coordinated Actions of SLX1-SLX4 and MUS81-EME1 for Holliday Junction Resolution in Human Cells. Molecular Cell, 52(2), 234–247.

Xie, F., Ye, L., Chang, J. C., Beyer, A. I., Wang, J., Muench, M. O., & Kan, Y. W. (2014). Seamless gene correction of β-thalassemia mutations in patient-specific iPSCs using CRISPR/Cas9 and piggyBac. Genome Research, 24(9), 1526–1533.

Xu, D., Muniandy, P., Leo, E., Yin, J., Thangavel, S., Shen, X., Ii, M., Agama, K., Guo, R., Fox, D., Meetei, A. R., Wilson, L., Nguyen, H., Weng, N., Brill, S. J., Li, L., Vindigni, A., Pommier, Y., Seidman, M., & Wang, W. (2010). Rif1 provides a new DNA-binding interface for the Bloom syndrome complex to maintain normal replication. The EMBO Journal, 29(18), 3140–3155.

Xu, S., Wu, X., Wu, L., Castillo, A., Liu, J., Atkinson, E., Paul, A., Su, D., Schlacher, K., Komatsu, Y., You, M. J., & Wang, B. (2017). Abro1 maintains genome stability and limits replication stress by protecting replication fork stability. Genes & Development, 31(14), 1469–1482.

Xue, H., Bhardwaj, A., Yin, Y., Fijen, C., Ephstein, A., Zhang, L., Ding, X., Pascal, J. M., VanArsdale, T. L., & Rothenberg, E. (2022). A two-step mechanism governing PARP1-DNA retention by PARP inhibitors. Science Advances, 8(36), eabq0414.

Xue, X., Raynard, S., Busygina, V., Singh, A. K., & Sung, P. (2013). Role of replication protein A in double holliday junction dissolution mediated by the BLM-Topo IIIα-RMI1-RMI2 protein complex. The Journal of Biological Chemistry, 288(20), 14221–14227.

Yamada, T., Horimoto, H., Kameyama, T., Hayakawa, S., Yamato, H., Dazai, M., Takada, A., Kida, H., Bott, D., Zhou, A. C., Hutin, D., Watts, T. H., Asaka, M., Matthews, J., & Takaoka, A. (2016). Constitutive aryl hydrocarbon receptor signaling constrains type I interferon-mediated antiviral innate defense. Nature Immunology, 17(6), 687–694.

Yan, Q., Xu, R., Zhu, L., Cheng, X., Wang, Z., Manis, J., & Shipp, M. A. (2013). BAL1 and Its Partner E3 Ligase, BBAP, Link Poly(ADP-Ribose) Activation, Ubiquitylation, and Double-Strand DNA Repair Independent of ATM, MDC1, and RNF8. Molecular and Cellular Biology, 33(4), 845–857.

Yan, Z., Delannoy, M., Ling, C., Daee, D., Osman, F., Muniandy, P. A., Shen, X., Oostra, A. B., Du, H., Steltenpool, J., Lin, T., Schuster, B., Décaillet, C., Stasiak, A., Stasiak, A. Z., Stone, S., Hoatlin, M. E., Schindler, D., Woodcock, C. L., … Wang, W. (2010). A histone-fold complex and FANCM form a conserved DNA-remodeling complex to maintain genome stability. Molecular Cell, 37(6), 865–878.

Yaneva, M., Kowalewski, T., & Lieber, M. R. (1997). Interaction of DNA-dependent protein kinase with DNA and with Ku: Biochemical and atomic-force microscopy studies. The EMBO Journal, 16(16), 5098–5112.

Yang, C.-S., Jividen, K., Spencer, A., Dworak, N., Ni, L., Oostdyk, L. T., Chatterjee, M., Kusmider, B., Reon, B., Parlak, M., Gorbunova, V., Abbas, T., Jeffery, E., Sherman, N. E., & Paschal, B. M. (2017). Ubiquitin Modification by the E3 Ligase/ADP-ribosyltransferase Dtx3L/Parp9. Molecular Cell, 66(4), 503-516.e5.

Yang, F., Chen, J., Liu, B., Gao, G., Sebastian, M., Jeter, C., Shen, J., Person, M. D., & Bedford, M. T. (2021). SPINDOC binds PARP1 to facilitate PARylation. Nature Communications, 12(1), Article 1.

Yang, H., Jeffrey, P. D., Miller, J., Kinnucan, E., Sun, Y., Thoma, N. H., Zheng, N., Chen, P.-L., Lee, W.-H., & Pavletich, N. P. (2002). BRCA2 function in DNA binding and recombination from a BRCA2-DSS1-ssDNA structure. Science (New York, N.Y.), 297(5588), 1837–1848.

Yang, L., Sun, L., Teng, Y., Chen, H., Gao, Y., Levine, A. S., Nakajima, S., & Lan, L. (2017). Tankyrase1-mediated poly(ADP-ribosyl)ation of TRF1 maintains cell survival after telomeric DNA damage. Nucleic Acids Research, 45(7), 3906–3921.

Ying, S., Chen, Z., Medhurst, A. L., Neal, J. A., Bao, Z., Mortusewicz, O., McGouran, J., Song, X., Shen, H., Hamdy, F. C., Kessler, B. M., Meek, K., & Helleday, T. (2016). DNA-PKcs and PARP1 Bind to Unresected Stalled DNA Replication Forks Where They Recruit XRCC1 to Mediate Repair. Cancer Research, 76(5), 1078–1088.

Ying, S., Hamdy, F. C., & Helleday, T. (2012). Mre11-Dependent Degradation of Stalled DNA Replication Forks Is Prevented by BRCA2 and PARP1. Cancer Research, 72(11), 2814–2821.

Yuan, J., Xu, W. W., Jiang, S., Yu, H., & Poon, H. F. (2018). The Scattered Twelve Tribes of HEK293. Biomedical and Pharmacology Journal, 11(2), 621–623.

Yuan, S. S., Lee, S. Y., Chen, G., Song, M., Tomlinson, G. E., & Lee, E. Y. (1999). BRCA2 is required for ionizing radiation-induced assembly of Rad51 complex in vivo. Cancer Research, 59(15), 3547–3551.

Zadorozhny, K., Sannino, V., Beláň, O., Mlčoušková, J., Špírek, M., Costanzo, V., & Krejčí, L. (2017). Fanconi-Anemia-Associated Mutations Destabilize RAD51 Filaments and Impair Replication Fork Protection. Cell Reports, 21(2), 333–340.

Zahn, K. E., Jensen, R. B., Wood, R. D., & Doublié, S. (2021). Human DNA polymerase θ harbors DNA end-

Zandarashvili, L., Langelier, M.-F., Velagapudi, U. K., Hancock, M. A., Steffen, J. D., Billur, R., Hannan, Z. M., Wicks, A. J., Krastev, D. B., Pettitt, S. J., Lord, C. J., Talele, T. T., Pascal, J. M., & Black, B. E. (2020). Structural basis for allosteric PARP-1 retention on DNA breaks. Science (New York, N.Y.), 368(6486), eaax6367.

Zellweger, R., Dalcher, D., Mutreja, K., Berti, M., Schmid, J. A., Herrador, R., Vindigni, A., & Lopes, M. (2015). Rad51-mediated replication fork reversal is a global response to genotoxic treatments in human cells. The Journal of Cell Biology, 208(5), 563–579.

Zeman, M. K., & Cimprich, K. A. (2014). Causes and consequences of replication stress. Nature Cell Biology, 16(1), 2–9.

Zhang, F., Shi, J., Bian, C., & Yu, X. (2015). Poly(ADP-ribose) mediates the BRCA2-dependent early DNA damage response. Cell Reports, 13(4), 678–689.

Zhang, F., Shi, J., Chen, S.-H., Bian, C., & Yu, X. (2015). The PIN domain of EXO1 recognizes poly(ADP-ribose) in DNA damage response. Nucleic Acids Research, 43(22), 10782–10794.

Zhang, Y., Wang, J., Ding, M., & Yu, Y. (2013). Site-specific characterization of the Asp- and Glu-ADP-ribosylated proteome. Nature Methods, 10(10), Article 10.

Zhao, H., & Piwnica-Worms, H. (2001). ATR-Mediated Checkpoint Pathways Regulate Phosphorylation and Activation of Human Chk1. Molecular and Cellular Biology, 21(13), 4129–4139.

Zhao, B., Rothenberg, E., Ramsden, D. A., & Lieber, M. R. (2020). The molecular basis and disease relevance of non-homologous DNA end joining. Nature Reviews Molecular Cell Biology, 21(12), Article 12.

Zhao, H., Watkins, J. L., & Piwnica-Worms, H. (2002). Disruption of the checkpoint kinase 1/cell division cycle 25A pathway abrogates ionizing radiation-induced S and G2 checkpoints. Proceedings of the National Academy of Sciences of the United States of America, 99(23), 14795–14800.

Zhao, W., Steinfeld, J. B., Liang, F., Chen, X., Maranon, D. G., Jian Ma, C., Kwon, Y., Rao, T., Wang, W., Sheng, C., Song, X., Deng, Y., Jimenez-Sainz, J., Lu, L., Jensen, R. B., Xiong, Y., Kupfer, G. M., Wiese, C., Greene, E. C., & Sung, P. (2017). BRCA1-BARD1 promotes RAD51-mediated homologous DNA pairing. Nature, 550(7676), 360–365.

Zhong, Q., Chen, C. F., Li, S., Chen, Y., Wang, C. C., Xiao, J., Chen, P. L., Sharp, Z. D., & Lee, W. H. (1999). Association of BRCA1 with the hRad50-hMre11-p95 complex and the DNA damage response. Science (New York, N.Y.), 285(5428), 747–750.

Zhong, Q., Gao, W., Du, F., & Wang, X. (2005). Mule/ARF-BP1, a BH3-Only E3 Ubiquitin Ligase, Catalyzes the Polyubiquitination of Mcl-1 and Regulates Apoptosis. Cell, 121(7), 1085–1095.

Zhou, T., Lee, J. W., Tatavarthi, H., Lupski, J. R., Valerie, K., & Povirk, L. F. (2005). Deficiency in 3'-phosphoglycolate processing in human cells with a hereditary mutation in tyrosyl-DNA phosphodiesterase (TDP1). Nucleic Acids Research, 33(1), 289–297.

Zhu, C., Iwase, M., Li, Z., Wang, F., Quinet, A., Vindigni, A., & Shao, J. (2022). Profilin-1 regulates DNA replication forks in a context-dependent fashion by interacting with SNF2H and BOD1L. Nature Communications, 13(1), Article 1.

Zhu, Z., Chung, W.-H., Shim, E. Y., Lee, S. E., & Ira, G. (2008). Sgs1 helicase and two nucleases Dna2 and Exo1 resect DNA double-strand break ends. Cell, 134(6), 981–994.

Zimmermann, M., Lottersberger, F., Buonomo, S. B., Sfeir, A., & de Lange, T. (2013). 53BP1 regulates DSB repair using Rif1 to control 5' end resection. Science (New York, N.Y.), 339(6120), 700–704.

Zimmermann, M., Murina, O., Reijns, M. A. M., Agathanggelou, A., Challis, R., Tarnauskaitė, Ž., Muir, M., Fluteau, A., Aregger, M., McEwan, A., Yuan, W., Clarke, M., Lambros, M. B., Paneesha, S., Moss, P., Chandrashekhar, M., Angers, S., Moffat, J., Brunton, V. G., … Durocher, D. (2018). CRISPR screens identify genomic ribonucleotides as a source of PARP-trapping lesions. Nature, 559(7713), 285–289.

Zlatanou, A., Sabbioneda, S., Miller, E. S., Greenwalt, A., Aggathanggelou, A., Maurice, M. M., Lehmann, A. R., Stankovic, T., Reverdy, C., Colland, F., Vaziri, C., & Stewart, G. S. (2016). USP7 is essential for maintaining Rad18 stability and DNA damage tolerance. Oncogene, 35(8), Article 8.

Zong, D., Adam, S., Wang, Y., Sasanuma, H., Callén, E., Murga, M., Day, A., Kruhlak, M. J., Wong, N., Munro, M., Chaudhuri, A. R., Karim, B., Xia, B., Takeda, S., Johnson, N., Durocher, D., & Nussenzweig, A. (2019). BRCA1 haploinsufficiency is masked by RNF168-mediated chromatin ubiquitylation. Molecular Cell, 73(6), 1267-1281.e7.

Zou, L., & Elledge, S. J. (2003). Sensing DNA damage through ATRIP recognition of RPA-ssDNA complexes. Science (New York, N.Y.), 300(5625), 1542–1548.

Zou, L., Liu, D., & Elledge, S. J. (2003). Replication protein A-mediated recruitment and activation of Rad17 complexes. Proceedings of the National Academy of Sciences, 100(24), 13827–13832.

8. Appendices

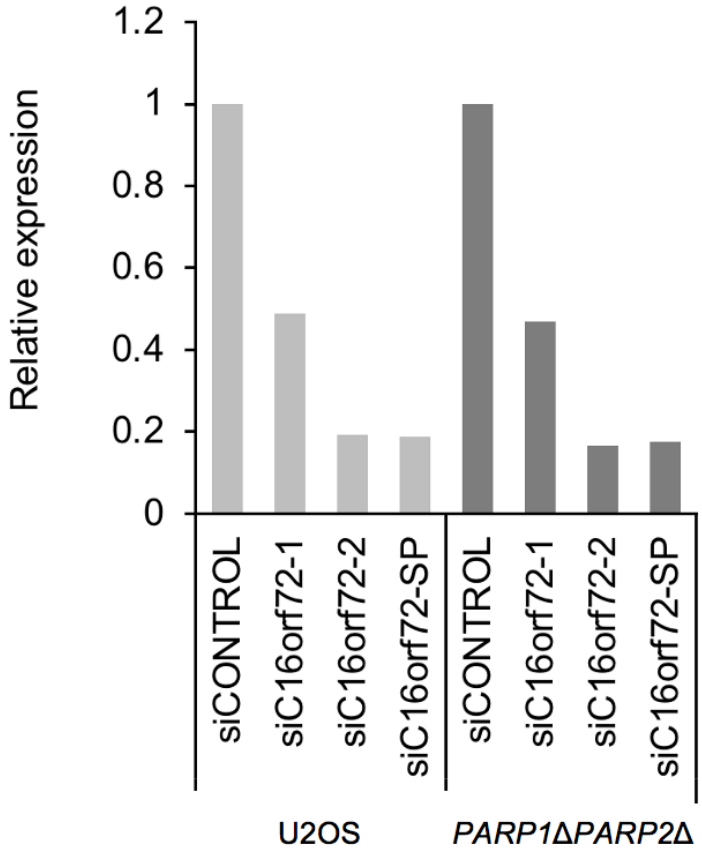


Figure 8.1: Validation of C16orf72 knockdown in U2OS, *PARP1Δ* and *PARP1ΔPARP2Δ* cells. Wild type U2OS and *PARP1ΔPARP2Δ* cell lines were transfected with non-targeting control siRNA (siCONTROL) or with C16orf72-targeting siRNA#1 (siC16orf72-1), C16orf72-targeting siRNA#2 (siC16orf72-2), or C16orf72-targeting SMARTpool siRNA (siC16orf72-SP). Relative expression of *C16orf72* in each of the conditions was quantified via RT-qPCR. The data represents one independent biological repeat. This experiment was performed by Dr Khairul Ramlee.

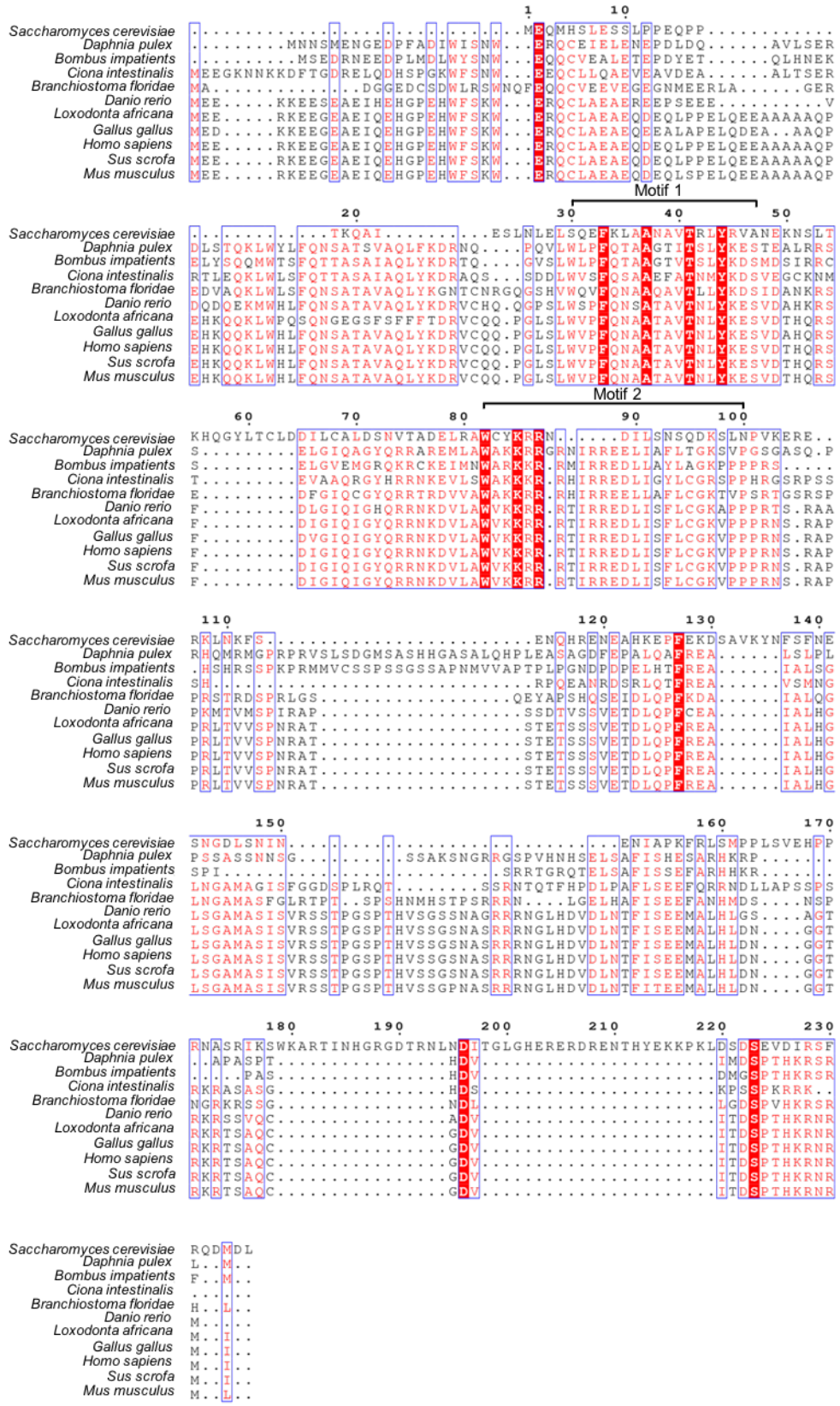

Motif 1
Motif 2
Saccharomyces cerevisiae
Daphnia pulex
Bombus impatients
Ciona intestinalis
Branchiostoma floridae
Danio rerio
Loxodonta africana
Gallus gallus
Homo sapiens
Sus scrofa
Mus musculus

Figure 8.2: Extended alignment of C16orf72 orthologues from chordates, arthropods and ascomycetes. Alignment of C16orf72 orthologues from *Saccharomyces cerevisiae*, *Daphnia pulex*, *Bombus impatients*, *Ciona intestinalis*, *Danio rerio*, *Loxodonta africana*, *Gallus gallus*, *Homo sapiens*, *Sus scrofa* and *Mus musculis*. The alignments were prepared with Clustal Omega and visualised with EndScript 3.0 (Robert & Gouet, 2014; Sievers et al., 2011, 2020; Sievers & Higgins, 2018). Completely conserved amino acids are indicated with white letters on a red background. Similar amino acids are indicated with red letters on a white background and are surrounded by a blue box. Amino acids with low similarity are indicated with black letters on a white background.

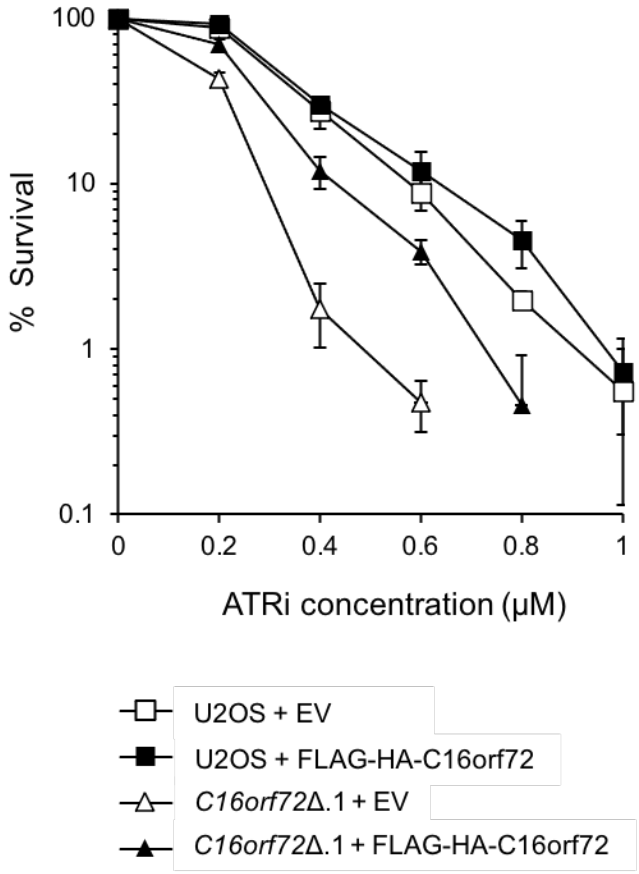
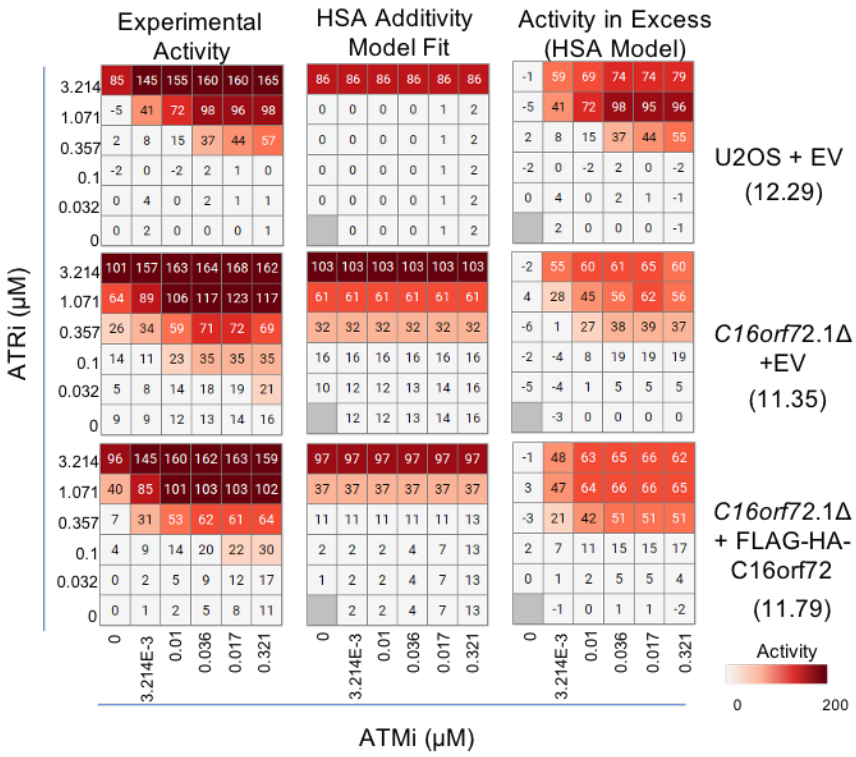
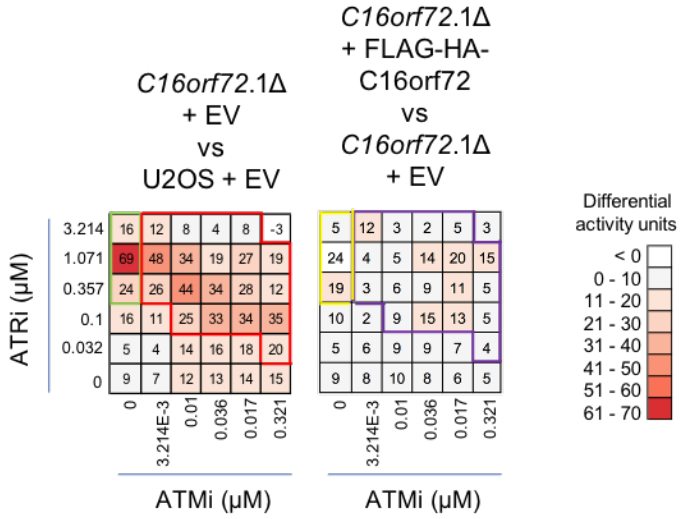


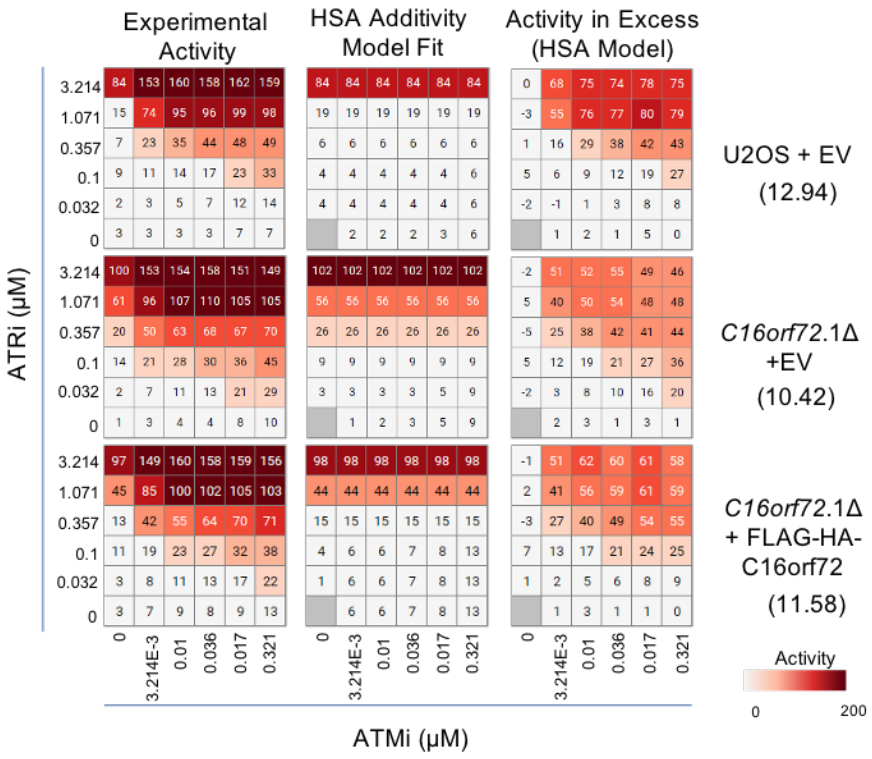
Figure 8.3: Loss of C16orf72 sensitises further sensitises U2OS cells to ATRi (a) U2OS + EV, U2OS + FLAG-HA-C16orf72, *C16orf72Δ*.1 + EV, *C16orf72Δ*.1 + FLAG-HA-C16orf72 cells were treated with ATRi for 9 days and their ability to form colonies was analysed via clonogenic survival assay. Error bars at each data point represent the standard error of the mean from three separate biological replicates. A two-way ANOVA with Tukey's post hoc analysis was used to determine the statistical significance between conditions. The experiments presented in this figure were performed by Dr Khairul Ramlee and Amy Wolstenholme.

a


Experimental Activity
HSA Additivity Model Fit
Activity in Excess (HSA Model)
U2OS + EV (12.29)
C16orf72.1Δ +EV (11.35)
C16orf72.1Δ + FLAG-HA-C16orf72 (11.79)
ATRi (μM)
ATMi (μM)
Activity
0
200
3.214
1.071
0.357
0.1
0.032
0
3.214E-3
0.01
0.036
0.017
0.321


C16orf72.1Δ + EV vs U2OS + EV
C16orf72.1Δ + FLAG-HA-C16orf72 vs C16orf72.1Δ + EV
ATRi (μM)
ATMi (μM)
ATMi (μM)
Differential activity units
< 0
0 - 10
11 - 20
21 - 30
31 - 40
41 - 50
51 - 60
61 - 70

b


Experimental Activity
HSA Additivity Model Fit
Activity in Excess (HSA Model)
ATRi (μM)
3.214
1.071
0.357
0.1
0.032
0
U2OS + EV
(12.94)
C16orf72.1Δ +EV
(10.42)
C16orf72.1Δ + FLAG-HA-C16orf72
(11.58)
0
3.214E-3
0.01
0.036
0.017
0.321
ATMi (μM)
Activity
0
200

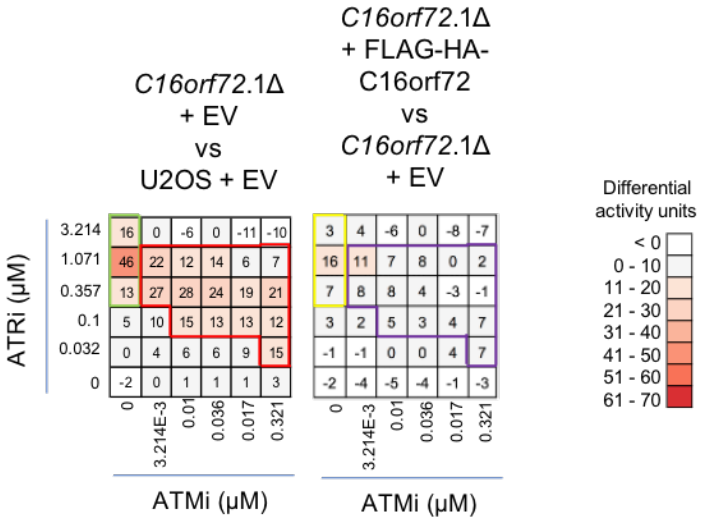

C16orf72.1Δ + EV vs U2OS + EV
C16orf72.1Δ + FLAG-HA-C16orf72 vs C16orf72.1Δ + EV
ATRi (μM)
3.214
1.071
0.357
0.1
0.032
0
0
3.214E-3
0.01
0.036
0.017
0.321
ATMi (μM)
ATMi (μM)
Differential activity units
< 0
0 - 10
11 - 20
21 - 30
31 - 40
41 - 50
51 - 60
61 - 70

Figure 8.4: *C16orf72* deletion further sensitises U2OS cells to ATRi-ATMi combinations. Heatmaps of U2OS + EV, *C16orf72Δ*.1 + EV and *C16orf72Δ*.1 + FLAG-HA-C16orf72 cells exposed to a 6x6 ATRi-ATMi combination matrix for 5 days. Experimental activity signifies extent of growth inhibition or cytotoxicity for a given concentration combination. An experimental activity of < 0 indicates that a treatment promotes the growth of cells. An experimental activity of 0 – 100 indicates that a treatment causes a cytostatic effect. An experimental activity of 101-200 indicates that a treatment causes a cytotoxic effect. Activity in excess signifies the excess experimental activity observed compared to the highest single agent (HSA) additivity model. For each cell line, activity in excess was used to calculate a synergy score (in brackets). Differences in experimental activity between indicated cell lines is signified with differential activity. Green box indicates further sensitisation of *C16orf72Δ*.1 + EV cells to ATRi relative to U2OS + EV cells. Red box indicates further sensitisation of *C16orf72Δ*.1 + EV cells to ATRi-ATMi combinations relative to U2OS + EV cells. Yellow box indicates partial rescue of ATRi sensitivity in *C16orf72Δ*.1 + FLAG-HA-C16orf72 cells relative to U2OS + EV cells. Purple box indicates partial rescue of ATRi-ATMi sensitivity observed in *C16orf72Δ*.1 + FLAG-HA-C16orf72 relative to U2OS + EV cells. Three independent biological repeats of this screen were performed. **(a)** and **(b)** represent two of the independent biological repeats of this experiment.